AFSWP-895

THIS DOCUMENT CONSISTS OF 570 PAGES
OF 325 COPIES, SERIES A

107366

FALL - OUT SYMPOSIUM ([redacted)

JANUARY 1955

[redacted]

ARMED FORCES SPECIAL WEAPONS PROJECT
WASHINGTON 25, D.C.

[redacted]

[redacted] ATOMIC ENERGY ACT 1954

[redacted]

AFSWP-895

FALL-OUT SYMPOSIUM

JANUARY 1955

This document contains information affecting the national defense of the United States within the meaning of the Espionage Laws, Title 18, U.S.C., Sections 793 and 794. The transmission or the revelation of its contents in any manner to an unauthorized person is prohibited by law.

This document contains RESTRICTED DATA within the meaning of the Atomic Energy Act of 1954. Its transmission or the revelation of its contents, in any manner not authorized by that Act, is prohibited by law.

[redacted]

[redacted]DATA

2

7/18/88

INCOMPLETE DOCUMENT REFERENCE SHEET

The archive copy of this document is incomplete.

Pages missing ii

Enclosures missing _____

_____

Attachments missing _____

_____

Other _____

CAS
signature

2-11-92
date

2A

[redacted]

LETTER OF PROMULGATION

A fall-out symposium sponsored by the Armed Forces Special Weapons Project was held in the Pentagon on 10, 11, and 12 January 1955. Thirty papers were presented during the three day meeting. This report is a collection of the papers presented at the symposium; it includes a major part of the discussions which followed a number of papers and is aimed at reporting accurately an unbiased representation of those reports and discussions.

The AFSWP appreciates the wholehearted cooperation extended by the numerous Department of Defense and Atomic Energy Commission laboratories and departments and private research organizations whose personnel presented papers. The meetings were well attended and it is believed that the papers presented and the discussions which resulted served to bring into focus the numerous technical problems which exist in this important field of weapons effects.

G. R. Luedecke

A. R. LUEDECKE
Major General, USAF
Chief, AFSWP

[redacted]

[redacted]

INCOMPLETE DOCUMENT REFERENCE SHEET

The archive copy of this document is incomplete.

Pages missing IV

Enclosures missing _____

_____

Attachments missing _____

_____

Other _____

CAS
signature

2-11-92
date

[redacted]

TABLE OF CONTENTS

[redacted]

[redacted]

[redacted]

TABLE OF CONTENTS

[redacted]

[redacted]

[redacted]

TABLE OF CONTENTS

[redacted]

[redacted]

[redacted]

TABLE OF CONTENTS

[redacted]

[redacted]

7

[redacted]

OPENING REMARKS

BRIGEN L. K. Tarrant, USA
Armed Forces Special Weapons Project

I am General Tarrant, Deputy Chief of AFSWP. General Luedecke, who is out of town and unable to attend, has asked me to convey to you his regret at being unable to personally welcome you to this Symposium. It is my pleasure to extend to you General Luedecke's and my own personal and official welcome.

Significant contributions have been made in this field by a large number of agencies and individuals working on various aspects of the fall-out problem and it appeared desirable for us to provide an opportunity for a meeting of the many diverse groups involved to insure that the basic information necessary to fix a point of departure is available to all concerned, as well as to promote a free exchange of new ideas and approaches to the problem.

While we cannot minimize the inherent complexity of the fall-out processes, we do, nevertheless, recognize the urgent need for a simple, workable solution which can be applied in the operational planning by both the military and civil defense elements of our government.

We realize that close-in fall-out is only one facet of the whole contamination problem and that contamination, in turn, is only a part of the entire weapons effects picture. However, the tremendous potential effect of planned or accidental fall-out contamination makes it imperative that we achieve, as rapidly as possible, the answers which are required.

In looking at the agenda I see that you have a great deal of material to cover in the next three days, so I believe the best contribution I can make is to cut short my remarks and let you get on with it. Before I close, I feel that I must mention the ever-present security problem. First, in spite of the many recent articles in the news media, we are directed to maintain this subject in a classified category of information. Second, it is desired to maintain the fact of the occurrence of this Symposium in a classified category. Third, it has been determined that it is not in the best interests of national security for any agency to make a public release on anything related to fall-out at this time.

I thank you for the interest you have shown in this meeting both by your attendance and the work that has gone into the preparation of the papers to be given.

[redacted]

[redacted]

8

[redacted]

PROJECTS 2.5a AND 2.6a RESULTS, OPERATION CASTLE

Edward R. Tompkins
U. S. Naval Radiological Defense Laboratory

This report summarizes the operational plan, the experimental approach, and the results of Projects 2.5a and 2.6a, Operation CASTLE, Detailed accounts of these projects are contained in the final reports. Certain specific properties of the atomic bomb debris and its distribution will be discussed at this symposium by other members from NRDL: C. F. Miller will discuss the physical and chemical nature of the contaminant; N. E. Ballou, the decay characteristics as related to the radiochemical composition; C. S. Cook, the source gamma spectra; and E. A. Schuert, the derivation of radiation contours. If some of these items are not covered in very great detail in this presentation, it is because they will be discussed later.

Objectives

The objectives of these projects were (a) to determine the radiation contours which resulted from fall-out of atomic bomb debris, and (b) to characterize this material as to its physical, chemical and radiochemical properties. This information has been useful in developing a method for predicting the fall-out patterns from detonations of weapons of various yields at different locations and for estimating the radiation hazard and the problems associated with the contamination of military bases and other targets of military importance.

Status of Knowledge Prior to Operation CASTLE

Nuclear Weapons Tests

Studies of several other contaminating events had been made prior to Operation CASTLE. At Operation CROSSROADS, the Baker shot spread radioactive contaminants over a large area around the point of detonation, but neither its distribution nor its characteristics were determined adequately.

Good measurements of the nature and distribution of the atomic bomb debris were made at Operation JANGLE for both the surface and underground shots. Here it was possible to measure the radiation field directly by the use of survey instruments. Measurements were also made of the quantity of fall-out and its rate of arrival around the shot point.

At Operation IVY, the extent of the cross and upwind fall-out zone and the time and rate of arrival were measured. No samples of fall-out were collected in the down-wind direction. The pattern in the cross and

[redacted]

[redacted]

upwind directions, particularly in regard to the radiation levels, was considerably different from that predicted by scaling up JANGLE results. This indicated the need for a more refined scaling method or a model which could predict the fall-out pattern more closely.

High Explosive Model Tests

In addition to these contaminating events, high explosive model tests using charges ranging in size from 150 lbs. to about 50 tons have been carried out. These shots were detonated both on land and water at different depths below the surface. Non-radioactive tracers were incorporated into the charges. The fall-out was collected around the shot points. Information as to the mass of material and the fraction of the device falling per unit area and its rate of arrival at various locations was obtained. Attempts were made to scale the high explosive model results so as to compare them to JANGLE results. It was found that many parameters scaled roughly as the cube root of the yield.

Plan of Attack at Operation CASTLE

In planning for Operation CASTLE, an attempt was made to develop a method for measuring the distribution of the fall-out and to estimate the radiation levels that would have existed around the shot point had the fall-out occurred over land. The method adopted provided for (a) the collection of fall-out over water and on the islands of the atoll to determine the amount falling per unit area at various locations around the shot point, and (b) the measurement of the radiation fields on the islands adjacent to the collection points. Then by using the simple assumed relationship,

$$R_W = R_L \frac{FO_W}{FO_L}$$

where R_L = radiation field measured over land

FO_W = the fall-out collected over water

FO_L = the fall-out collected over land

the values for the radiation levels R_W at various locations which would have occurred had the fall-out arrived over land could be estimated and iso-radiation level lines drawn.

Planned Locations of Sampling Stations

The general array of sampling stations which was planned is shown in Figure 1. The stations were to be located at the intercepts of circles, 5, 10, 20, 35 and 50 miles in radius and radii 18° apart extending from

[redacted]

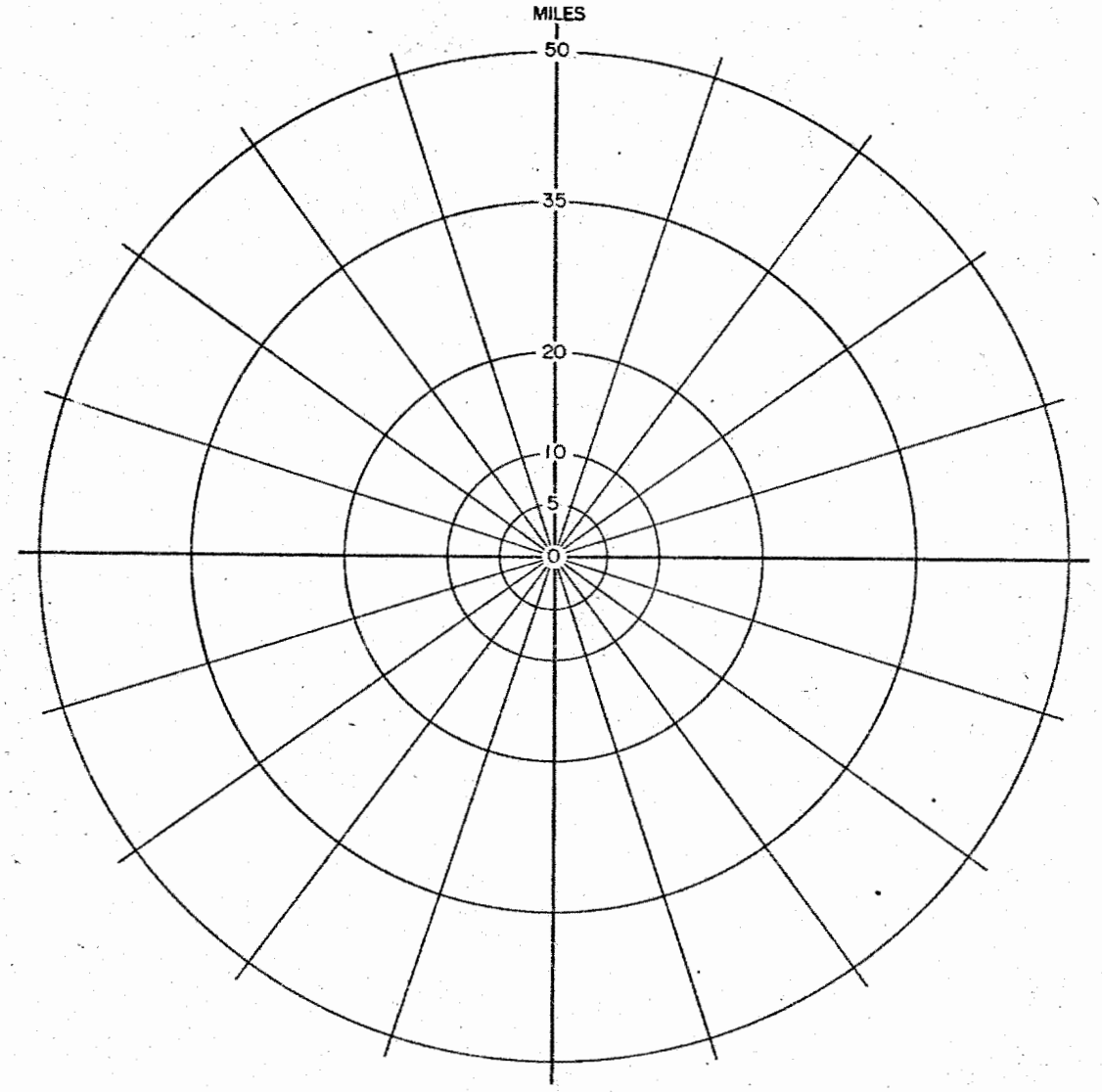

Figure 1
Basic Sampling Array Proposed for All Shots Except Echo where a Smaller Array was Planned for the Lower Yield Test

[redacted]

11

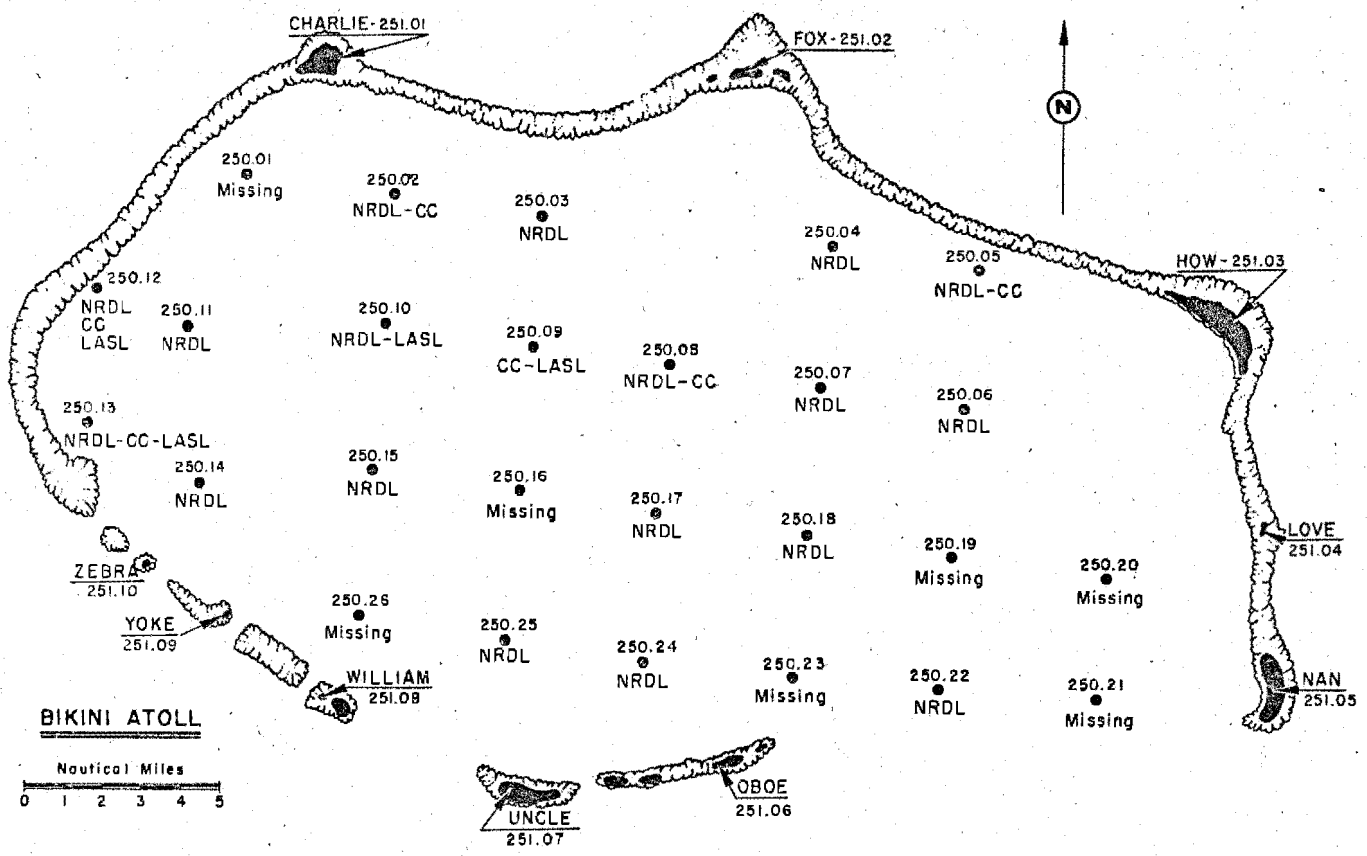

Figure 2
Lagoon and Island Station Array for Bikini Atoll

[redacted]

the shot point. The majority of these points were located at sea thus requiring floating stations. The island and lagoon stations were not located in conformity with this pattern. The land stations were placed on high, clear ground toward the center of the islands. The lagoon stations were located on a rectangular grid. Figure 2 shows these station locations at Bikini atoll.

Description of Stations

Three types of stations were used: land, lagoon and sea stations.

Most instrumentation at the land stations was placed in pits to shield it from blast. Total fall-out collectors and film badge dosimeters were used at all locations. Differential fall-out collectors for determining the time and rate of arrival of fall-out were located at most of the land stations. Radiation intensity recorders were located on two island stations, but only the one on station 251.03 collected useful data. Auxiliary equipment was used for starting and stopping the instruments and for furnishing power. Prototype collectors of several types were located at several island stations to test their value for use in future operations.

The lagoon stations consisted of moored rafts 7 ft. x 11 ft. Figure 3 shows one of these stations being lowered into the water. The instrumentation on these stations was similar to that at the island stations with the exception of the radiation intensity recorders. The sea stations were free-floating buoys as shown in Figure 4. They carried total collectors and film badge dosimeters. They were provided with radio transmitters for identification by the Security Force and to aid in locating them during the recovery operation.

Sample Collection from the Various Shots

Although plans had been developed for adequate sampling of each event, a number of unforeseen circumstances made it impossible to gather more than a small fraction of the data planned. Unforeseen delays in the shot schedule and the unexpectedly rough sea conditions were the primary hindrances. As a result, most of the free-floating buoys were lost without collecting data. Also, because of the severity of the blast from Shot 1, a number of lagoon stations capsized and a fire was started on Tare which destroyed a large part of the spare equipment needed for subsequent shots. Useful information was obtained from the island stations and the surviving lagoon stations. Measurement of the radiation levels and the fall-out which arrived on the atolls east of Bikini after Shot 1 provided valuable data to assess the downwind pattern of fall-out from super weapons detonated over land. Samples collected on the Project 6.4 YAG's were useful for determining the

[redacted]

[redacted] ATA

13

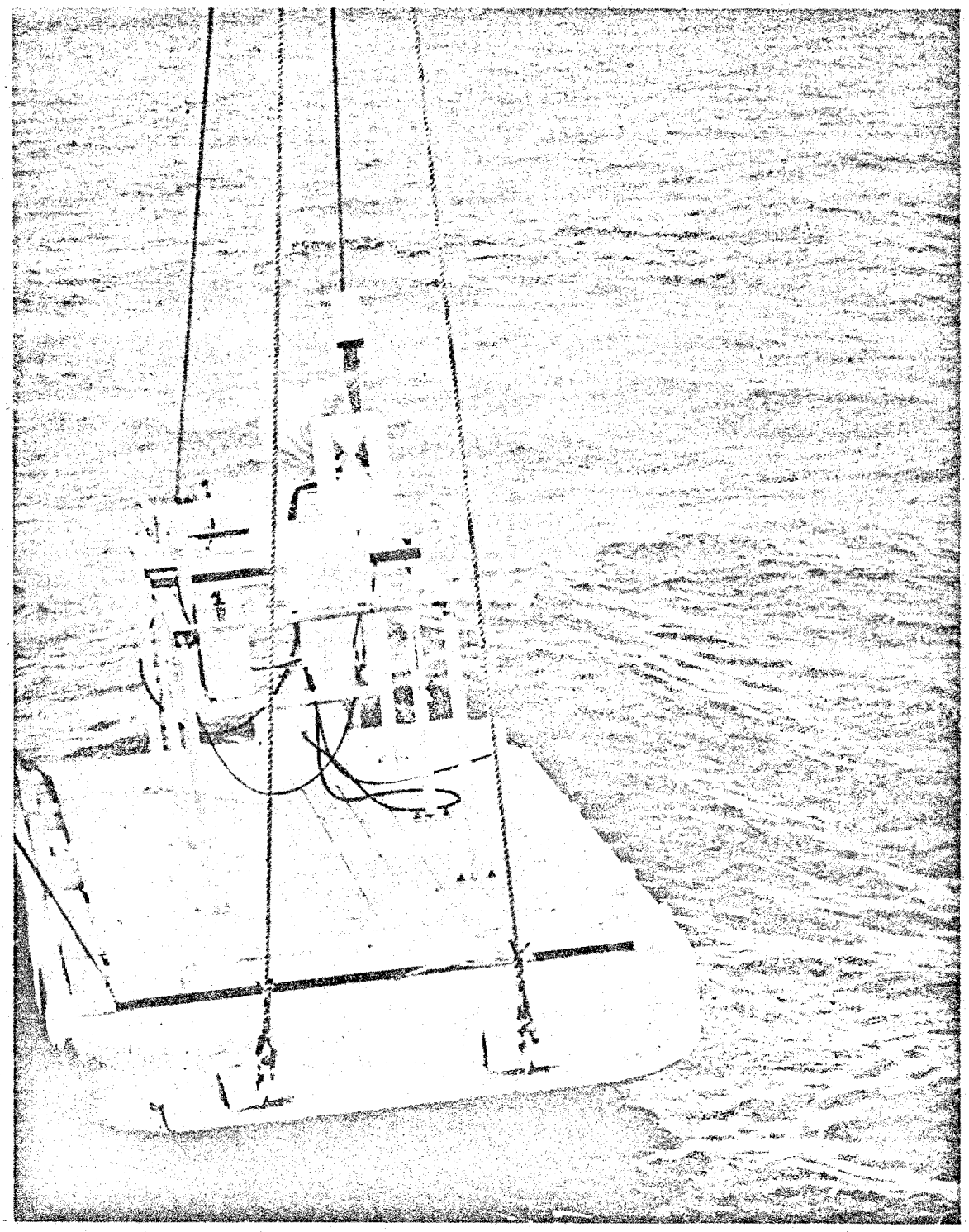

Figure 3
Lagoon Station Being Placed

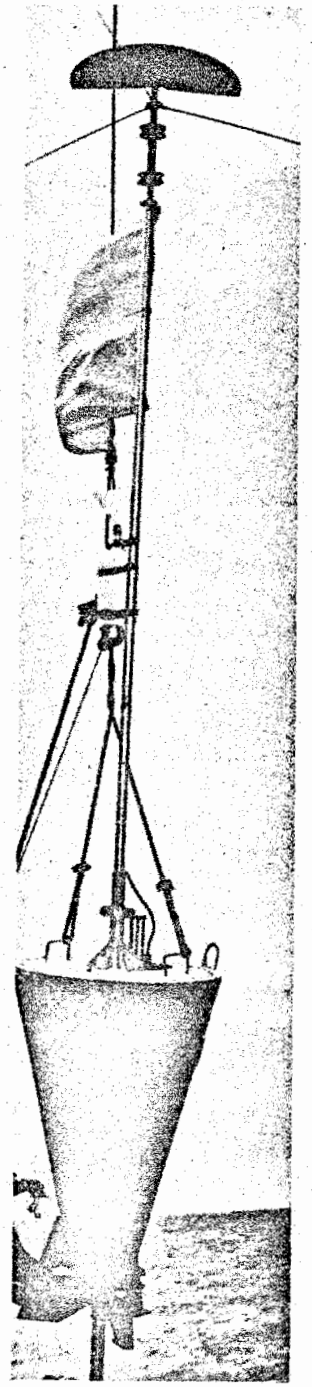

Figure 4
Free-Floating Sea Station being Launched

properties of the contaminant. On Shot 2, no fall-out arrived on the island or lagoon stations. The only samples collected were on the free-floating buoy stations. Figure 5 shows the locations of those stations which were recovered after that shot. It will be noted that the set and drift varied a great deal around the atoll. This made it difficult to determine where the buoys should be dropped in order for them to drift to the correct location at shot time. Collections were made from lagoon and island stations for Shots 3, 4 and 6. Water sampling on Shots 5 and 6 supplemented this data. This operation will be discussed by Dr. Folsom and Dr. Werner.

Instrumentation

Two types of total collectors were used. One was a polyethylene bottle with a 7-in. diameter funnel as shown in Figure 6; the other was a piece of gummed paper about a foot square placed in a horizontal position. The differential fall-out collector, shown in Figure 7, collected the samples in a number of small polyethylene jars through openings in a belt that was drawn over the jars. The film badge packs were supplied by Project 2.1. The radiation intensity recorder was of the same type as that used on the YAG's by Project 6.4.

Evaluation of Sampling Methods

In the past, it had been assumed that the material which fell on a collecting surface of a collector was representative of what would have fallen on the same area had the collector not been there. At CASTLE, this assumption was tested.

The precision which could be expected from collections over very limited areas was tested by comparing the quantities collected in total fall-out collectors located adjacent to each other and on the circumference of a circle of 50-ft. radius. These tests showed that with either type of total collector, the largest variation between them was less than a factor of two and most values were within $\pm$ 25% of the mean.

An attempt was made to assess the accuracy of the collections by plotting the radiation field readings against the gamma activity of the material collected at stations located various distances from the shot point. These results shown in Figures 8 and 9 indicate that the collections on the gummed paper are proportional to the field readings while the efficiency of the bottle and funnel collector varies considerably with distance from the shot point.

Because of the uncertainty of the efficiencies of various types of collectors, more extensive tests of this type are being planned for Operation TEAPOT. The accuracy and precision of several sampling methods at various locations around the shot point will be evaluated.

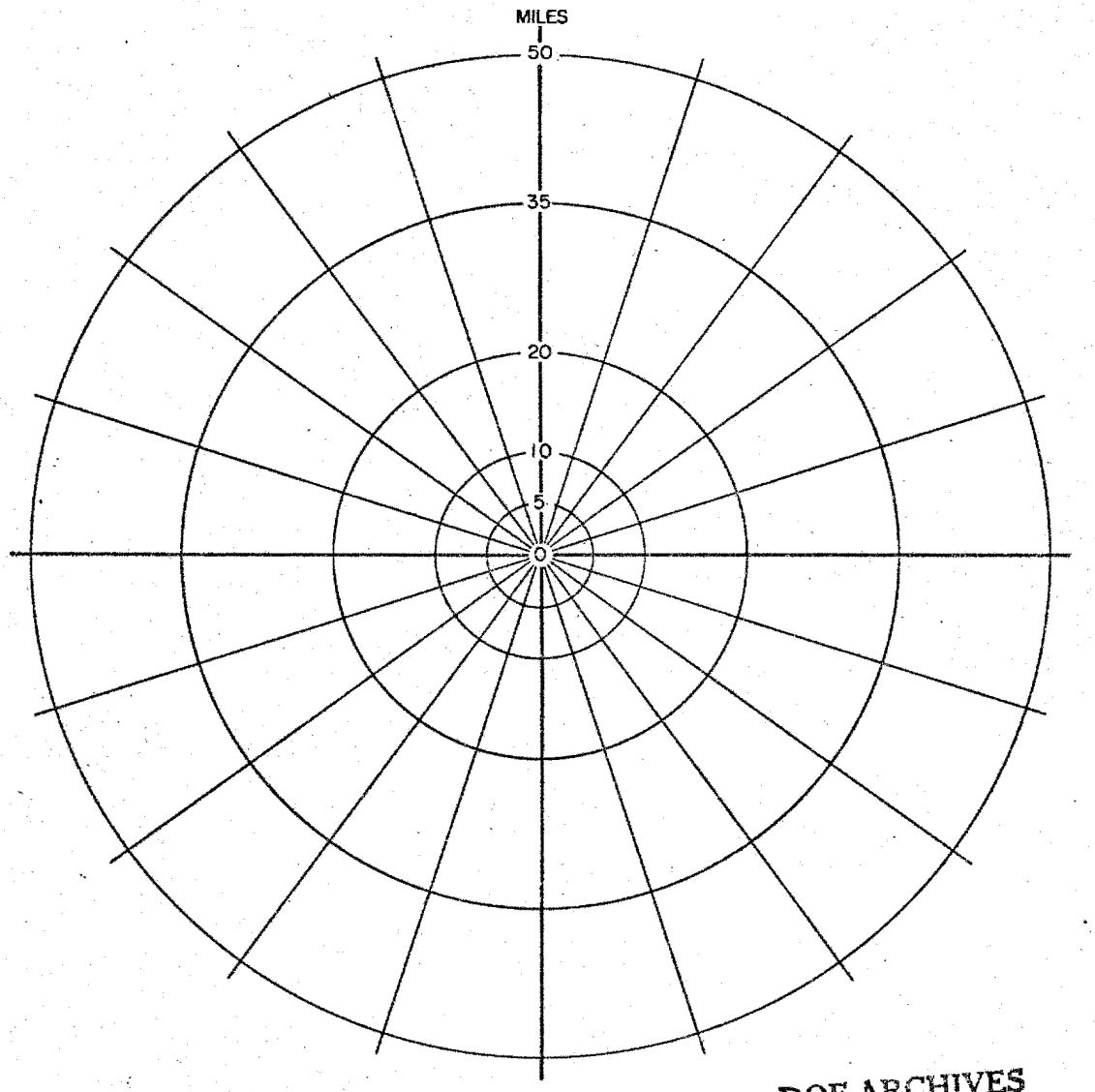

Figure 5
Shot 2, Sea Station Array

17

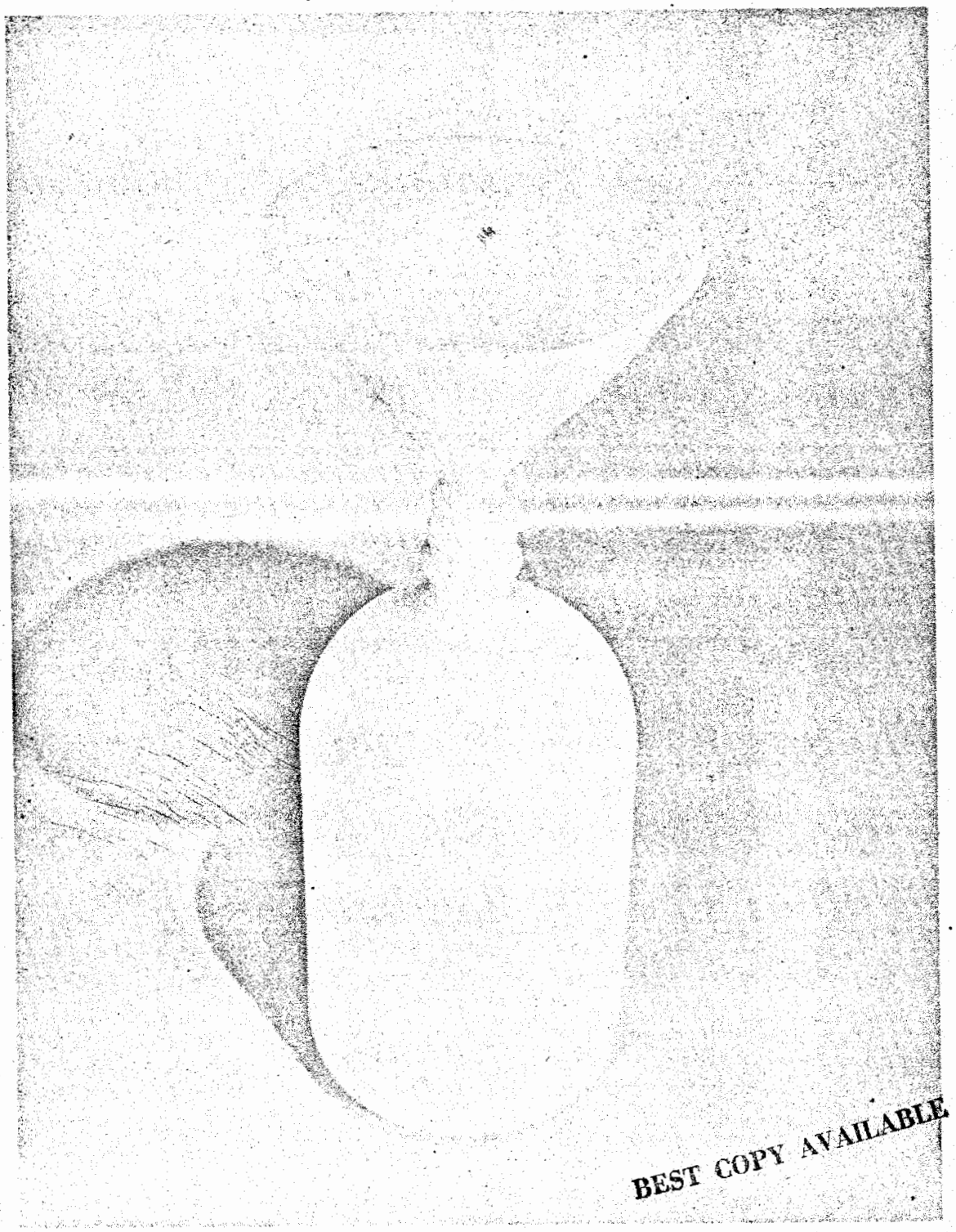

Figure 6
Total Collectors

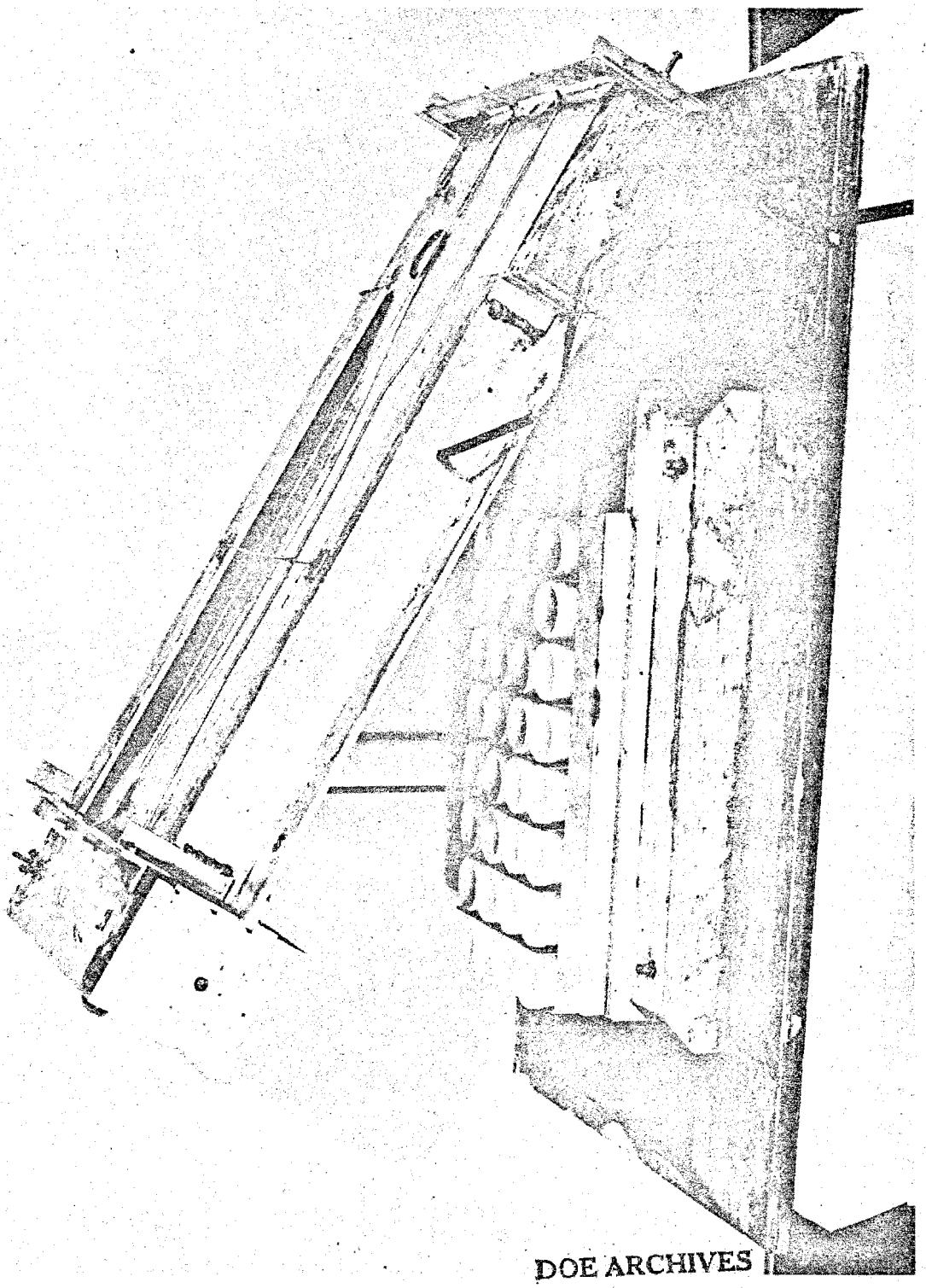

Figure 7
Differential Fall-out Collector

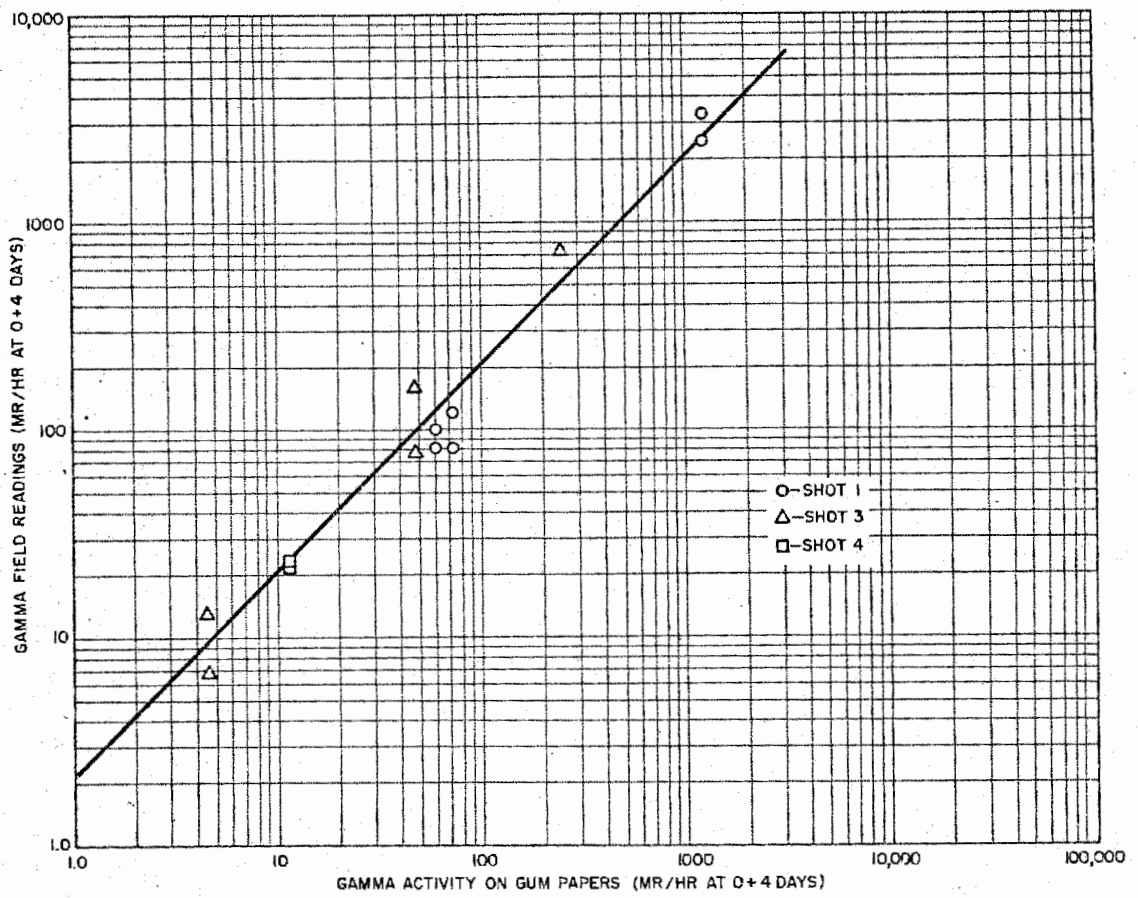

Figure 8
Ratio of Gamma Infinite Field Measurements to Equivalent Gamma Measurements from the Gummed Paper Collector (mr/hr at 0+4 days)

[redacted]

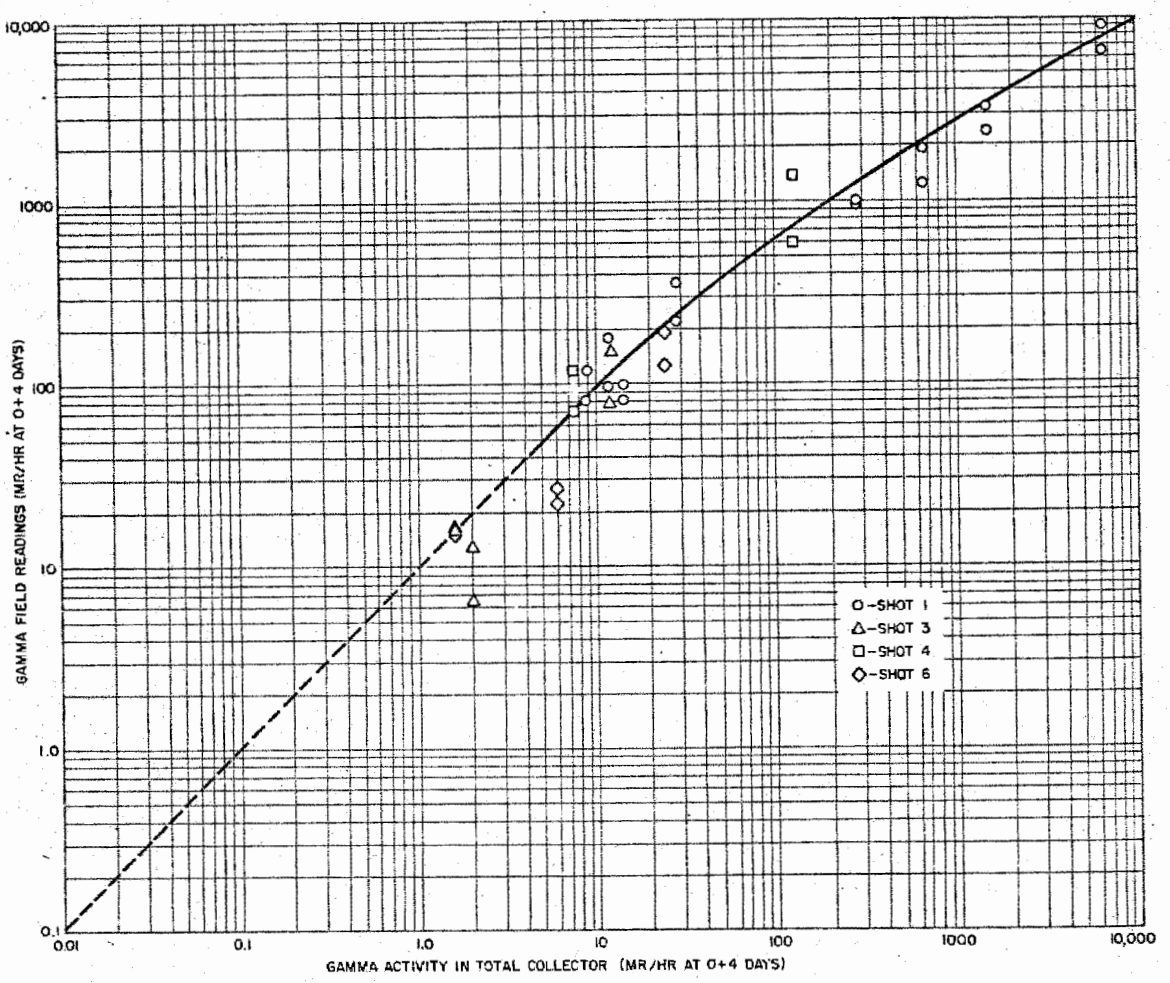

Figure 9
Ratio of Gamma Infinite Field Measurements to Equivalent Gamma Measurements From the Total Collector (mr/hr at 0+4 days)

[redacted]

Collection and Treatment of Samples

Samples were collected by the field teams and taken to the mobile laboratory on Elmer. The approximate radiation level of each sample was determined with a survey meter. Aliquots of some samples were taken for further measurements at the site. The samples were then packaged and shipped to the Zl for further analyses.

The measurements made at the site were limited to those which needed to be made at early times after the detonation. Gross decay measurements were started. Aluminum and lead absorption curves and gamma spectrometry measurements were made at several times starting as soon as the samples could be prepared. Analyses were performed to determine the contributions of several short-lived radionuclides including those formed by neutron reactions in the bomb components and environmental substances.

The portion of the radioactivity associated with the solid, ionic and colloidal phases was determined in the forward area after separating the phases by centrifugation and ultrafiltration. Special ion-exchange methods were developed to aid in some of the radionuclide separations. It was planned to make these measurements and determinations of some short-lived radionuclides at very early times after detonation. This was not possible because of the difficulties in collecting and transporting samples to the field laboratory.

At USNRDL, the gross decay and absorption and spectral measurements were continued. The details of these measurements will be discussed by Dr. Ballou and Dr. Cook. Also, the physical, chemical and radiochemical properties of the contaminant were studied further. The gross chemical composition was determined by spectrographic, spectrochemical and other analytical methods. Radiochemical analyses for selected species were carried out. The physical measurements included particle size and density determinations, X-ray diffraction measurements and petrographic studies.

Summary of Results

Because results of these studies will be discussed in detail by other participants of this symposium, only a summary will be given here.

Close-in Fall-out Patterns

The fall-out patterns in the lagoon area were well documented for most of the shots. Samples from island and lagoon stations and radiation measurements on the islands furnished enough data to draw reliable contour lines. The patterns for Shots 1, 3, 4 and 6 are shown in Figures 10 through 13. Figure 14 shows estimated contours for Shot 2. These are based on the activity levels of the samples collected on the free-

[redacted]

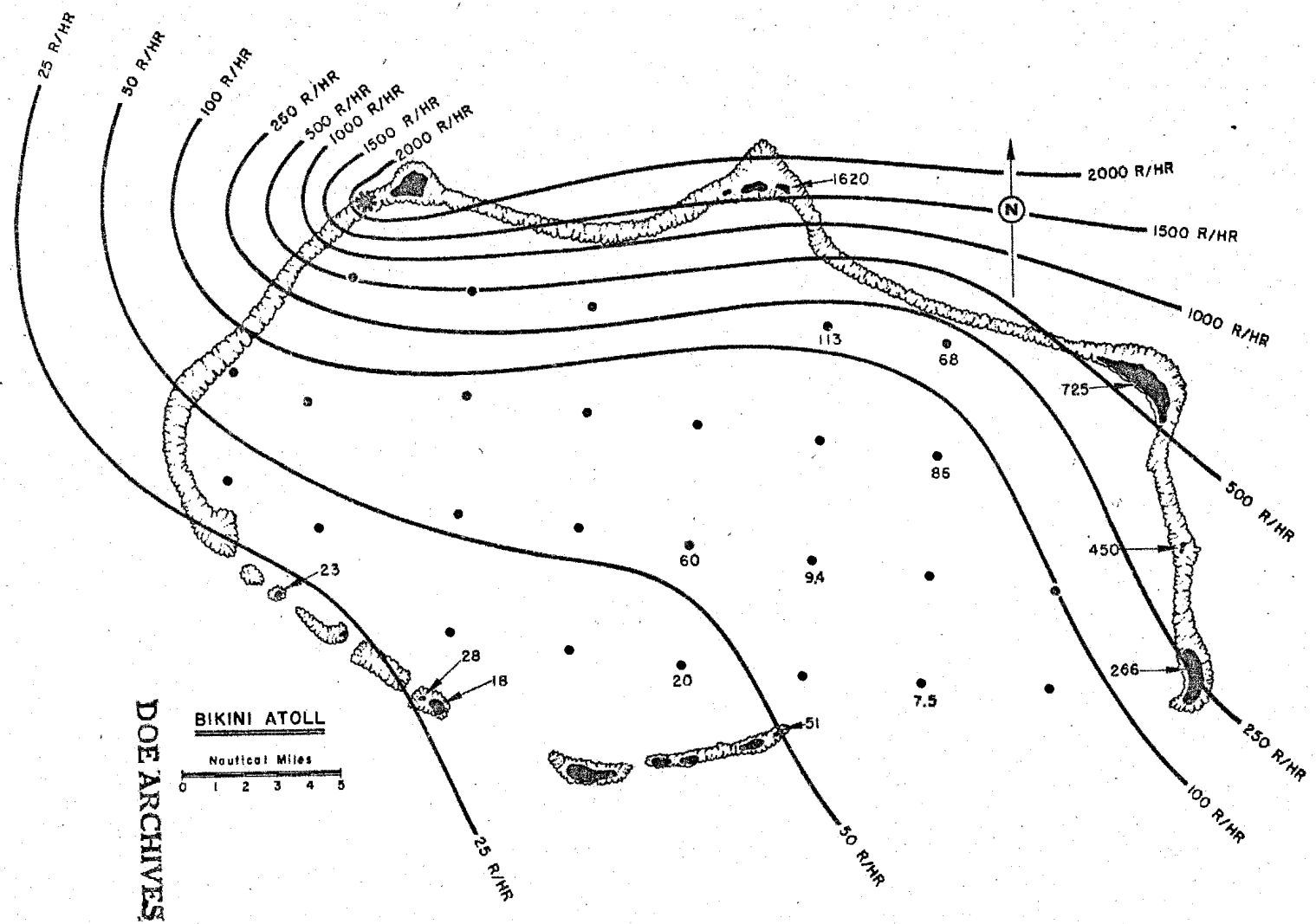

Figure 10
Shot 1, Close-in Gamma Fall-out Pattern (r/hr at 1 hr)

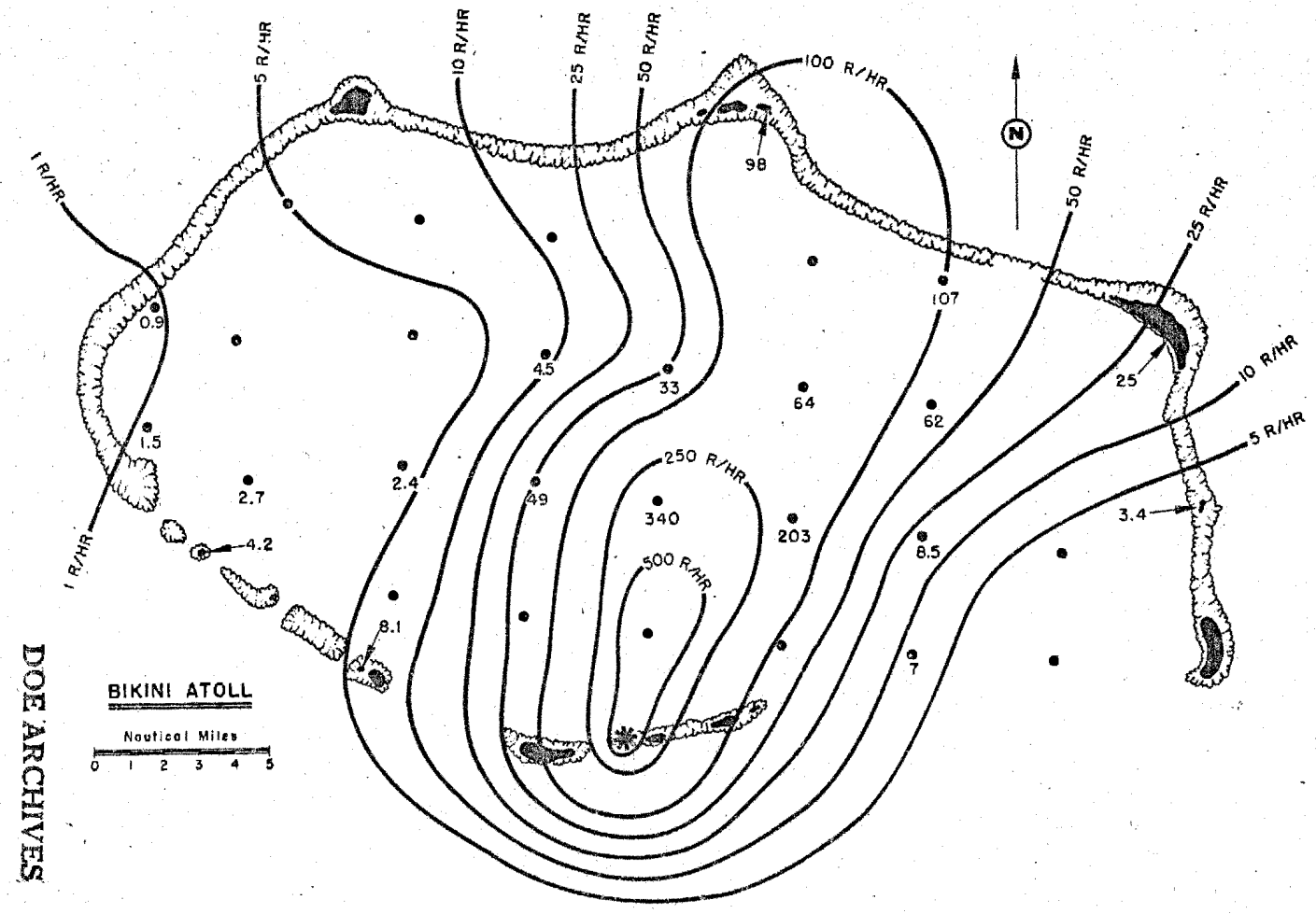

Figure 11
Shot 3, Close-in Gamma Fall-out Pattern (r/hr at 1 hr)

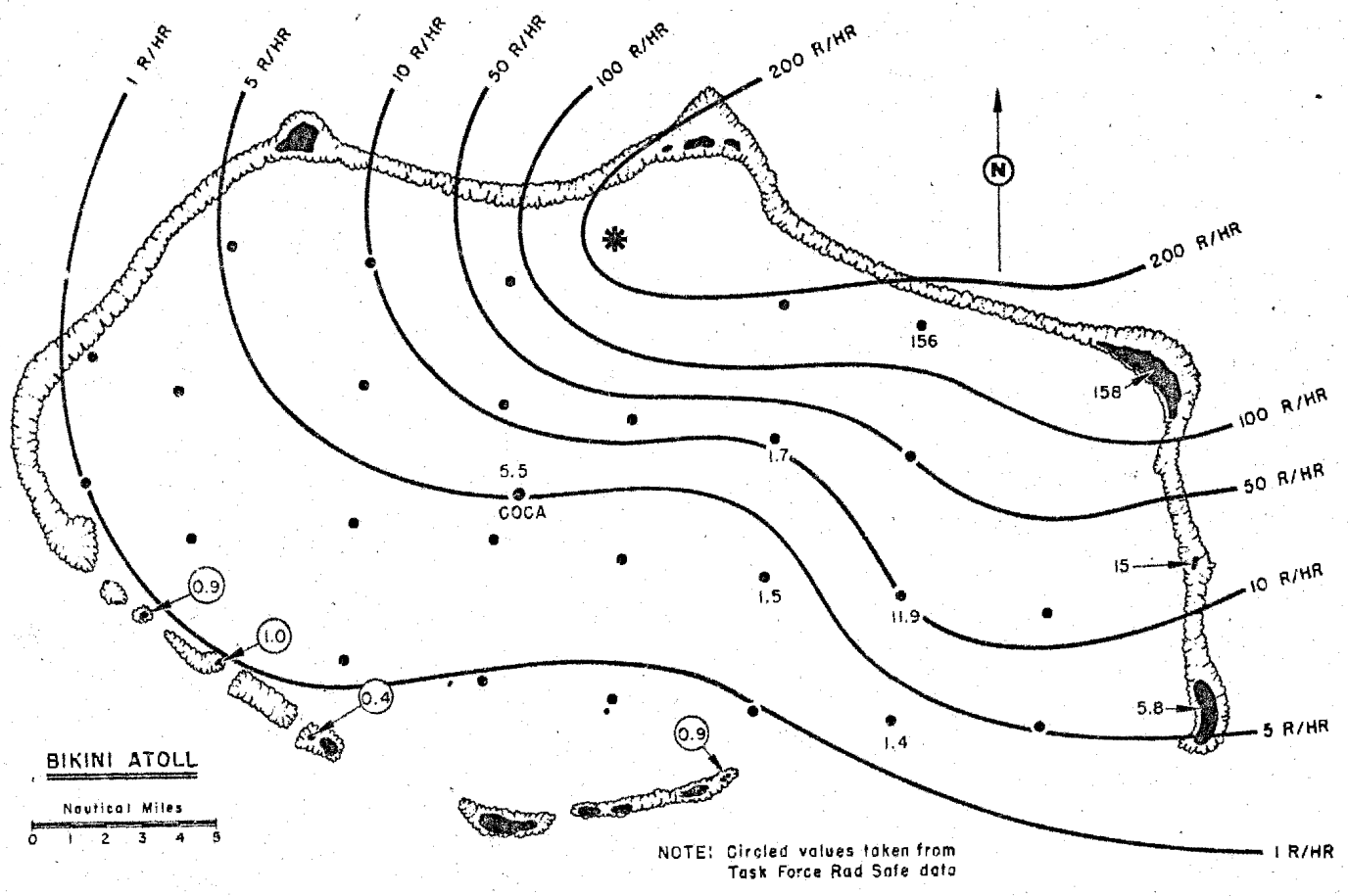

Figure 12
Shot 4, Close-in Gamma Fall-out (r/hr at 1 hr)

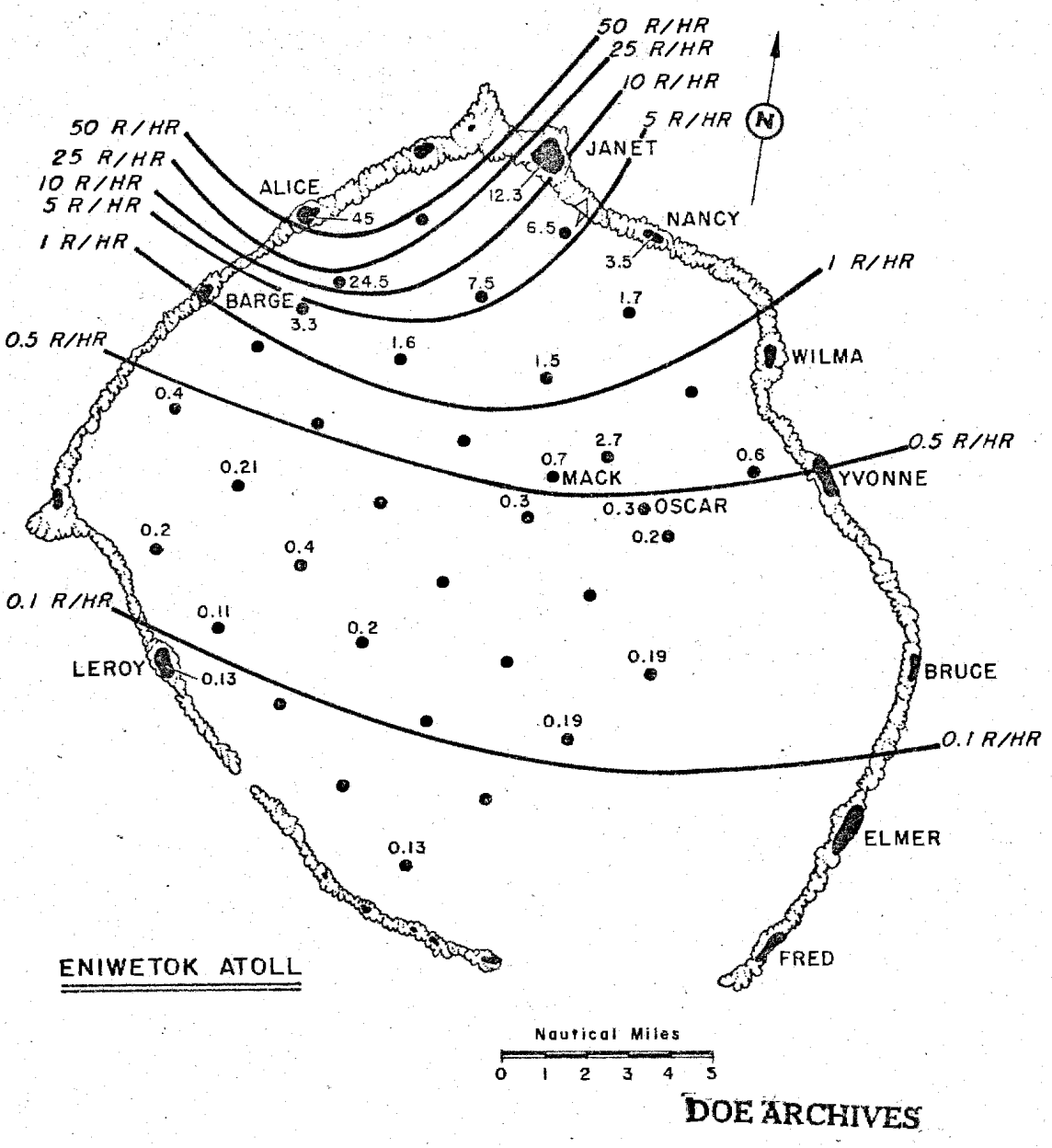

Figure 13
Shot 6, Close-in Gamma Fall-out Pattern (r/hr at 1 hr)

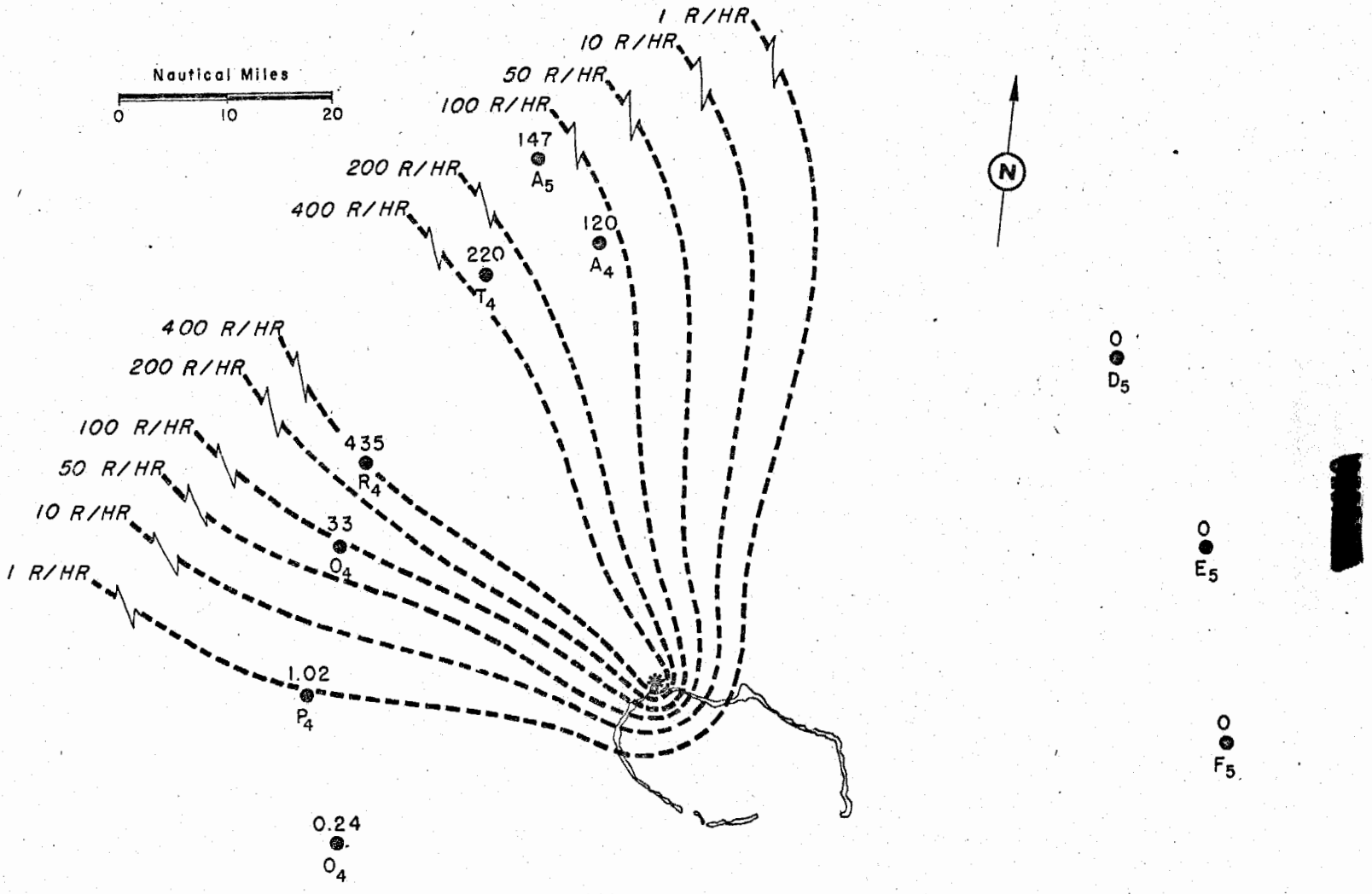

Figure 14
Shot 2, Fall-out Pattern (r/hr at 1 hr)

27

[redacted]

floating buoy stations. No fall-out arrived at the Project 2.5a island or lagoon stations following this shot.

Physical Characteristics of the Fall-out

The nature of the fall-out was determined by the point of detonation and the weapon yield. Figure 15 shows a gummed paper collector from one of the lagoon stations covered with fall-out from Shot 1. This fall-out consisted largely of coral-like material, a majority of which was of large particle size. The ratio of radioactivity/mass of the particles varied considerably. No correlation was found between this ratio and the particle size. Many of the particles were fragile and could not be sieved without breaking them; therefore, the determinations of activity/unit mass of the various sized particles would not be representative of the actual fall-out. The microscopic studies of individual large particles showed that they varied considerably both as to composition and radioactivity.

The nature of the particles from the barge shots is uncertain. No visible bomb debris was collected in the total collectors. Filter samples and their radioautographs were studied microscopically. There were some small droplets observed, but it is uncertain whether these were fall-out or originated from ocean spray. Most of the particles were too small to be observed through the optical microscope, but their presence was shown by radioautography. The radioactivity in the samples from the total collectors which had collected rain after the fall-out period was found to be largely in the liquid phase. These observations as well as the contamination behavior of this fall-out as reported by Projects 6.4 and 6.5 indicate that it consisted largely of extremely fine aerosols containing the bomb debris and substances derived from sea water with a very limited amount of coral constituents.

Particle Size Distribution

The particle size distribution was determined by carefully mounting the fall-out samples from the differential samplers on transparent backing material and measuring them by observation through a microscope with an ocular micrometer. A radioautograph of the mounted particles was made on stripping film mounted over the backing. This was developed in place and thus permitted the identification of the radioactive particles. Nearly 7000 radioactive particles from Shot 1 were measured. Figure 16 shows the distribution of all of these particles. The distribution of the fall-out collected on several of the atoll islands east of Bikini is shown in Figure 17. The application of this information for estimating the fall-out distribution will be discussed by Mr. Schuert.

[redacted]

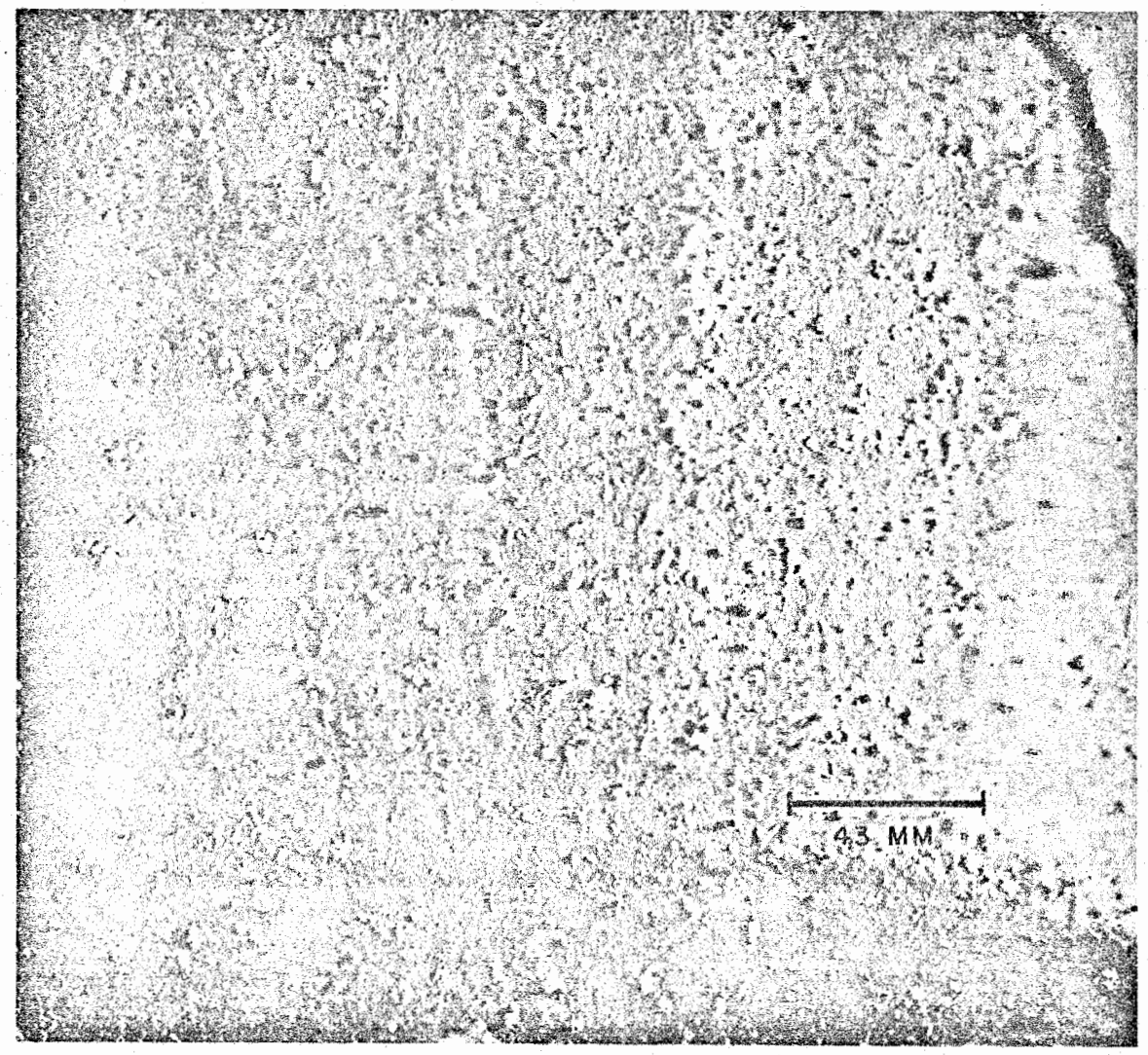

Figure 15
Shot 1, Fall-out Particulate, Station 250.04

[redacted]

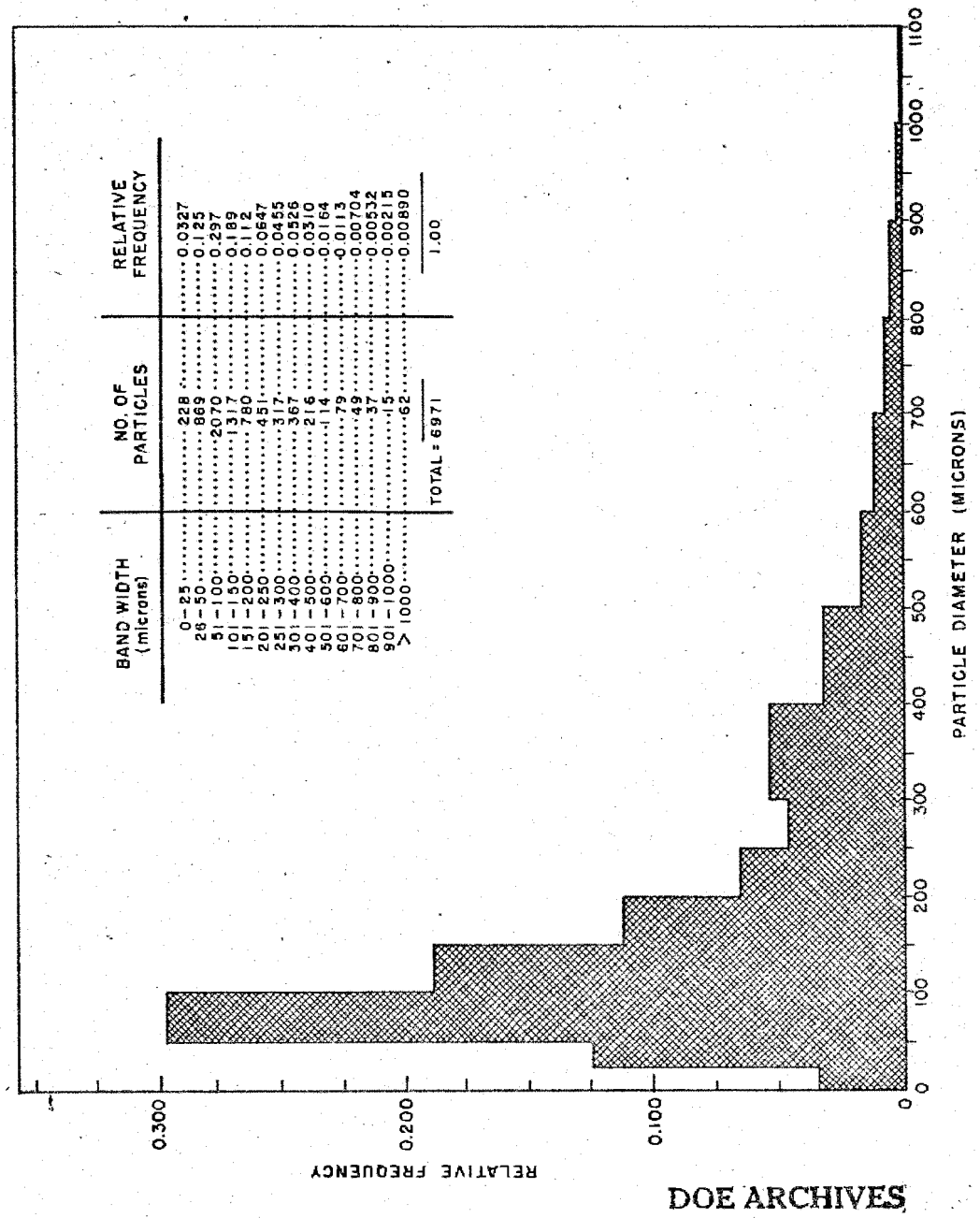

Figure 16
Shot 1, Composite Particle Size Distribution

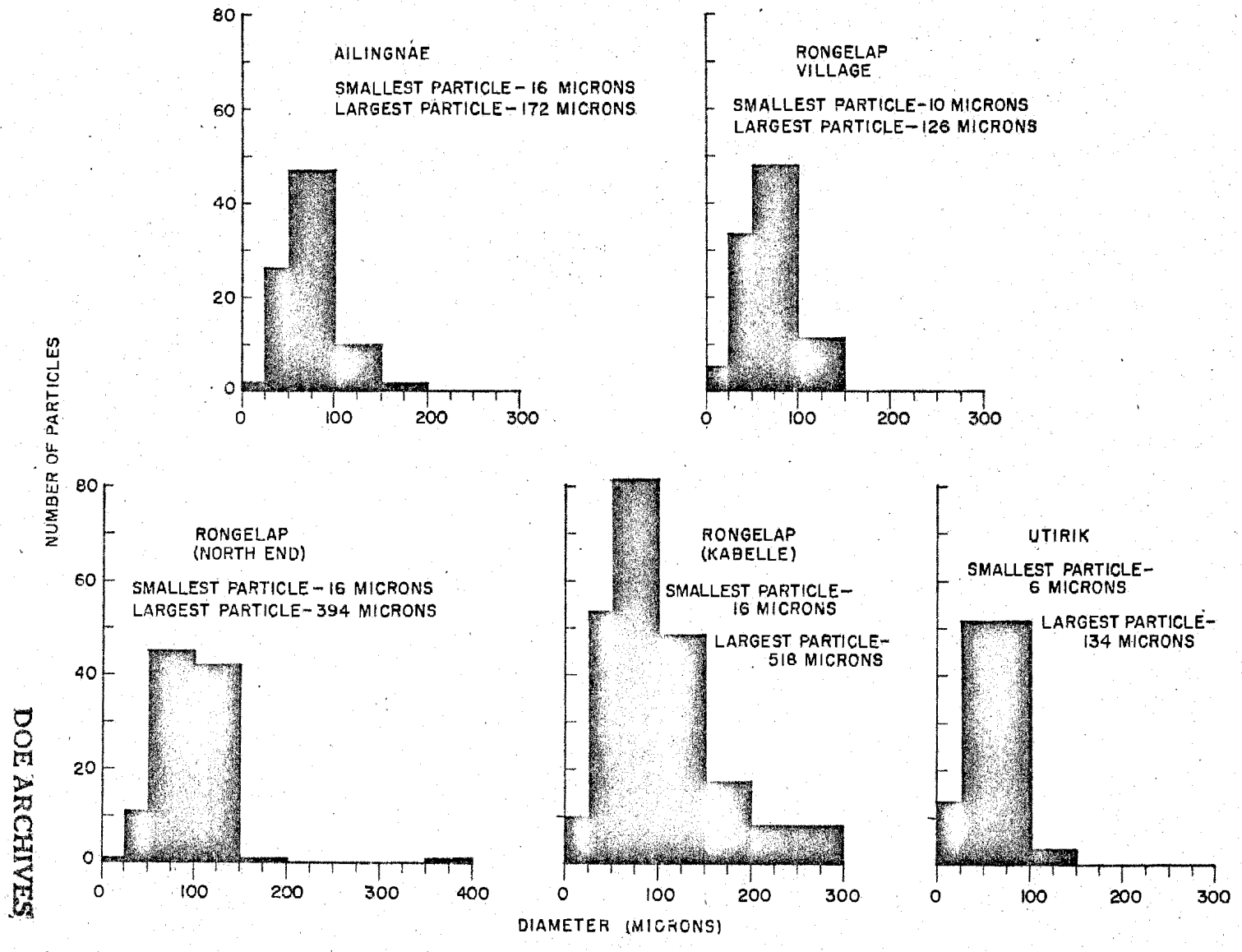

Figure 17
Shot 1, Outer Atoll Particle Size Distribution

[redacted]

Integrated Dosage at an Island Station

The data from the time-intensity recorder located at station 251.03, plotted as total dose vs. time is shown in Figure 18. This station lay in the heavily contaminated, downwind area. It may be seen from this graph that anyone caught in the open on this island would have received a lethal dosage of radiation by 4 to 5 hours after the detonation.

Chemical and Radiochemical Properties of the Fall-out

These properties of the contaminant will be discussed by Dr. Miller and Dr. Ballou. It may be interesting here to note briefly a few results obtained in the forward area by an ion-exchange procedure developed there. Early analyses of Shot 1 fall-out for Na^{24} by standard radiochemical procedures had failed to give conclusive results because of the difficulty of purifying the sodium fraction. To eliminate this difficulty, a preliminary purification step was introduced. This consisted of passing the dissolved fall-out through a cation exchange column, washing the column with water and then eluting the alkali metal ions with dilute HCl. This fraction was then analyzed for Na^{24} in the usual manner.

The elution curve of the radionuclides as measured by a recording rate meter for one of these experiments is shown in Figure 19. Attempts were made to identify the species in some of the other fractions as well as to ascertain the purity of the alkali metal fraction. Decay data and gamma spectra measurements led to the identification of the constituents in some of these fractions. The details of these analyses will be found in the final report of Project 2.6a.

Summary

From this and subsequent presentations, it will be seen that a great deal of information useful in fulfilling the objectives of these projects was obtained. However, much remains to be done. The nature of the contaminant from surface land shots of super weapons over coral is well defined. More information is needed regarding its distribution. The chemical and radiochemical properties of the fall-out from surface water shots was determined. More information is needed concerning the physical characteristics and distribution of fall-out from this type of detonation. While the size and shape of the clouds have been determined photographically, the distribution of radioactivity and mass within their boundaries are entirely unknown.

Information is also needed regarding the properties of the contaminants and their distributions from weapons of different yields in other environments. Of particular importance for the weapon effects program are detonations in clay soil and in shallow harbors of weapons of several yields.

[redacted]

[redacted]

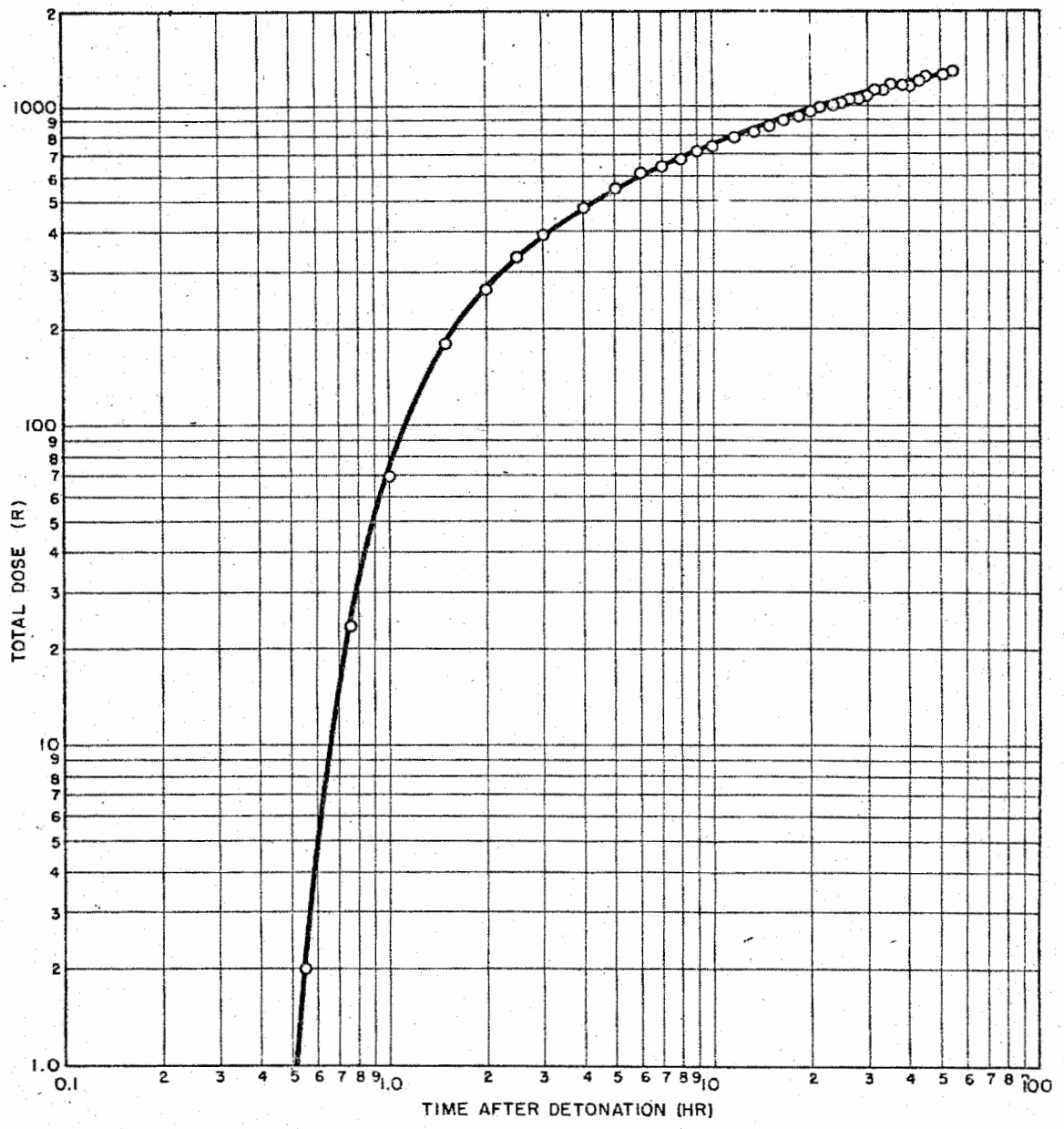

Figure 18
Shot 1, Integrated Gamma Dose, Station 251.03

[redacted]

[redacted]

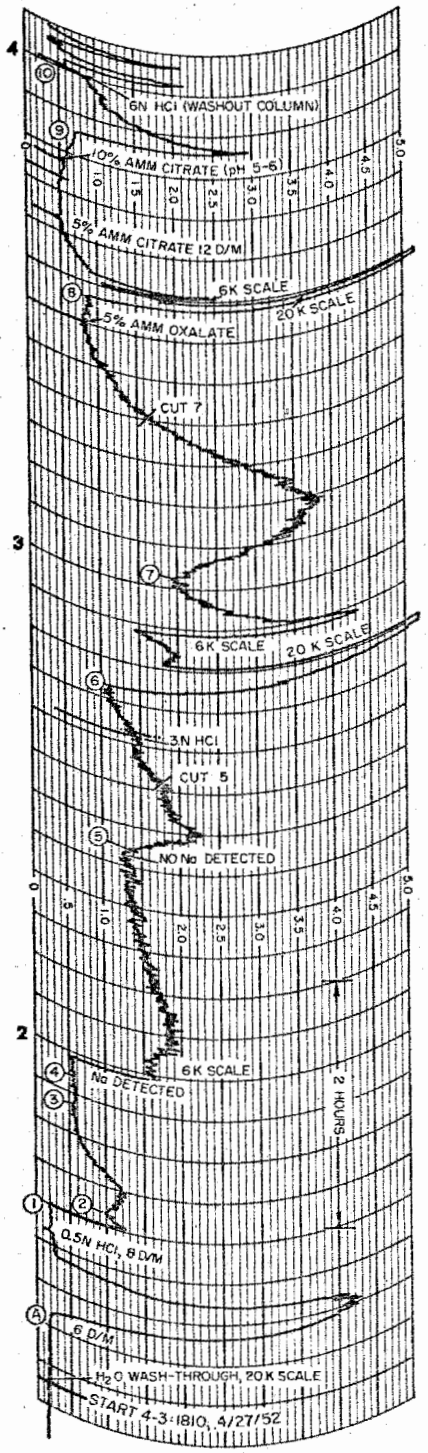

Figure 19
Facsimile of Chromatogram Taken From the Esterline-Angus Recorder

[redacted]

PROJECT 2.5b AND 2.6b RESULTS, OPERATION CASTLE

Dr. Benjamin Barnett
Chemical and Radiological Laboratories

Introduction

The objectives of Project 2.5b and 2.6b were to document the fall-out and to determine the properties of the material.

The data were used to evaluate the contamination hazard, and to arrive at some conception of how active particles form in the fireball.

Apparatus

To carry out these objectives two types of samplers were used. The first is shown in figure 1. This is the CmlC differential sampler. The top only is illustrated and the cover, which can be opened at any desired time after blast, is shown exposing the opening through which the fall-out enters the collecting, wedge-shaped segments, which are shown in figure 2. There are 24 of these sections on a tray, and the tray is rotated so as to expose each section for the required times.

Since samples free of aqueous fall-out were required for some of the work, a new type of sampler shown in figure 3, was devised. This consisted of a cone containing a mixture of carbon tetrachloride and chlorobenzene (together with a little aerosol OT to reduce the surface tension). Fall-out arriving at the surface was rapidly separated into an aqueous phase which remained on top, and the solid material which settled out.

Operations

These instruments were set out at the positions shown in figure 4. The squares show where both types of samplers were located, and the circles where only the CmlC differential samplers were placed.

We also had samplers on rafts at the Bikini stations, but almost all of these were lost owing to high seas, so that our projected work on base surge could not be carried out.

Results

It seems probable that most of the activities measured came from the column, rather than the cloud, so that especially for the larger shots early arrival of fall-out was to be anticipated.

[redacted]

[redacted]

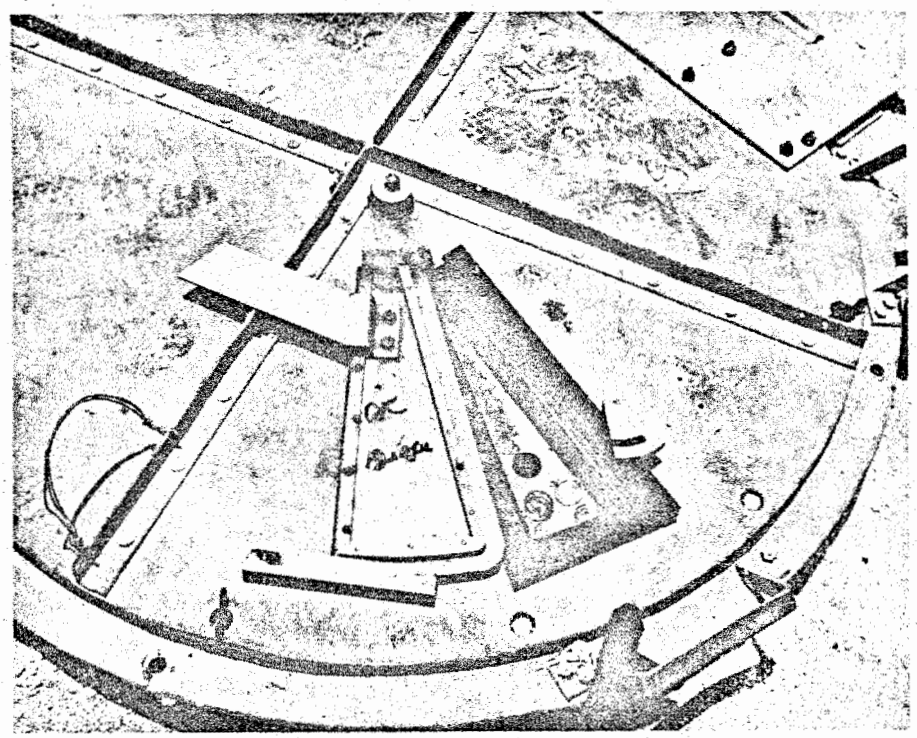

Figure 1
Top of Chemical Corps Differential Sampler

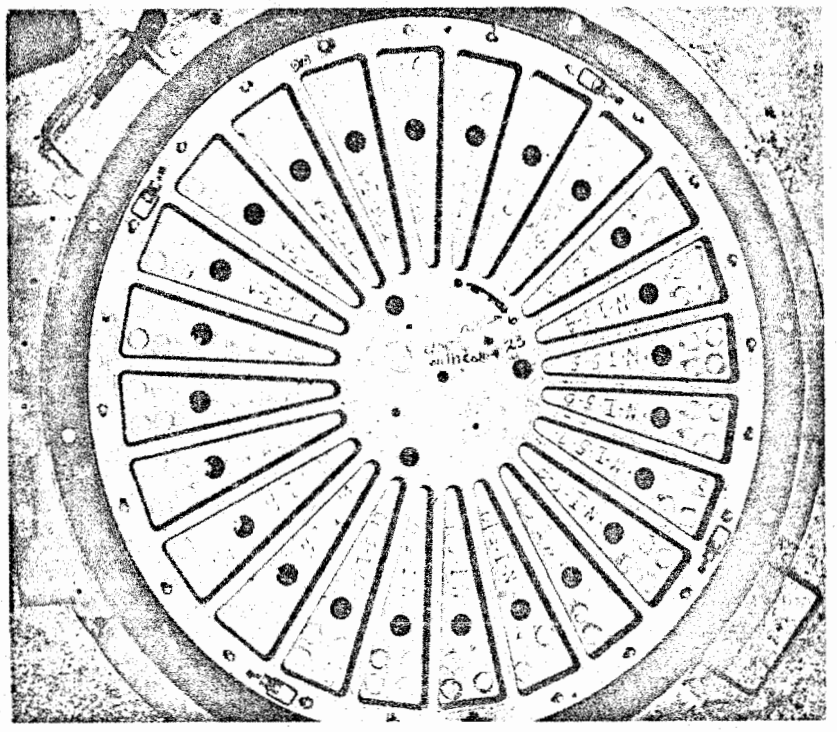

Figure 2
Wedge-Shaped Sampling Sections of Chemical Corps Sampler

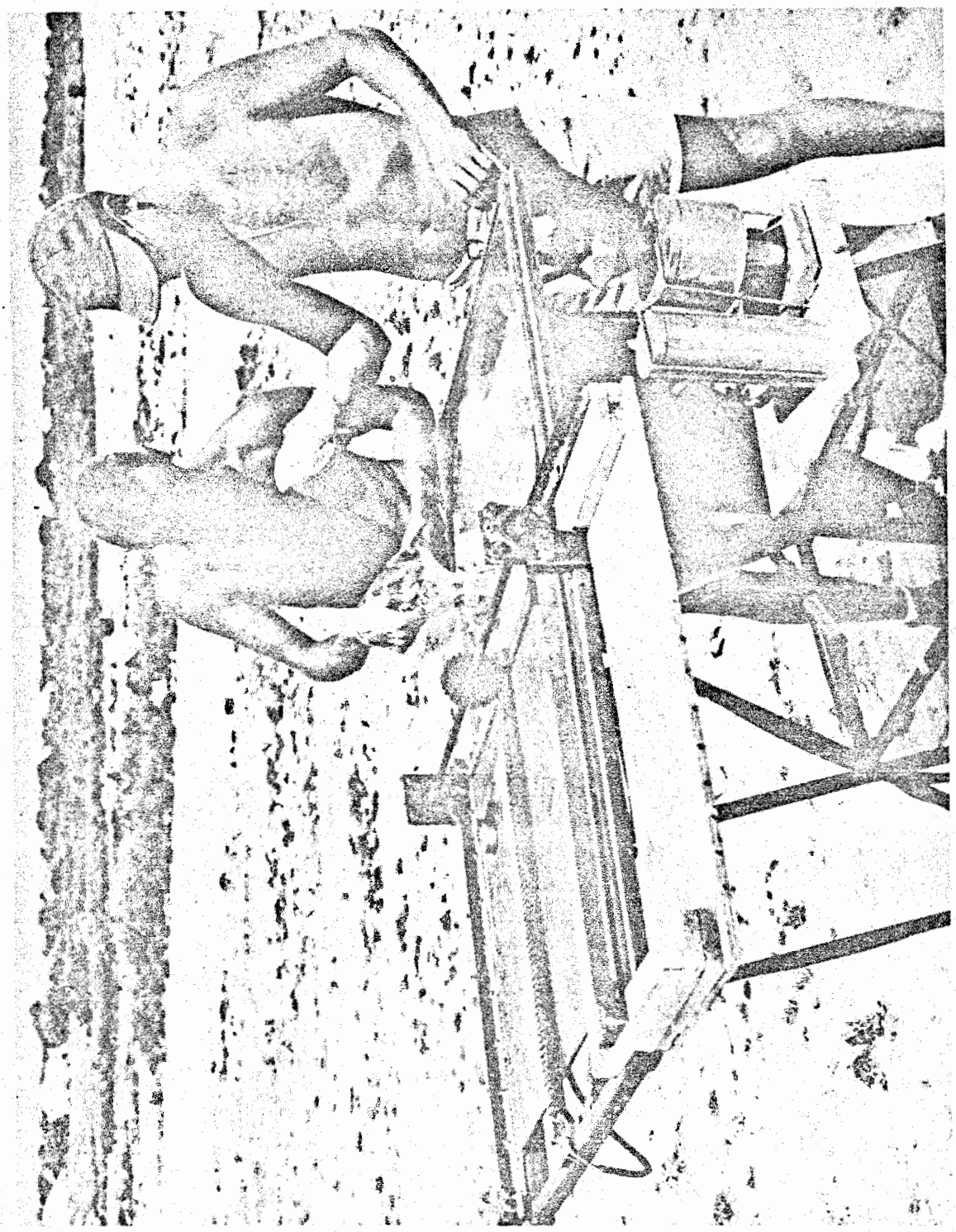

Figure 3
New Cone Sampler

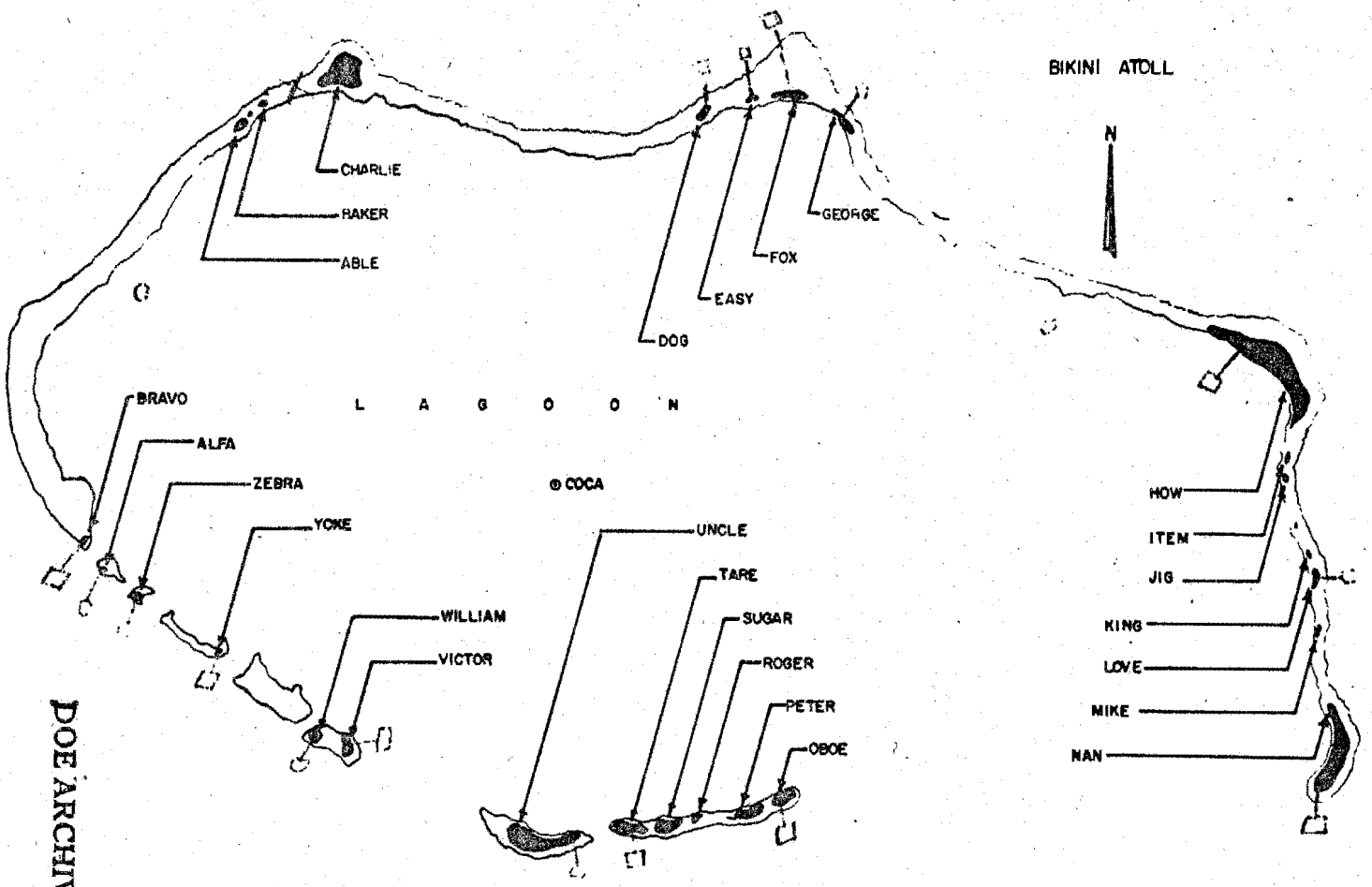

Figure 4
Sampling Stations

[redacted]

The collector located at Nan, 23 miles from ground zero, indicated that radioactive material arrived during the first six minutes sampling interval following the Bravo detonation.

In the case of the Union shot the highest activity arrived within two minutes after shot within two miles west from ground zero, whereas at stations 14 miles north fall-out arrived between $\frac{1}{2}$ hour to $1\frac{1}{2}$ hours after shot.

In the case of the Bravo [redacted] device the maximum activity generally arrived during the first hour after burst.

For this case the maximum β -field strength was 62c/ft^2. The strength of the field fell off very rapidly, as is shown in figure 5, despite the fact that fall-out continued to arrive all along this curve. This shows how rapidly the actual β - hazard falls off, despite the arrival of further fall-out.

Figure 6 shows isodose lines, plotted from Rad-Safe data, for gamma radiation, for the Bravo shot. The maximum dose rate at M+6 hour was 340 r/hr at Able Island. Ground zero was on the reef off Charlie Island.

A similar plot is shown in figure 7 for the third shot. The maximum dose rate was 50 r/hr at Uncle Island, and the total dose for infinite stay time was 1450 r. Ground zero was on Tare Island.

Active fall-out from surface shots of the Bravo type can give rise to illness and even death at distances far beyond those where blast and thermal effects are hazardous.

It seems also that because of the high proportion of activity in small particles, an inhalation hazard may exist for shots of this type. Figure 8 shows a plot of the total activity against particle size for a typical sample of Bravo fall-out. For all particles up to 10 μ the activity amounts to as much as 15% of the total. The active particles amounted to 43% of the total particles. This evidence that activity continued down to small particles led to a study of activity as a function of particle size.

A more intimate study of the activities of these active particles was made based on the relation

$$A^o = kd^m \qquad (4.1)$$

[redacted]

[redacted]

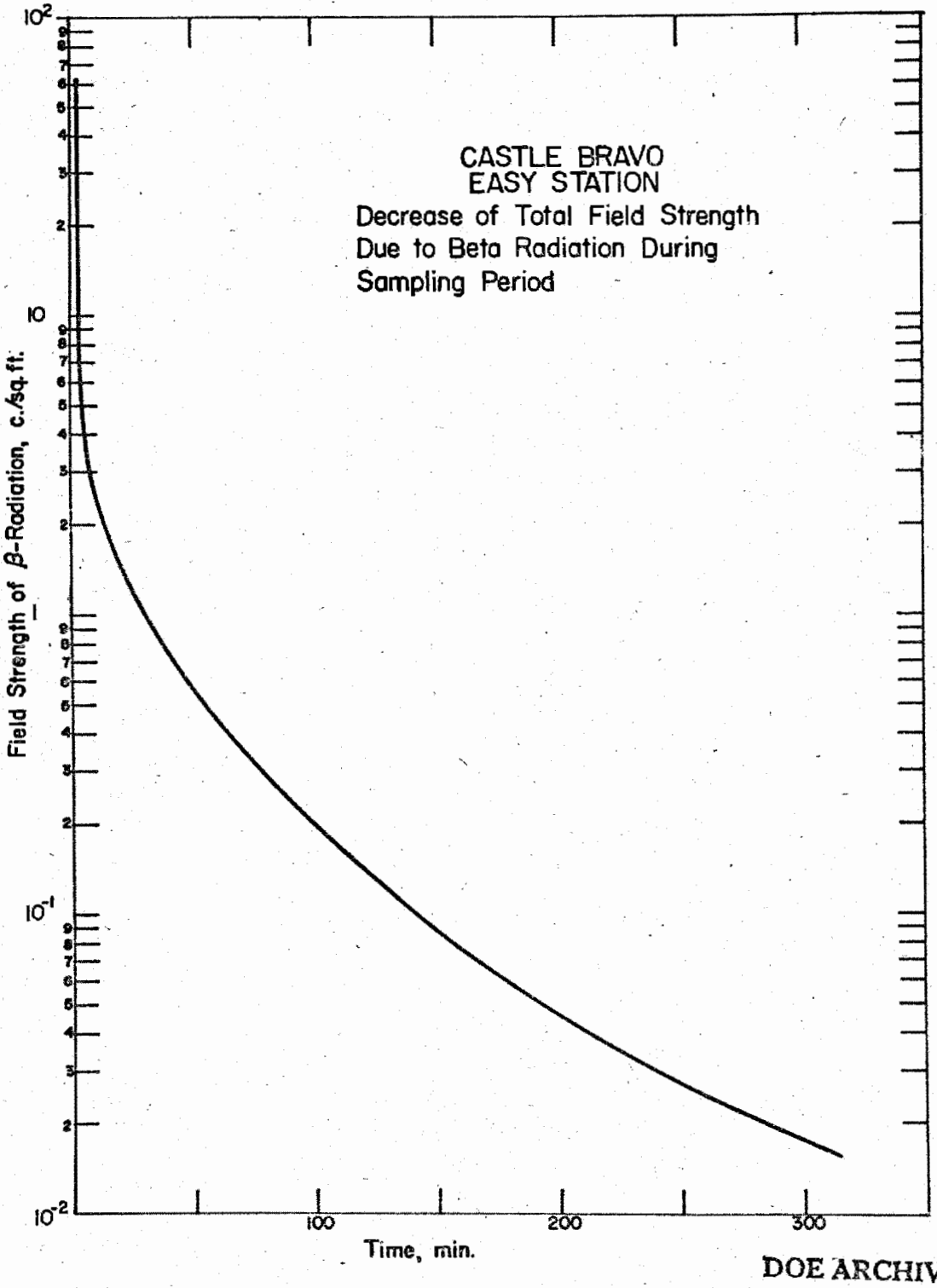

Figure 5

[redacted]

4D

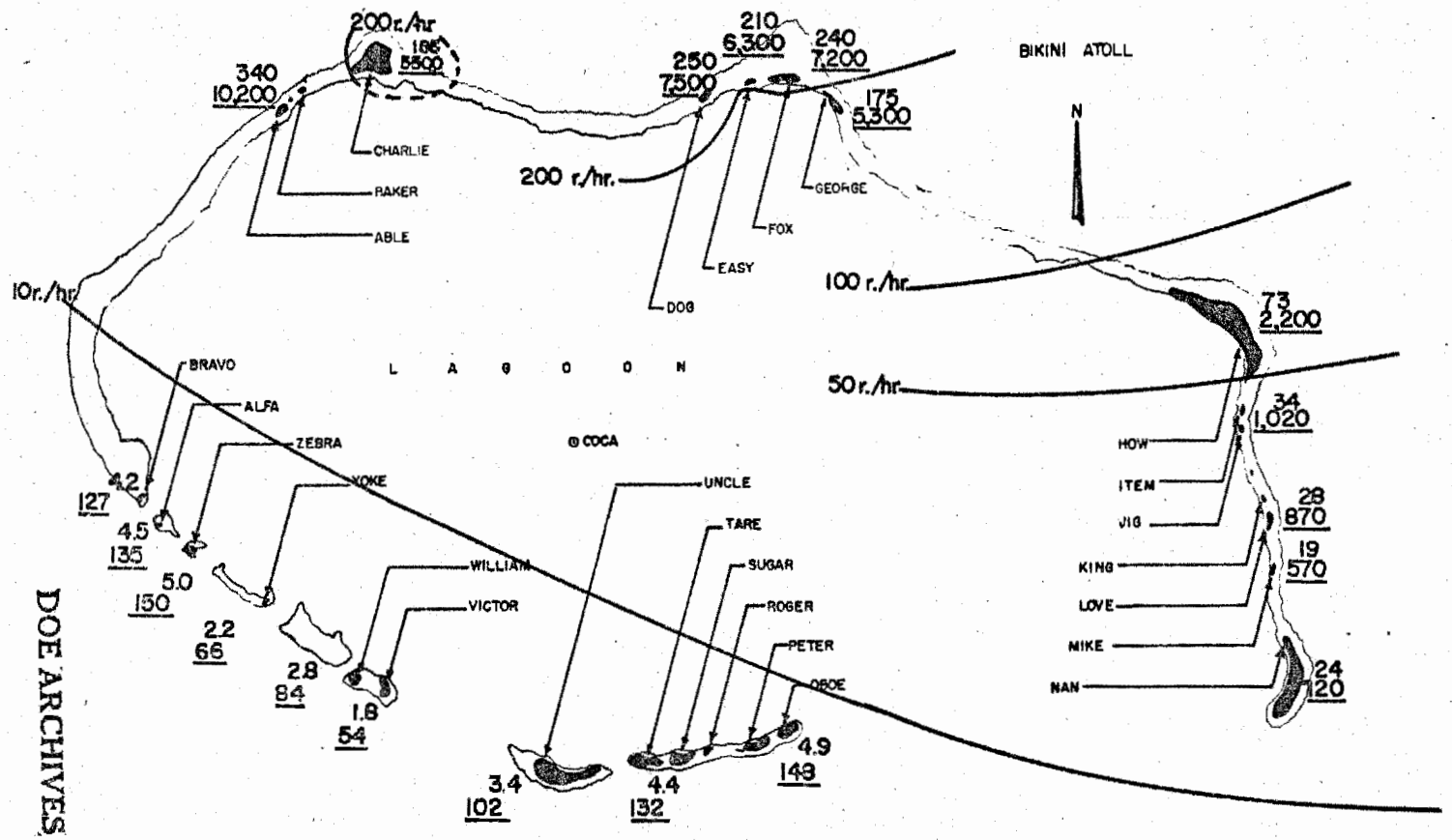

Figure 6
Isodose Lines for First Shot

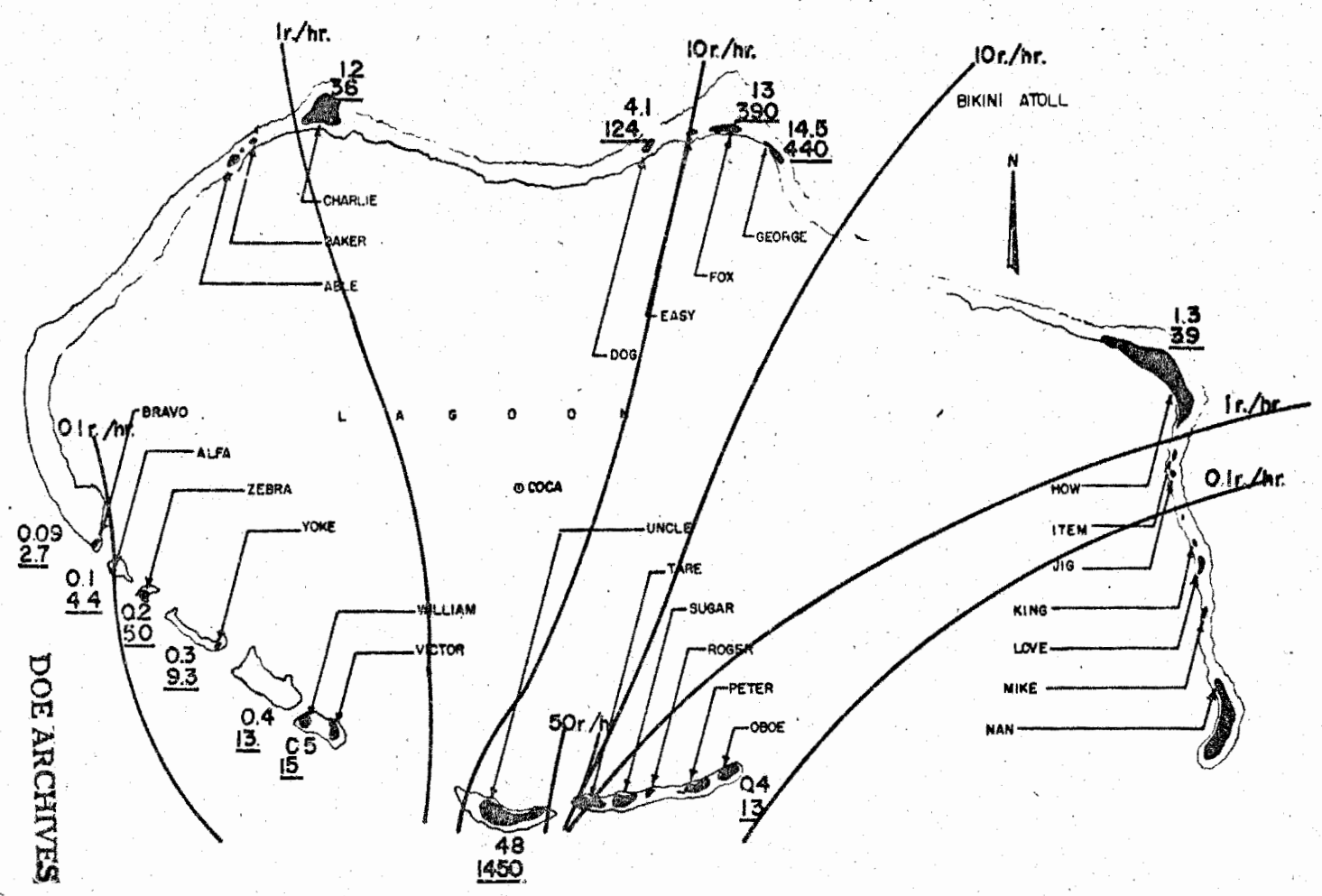

Figure 7
Isodose Lines for Third Shot

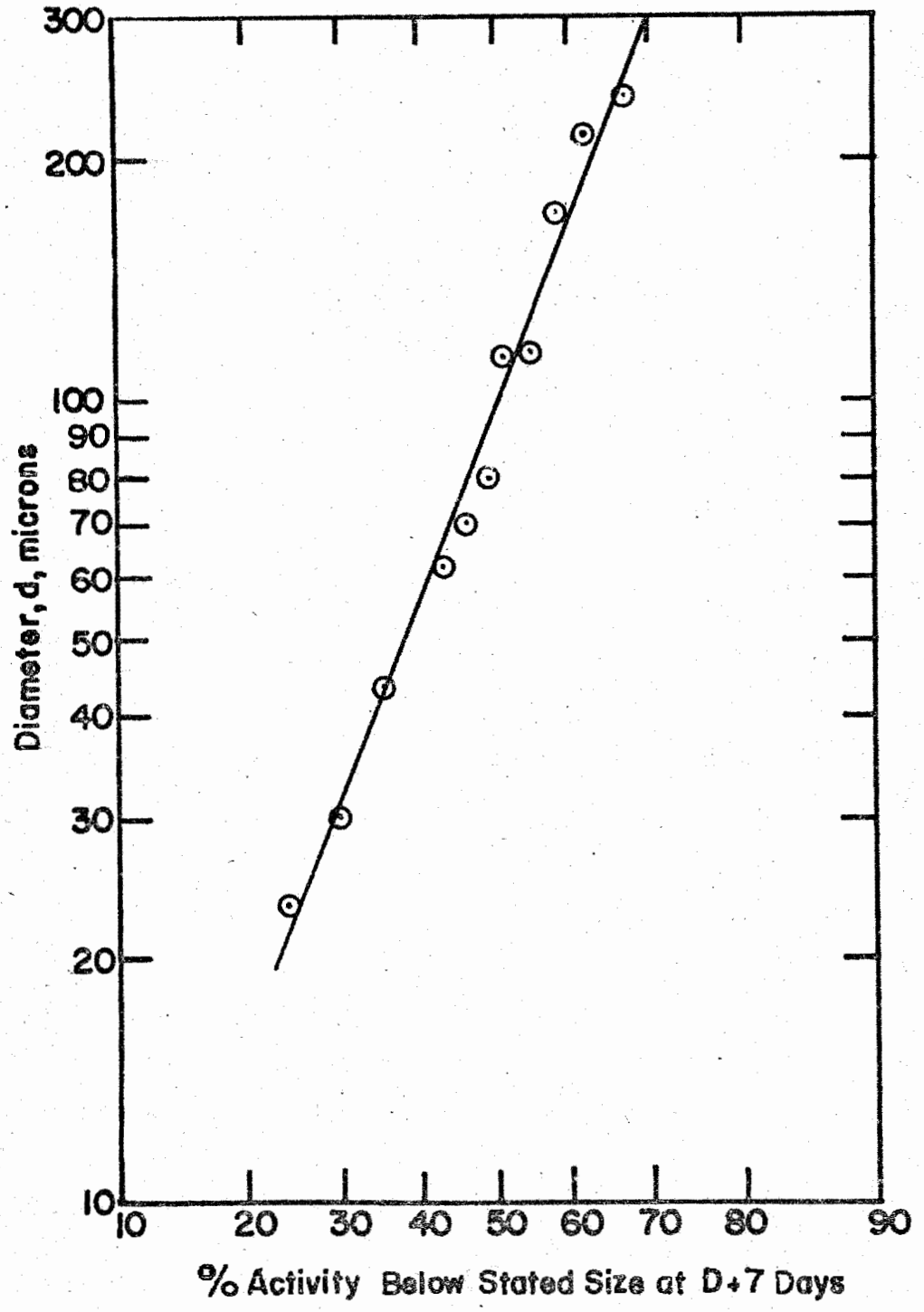

Figure 8

[redacted]

A study of the constant m in equation (4.1), together with other data, led to an insight into the processes in the fireball leading to the formation of active particles. In this equation k and m are constants, and A^o, the activity at zero time.

Our work has brought out the meaning of the sign and magnitude of the exponent, m. Most of the particles we studied were agglomerates and when these were broken down into their individual particles, the specific activities of the individual nuclides present in the smaller particles increased as their diameter decreased, i.e., m was negative.

We used the Roller Analyzer for reducing the agglomerates. This is a device for size-grading particles in an air-stream.

As an example, the next figure (9) shows a plot of the Sr^{89} specific activity against particle size for a Bravo sample. (A similar curve was obtained for Ba^{140}). This is a plot of the specific activity of Sr^{89} against the particle size. The slope of the line below 50 μ is -0.88. For Ba^{140} it is -0.91.

The sharp break at 50μ is due to our size-grading procedure with the Roller Analyzer. To the right of the dotted line we have the sieve-graded aggregates, and to the left the individual particles.

The next figure (10) shows a similar plot for Ce^{144}. Note that the slope of this is much less than that for Sr^{89}.

The significance of the numerical value of m can be shown in the following way.

For any nuclide with specific activty A^o at zero time,

$$A^o = kd^m \qquad (4.1)$$

The activity referred to the whole particle, is

$$(A^o)^1 = \frac{1}{6} \pi \rho \, kd^{3+m} \qquad (4.2)$$

where $\frac{1}{6} \pi \rho \, d^3$ is the mass of the particle, assuming spherical particles and ρ is the density.

Then, if experimentally, we find m = -1, the activity is proportional to the square of the diameter, i.e., to the surface area of the particle.

[redacted]

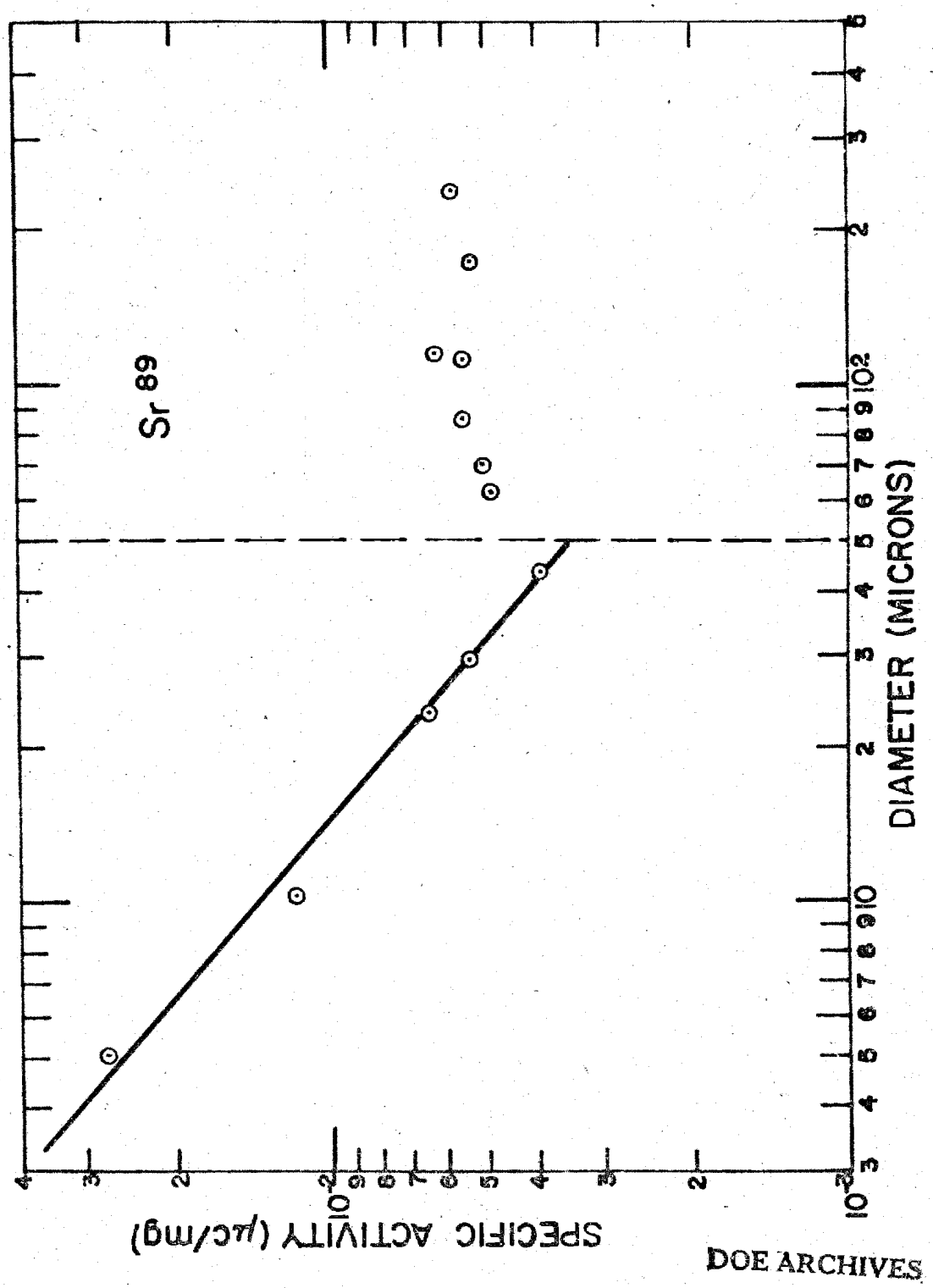

Figure 9

45

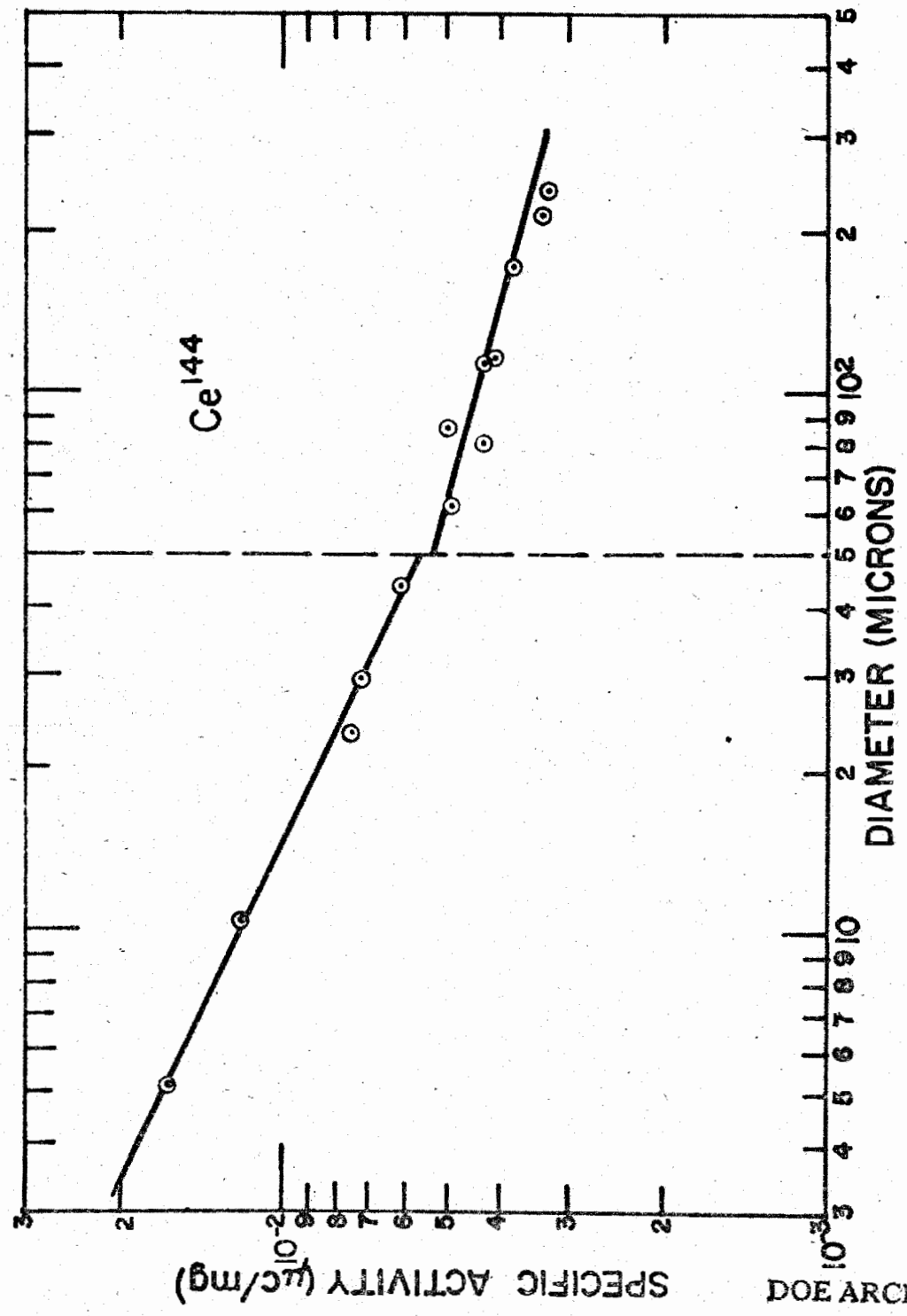

Figure 10

As was shown in the figure for Sr^{89} the value of m was -0.88, and for Ba^{140} it was -0.91. Consequently, these two nuclides were concentrated essentially on the surface, as would be expected for nuclides with long-lived precursors.

If the exponent, m, were zero, the activity in equation (4.2) would be proportional to the volume, so that the activity would be distributed uniformly throughout the volume.

For activity concentrated at the center, the activity per particle is constant, and m = -3.

We have actually found values of m as low as -0.32. For example, for Ce^{144} we found -0.47; for Mo^{99}, -0.48, and for Zr^{95}, -0.32. In these cases the activity is distributed in some irregular way throughout the volume. It appears that this could happen if, as particles are growing in cooler parts of the fireball, they pass across concentration gradients, i.e., there is incomplete mixing in the fireball.

Returning to equation (4.1), it is possible to relate this expression, in a formal way, with the decay slope. Since by definition

$$n = \frac{d \ln \sum A_i}{d \ln t} = -t \frac{\sum \lambda_i A_i^o e^{-\lambda_i t}}{\sum A_i^o e^{-\lambda_i t}} \qquad (4.3)$$

We need only substitute equation (4.1) for every nuclide, i, to obtain the desired relation.

There is also a useful relation between equation (4.1) and fractionation, as indicated by changes in the R-factor. An equation like (4.1) can be written for any two nuclides:

$$A_i^o = k_i d^{m_i} \qquad (4.4)$$

$$A_j^o = k_j d^{m_j} \qquad (4.5)$$

so that

$$\frac{A_i^o}{A_j^o} = \frac{k_i d^{m_i - m_j}}{k_j} \qquad (4.6)$$

and we can see that the left side is proportional to R, the proportionality constant being the value of A_i^o/A_j^o for pile fission of these two nuclides.

Note that if $m_i \neq m_j$, the fractionation observed will depend on the particle size, but if $m_i = m_j$, fractionation, if still present, is independent of the particle size. The same size particle has been assumed throughout.

We found evidence for fractionation in our CASTLE samples. Union shot samples were low in Sr^{89} and Ba^{140}. Table 1 shows the R-factor for Sr^{89} and other nuclides, as a function of particle size. The trend in the R-factors is obvious.

Table 1

R Factor from Intermittent Fall-Out Collector
Union Shot, Bikini Island

Time (after Shot) of Sample Collection in Hrs	Sr^{89}/Mo^{99}	Ba^{140}/Mo^{99}	Ce^{144}/Mo^{99}	Gross Decay Slope (10-20 das)
1.5- 3	0.702	0.788	0.50	-1.73
3.5- 5	1.15	1.64	-	-1.36
8- 9	0.538	0.661	0.460	-1.54
9-10	1.56	1.53	0.656	-1.60
10-11	1.81	1.43	0.31	-1.37
11-12	1.80	1.71	3.4	-1.04

We may deduce from this result that if base surge is active it will be low in Sr^{89} and Ba^{140}, because the base surge is due to material from the column falling back to earth shortly after shot. Since this activity leaves the fireball early, it may be low in nuclides with long-lived ancestors, so that the base surge will also be low in these.

We have found active particles in our fall-out samples which apparently must be assumed to have appeared in the base-surge. An

[redacted] ENERGY AC[redacted]

example of such a particle is shown in figure 11. The particle, which was partially calcined coral inside, was covered, but not uniformly, with activity on the surface. Particles of this kind were found above about 200 μ , and were prepared for autoradiography by thin-sectioning.

Our decay data showed that the activities of shot 1 samples were given by equation (4.7).

DELETED

A typical decay curve, extrapolated to low times, is shown in figure 12.

DELETED

The observed decay rates of samples from certain other shots showed interference by activity due to the Bravo shot. The data for shot 2 could be represented, for example, by

$$A = A_1 (t+623)^n \qquad (4.8)$$

where 623 was the time between the first and second shot, in hours; in other words, all the activity of shot 2 samples was due to shot 1. The samples from shot 3 were less affected by shot 1 activity.

Discussion

The results may now be collected to outline our conception of the reactions in the fireball leading to the formation of active particles.

The fireball, at the start, has, near the ground, a layer of vaporized ground material (here CaO) at the bottom, of greater density than at other points. As the hot bubble containing fission and other products rises, it carries up trailing behind it, currents of the heavier ground material layer, thus giving rise to varying concentration gradients, and to lateral eddies; in other words, conditions in the

[redacted]

Figure 11
Non-uniform Surface Activity on a Large Particle (> 200 μ)

[redacted]

[redacted] ENERGY ACT [redacted]

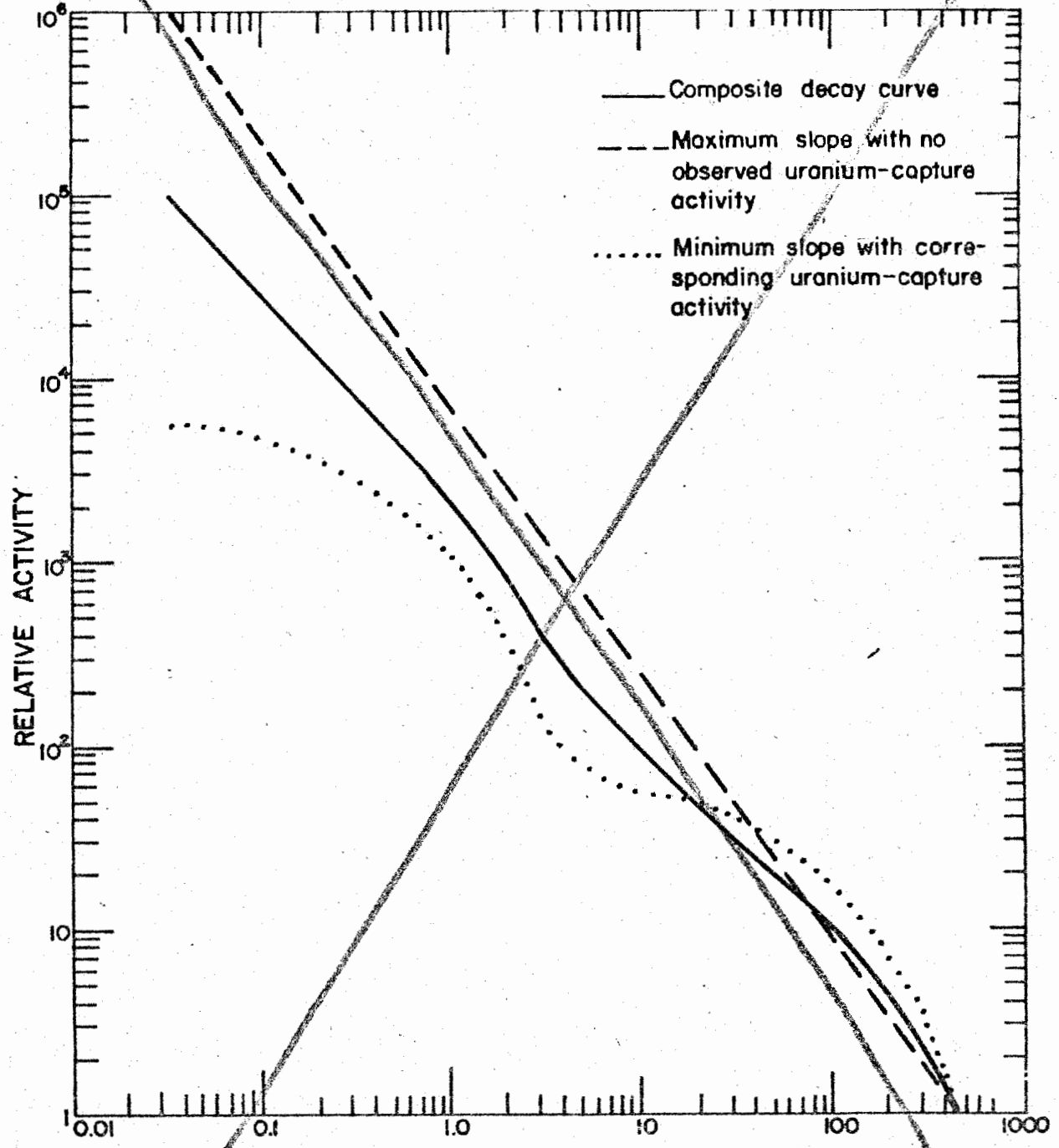

Figure 12
Typical Gross Decay Curve

[redacted]

fireball are such that there is poor mixing. This conclusion is supported by the low values of the exponent m in equation (4.1) for such nuclides as Ce^{144} and Zr^{95}, since such low values indicate particle formation under different concentration conditions.

Contamination of the Column and Base-Surge

At the edge of the fireball some material condenses early to fall-out, and owing to the vortex action this could be active since the eddies in the fireball may bring fission products to the edge. This fall-out, "peeling-off" and falling, may be sucked up again in the thermal draft, and become impacted on inactive material in the column. Since the base surge is believed to originate from the lower part of the column, it appears that contamination in the base surge might be explained on this basis.

The activities found would appear to be due to this effect because our stations were too close in to have received fall-out from the cloud. The photograph on figure 13 of the column collapsing over the atoll supports this.

Summary

We have presented isodose lines, based on Rad-Safe Data, for the total hazard, for the various CASTLE shots.

On the basis of our decay studies, high values of the decay slope were attributed to the presence of certain capture products.

These, at 250 hrs. after the Bravo shot, corresponded to about 44% of the total activity.

Our work has advanced our more intimate understanding of the mechanism of the formation of active fall-out, and has led to a possible explanation of how the column, and eventually the base-surge, can become contaminated.

[redacted]

[redacted]

Figure 13
Collapse of Column over Atoll

[redacted]

[redacted]

INCOMPLETE DOCUMENT REFERENCE SHEET

The archive copy of this document is incomplete.

Pages missing 48

Enclosures missing _____

_____

Attachments missing _____

_____

Other _____

CPS
signature

2-11-92
date

[redacted]

METHODS, FINDINGS, AND OCEANOGRAPHIC FACTORS OF PROJECT 2.7, OPERATION CASTLE

Dr. Theodore R. Folsom
Scripps Institution of Oceanography

Introduction

I have been asked to discuss certain aspects of a fall-out survey which was made just following Shot 5 of the CASTLE operation by personnel of both United States Naval Radiological Defense Laboratory and Scripps Institution of Oceanography operating as Project 2.7 of Task Unit 13. This survey covered a large area of open sea east of Bikini atoll, and relied to a great extent upon oceanographic methods for bringing back an evaluation of the extent of the fall-out. I will direct my remarks towards the oceanographic factors here introduced into fall-out studies for the first time, and Dr. Werner of NRDL will, in the following paper, stress the quantitative radiological results.

This expedition was planned and implemented on very short notice, and it could not have succeeded without the effective cooperation of numerous agencies and individuals within the task force. Unfortunately many of the acknowledgements, which are certainly due, will have to be omitted here.

Outfitting in Haste

This was perhaps the first time anyone had set out seriously to catch fall-out by using the ocean itself as a trap; but it so happened that no specialized and well-equipped oceanographic ship was in the Marshalls region during this particular operation. For this reason the USS SIOUX, an ATF tug which was already assigned for NRDL project work, was hastily outfitted. A contractor's winch was acquired from the Holmes and Narver yard along with about 3,000 feet of light (and very doubtful) cable. And a wire-measuring wheel, a set of standard oceanographic Nansen-type water-sampling bottles, and a set of twelve specialized oceanographic thermometers, and also a Bathythermograph and several cases of citrate bottles were loaned by the Hydrographic Office representative, Mr. Hammond. Another bathythermograph was loaned by the destroyer, USS EPPERSON.

The gasoline driven winch was welded to the ship's fan-tail deck, and a hydrographer's platform and boom was rigged outboard. Project 2.5 personnel secured a rush shipment by air of gallon-sized plastic bottles for transporting water samples; and it was later found possible

[redacted]

[redacted]

54

[redacted]

to improvise from these bottles some very satisfactory though clumsy "snap-samplers" of a type which minimizes the loss of highly diluted materials.

All this was put together in about one week. One of those particular weeks memorable to many of us as "weeks of the flexible time scale" when there were several "Y - 2 days" and consequently were several repeated, disappointing, false starts. But, when the ATF SIOUX finally left Eniwetok on 4 May, she had aboard the bare elements of a hydrographer's equipment; and some of the mechanically-weak and therefore dangerous features of this equipment were remarkably well compensated for by the skill and enthusiasm discovered in a young seaman who volunteered to become the winch operator. He was a red-headed farm boy nicknamed "Booga" who apparently had learned to love the hoisting of hay gently into hay lofts. He became very good at it and for unexpected skill, we who stood at the flimsy Hydro wire will always be grateful.

Direct Reading Gamma Detecting Devices

The ocean is very large and very deep, and the taking of three-dimensional samplings of it is a very slow and tedious process even with the best equipment. Two hours, for example, may be required for each deep sampling cast, and four or five days may be required to merely traverse the area influenced by modern weapons. Sooner or later the oceanographer always turns to methods for interpolating between the careful measurements which he makes at "stations". Very fortunately for this particular survey a convenient interpolating device was known to be available but in sad physical condition momentarily. It was a geiger counter which had been removed from a standard Radsafe hand set and had been installed inside a section of steel tubing. It was entirely water-tight; it could be lowered to depths of about 200 feet; the gamma signals could be read on deck. It could be towed behind a ship; and it had just been tested in Bikini lagoon by Scripps people interested mainly in lagoon circulation.

At the time the request for it came to Bikini, this so-called Mark I prototype, underwater, marine geiger, gamma detector was in pieces in a cardboard box, under a bench, on a ship in the lagoon. It had just passed through the propellor of an "M" boat, the captain of which having forgotten he had behind him a "tow". But so promising were the data-extending possibilities of this crude instrument, it was shipped in pieces to Parry and rebuilt. And two more, somewhat similar, underwater gamma detectors also were put together from hand set components during that period when the weather, or something, delayed the

[redacted]

55

"Yankee" event. These were really crudely-made devices; it was hoped merely that at least one of the three would survive the rough treatment expected at sea.

The Track of the SIOUX

Ultimately, on the morning of 5 May the ATF SIOUX, outfitted as just described, proceeded to a point south and east of Bikini, made shake down tests of all gear, took deep samples of clean water for control purposes, and then waited for permission to make a section through the fall-out area. At about 2000 hours, 5 May, the first section was started, intended to pass ground zero at a radius of about 25 miles. The gamma detecting gear was streamed out.

Figure 1 is shown to aid description of the unconventional gear used on this cruise. The cylindrical gamma detectors were towed about 200 feet astern by rubber light cords; these detectors sank six feet below the surface at the 7 to 13 knot speed which was generally held. The meters were read on deck; whenever possible two or more instruments were towed together.

Another gamma detector, an AN/PDR-T1B handset inside a steel tank was supported six feet outboard at about six feet elevation above the sea surface. It served several functions to be discussed later.

The SIOUX steamed almost 900 miles through the contaminated area during the next four days.

Along the ship's track shown in Figure 2 has been plotted the relative gamma intensity corresponding roughly to mr/hr, and the eight stations have been identified with circles. The gamma signal is plotted to the right of the track.

Somewhat before midnight the SIOUX broke abruptly into "hot" water - rapidly getting "hotter". Those who were aboard will not soon forget the ominous effect caused by the meters' climbing continuously upward and going off scale one by one. Only the above-water detector (the T1B instrument) managed to stay on scale, partly due to its heavily shielded condition.

At just fifteen minutes after midnight it was discovered that the ship was reversing its course, and a dash up to the bridge brought to light the fact that the ship's Radsafe officer had been fully instructed as to procedures to carry out in the event of fall-out - but had not been prepared to recognize that event where nothing was falling on the deck but where the sea itself was radiating intensely for miles around. It also appeared from the ensuing conversation that during an earlier

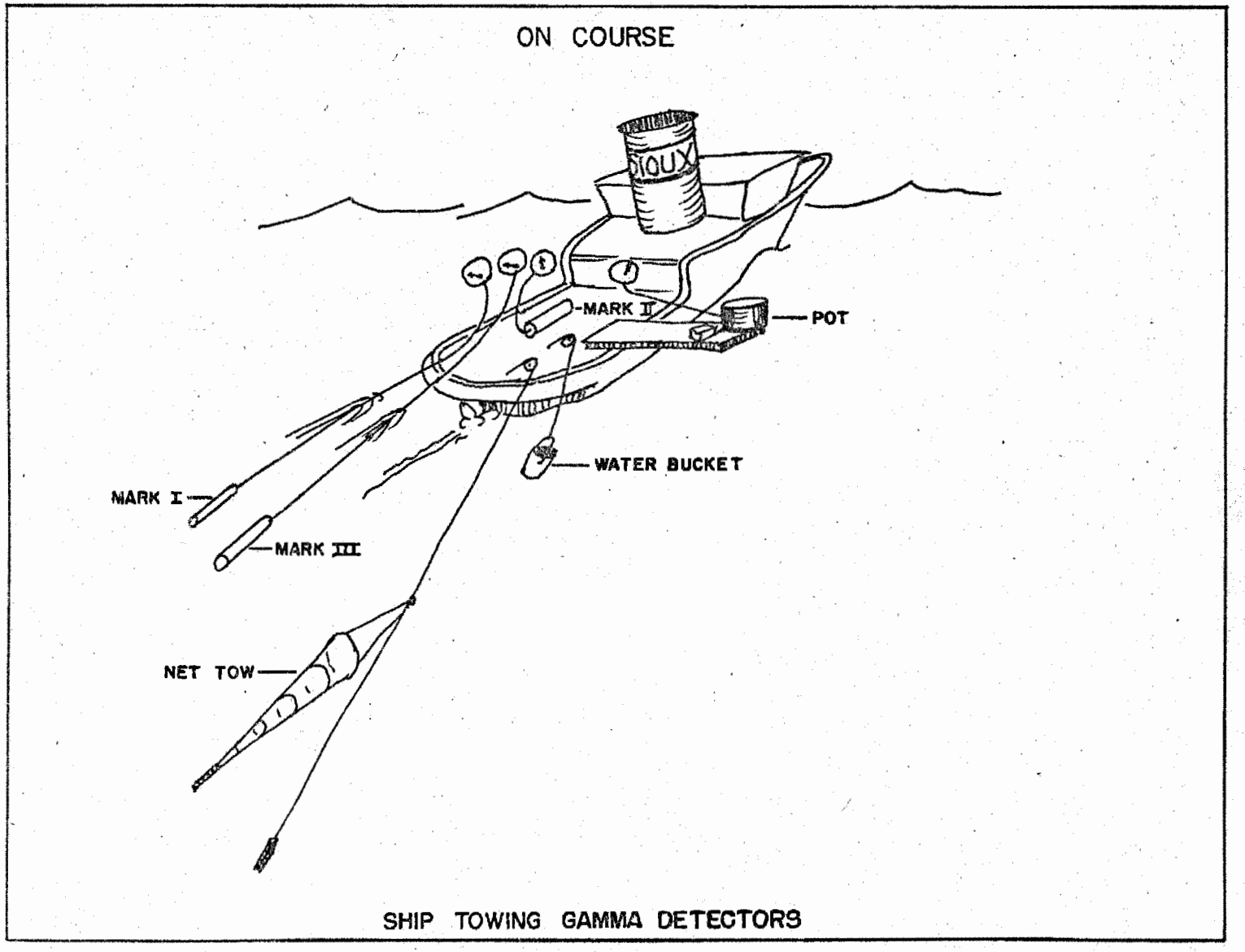

Figure 1

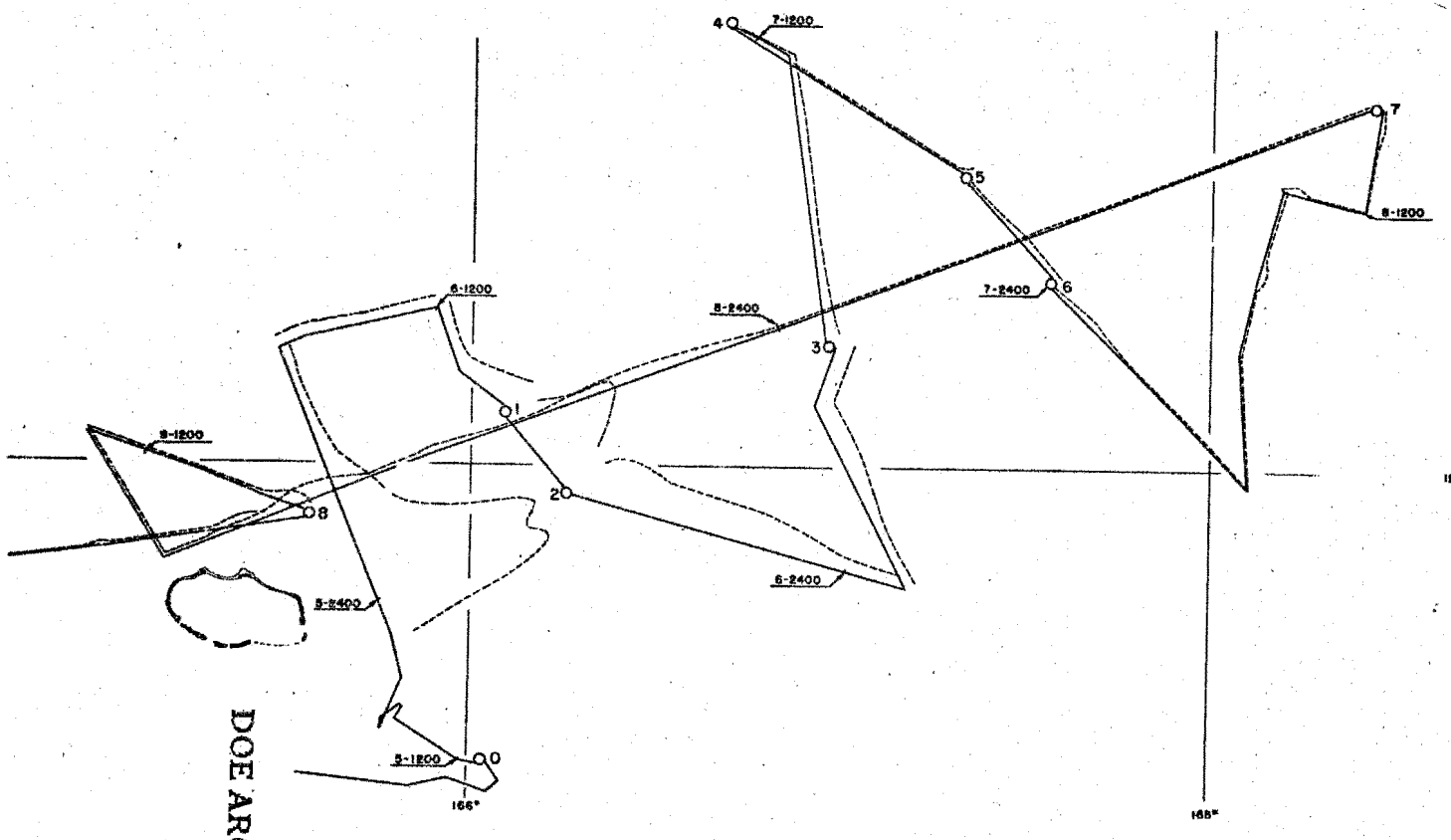

TRACK OF THE SIOUX, WITH RAW GAMMA SIGNAL

Figure 2

[redacted]

cruise when a similar physical situation must have existed, contaminated sea water had been pumped over the comparatively clean decks of this ship.

A simple test was demonstrated of raising the Radsafe monitoring instrument above the steel windscreen on the bridge so as to cause better exposure from the sky, and the cruise was thus prevented from ending then and there.

It will be seen that the track intercepts six areas where gamma activities far above background were detected. Since four days passed during the survey, decay alone produced a great deal of attenuation, the signals became progressively weaker, but always remained measurable.

All the gamma measurements cannot be presented in detail here, they were made at over 450 points. But some of the signal variations witnessed during the first day will be illustrated later after the measurements at fixed stations are discussed.

The winch, meter wheel, hydrographer's platform (carrying the T1B instrument in it), are shown schematically (Figure 3), as are the string of sampling bottles on the hydrographic wire.

On the left is indicated the method of lowering the Mark II gamma detector to measure the gamma intensity profile. This slide will be shown again later, but the work at fixed stations can be listed at this time.

During the eight main stations there were made:

One cast to 800 meters with seven samplers

Four casts to 500 meters with six samplers

Four casts to 175 meters with six samplers

Two casts with a plankton net towed at two knots.

Four short additional stations were made where only BT instruments were lowered; all told BT's were made at 12 positions along the track.

At three stations the vertical profile of gamma signal was measured directly with the Mark II instrument.

Each Nansen bottle carried two reversing thermometers.

[redacted]

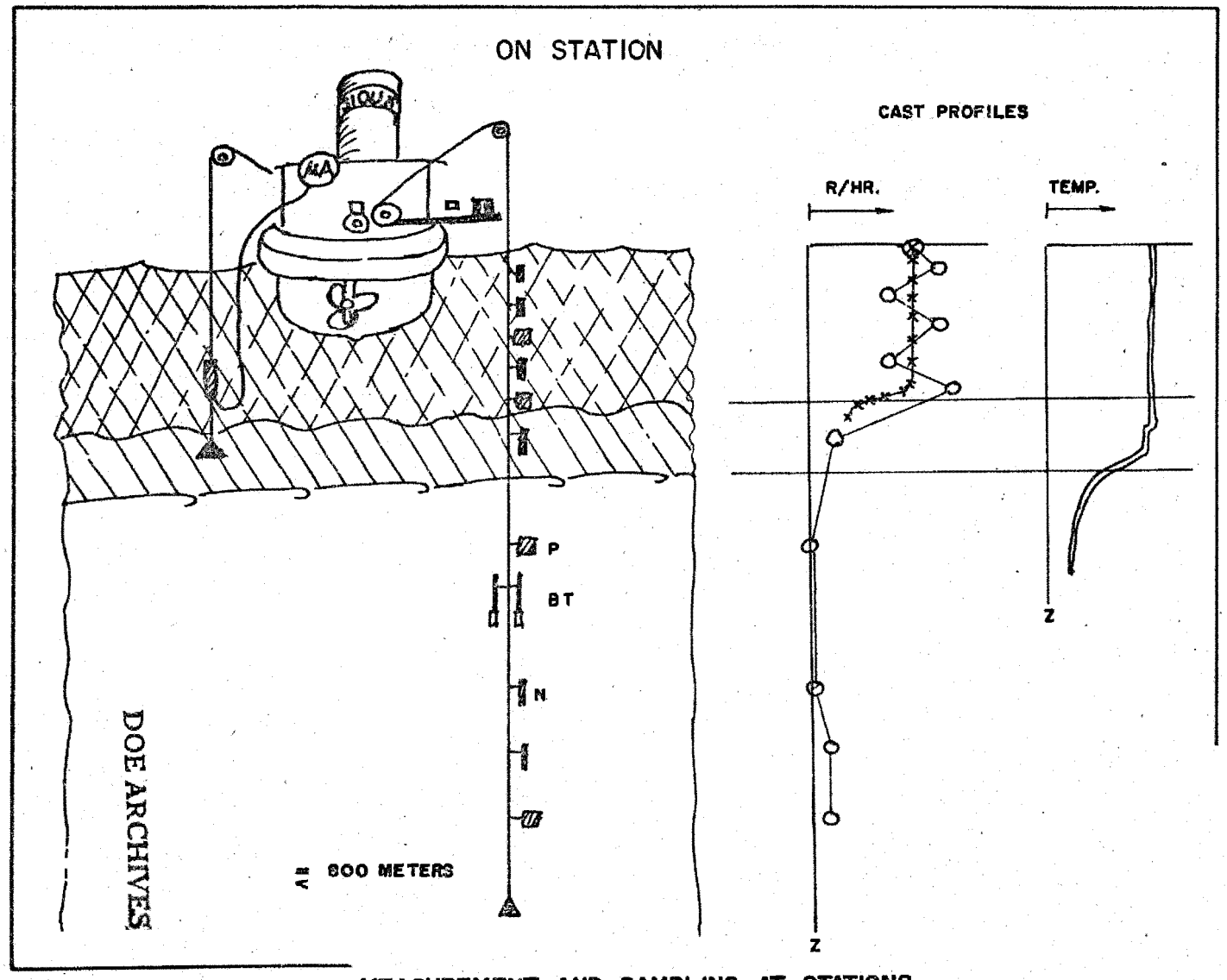

MEASUREMENT AND SAMPLING AT STATIONS

Figure 3

[redacted]

Always four of the special plastic bottles were used.

Surface water samples were taken at stations as well as along the track.

Disposal of the Water Samples

The water samples taken at these stations as well as samples taken at the surface during the cruise, were rushed by plane to NRDL for analysis. Dr. Werner will discuss the results of these analyses and the conclusions which can be drawn from them somewhat independent of the direct gamma measurements which will now be discussed in detail.

The Direct Gamma Measurements

Most of the direct measurements of dose rate were made with geiger instruments; these had many ranges and had ample sensitivity, but as with the measurements of any geiger instrument these measurements must be used with care. In this particular marine usage a number of additional reductions have to be applied to the readings to yield the approximate true dosage rates.

Contamination and Background

A number of steps of calibration and correction were carried out.

Several instruments were used together whenever feasible. They were intercalibrated and tested against the hand sets on board ship several times. These were new, untried instruments.

The separate records come into satisfactory numerical agreement after calibrations are applied.

At each station - and sometimes between - the towed instruments were hauled aboard and carefully washed. The slide (Figure 4) shows the result of this washing upon the signal.

At these wash-off points a reliable correction for contamination can be made; but between these positions an interpolation had to be resorted to. A simple linear proportionality was assumed for relating the rate of surface "pick-up" and concentration of activity on the sea.

Considerable thought has been given to methods to reduce pick-up and to make better corrections later -- but nothing more can be presented here.

[redacted]

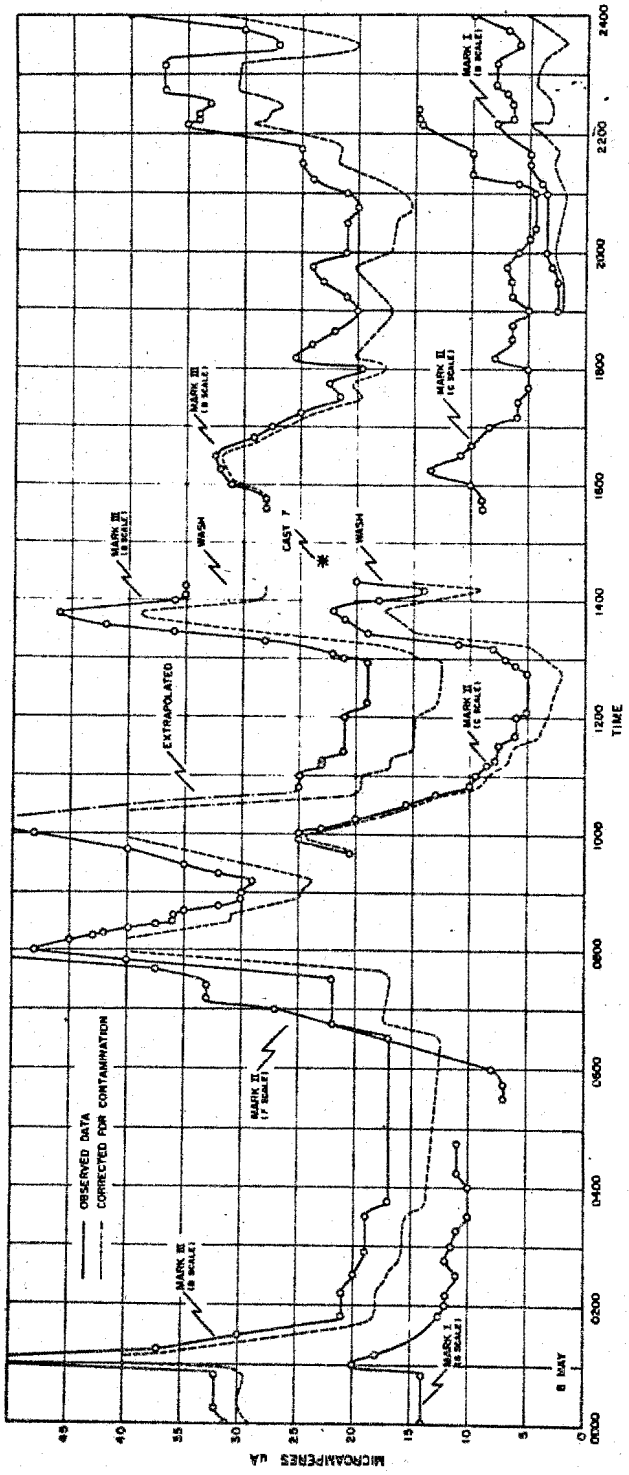

DETAILS OF SIGNAL ALONG TRACK

Figure 4

62

Calibration

All three of the towed instruments were calibrated on 10 May 1954 immediately after the cruise, at Parry Island RadSafe and against a large radium point source.

Then these instruments were immediately boxed and shipped to the United States Bureau of Standards. At the Bureau, the radium calibrations were repeated, and the instruments were then exposed to radiations having photon energies ranging from as low as 58 KEV up to 1.2 MEV.

These exposures were repeated from all incident beam angles so that a mean response corresponding to a broad source could be estimated.

The variations of response of the Mark II instrument with beam energy is shown in Figure 5.

A computed mean of responses for all angles is shown in Figure 6. This relates to a submerged exposure of the instrument inside a large, monochromatic, hypothetical, distributed source, i.e., a 4π monochromatic source.

Response to Estimated Field Source

Estimates of the source energy spectra which might have existed in the sea during the period of the survey were supplied by Dr. Werner of NRDL and by Dr. Scoville of the Armed Forces Special Weapons Project. An average of the estimated spectra for D+1, D+2, D+3, and D+4 days is shown in the figure second from the bottom.

By following the technique outlined in the Technical Analysis Report issued January 1954 by the Weapons Effects Division of AFSWP (AFSWP-502A), a dose histogram was computed. This represents an estimate of what energy distribution was actually "seen" by the submerged instrument. It is shown in Figure 6.

Final Calibration Curves

The results of the monochromatic response constants of the instrument may now be combined with the computed, in situ dosage spectrum to give an estimate of the response of the instrument to the mixed activity believed to exist in the sea.

Before final application of these calibrations to the field measurements, account had to be made of the slight non-linearity of

[redacted]

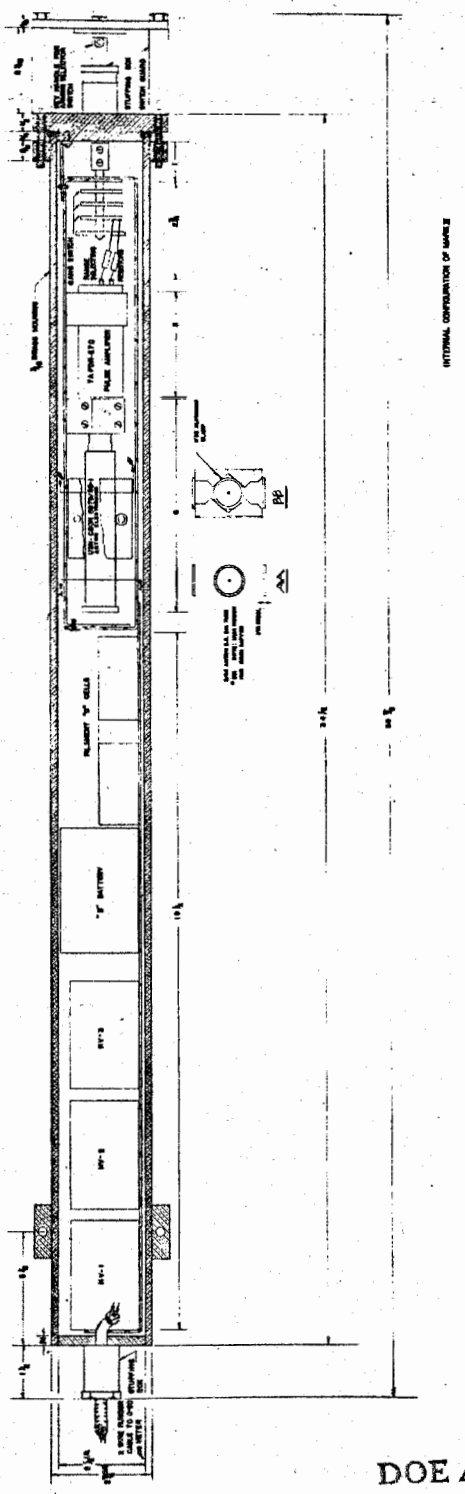

DETAILS OF MARK II INSTRUMENT

Figure 5

[redacted]

[redacted]

64

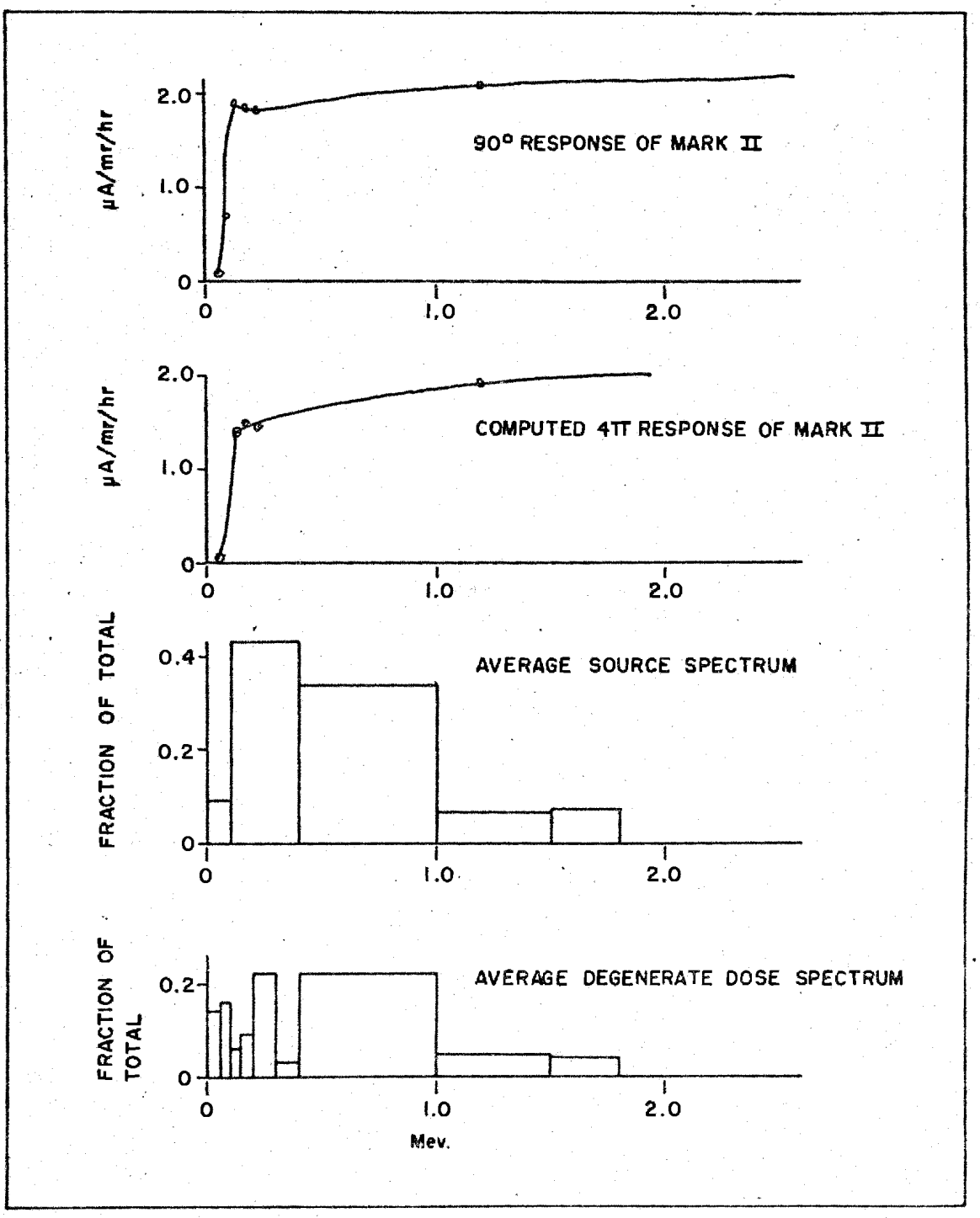

SUMMARY OF CALIBRATION STEPS

Figure 6

[redacted]

monochromatic response of the instrument, that is the μA-versus-mr/hr response.

The shape of the responses to radium rays is shown (Figure 7); the results from Parry Island and from the Bureau's calibrations are compared here, but for only one range.

The correction for use of the Mark II instrument inside a large distributed source of the type expected can be summarized by saying the Parry Island radium calibration curves had to be shifted upward by a factor of 1.5.

That is, this instrument calibrated against radium, underestimates the dosage rate when used to measure softer, mixed radiations underwater.

So far nothing has been said about the effects of time and vertical and horizontal motions; but the gamma signals along the track can now be reduced to apparent mr/hr in situ - that is the ionization in an air cavity under water.

Reduction of Hypothetical Dose at Three Feet

An underwater dose estimate has limited usefulness except perhaps for computing the exposure of personnel below decks.

It is customary to normalize fall-out dosage to that which would exist at three feet. But even over land this computation must be simplified to that unlikely case where the land is perfectly smooth - a very large hypothetical billiard table; and this imaginary, uniform distribution spread over the imaginary catchment plane is not much harder to derive from measurements made at sea than from those made on land and certainly as real.

Absorption of Energy in Water

Apparent-dose in roentgens/hr under water can be reduced to density of radioactive energy fairly directly if the source is distributed uniformly and if the source spectrum is known.

In a large uniform distribution, energy-balance considerations require that the rate at which energy is absorbed in any unit volume of water is equal in the rate at which it is emitted from any neighboring identical volume element, that is, absorption in water equals activity density.

This equation can be utilized if the apparent roentgen in situ is known since the roentgen corresponds to the amount of energy absorbed

[redacted]

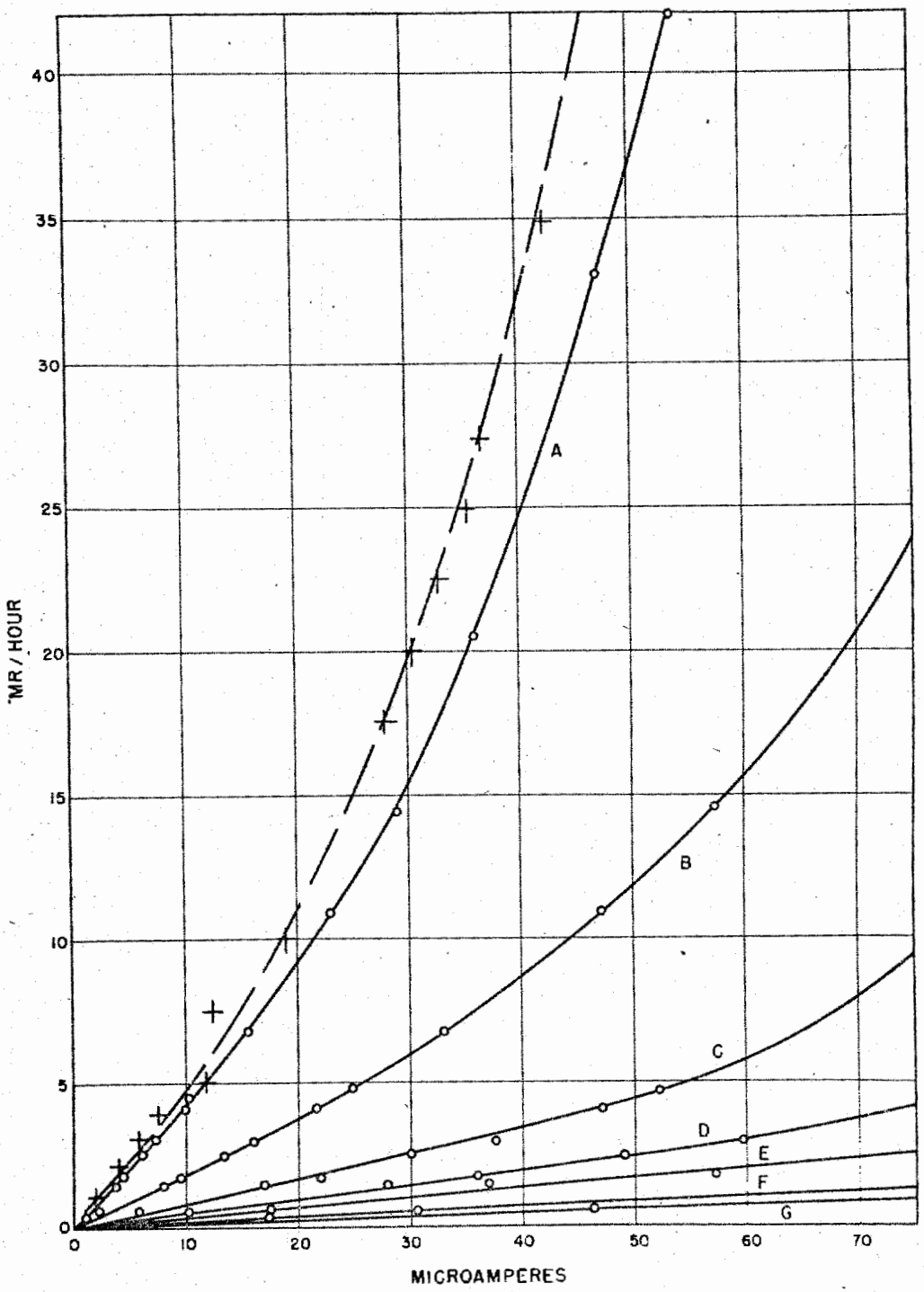

DOE ARCHIVES

CALIBRATION CURVE OF MARK II

Figure 7

[redacted]

[redacted] ENERGY ACT 19[redacted]

[redacted]

in a unit volume in air, which of course reduces to the energy which would have stopped in the same volume of water - by multiplying by the ratio of the appropriate "true" absorption coefficients.

Total Density in the Column

The total amount of fall-out energy per unit area can be obtained by summing up all activity in the water column. The field experiments indicate a surprisingly uniform mixing (Figure 8).

It can be estimated, even with the limited experimental data collected in this expedition alone, to what depth the contamination had penetrated at any time even though the cable was too short to permit direct measurement (Figure 9).

There are several reasons for giving the oceanographer confidence that the activity did not ever during the whole cruise penetrate below a fairly well established depth - the thermocline lying at about 100 meters. Twelve Bathythermograms were made during the cruise - 48 more were contributed by destroyers in the area. These and the thermometers on the hydrographic wire establish this ultimate depth of mixing within plus or minus 20%.

Only one single water sample showed any significant evidence of penetration below the thermocline. We attribute this finding to the sort of contamination which may be anticipated with Nansen-type of sampling bottles.

Thus the radioactive density which would have collected on the hypothetical fall-out catchment plane can be computed by simply multiplying the in situ density in MEV/cm^3/sec by the depth of mixing, measured or computed in terms of centimeters of course (Figure 10).

The final step of reduction requires the use again of the tables made available in the AFSWP-502A report.

Fortunately that special case involving radiation from a uniform distribution over a plane surface has been worked out in some completeness and is presented in tabular form in this monograph. The calculations are somewhat tedius, but are straightforward; but solution does take into account the contributions from scattered rays. That is, a "build-up" factor suitable for the problem at hand has been made available by modern electronic integration.

The final reduction can be summarized therefore by the formula shown at the bottom of Figure 10.

[redacted]

[redacted]

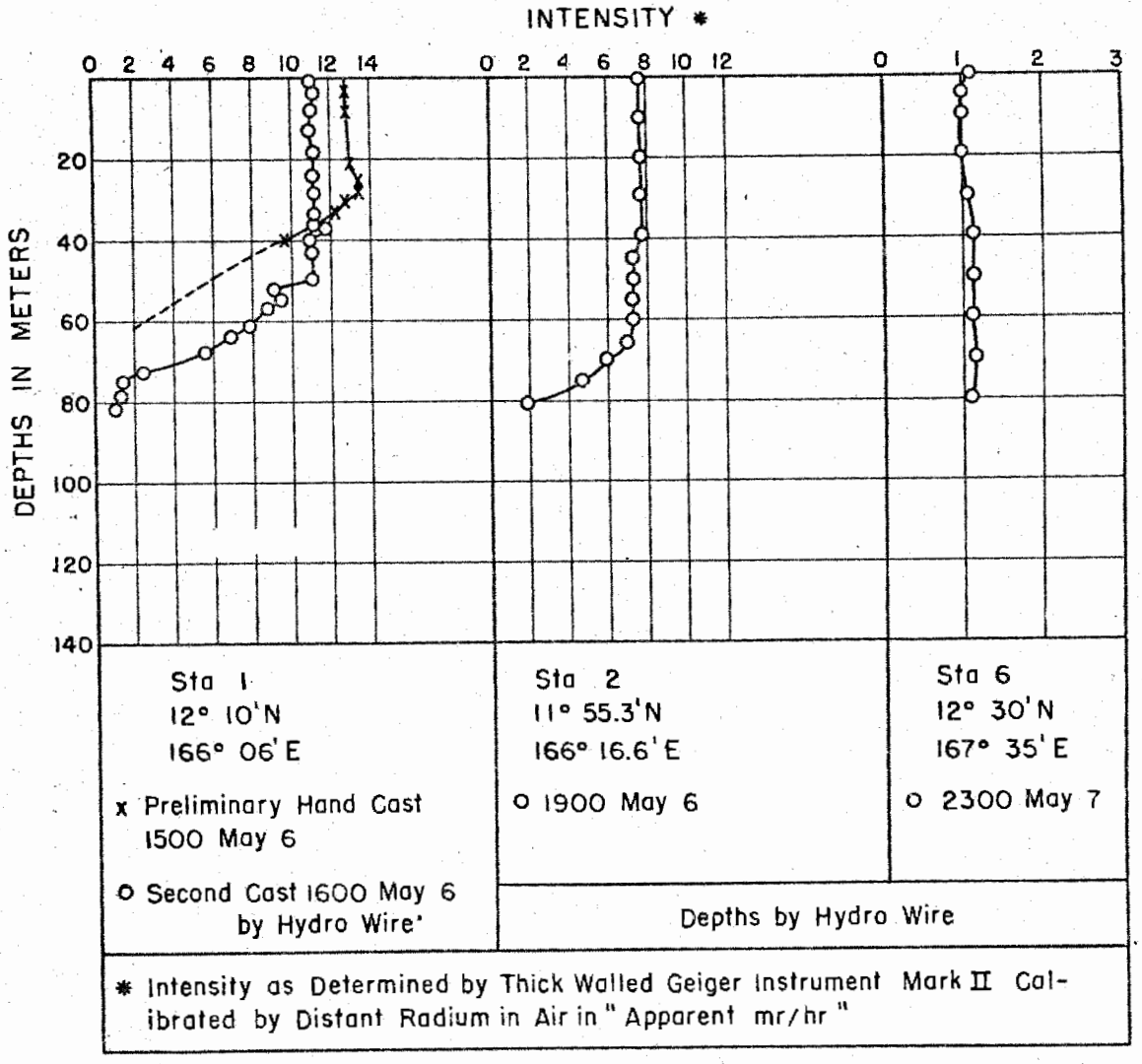

VERTICAL PROFILES OF CONTAMINATION

Figure 8

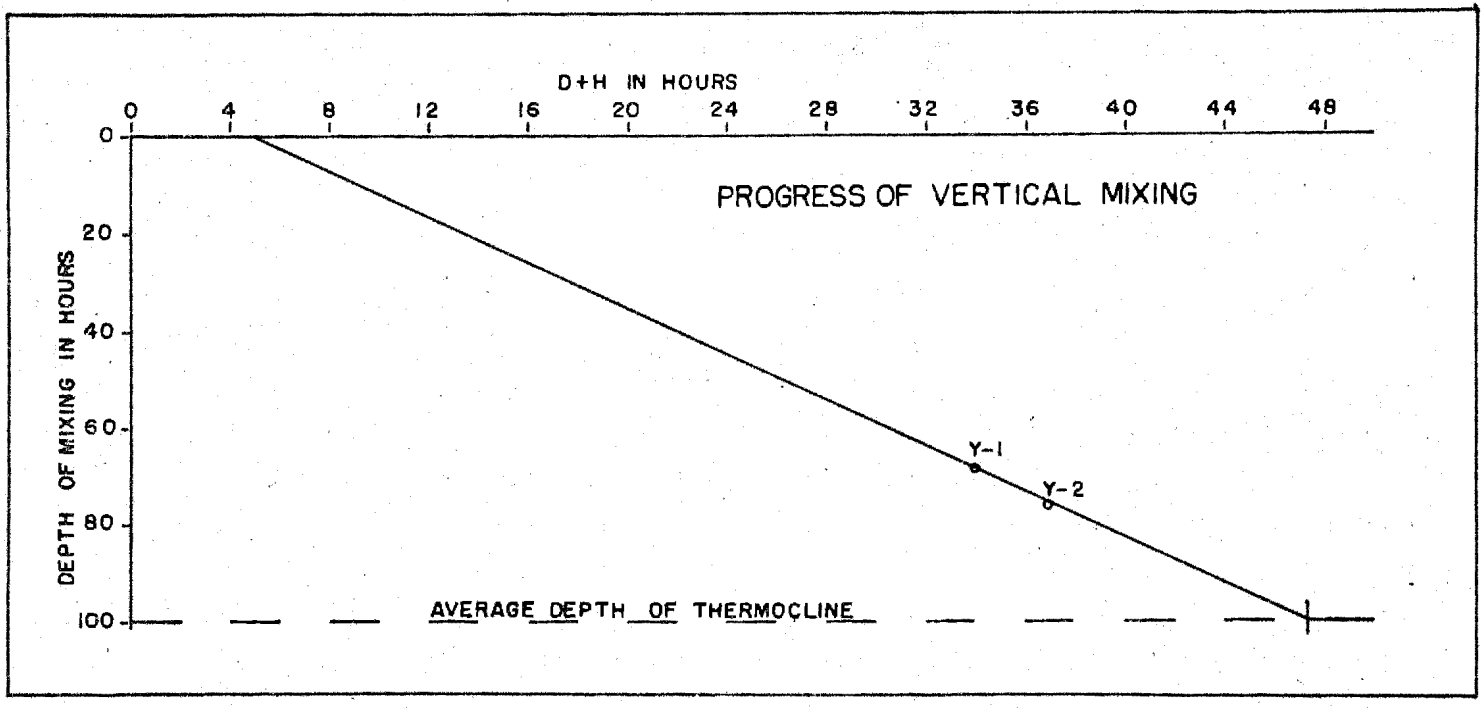

PROGRESS OF CONTAMINATION DOWNWARD

Figure 9

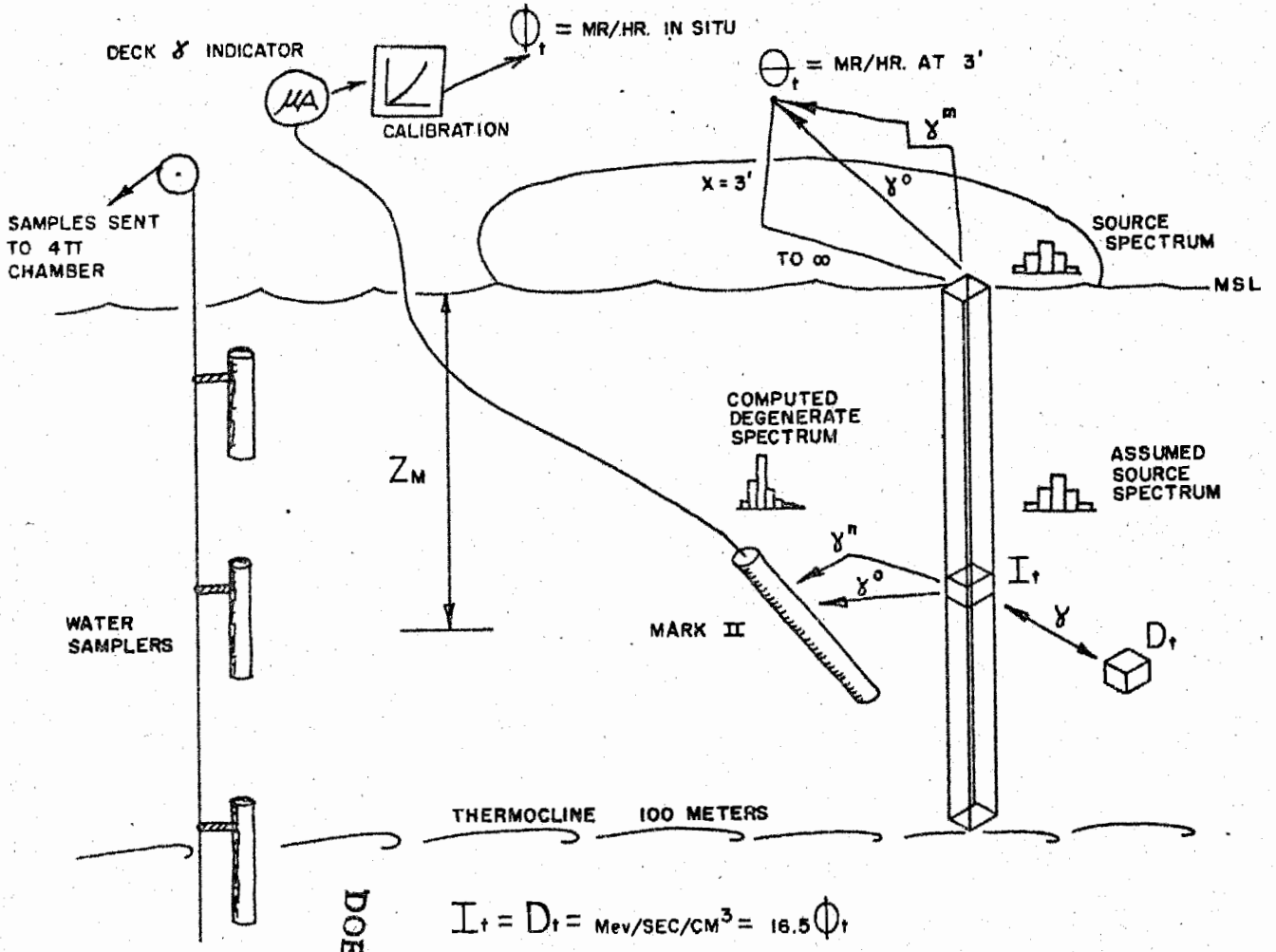

$$I_t = D_t = \text{Mev/SEC/CM}^3 = 16.5\,\Phi_t$$

$$\Theta_t = 8.2\,Z_M\,\Phi_t = \text{mr/HR}$$

SUMMARY OF REDUCTION

Figure 10

[redacted]

The dose in air at three feet above the standard, smooth, fall-out plane, in mr/hr is:

$$\Theta_t = 8.2\ Z_m \Phi_t = \text{mr/hr}$$

where Z_m is the mixing depth in meters and Φ_t is the apparent dose in mr/hr read by a properly corrected dosimeter submerged in the water.

So far lateral motion and decay of activity have not been introduced. Time is still a variable.

Decay

The amount by which the decay of the activity disguises the signals seen by a ship steaming on a slow traverse can be now illustrated. We shall now compare two plots made along the track, one of the signal unmodified (Figure 2) - the other shows it reduced to the synoptic time D+12 hours (Figure 11).

For final computations an experimental decay curve supplied by Dr. Werner was used. It differs from what is given by use of the familiar "1.2 decay law".

Lateral Displacement Due to Currents of the Sea

Finally, the effect of lateral displacement occurring after the fall-out arrives at the sea surface may now be taken into consideration.

The currents near Bikini unfortunately are not stable enough to be predicted in detail with any accuracy. However, there is a fairly persistent component from east to west (Figure 12).

For the present computations, a steady east to west current of $\frac{1}{2}$ knots was assumed. The type of error which might have been introduced is fairly apparent - it is mainly a distortion of shape of the fall-out field (Figure 13).

Hypothetical Synoptic Track

It now may be computed where the fall-out material actually contacted the sea surface. The ship's track must be displaced by amounts appropriate to the time of fall-out arrival and to the sea currents. This corresponds to a route which a "Jeep" might have taken over dry land to survey the fall-out.

[redacted]

[redacted]

72

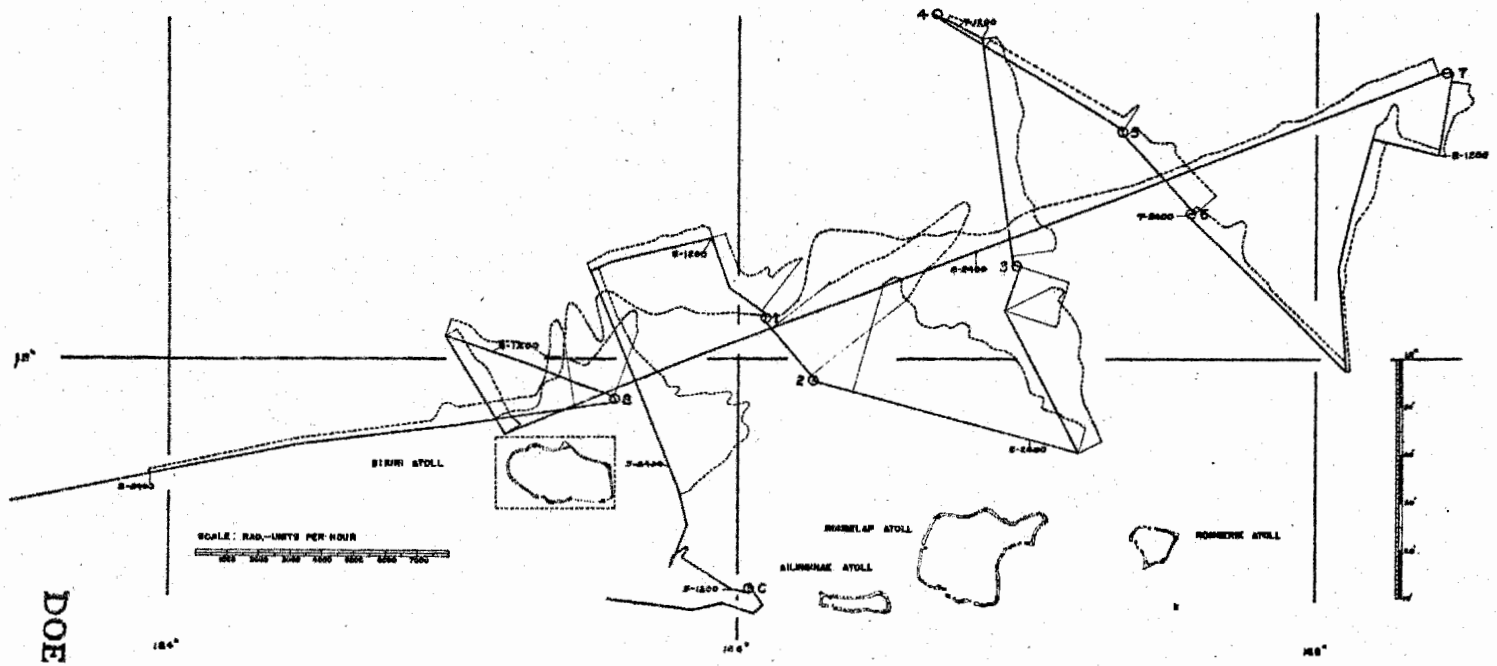

TRACK, APPARENT mr/hr REDUCED TO Y + 12 HOURS

Figure 11

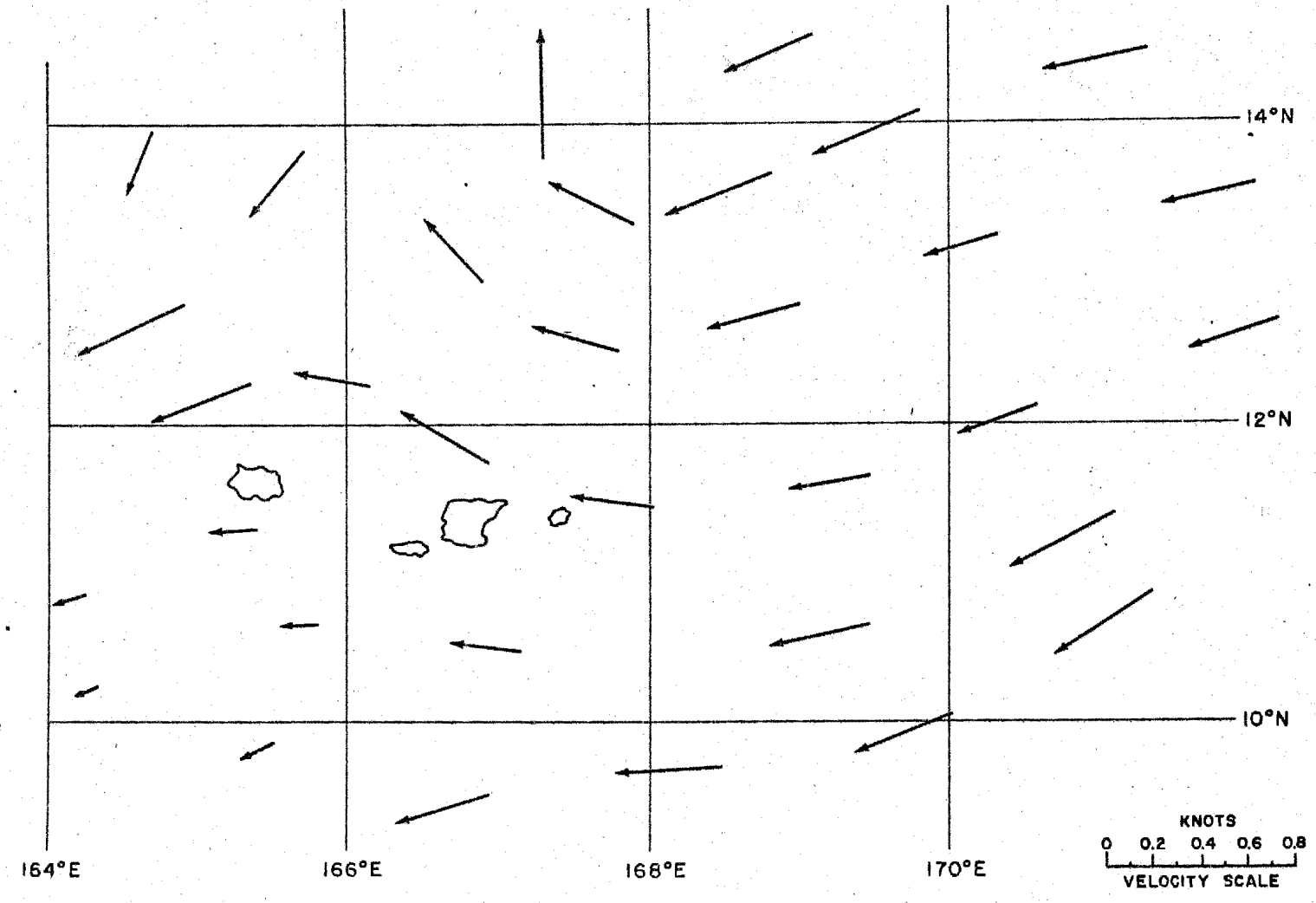

VECTOR SUMMARY OF 10 YEARS OF JAPANESE OCEANOGRAPHIC STUDY IN THE AREA

Figure 12

7/18/88

INCOMPLETE DOCUMENT REFERENCE SHEET

The archive copy of this document is incomplete.

Pages missing 70

Enclosures missing _____

_____

Attachments missing _____

_____

Other _____

CRS
signature

2-11-92
date

DHA

(Figure 13 shows the results from a preliminary computation which did not take into account the variation of fall-out arrival time.)

Graphic Summary of Fall-out

Along the plot of this displaced track the hundreds of measurements of local dose rates now can be redistributed and joined with isolines in the usual manner. Intuition and artistic impulse clash at this juncture with evidence and statistics.

Two time conventions generally are adopted in fall-out presentation; reduction to D+12 hours, and reduction to D+1 hours (Figure 14).

Dose-rate reduced to D+12 hours predicts less awful results than does that dose rate reduced to D+1 hours, but the first is far more realistic.

Table I

Intensity and Area in Each Contour

Iso-dose Rate Contours at 3 Foot Elevation

Contour No.	Area (Sq. Miles)	Dose Rate	
		At H+12 Hrs.	At H+1 hr. = 22.7×H+12
A	45	80	1820
B	450	60	1360
C	1190	40	910
D	3070	20	450
E	6320	10	230
F	10000	5	115
G	17850	1	25

The iso-dose contours (Figure 15) are more realistic, they imply what exposure would be accumulated by personnel on dry land within 50 hours following a large detonation. The significance of magnitudes such as these are apparent to everyone here.

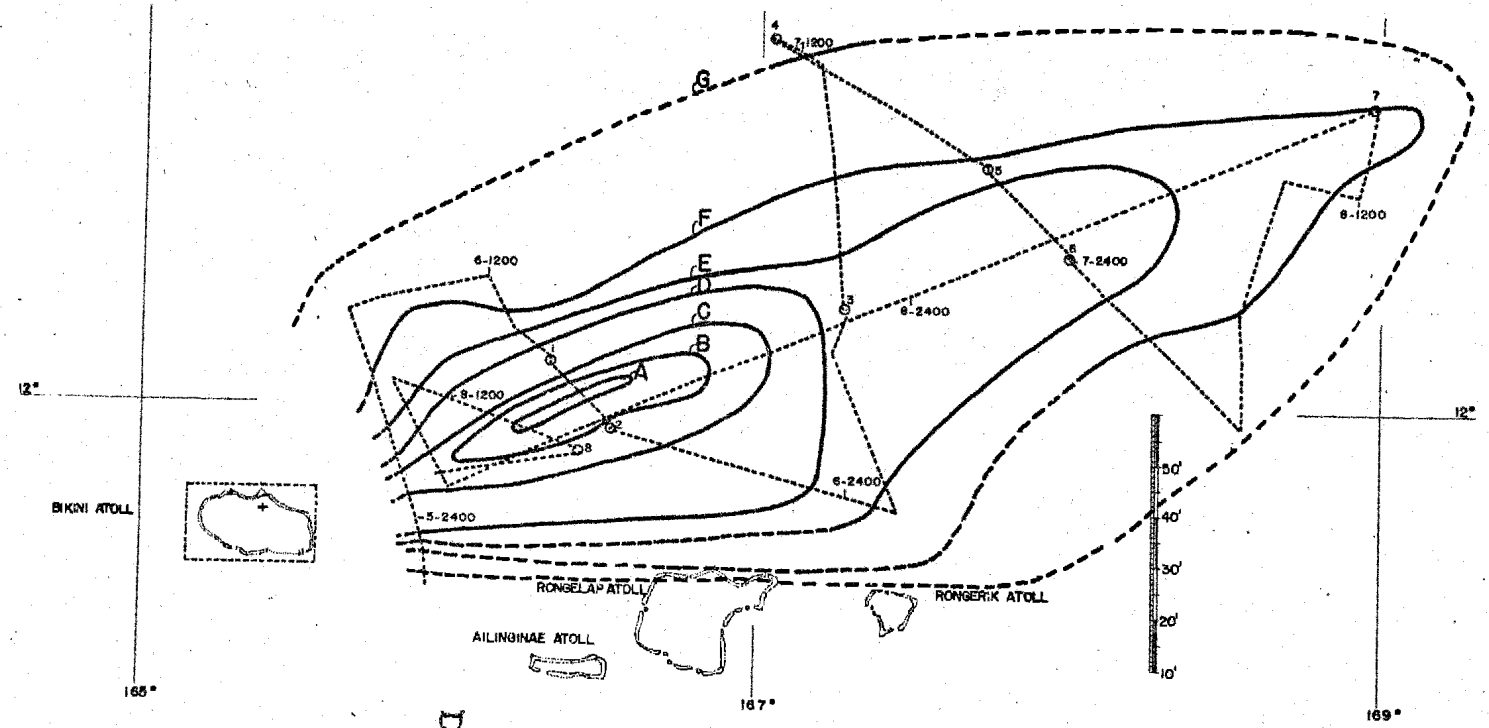

ISO—DOSE—RATE CONTOURS

Figure 14

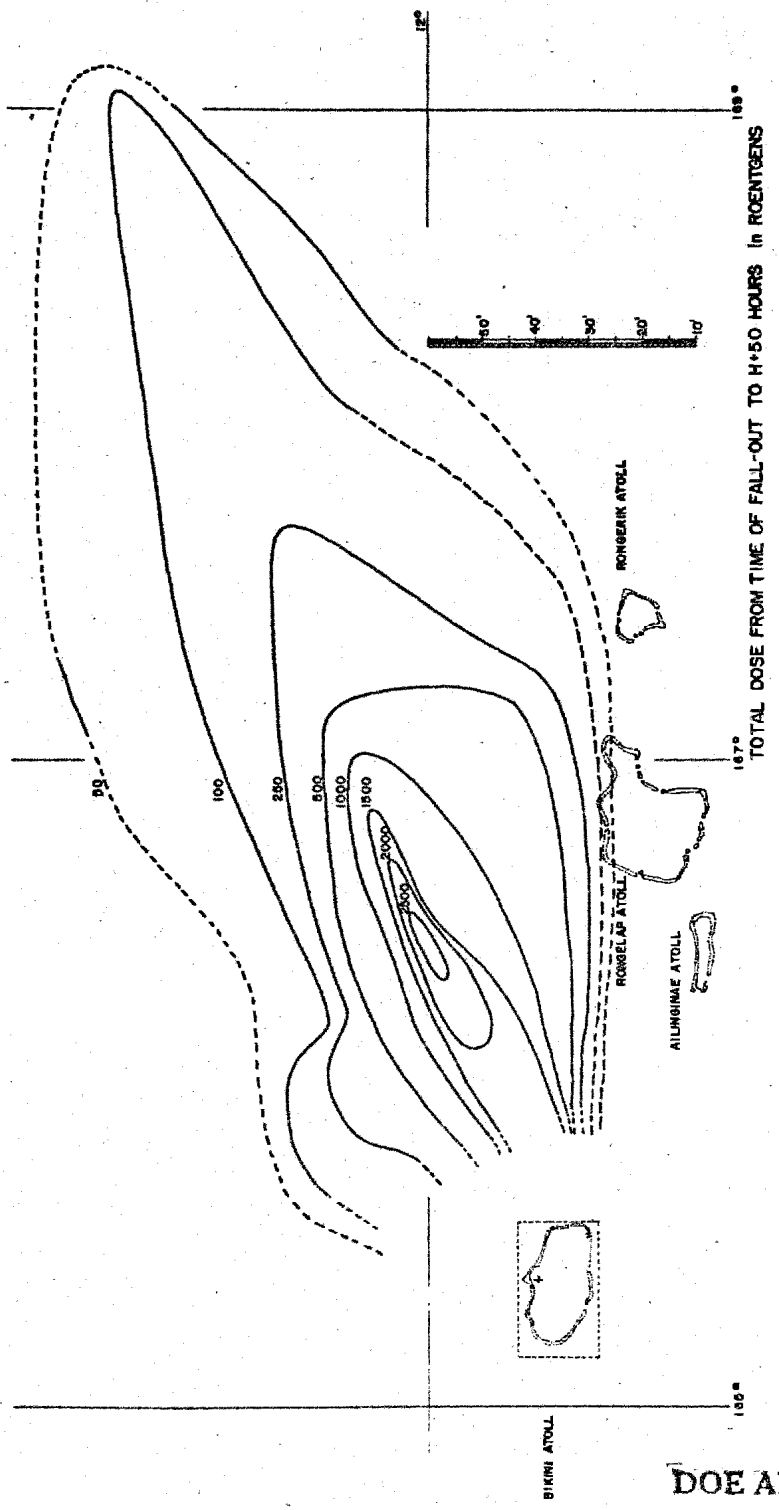

ISO-DOSE CONTOURS

Figure 15

[redacted]

Table II

Total Dose from Fall-out Arrival Until H+50 Hours

Contour No.	Area (Sq. Miles)	Total Dose in R (Shown in Figure Itself)
Innermost	32	2500
-	210	2000
-	610	1500
-	1400	1000
-	3000	500
-	4900	250
-	9350	100
Outermost	14350	50

Discussion of Results

I believe the three accomplishments of this survey are:

Its contribution of a basis for evaluation of a promising method of studying fall-out hazard.

The approximate numerical values representing the extent of contamination from one particularly large weapon.

Some contributions to pure science, for example some actual numerical values of the rate of downward turbulent mixing of the sea - a subject of particular interest to oceanographers.

The first outcome can be amplified a little further. It does appear feasible to use the sea itself as a sampling collector - in fact there does not seem to have been a better collector devised for catching and holding in place an aerosol or fine powder. Meteorologists are aware that no instrument catches snow like a snowfield does. It appears that samples representing many of the more important features of fall-out can be retrieved safely and economically from the sea. And it appears that eventually even such data as the time of arrival of particles at distant surface points may be deduced from oceanographic measurement.

Concerning the numerical fall-out values given here for a particular detonation, little more will be said, except that Dr. Werner of NRDL has recently reported that results of the water sample analyses are in surprising agreement with the direct gamma measurements just described. As to the total energy picture, it just is not

[redacted]

78

[redacted]

fair to expect a single little tug boat to go forth alone and bring home an accurate detailed synoptic picture of <u>any</u> aspect of 10,000 square miles of sea.

Conclusions

In conclusion it would appear that the greatest possible use should be made of the ocean itself during further trials.

[redacted]

[redacted]

THIS PAGE IS BLANK

[redacted]

80

[redacted]

PROJECT 2.7 RADIOLOGICAL ASPECTS, SHOT 6, OPERATION CASTLE

L. B. Werner
U. S. Naval Radiological Defense Laboratory

The method described in this paper constitutes a means of obtaining fall-out data needed for the development and improvement of fall-out models. The method is complementary to that described by Dr. Folsom in an earlier paper and comprises a part of the Operation CASTLE Project 2.7 work. The objective of this work was to determine the dose rate above a plane which had received fall-out. The fall-out was received over wide areas of ocean surface and subsequently was mixed with sea water. The experimental approach was the collection of sea water samples and their subsequent analysis for gamma activity. Other details of the experimental method are described in the paper by Dr. Folsom. The calculation of radiation intensities was comprised of first the determination of the total gamma energy emission rate of fall-out deposited upon the ocean surface and second calculation of the dose rate for a given gamma emission rate. The method for calculating the dose rate has been described by L. D. Gates, Jr. and C. Eisenhauer in AFSWP 502A and 502A Supplement "Spectral Distribution of Gamma Rays Propagated in Air". A summary of the method is given in Tables 1 and 2.

Table 1

Calculate total dose rate d at height x = 3 ft above an infinitely contaminated plane having a total energy emission rate of 1 Mev cm^{-2} min^{-1}

$$d = \sum_i n_i d_i$$

where

d_i = dose rate in Mev cm^{-3} min^{-1} at height x above an infinite plane emitting photons of initial energy E_i isotropically at the rate of 1 photon cm^{-2} min^{-1}

n_i = number of photons cm^{-2} min^{-1}

[redacted]

[redacted] 91

[redacted]

Table 2

$$d = \sum_i n_i d_i$$

$$d_i = \frac{E_i\, h(E_i)}{2} \int_{t_i}^{\infty} \frac{e^{-s}}{s}\, ds \; B_i(t_i)$$

where

E_i = initial photon energy

$h(E_i)$ = "true" linear absorption coefficient for air

$t_i = \mu_i x$

x = 3 ft

μ_i = total linear absorption coefficient for photons of energy E_i

$B_i(t_i) = \frac{1}{1-y_i}$ = build-up factor or ratio of dose from all photons to that from unscattered photons

and

y_i = fraction of dose from source energy E_i, delivered by scattered photons; y_i is obtained from Curve A, Fig 20, AFSWP 502A.

Using this method and gamma spectra supplied by Dr. C. S. Cook of NRDL a calculation of the dose rate produced by a source emitting 1 Mev cm^{-2} min^{-1} is shown in Table 3.

[redacted]

Table 3

Calculation of dose rate d at height x = 3 ft above an infinitely contaminated plane having a total energy emission rate of 1 Mev cm^{-2} min^{-1}

Shot 5 at D + 8 days					Shot 6 at D + 7 days			
E_i	$\frac{n_i}{\sum n_i}$	n_i	$B_i(t_i)$	$n_i d_i \times 10^6$	E_i	$\frac{n_i}{\sum n_i}$	n_i	$n_i d_i \times 10^6$
.05	.261	.760	≈2.5	≈ 7	.05	.271	.796	≈7.3
.15	.245	.713	~1.8	~10.5	.15	.21	.617	~ 9.1
.25	.140	.407	1.55	10.0	.25	.17	.50	12.4
.35	.016	.047	1.45	1.6	.35	.026	.076	2.69
.45	.095	.276	1.40	12.4	.45	.069	.203	9.14
.65	.087	.253	1.33	16.2	.65	.096	.282	18.1
.75	.097	.282	1.31	20.6	.75	.094	.276	20.2
.85	.0135	.039	1.29	3.1	.85	.029	.085	6.96
1.55	.0455	$\frac{.132}{2.91}$	1.20	$\frac{17.3}{98.7}$	1.55	.035	$\frac{.103}{2.94}$	$\frac{13.5}{99.5}$
.344	1.00	2.91	1.45	100	.340	1.00	2.94	100
∴ 1 Mev $cm^{-2}min^{-1}$ gives ∴ 9.37×10^{-8} r/hr					1 Mev $cm^{-2}min^{-1}$ gives 9.45×10^{-8} r/hr			

The calculation of energy emission rate per unit volume of radioactive sea water is demonstrated in following tables.

The gamma energy emission rate of all water samples was inferred from the response produced by the samples in a high efficiency 4 π geometry ionization chamber, the type described by Jones and Overman.

83

[redacted]

Table 4 shows the calculation of the ratio of energy emission rate to the ionization chamber response for an arbitrary 2.22 x 10^6 gamma photons per min, and using spectral data supplied by Dr. Cook.

Table 4

Calculation of Ratio of Energy Emission Rate (Mev/min) to 4π Ionization Chamber Reading (i)

Shot 5 at D + 8 days					Shot 6 at D + 7 days				
E_i	$\frac{n_i}{\sum n_i}$	I_i	$\frac{I_i^{n_i}}{\sum n_i}$	(Mev/min) x 10^{-6}	E_i	$\frac{n_i}{\sum n_i}$	I_i	$\frac{I_i^{n_i}}{\sum n_i}$	(Mev/min) x 10^{-6}
.05	.261	.08	.0209	.0290	.05	.271	.08	.0217	.0301
.15	.245	.12	.0294	.0816	.15	.210	.12	.0252	.0700
.25	.140	.16	.0224	.0777	.25	.170	.16	.0272	.0943
.35	.016	.21	.0034	.0124	.35	.026	.21	.00546	.0202
.45	.095	.25	.0237	.0950	.45	.069	.25	.0172	.0690
.65	.087	.34	.0296	.1254	.65	.096	.34	.0326	.139
.75	.097	.38	.0368	.1614	.75	.094	.38	.0357	.157
.85	.0135	.42	.0057	.0255	.85	.029	.42	.0122	.0547
1.55	.0455	.70	.0318 / .2037	.1565 / .7645	1.55	.035	.70	.0245 / .2176	.120 / .7543
$\frac{(\text{Mev/min})}{I} = \frac{0.7645}{0.2037} \times 10^6 =$ 3.75×10^6					$\frac{(\text{Mev/min})}{I} = \frac{0.7543}{0.20176} =$ 3.74×10^6				

The data in column 3 headed I_i were obtained from a calibration curve determined by W. E. Shelberg. This curve was determined with the use of absolute standards varying in energy from approximately .2 Mev to 2 Mev. In actuality most samples were too low in intensity to permit

[redacted]

84

direct measurement in the 4π ionization chamber. The low activity samples were therefore measured with the use of gamma scintillation counters and converted to equivalent Mev/min according to the method shown in Table 5.

Table 5

Calculation of Ratio of Mev/min emitted by Sampler to Counts/min in the Gamma Scintillation Counter

Five samples of sea water collected following Shot 5 were measured on D + 10 days in both gamma scintillation counter and the 4π ionization chamber:

$$\frac{(I)}{(c/m)} = 1.59 \times 10^{-6}$$

since

$$\frac{(Mev/min)}{I} = 3.75 \times 10^{6}$$

$$(Mev/min) = 5.96 \times (c/m)$$

Finally the dose rate in r/hr at time of analysis of the samples (9 days for Shot 5 and 7 days for Shot 6) was calculated with the relationship summarized in Table 6.

Table 6

Dose Rate at 12 hr in r/hr at height x = 3 ft Above an Infinitely Contaminated Plane - Calculated from Counts $cm^{-3}min^{-1}$ at D + 9 Days

Since $(Mev/min) = 5.96 \times (c/m)$

$1\ Mev\ cm^{-2}\ min^{-1} = 9.41 \times 10^{-8}$ r/hr

$$(r/hr)_{9\ days} = 9.41 \times 10^{-8} \times 5.96 \times (c/m)_{9\ days} \times (cm^{-3}) \times Z$$

where Z = depth (cm) of mixing obtained from graph, time of mixing vs depth of mixing

$$(r/hr)_{12\ hr} = \frac{0.044}{0.00135} (r/hr)_{9\ days}$$

[redacted]

Account has been taken of the depth of the mixed radioactive surface layer of sea water as determined from the curve of time of mixing vs depth of mixing provided earlier by Dr. Folsom. The time of mixing was the difference between the time of sample collection and the time of arrival of fall-out at various distances as estimated by E.A. Schuert of NRDL. The gamma intensity in r/hr at an arbitrary reference time of 12 hours was calculated from the intensity at 9 days by use of the gamma field decay curve as given in the final report of Project 2.5a Operation CASTLE. The iso-intensity contours derived from the data for Shot 6 are shown in Figure 1. The points indicated on the figure represent the position of the sample water at the estimated time of arrival of fall-out. The areas inclosed by various dose rate contours are shown in Table 7.

Table 7

Areas Inclosed by Various Dose-Rate Contours at 12 hrs - Shot 6

Dose Rate	Area (sq mi (stat.))
50	60
40	200
30	550
20	1600
10	3500
5	5250
1	7750

Some estimate of the reliability of the method is provided by the qualitative comparison of contours with aerial survey data kindly provided us by Mr. Levine, Head of Instrumentation Branch, NYOO, as shown in Figure 2. An indication of the precision of the method is provided by the comparison shown in Table 8.

[redacted]

[redacted]

86

[redacted]

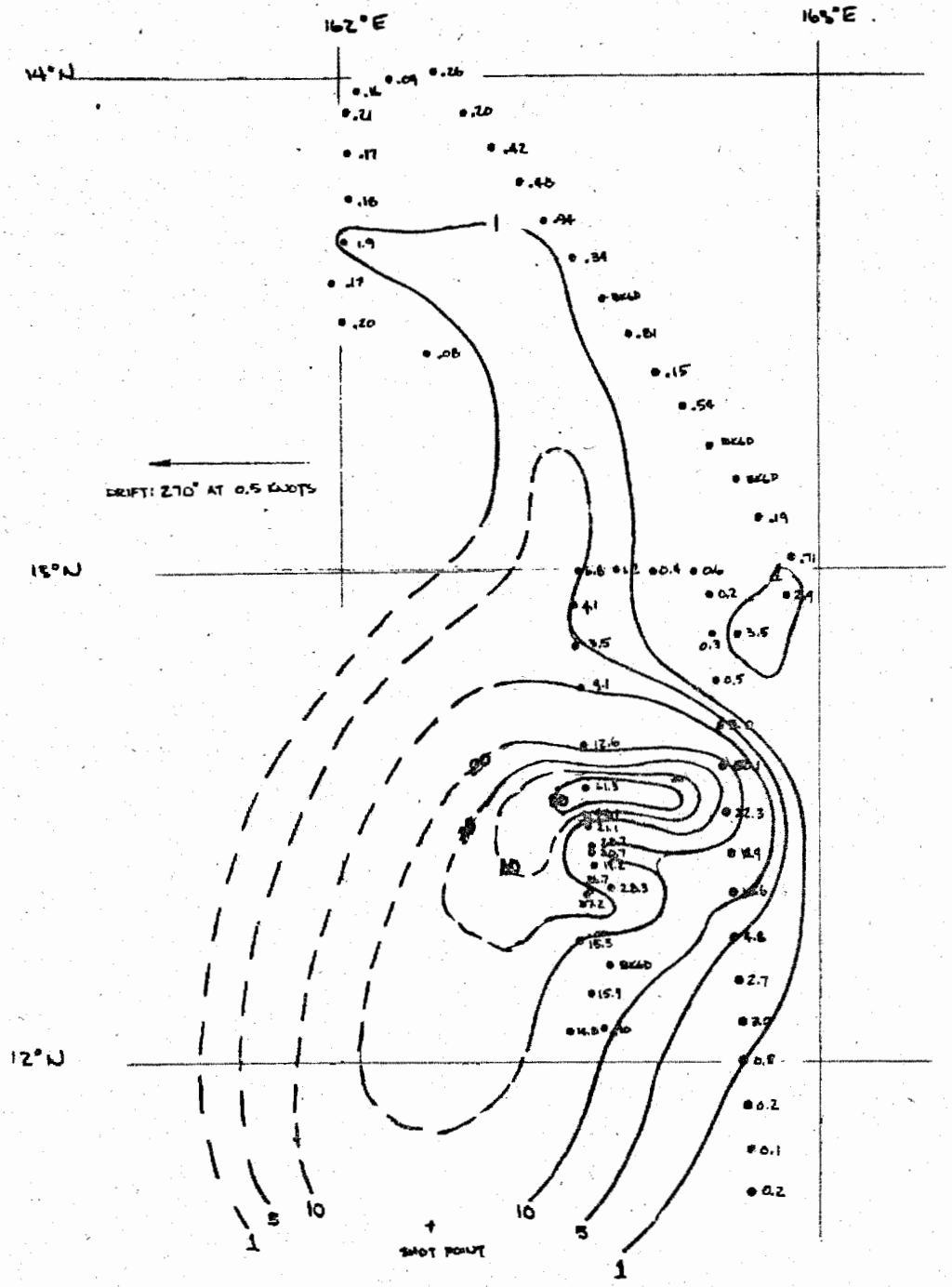

SHOT 6 FALLOUT PATTERN

RADIATION LEVELS IN R/HR AT D+12 HOURS

• DENOTES SAMPLE POSITION AT MEAN ARRIVAL TIME

Figure 1
Shot 6 Fall-out Pattern

[redacted]

[redacted]

87

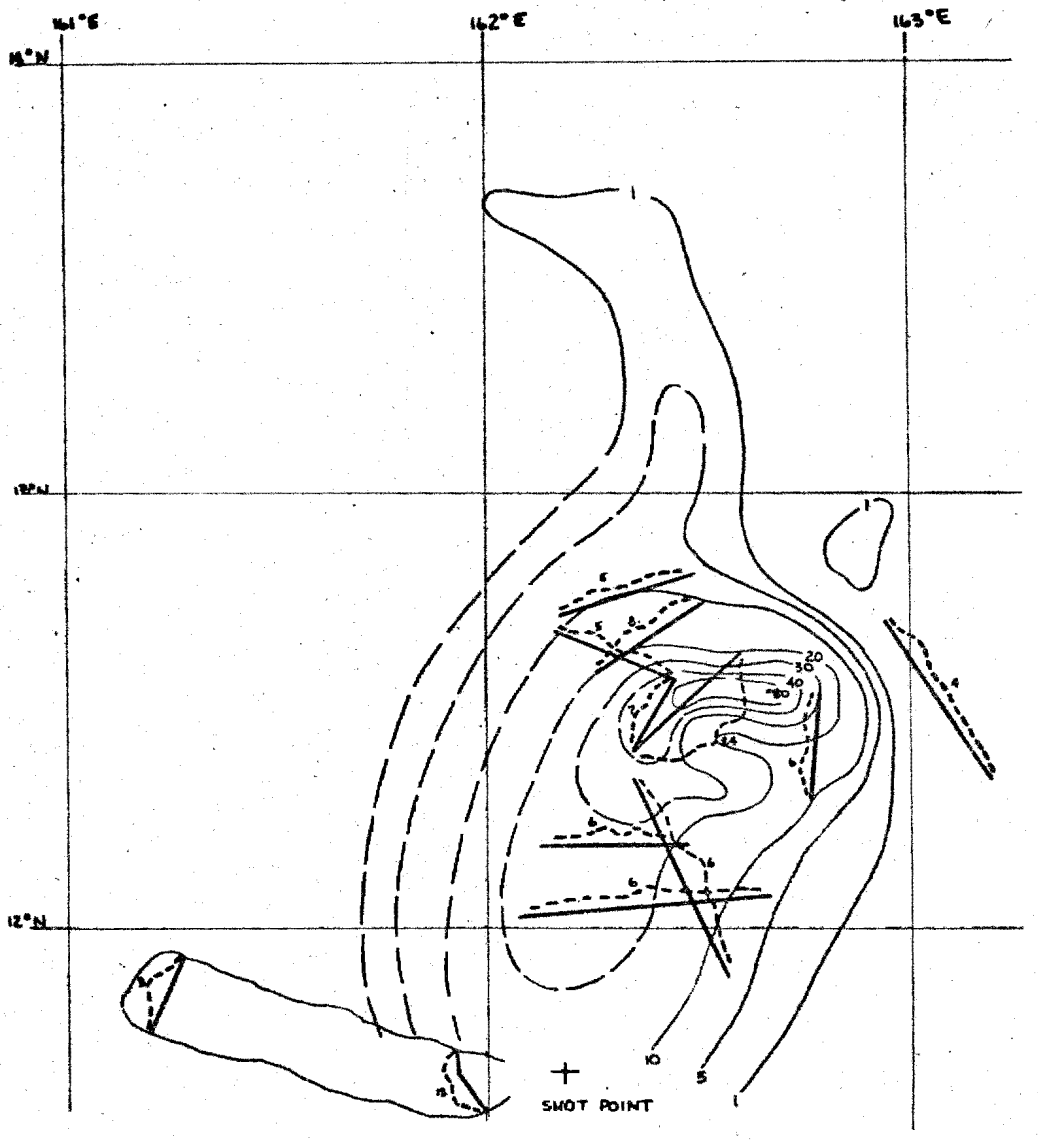

SHOT 6 DOSE RATE CONTOURS AT 0412 HRS.

QUALITATIVE COMPARISON OF AERIAL SURVEY WITH WATER SAMPLING RESULTS

Figure 2
Shot 6 Dose Rate Contours at 0412 hrs.

[redacted]

Table 8

Comparison of Shot 5 Gamma Field Intensities at 12 hr as Calculated from (1) Towed Probe Data; (2) Water Analysis Data; (3) Water Analysis Data and Observed Ratio of Field Gamma Intensities to Radioactivity Per Unit Area (CASTLE Project 2.5a) r/hr

Station	1	2	3
1	23	43	25
Surface	64	63	37
Surface	77	60	36
2	35	26	15
Surface	9.5	2.6	1.6
3	13	15	8.8
4	1.5	2.0	1.2
Surface	2.9	2.3	1.8
5	7.5	3.9	2.3
6	6.4	4.8	2.8
Surface	2.9	0.37	.22
Surface	18	15	8.6
Surface	8	4.9	2.7
Surface	18	16	9.3
Surface	6.1	4.2	2.5
Surface	4.5	1.8	1.1
Surface	15	11	6.7
7	8.9	6.1	3.6
Surface	38	57	34
Surface	11	13	7.9
Surface	43	56	33
Surface	7.6	9.2	5.4
8	42	52	31

Column one gives the field intensity as calculated from data taken with the towed probe as described by Dr. Folsom. The second column presents field intensity calculations from water analysis data as described in this paper. The third column presents field intensity calculations from the activity per unit area as derived from the water analysis data, and application of an observed ratio of field gamma intensity to radioactivity per unit area as presented in the CASTLE project 2.5a report. A ratio of 1:1 was considered to be most appropriate for this calculation. A third estimate of the reliability of the method is given by calculation of the fraction of the total

[redacted]

89

[redacted]

activity produced by the detonation which can be accounted for in fall-out.

DELETED

[redacted]

90

[redacted]

DELETED

In future operations it is apparent that far better supplementary data will be needed to improve the reliability of the calculations by this method. Such data must include (a) gamma spectra, (b) decay data both for source material and gamma fields, (c) characterization of the properties of fall-out throughout the area especially physical properties, (d) time of arrival data (e) careful measurement of gamma radiation fields produced on land areas and correlation of the fall-out area by unit area and correlation of the fall-out activity per unit area.

As the 2.7 Project was initiated and undertaken under the stress of actual participation in Operation CASTLE much of the necessary supplementary information had to be approximated. Nevertheless although the project was initially conceived as a feasibility study it has gone far beyond the original expectations and has produced valuable estimates of the actual radiological conditions produced by Shots 5 and 6.

For maximum effectiveness future operations should combine technique of rapid aerial synoptic survey, (2) rapid survey by multiple naval units with frequent correlation between ship and aerial measurements (3) sea water collection, (4) rall-out collections especially for detonations producing large particle fall-out and (5) thorough oceanographic characterization of the expected fall-out areas.

It is essential that for full utilization of the above technique planning for field operations scheduled for 1956 should be started immediately.

[redacted]

[redacted] 91

[redacted]

THIS PAGE IS BLANK

[redacted]

[redacted]

[redacted]

PROJECT 9.1 (CLOUD PHOTOGRAPHY RESULTS), OPERATION CASTLE

Lt. Col. Jack G. James
Directorate of Weapons Effects Tests

Project 9.1, Cloud Photography, Operation CASTLE, was conducted on all shots. The purpose of this experiment was to determine the dimensions and altitude of each nuclear cloud as a function of time. Primary interest lies in the early stage during which the cloud rises to maximum altitude. Secondary interest is in the intermediate interval during which the cloud extends to its maximum diameter at the stabilized altitude. The late stages during which the cloud begins to disperse receives attention, also, but to a lesser extent than the first two stages of interest. The photographic method of recording this phenomena was chosen in view of its ability to record permanently and for leisurely analysis, every visible detail of the cloud at any desired time. The extreme large dimensions of the CASTLE clouds dictated the placement of cameras at considerable distances from ground zero. The use of aircraft as camera platforms was decided on in lieu of ground stations due to the geographic locations of suitable atolls and the probability of natural cloud cover obscuring the field of view. Several aircraft were required for the purposes of triangulating on the nuclear cloud to determine its position and to provide insurance against failure of any one station procuring satisfactory data. I think it would be of interest to most of you to know something of the operational plan in order that you may better understand the results obtained on this project.

Four aircraft were used; one RB-36 operating at 40,000 feet, and three C-54's working at 10,000-14,000 feet. The planes were forty to one hundred miles from ground zero, usually at the fifty mile range. Aerial cameras were installed on A-28 Stabilized Mounts and operated by the Lookout Mountain Laboratory, U. S. Air Force. Photographs were taken of the visible cloud, from several directions, as a function of time. Supporting data was photographed automatically, and the aircraft furnished navigation logs to document the ship's position at every instant. These logs were rather less complete and less accurate than had been expected; this is attributed primarily to the heavy load the crew members had to carry in flying the ships under unaccustomed conditions.

All four ships flew in every shot. Of the twenty-four missions, six were spoiled because of interference by natural clouds. Four of these were on Shot No. 3 which was fired under such bad weather conditions that, to the best of our knowledge, no decent photographs of any sort were taken from the ground or from the air.

[redacted]

[redacted]

93

[redacted]

The data obtained are more complete and more accurate than any obtained on previous operations. Good measurements of cloud height and diameter over a ten-minute interval have been worked up by Edgerton, Germeshausen and Grier, Inc. for the five shots which were photographed. It has been found possible to apply suitable corrections for the effects of earth curvature and atmospheric refraction, for the slight tilt of the camera platform, and for the altitude of the plane. The resulting data agree quite well from one plane to the other, and it has been possible to assign smaller uncertainty to the results than had been anticipated. Unfortunately, it has not been possible to evaluate the few data taken more than ten minutes after detonation.

On previous atomic tests, all cloud measurements were taken with ground-based cameras until Operation IVY when the first attempt was made at aerial documentation. The data obtained was far from perfect, but provided invaluable experience in planning the CASTLE program, and, as it turns out, the same statement can be made concerning the CASTLE results. Although the CASTLE data is incomplete, it is the best yet obtained and experience gained has shown us many ways in which our operation could have been improved. The original CASTLE 9.1 plan called for four high-altitude long-range aircraft; namely, RB-36 airplanes, but due to lack of parking space and a number of other factors, the cloud photography aircraft necessarily had to be shared with other participating projects.

Each plane was equipped with a type A-28 Automatic Stabilized Mount, which carried one modified K-17C camera and one 35mm Eclair motion picture camera. The 35mm cameras were intended to operate at about one frame per second, to document the rapid rise of the cloud during the first five minutes or so. They were equipped with timing clocks. The K-17C cameras were provided with special shutters, to permit long exposures under dim lighting conditions, and were planned to take three photographs every minute during the early stages, and to drop back to a slower schedule later on. The K-17C cameras were provided with data recording chambers to record: (a) the time at which each frame was exposed, (b) aiming of the camera by means of a gyro-controlled compass card, and (c) tilt of the stabilized platform by means of a bubble-level.

One installation was placed in the RB-36 aircraft, which was flown at about 40,000 feet on every shot. This plane was available to Program 9.1 for only the first ten minutes after detonation.

Similar installations were made in three C-54 aircraft, which flew at 10,000-14,000 feet for each shot. These planes were available for an hour or more, and were shared with Task Unit 9.

[redacted]

[redacted]

The original plan called for placement of all planes in the two western quadrants to permit photography of the cloud silhouette against the dimly illuminated eastern sky. Distances and lenses were specified to cover a field of view approximately 150,000 feet high and 350,000 feet across in the vertical plane at ground zero. This requirement was based on observations taken at IVY.

The ship's navigator was requested to supply information as to the distance and bearing to ground zero every minute, together with supplementary data on the plane's heading, course and speed.

Although the schedule was tight, all equipment was installed and trial runs were made before leaving the States. These runs were apparently satisfactory. Trial runs were also made in the forward area, with the primary object the determination of the pre-dawn sky light-levels. It was found that the available light was marginally weak, but still exceeded pessimistic expectations.

The plan of operation is relatively simple in principle, but success depends upon good luck as well as on proper functioning of individuals and equipment. Serious loss of data or even complete failure of the mission can result from the failure of a single link in the chain. For example, incomplete navigation data can spoil an otherwise perfect set of films. On the other hand, failure of a clock or of a shutter or of a power source is equally ruinous.

For those of you who are interested in the method of analysis employed by Edgerton, Germeshausen and Grier, Inc., I suggest you obtain a copy of the 9.1 preliminary report which outlines the analysis method in detail. Time does not permit discussion of each event and the results obtained from the photographs; consequently, I have chosen a few selected photographs made from the RB-36 on Shot 5 (Yankee). These pictures have been reduced to 35mm slide size from 9x9 inch serial negatives made with the K-17C camera and are fairly representative of the photography obtained on this project.

Figure 1 - This is zero time, Yankee event, 6:10 A.M. You will notice at the bottom of the picture the three recording instruments which were built into the cameras. The instrument on the left is the clock time, in the center is the tilt reading, and on the right the azimuth reading. These recording chambers operated very satisfactorily except in cases where the cameraman put the cameras on runaway; thus causing a vibration which made it almost impossible to read the instruments.

Figure 2 - There has been a period here of thirty seconds where the bomb light was too intense to record any rate of rise activity with the K-17 cameras.

[redacted]

[redacted]

95

[redacted]

Figure 3 - The time here is 32 seconds after zero and the cloud has reached an altitude of roughly 23,000 feet.

Figure 4 - The time here is 37 seconds after zero and you can note here the shock wave moving out across the lagoon.

Figure 5 - The time here is 41 seconds after zero and the top of the cloud at this point has reached approximately 32,000 feet.

Figure 6 - The cloud is still rising very rapidly and you can still note the shock wave in the lower right through the break in the natural cloud cover.

Figure 7 - The time here is 45 seconds after detonation and we are just at this time commencing to lose some of the extreme brilliance from the fireball.

Figure 8 - There has been a time lag here of about two minutes due to inadequate light conditions to photograph the cloud. As the cloud reaches these high-altitudes, we are able, through long exposures, to obtain reasonably good photography.

Figure 9 - The cloud is still rising quite rapidly and the characteristic skirts are forming over the stem. The white spot in the lower center foreground has nothing to do with the cloud phenomena. It is believed to be a light leak in the recording chamber.

Figure 10 - As the cloud increases in height, our chances for good photography are increased as the early dawn light is increasing rapidly at this time.

Figure 11 - Although it was not intended to do stereo pairs in this experiment, we have found that photographs, such as Figure 11, when matched under a stereoscope with a preceding picture, frequently give reasonably good stereo effects.

Figure 12 - The cloud is becoming fairly well stabilized at this time which is 4 minutes after detonation and the preliminary measurements show the top of the cloud to be at approximately 110,000 ft.

Figure 13 - We are now 4½ minutes after zero and the diameter of the cloud is extending very rapidly.

Figure 14 - At 5 minutes after zero, the cameraman is beginning to experience difficulty keeping the cloud within the camera's field of view.

[redacted]

[redacted] ENERGY ACT

[redacted]

Figure 15 - At 5 minutes and 25 seconds, the cameraman generally had to resort to switching the camera from a fixed position to a left and then to a right view. This was done in order to give Edgerton, Germeshausen and Grier, Inc. an opportunity to measure the cloud diameters on every other photograph.

Figure 16 - We are coming up on 10 minutes after zero time in this photograph. Light conditions have improved considerably and we are beginning to record detail in what remains of the stem. At about the 10 minute period, the CASTLE clouds completely outgrew the capability of the cameras in all four aircraft. The solution to this problem, of course, is very simple; to conduct accurate cloud measurements by aerial photography. It is absolutely essential that the aircraft be positioned at altitudes of 30,000 feet or higher and on anything in the megaton yield range aircraft should be located at a minimum of seventy nautical miles from ground zero. On this particular event that you have just seen on the screen, the cloud reached an altitude of 44,000 feet in one minute and a diameter of 34,000 feet in one minute. The maximum altitude was measured at 110,000 feet and a spread in diameter to 270,000 feet.

Figure 17 - This is a chart taken from the preliminary report which shows you a summary of the cloud parameters in thousands of feet. This is for all CASTLE shots except Shot 3 which, as I mentioned before, was obscured by natural cloud cover. For comparison purposes, the IVY-MIKE and IVY-KING shots are included.

In conclusion, it is believed that the basic plan used during Operation CASTLE is the correct one to use and that on future operations improvements can be achieved through careful attention to details rather than by drastically altering the method of operation. For continental tests, ground-based cameras will give the best results, but for Pacific operations, high-altitude aircraft is the only presently known method of accurately recording cloud phenomena. We believe that in future Pacific tests, the program should provide automatic means of recording every bit of information it needs without too much reliance on the aircraft crew; for example, it is essential to know aircraft position, altitude, course, attitude, air speed and ground speed, also, the camera parameters such as aiming, timing, aperture and shutter settings. Judgment is sometimes impaired while working at high-altitudes and the photography interval program should not be placed at the discretion of the operator. We firmly believe that the photographer must be free of as many manual duties as possible. He should not have too many cameras to operate and the controls should be simple, clearly labeled, and as automatic as possible. In fact, the camera installation should try and do the cameraman out of his job. If he has nothing to do except check for malfunctions, the probability of success on the mission should be very high. If and when we are called upon again to conduct a cloud photography program, I can assure you the lessons learned on CASTLE will be of tremendous value to us in planning and instrumenting on any future test series.

[redacted]

[redacted]

[redacted]

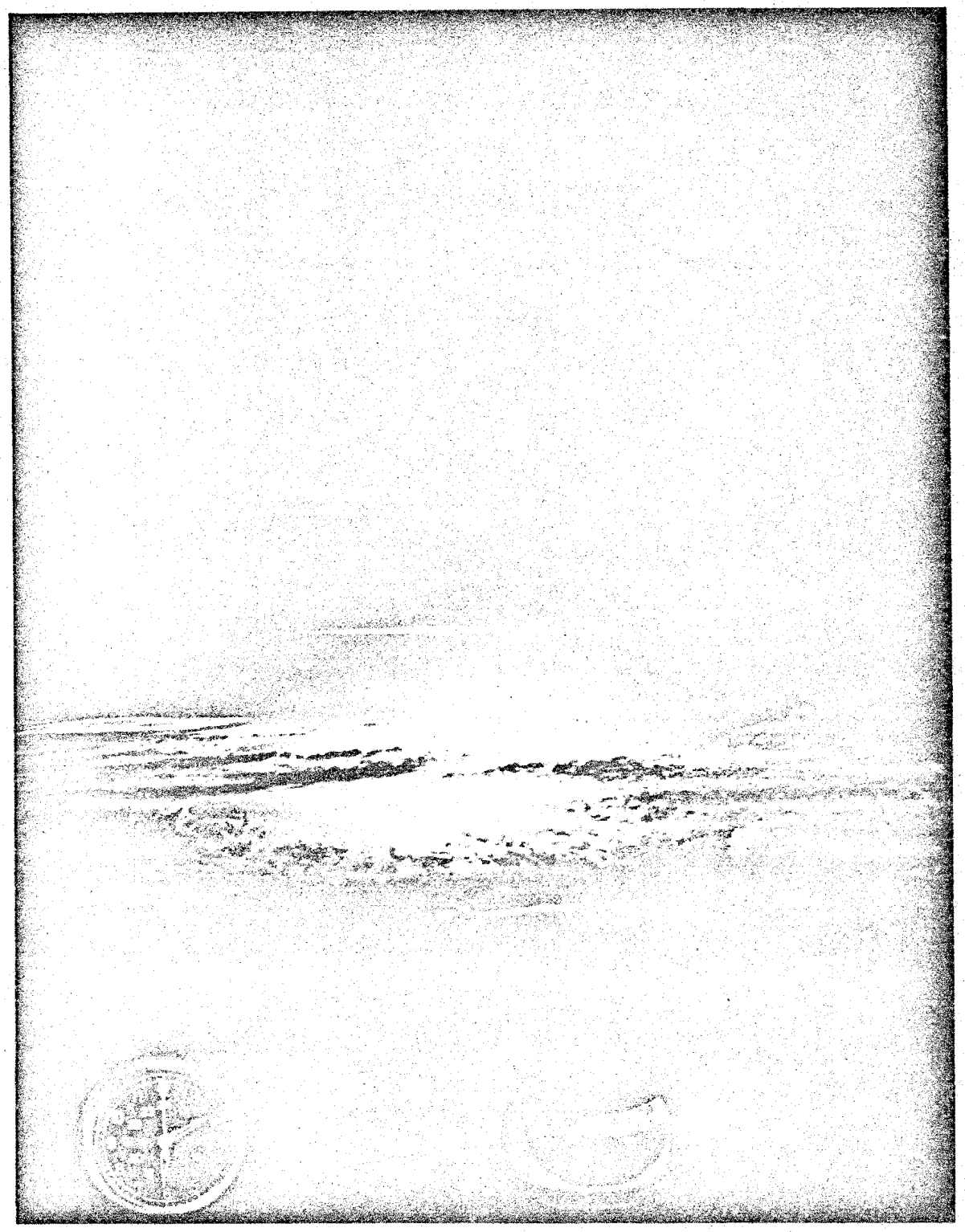

Figure 1
94

[redacted]

[redacted]

[redacted]

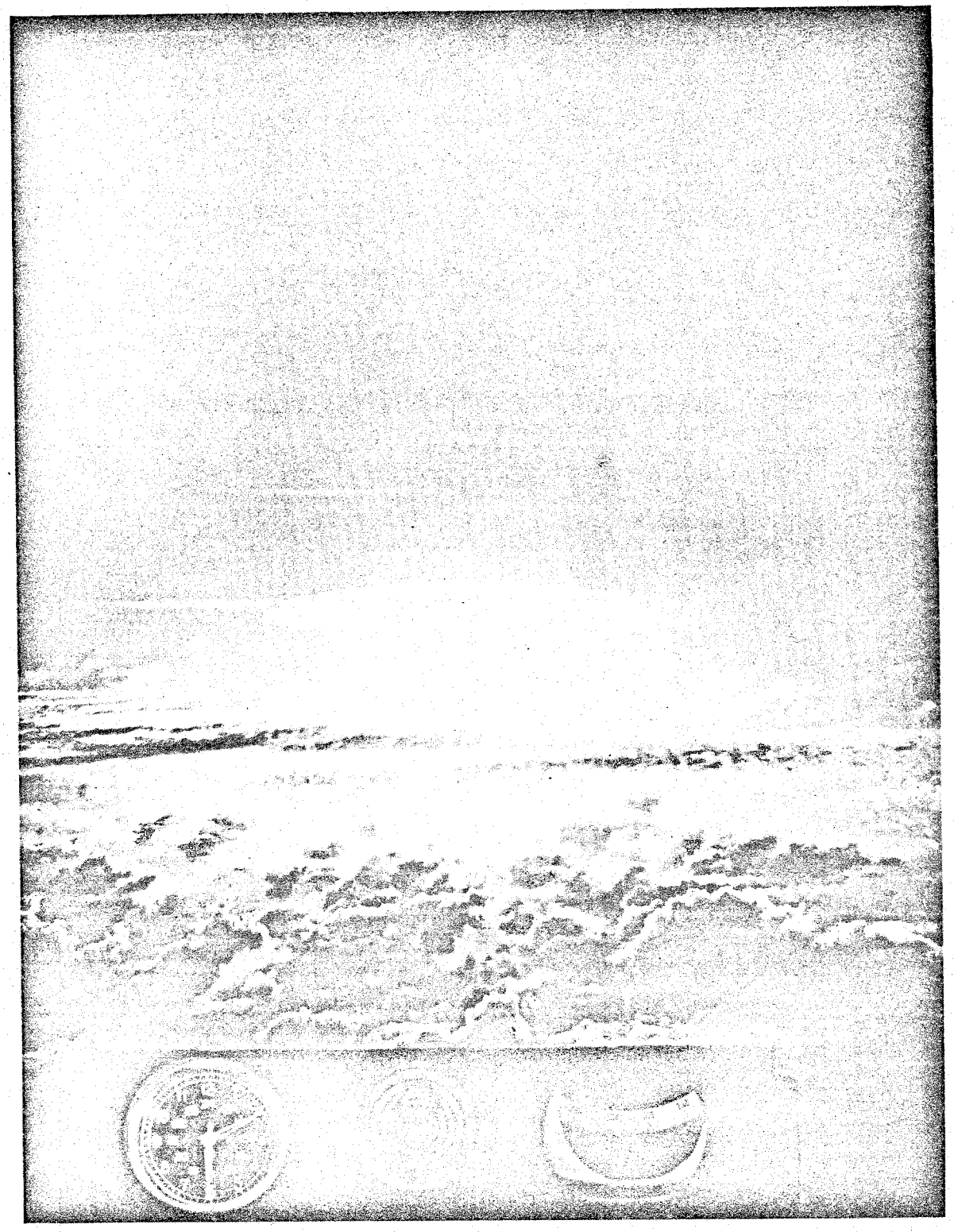

Figure 2

[redacted]

[redacted] DATA
[redacted] OMIC ENERGY AC[redacted]4

[redacted]

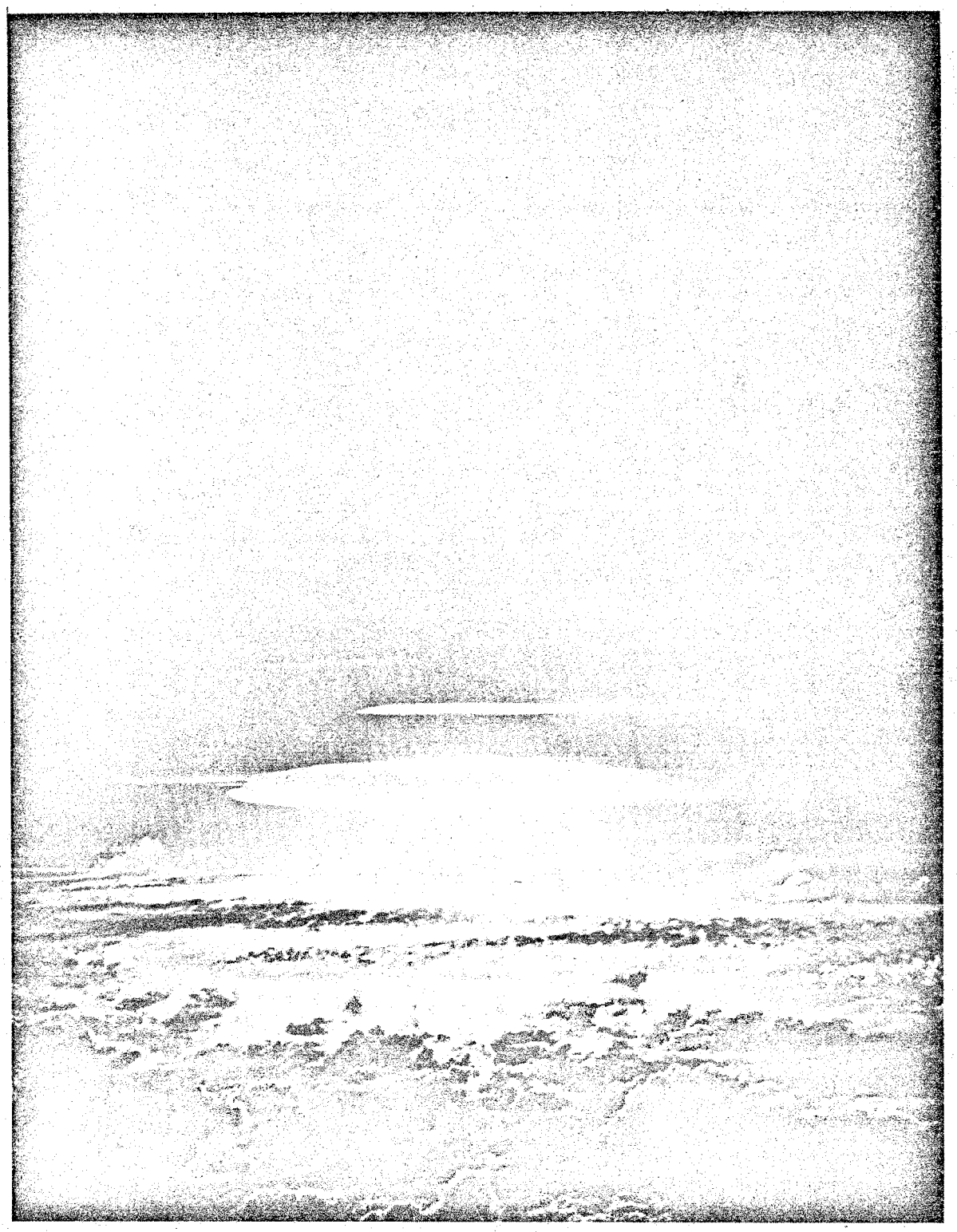

Figure 3

[redacted]

[redacted]

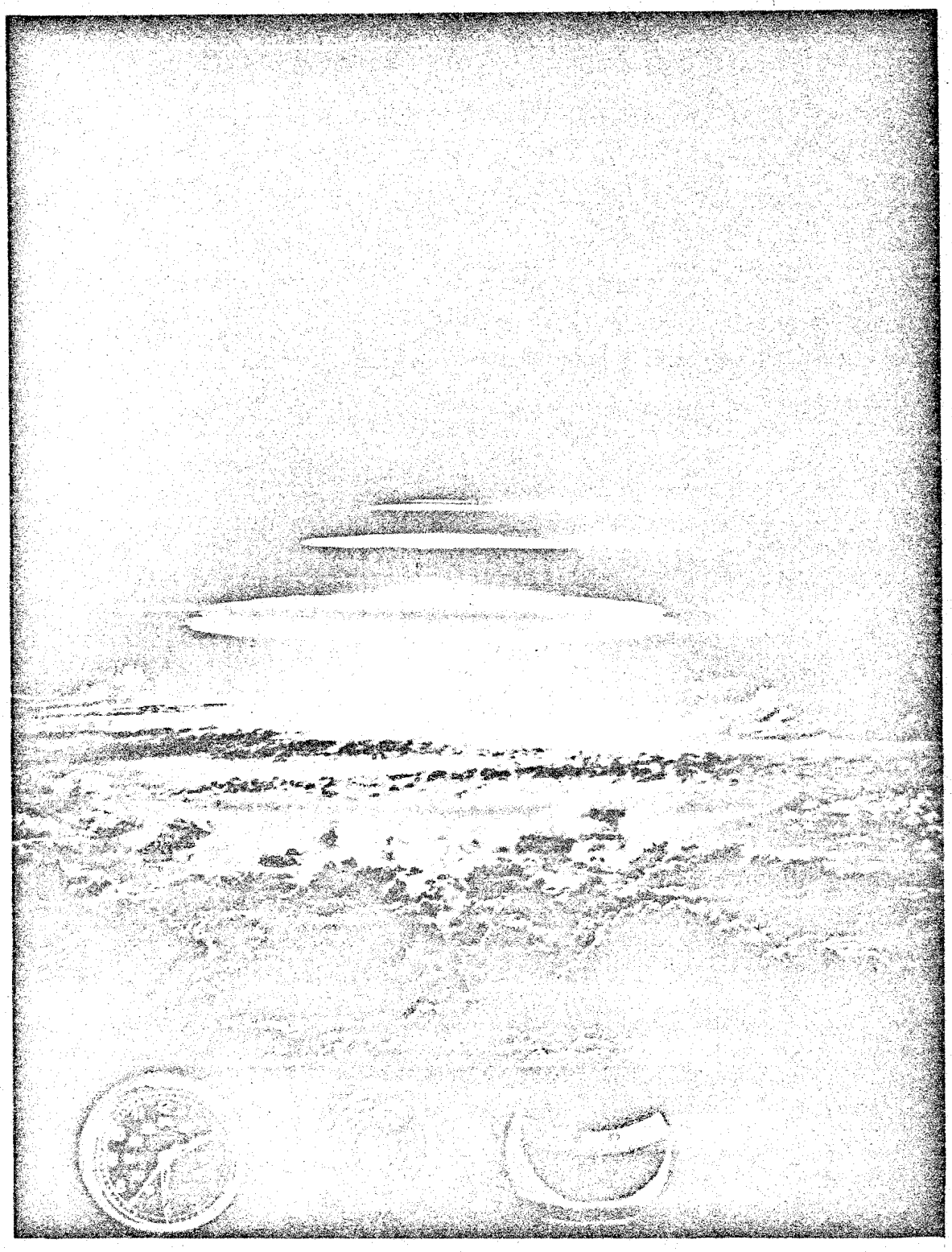

Figure 4

[redacted]

[redacted]

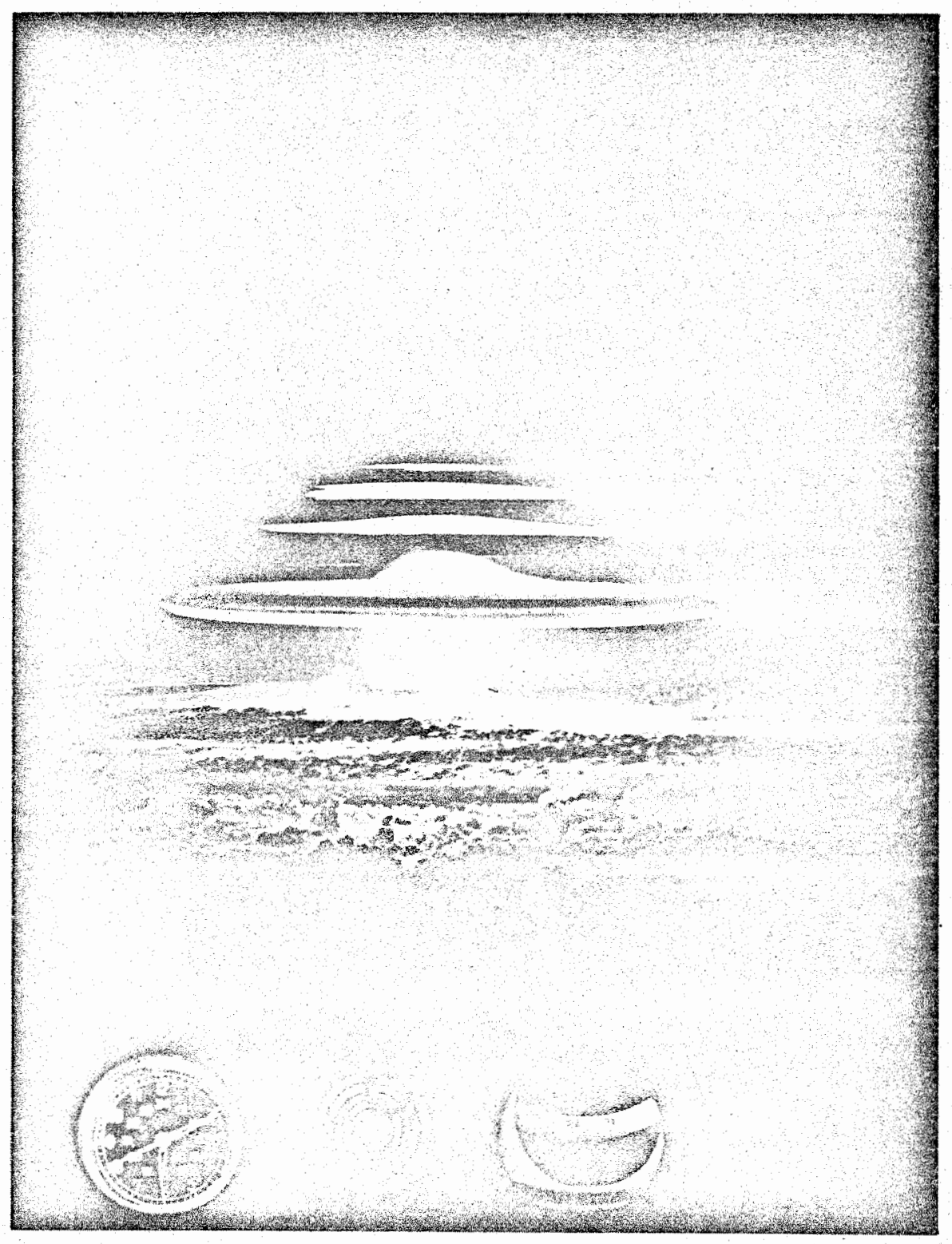

Figure 5
98

[redacted]

[redacted]

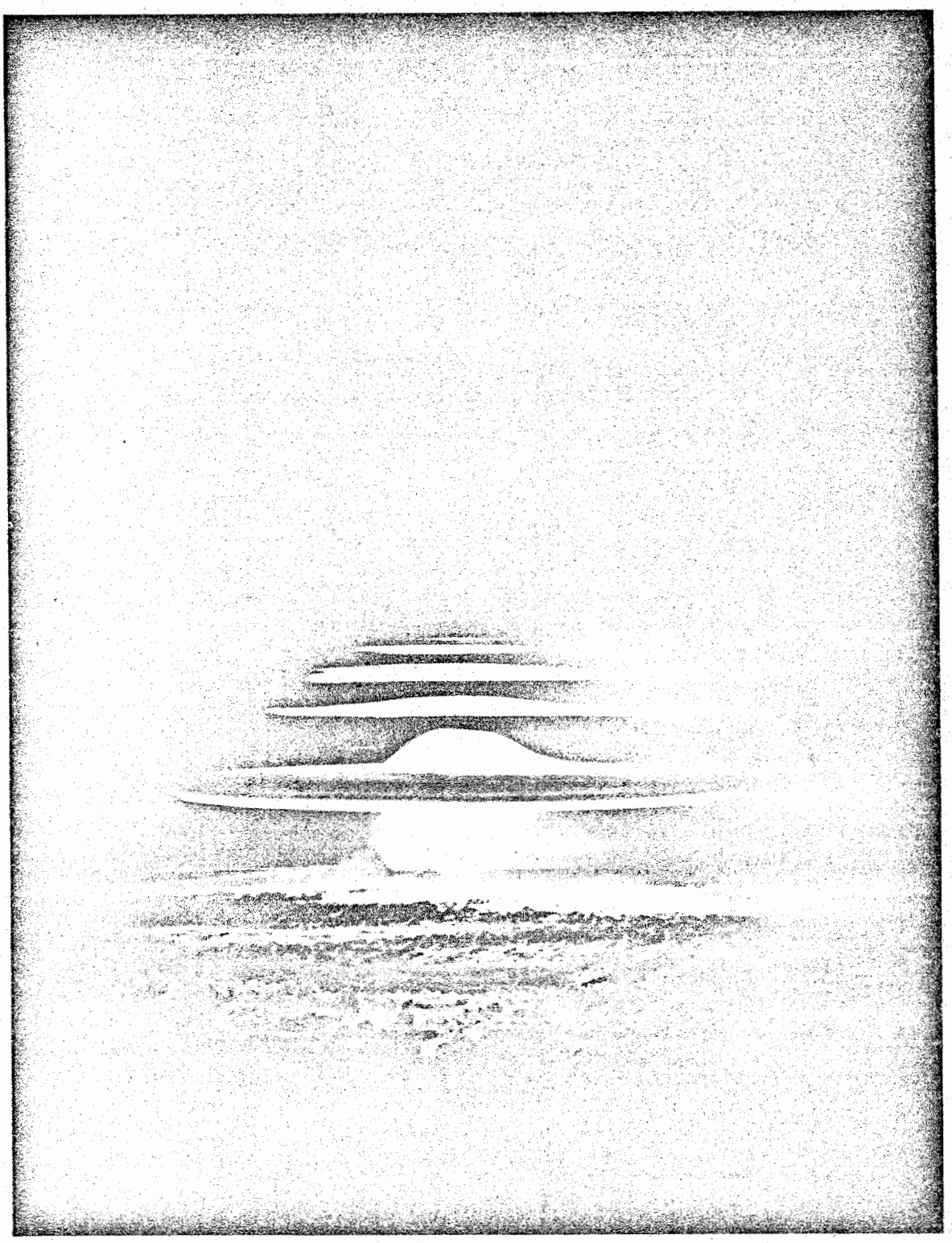

Figure 6

[redacted]

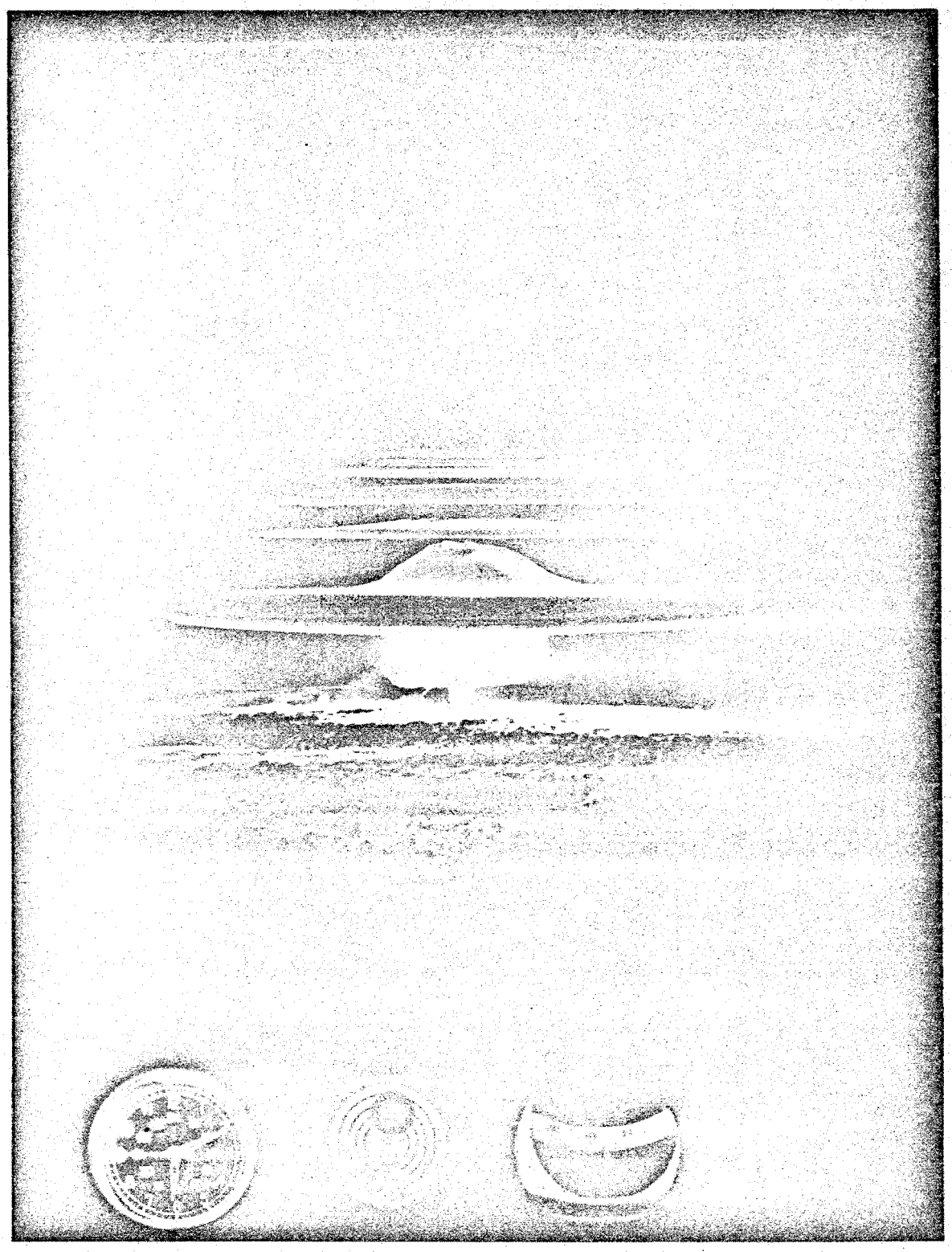

Figure 7

[redacted]

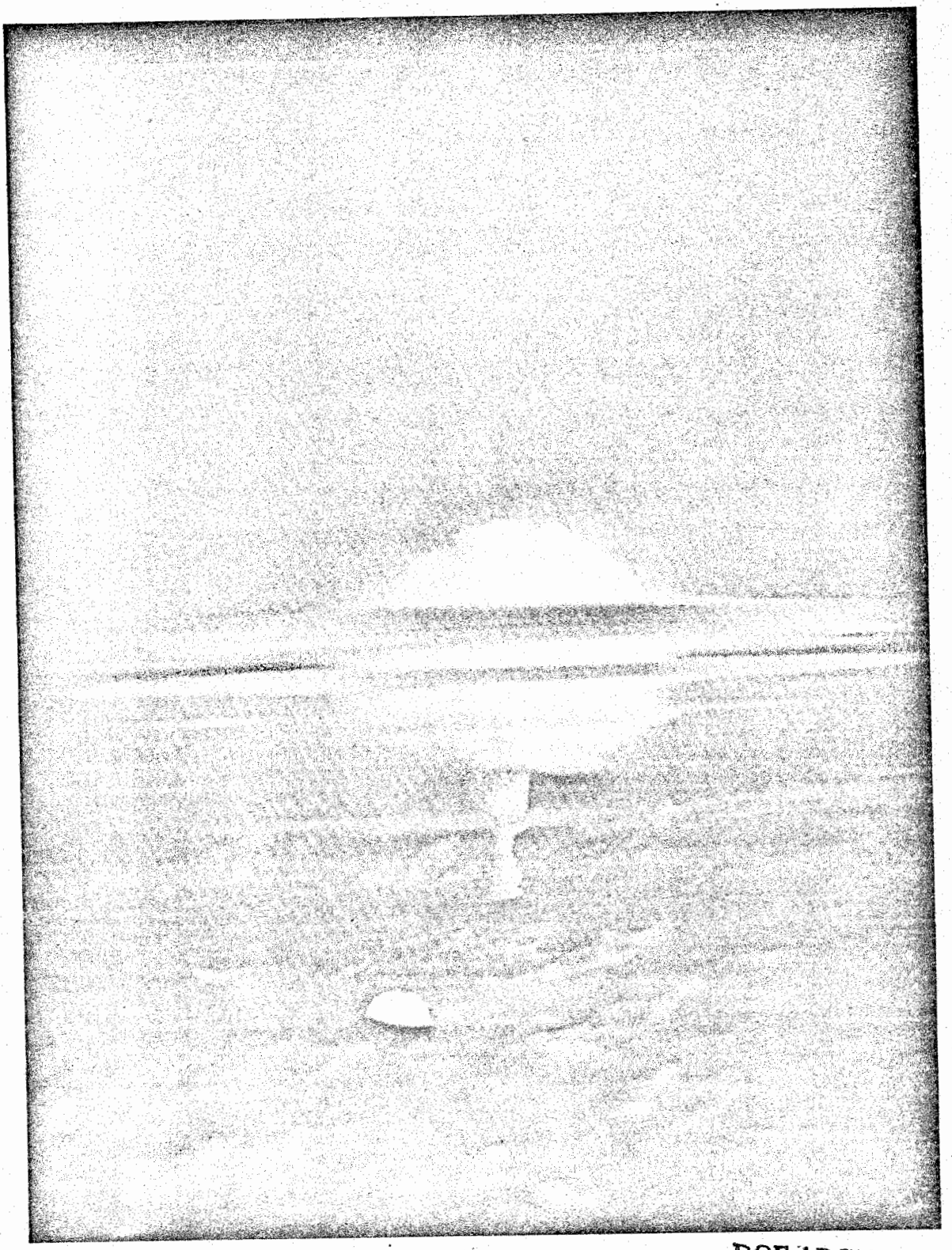

Figure 8

[redacted]

[redacted]

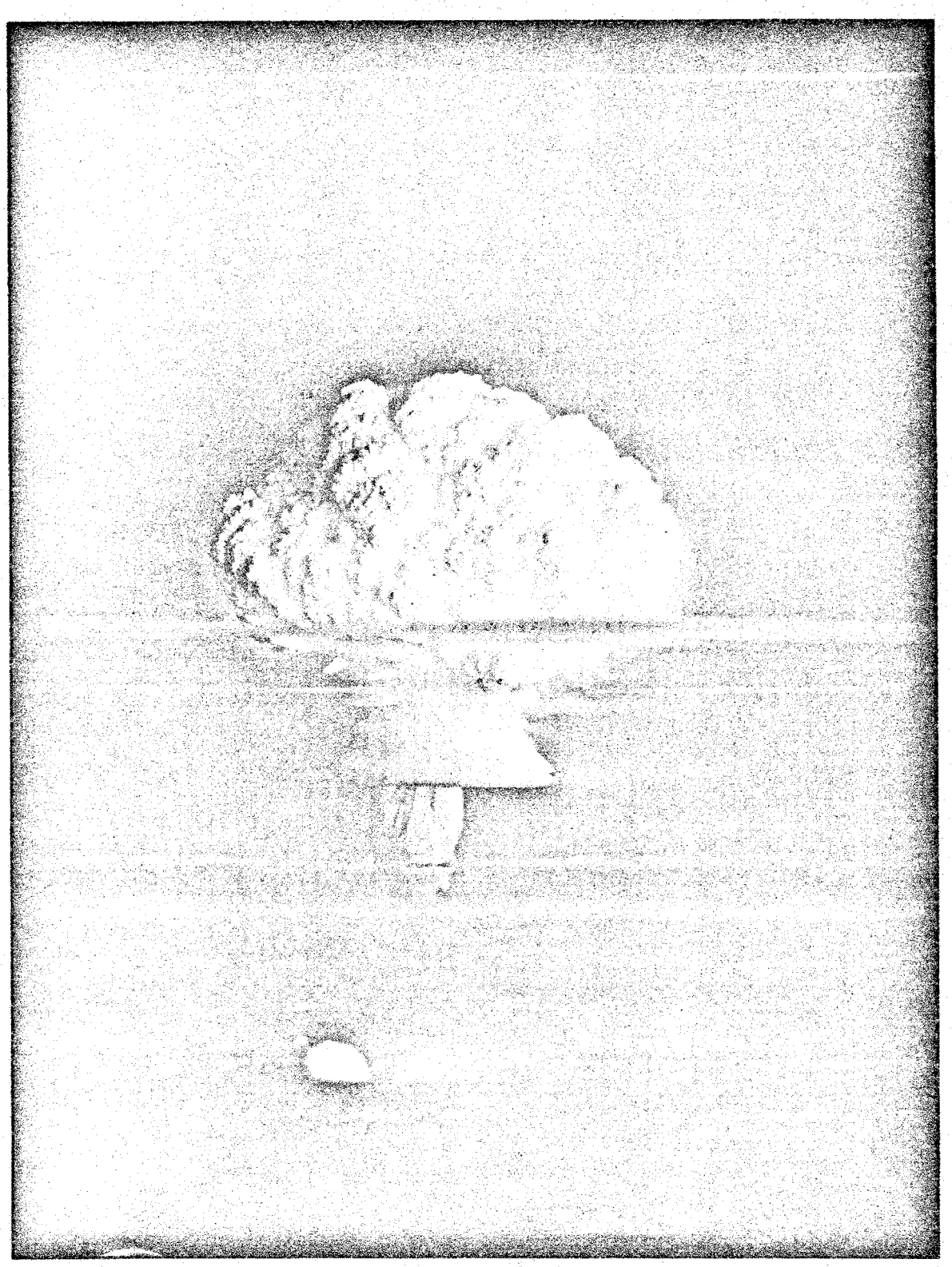

Figure 9

[redacted]

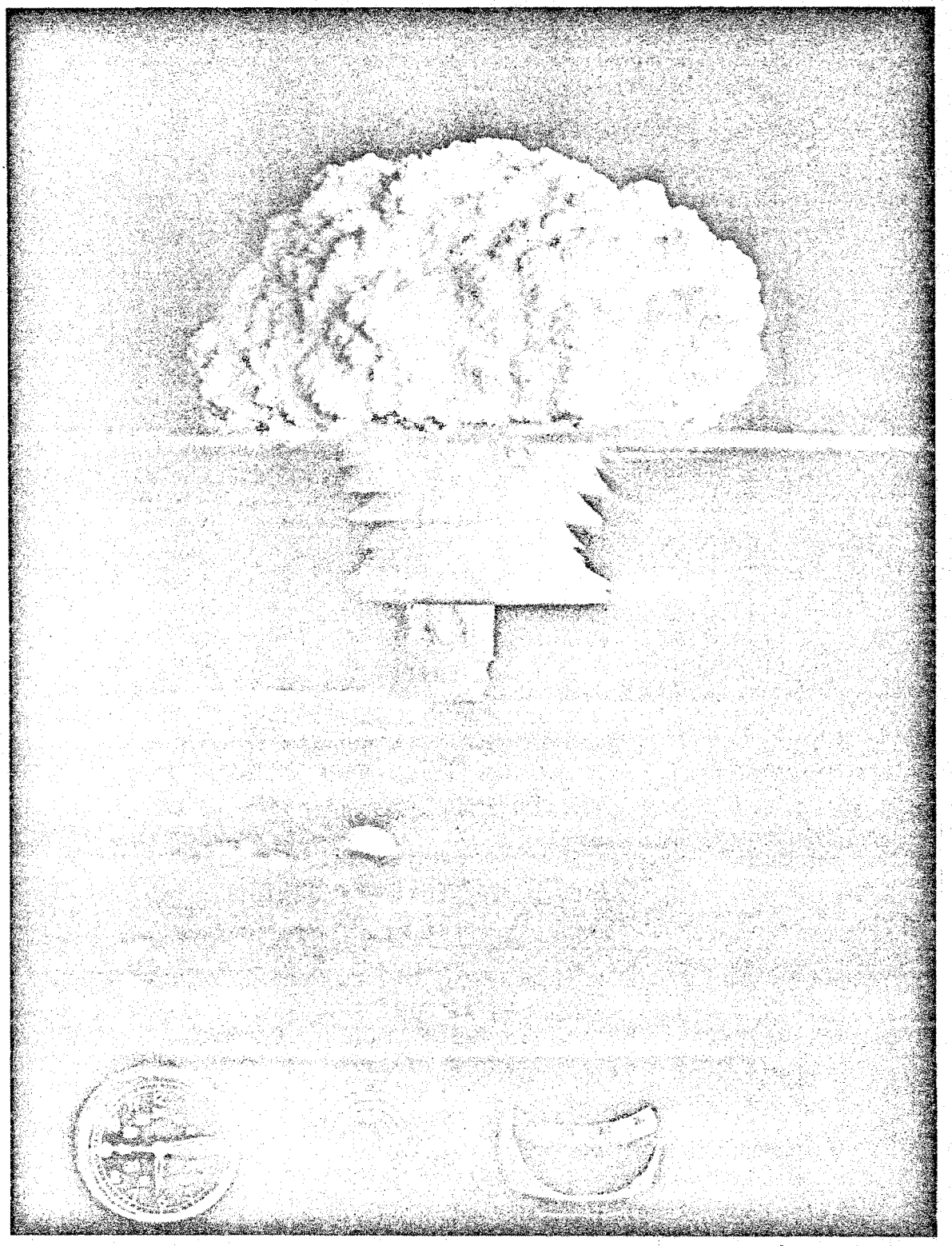

Figure 10

[redacted]

[redacted]

107

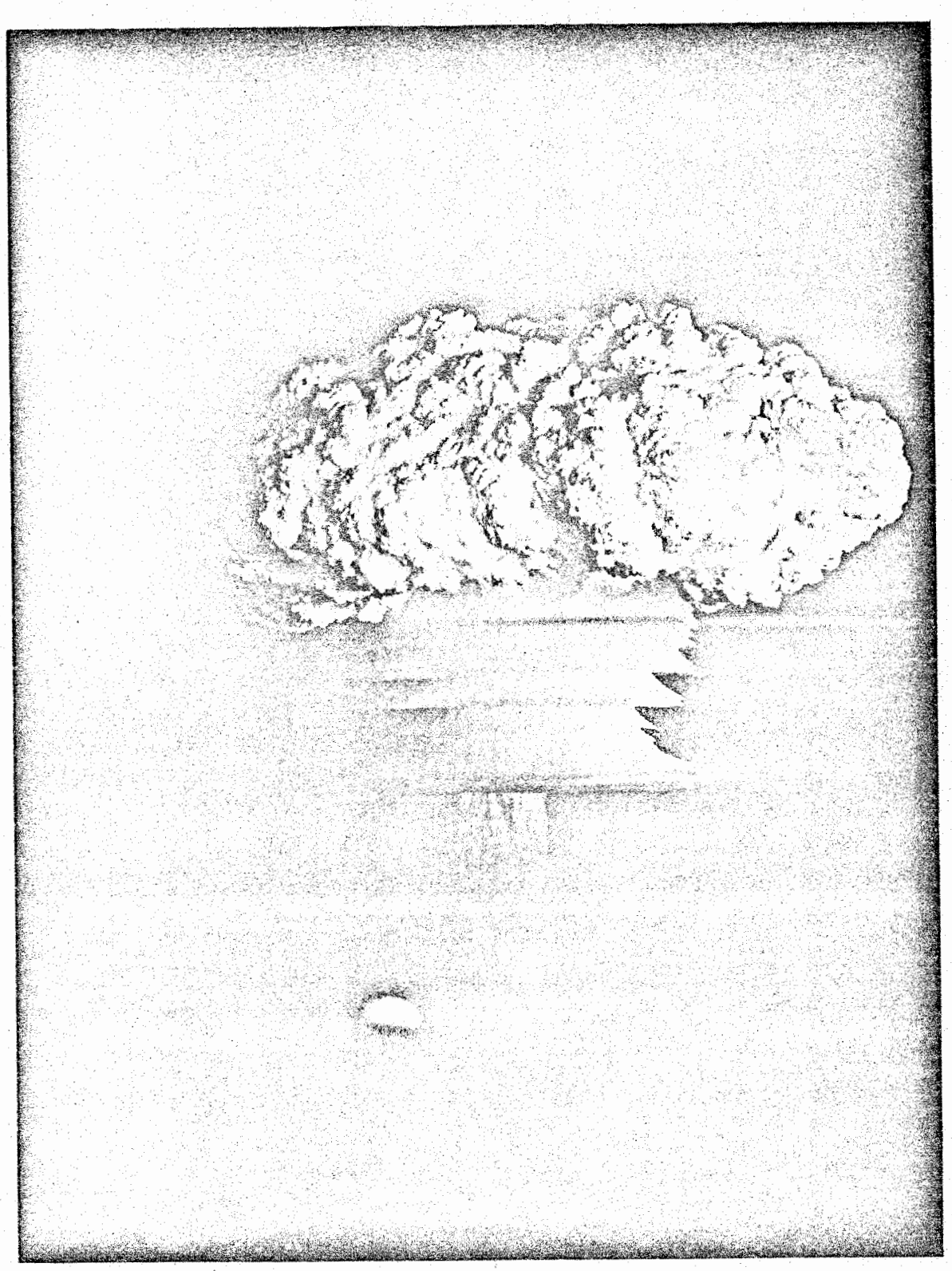

Figure 11

[redacted]

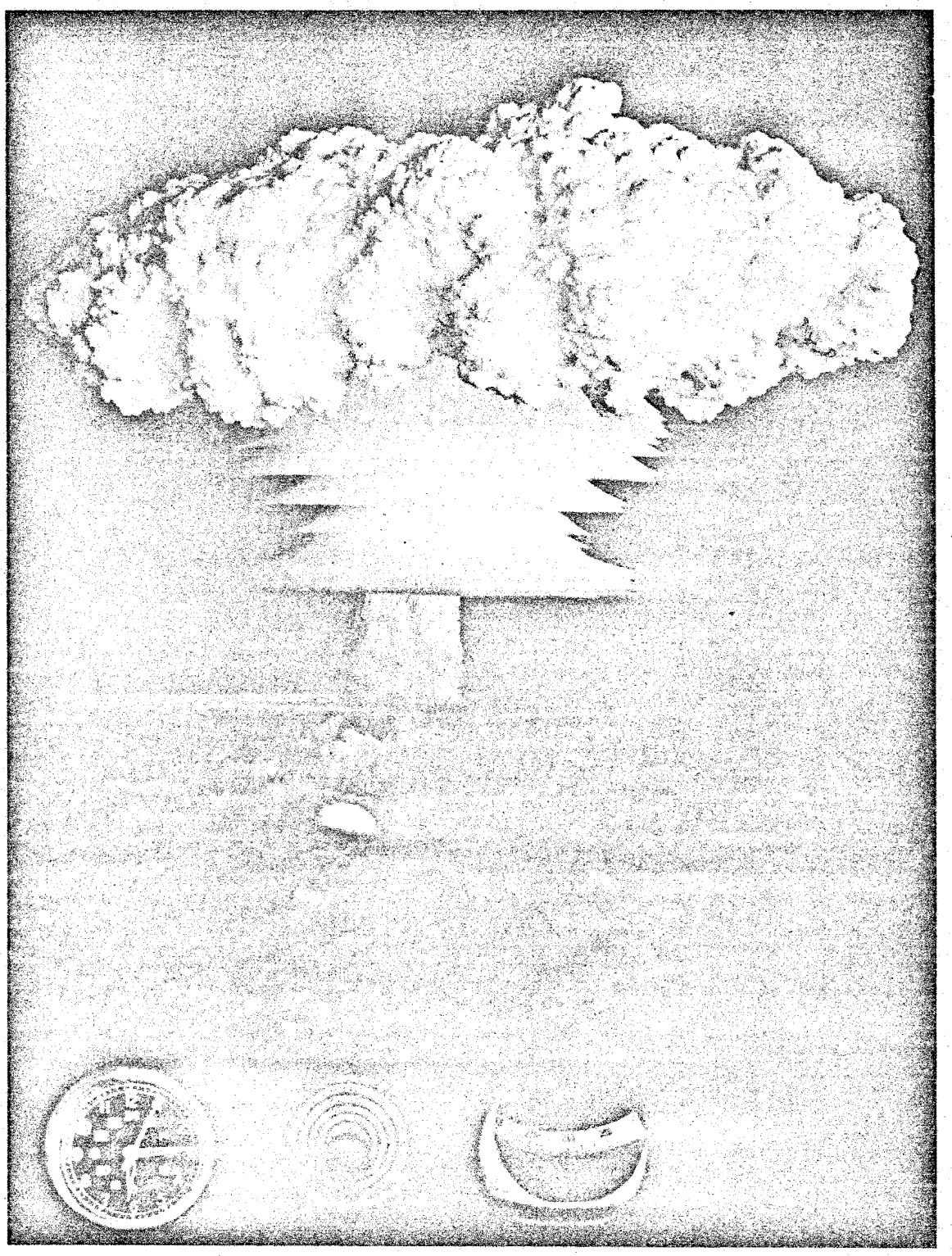

Figure 12

[redacted]

[redacted] ENERGY ACT

[redacted]

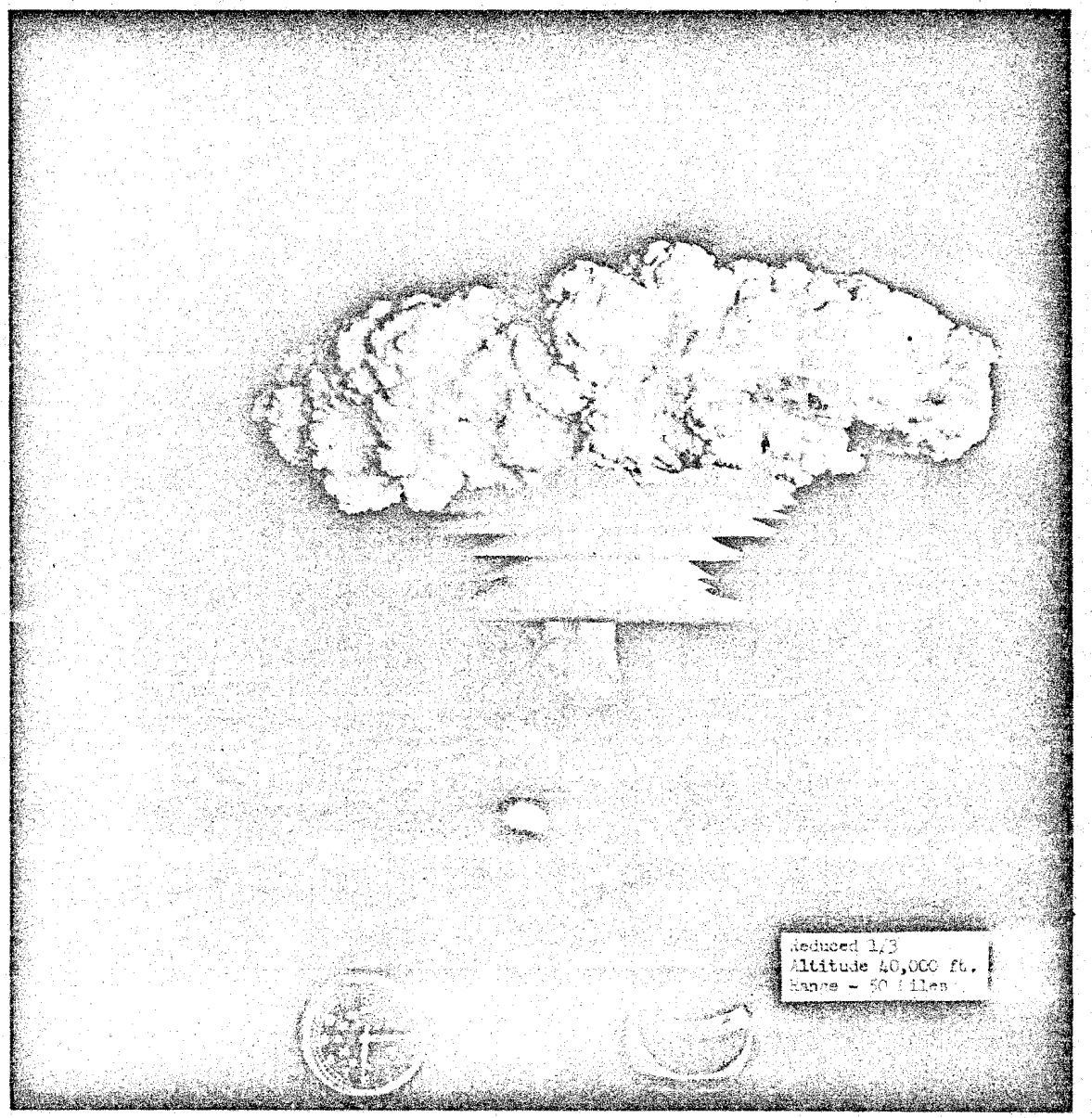

Figure 13
106

[redacted]

[redacted]

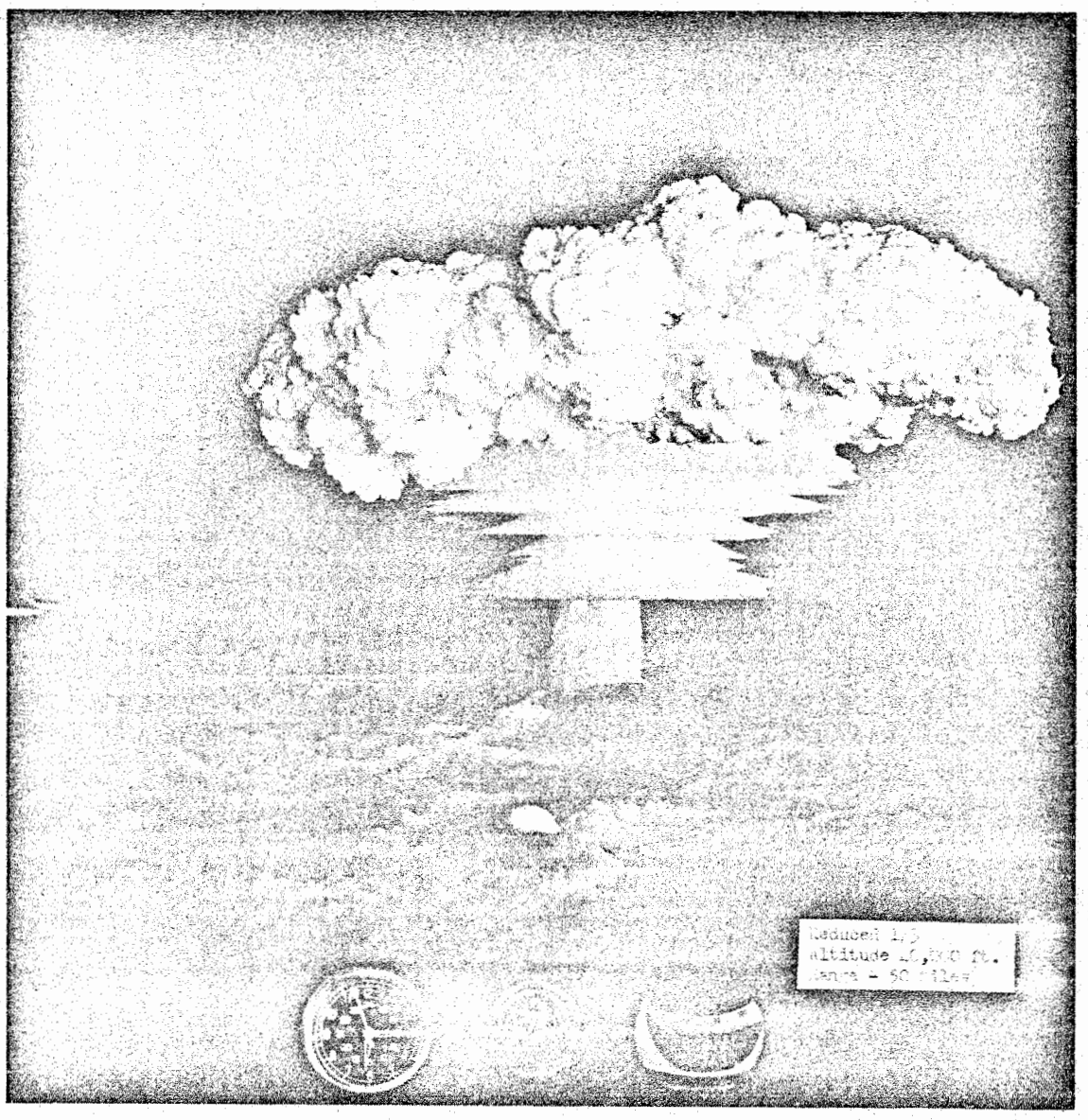

Figure 14

[redacted]

[redacted]

[redacted]

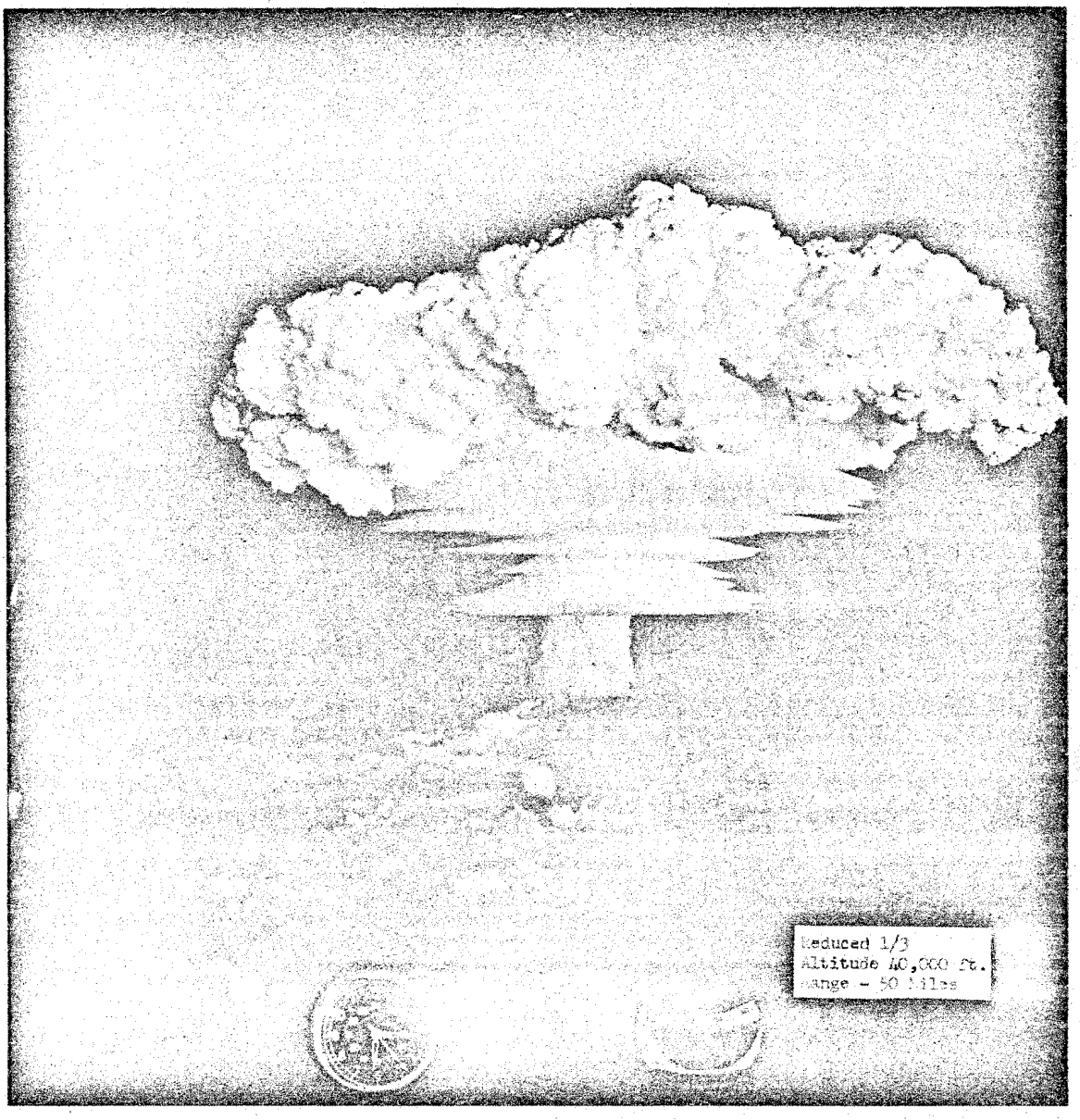

Figure 15

[redacted]

[redacted] ENERGY ACT [redacted]

[redacted]

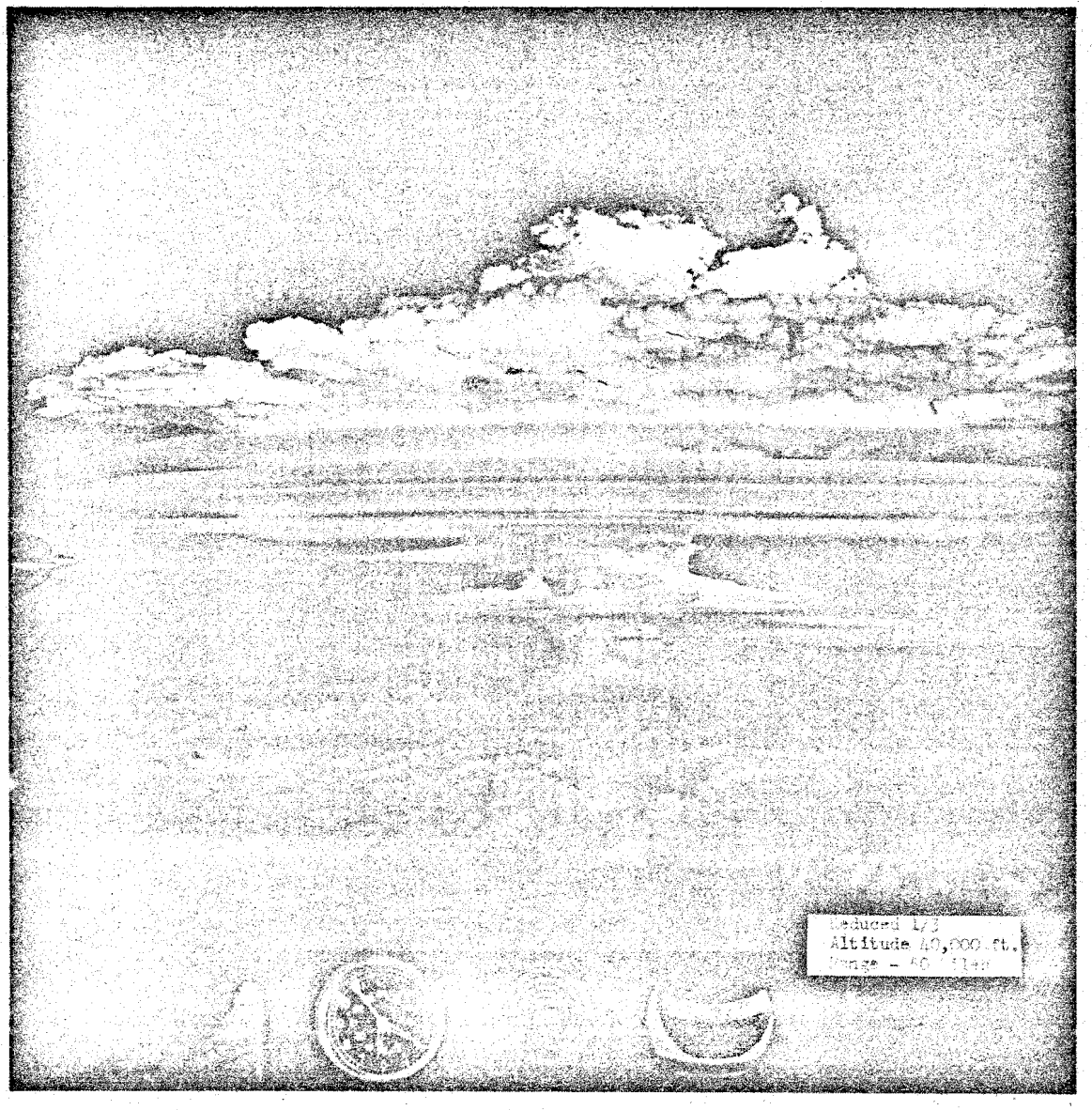

Figure 16

[redacted]

[redacted] 113

[redacted] ATOMIC ENER[redacted]

SUMMARY CLOUD PARAMETERS

THOUSANDS OF FEET

SHOT	HEIGHT — TOP		DIAMETER	
	MAX	1 MIN	1 MIN	10 MIN
CASTLE 1	114	47	38	370
CASTLE 2	110	44	33	316
CASTLE 4	94	35	26	125
CASTLE 5	110	44	34	270
CASTLE 6	72	25	19	147
IVY M	98	39	30	200
IVY K	76	28	11	90

Figure 17

[redacted]

PHYSICAL AND CHEMICAL NATURE OF THE CONTAMINANT; DIGEST OF OBSERVATIONS PRIOR TO CASTLE

R. D. Cadle
Stanford Research Institute

Pre-Jangle Fall-Out Studies

Most of the pre-Castle fall-out studies were made on three shots: Jangle Surface, Jangle Underground, and Ivy Mike. However, some investigations of cloud and fall-out particles were conducted at Sandstone and Greenhouse.

Cloud particles were sampled at Greenhouse by means of aircraft and were studied by means of an electron microscope. The median diameters were about 0.5 micron, although there was considerable variation from shot to shot and with altitude. Active fall-out particles collected at Greenhouse were classified either as spheres or as active coral grains. The median diameter of the spheres was about 5 microns and of the grains, about 20 microns.

Jangle Tests

Extensive sampling of the fall-out from the Jangle Surface and Underground shots was conducted by several groups. The fall-out consisted of both radioactive and inactive fractions. The inactive fraction appeared to be essentially unchanged soil and the active material appeared to have been formed by fusion or condensation. The particle size distribution of the gross fall-out was essentially that of the original soil. The percentage of active particles in the gross fall-out varied with particle size but was about 5% to 10% for both shots.

The general appearance of the active particles is shown in the photomicrographs in Figure 1. Most of the active particles contained glassy material which was often vesicular; they varied from almost colorless to jet black, the darker particles being the most active. Some of the particles appeared to contain essentially unchanged earth. Spherical particles were found in both surface and underground shot fall-out, although a larger percentage was found in the former. Possibly the surface shot particles were formed at a higher average temperature than the underground shot particles. Figure 2 is a photomicrograph of a particle found in the crater from the underground shot. It demonstrates the complex nature of many of the particles. When found, it was covered with a black, glassy, ferromagnetic crust which was removed.

[redacted]

115

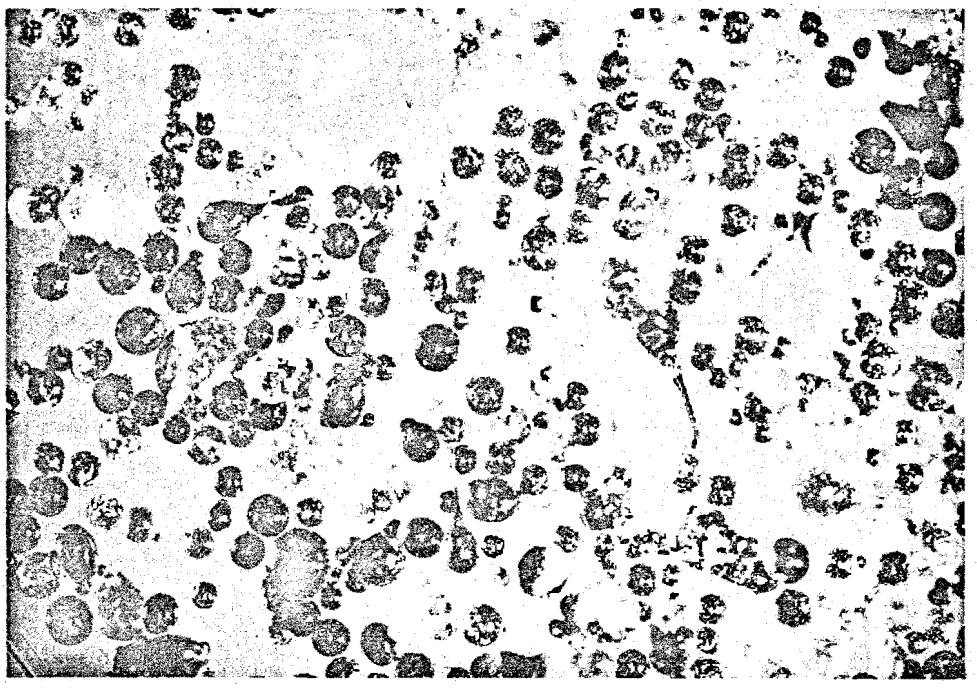

(a)

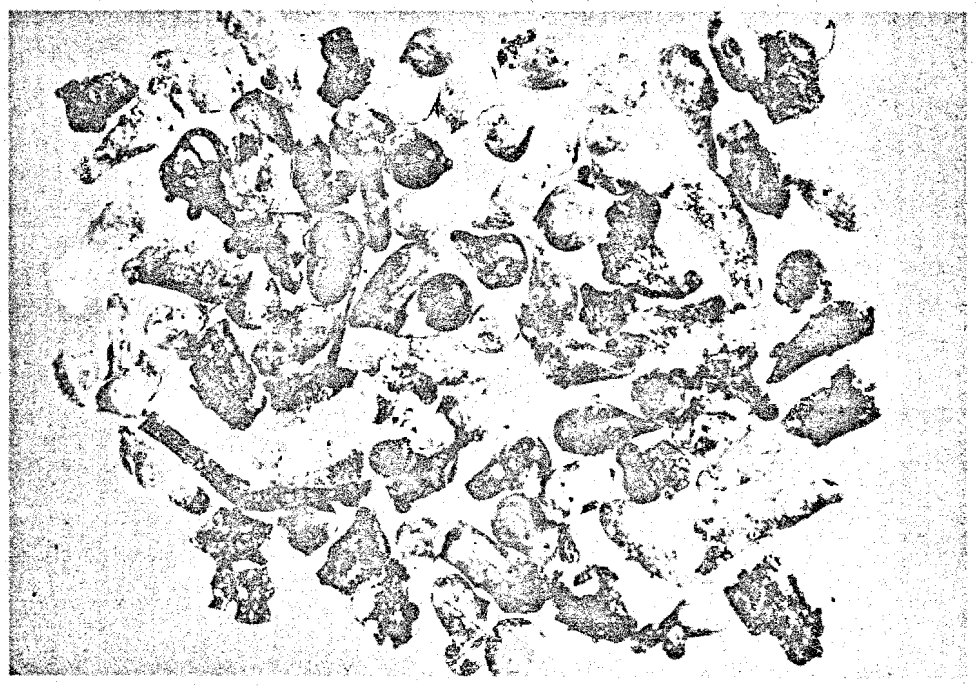

(b)

Figure 1
Typical Radioactive Particles from Fall-Out of Operation JANGLE
(a) Surface Shot, (b) Underground Shot

116

[redacted]

Several groups prepared thin sections of the particles and studied them with the petrographic microscope. The particles were found to contain, in addition to the glassy material, fragments of quartz, feldspar, olivine, serpentine, and other minerals which were presumably part of the original soil. A few active particles were found which contained small spheres or irregular fragments of a ferromagnetic metal, presumably iron (Figure 3). Since the black material with which so much of the activity was associated seemed to consist of iron oxides, the discovery of free metal suggested the interesting possibility that both reducing (or inert) and oxidizing conditions existed at various times or places within the clouds produced by the explosions.

Emission spectrographs of black glassy particles and of the original soil showed that the former contained much higher concentrations of iron and copper than the latter. The black particles were ferromagnetic and may have contained considerable iron oxide, possibly from the bomb casing. This dark material may have been produced by condensation of vapors of soil, bomb casing, and fission products, which constituted the "fireball."

More than 99% of the mass of the underground shot active fall-out was composed of particles larger than 10 microns in diameter, and 50% was larger than 180 microns. Few data are available concerning the size distribution of active fall-out from the surface shot, but work reported by NRDL shows that almost all activity of the surface shot fall-out was associated with particles larger than 100 microns in diameter.

Thin sections of active particles were autoradiographed. The autoradiographs were enlarged and compared with photomicrographs of the sections. Some of the results are shown in Figures 4 and 5. Activity was distributed rather uniformly throughout some particles but was mainly associated with specific regions of others. The darker portions of the particles were usually more active than the lighter portions. Very rarely the activity was concentrated near the outside of the particle. Apparently, glassy droplets of relatively low activity often came in contact with other droplets which were more active and usually dark colored. Various degrees of mixing occurred, depending on the viscosity (temperature?) of the droplets, the time which elapsed before cooling, and the turbulence of the gases bearing the particles.

Ivy Mike

Ivy Mike was a thermonuclear surface shot at Eniwetok. The active fall-out particles were usually white, hard grains having a

[redacted]

Figure 2
Part of a Large Radioactive Particle Found in a Sample of the Soil from the JANGLE Underground Shot Crater. The largest black sphere was 240 microns in diameter. A magnetized needle showed that the spheres were ferromagnetic.

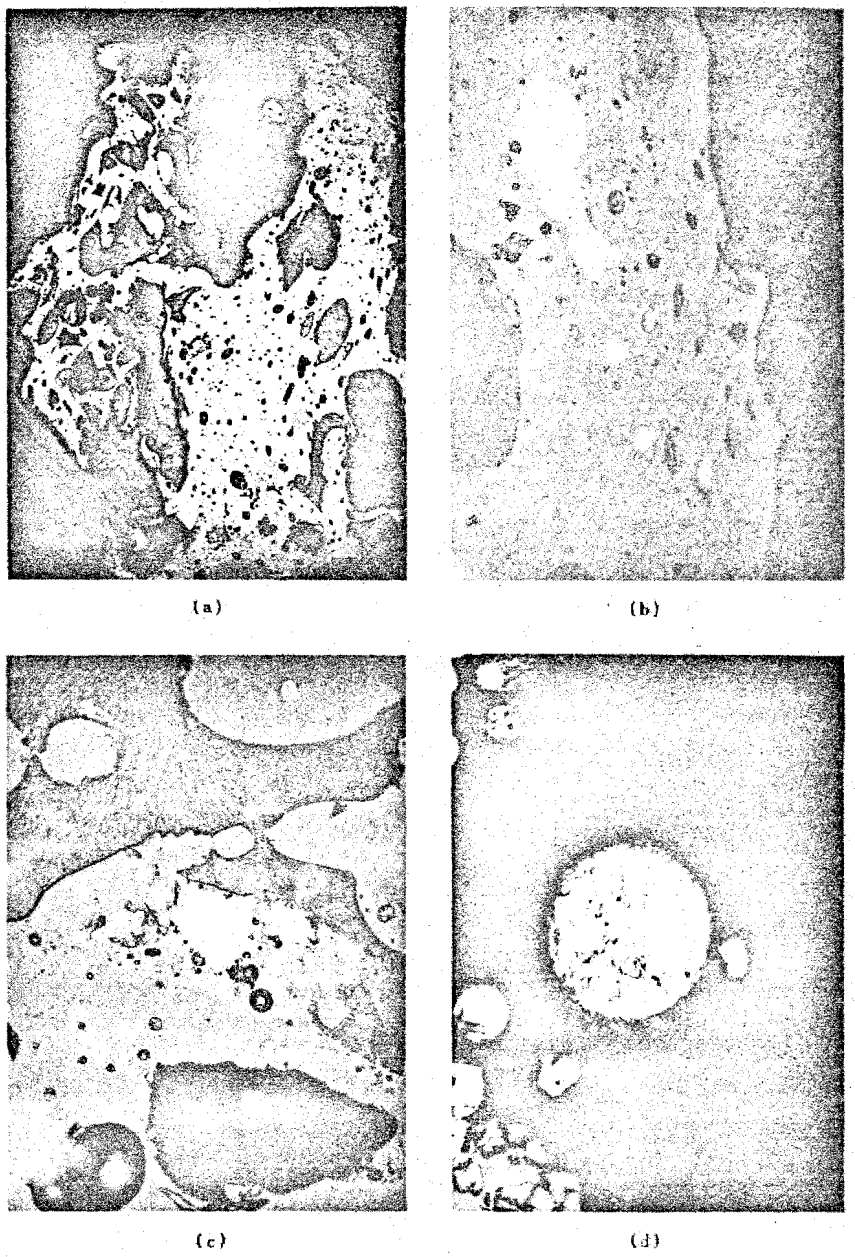

Figure 3
Photomicrographs of Thin Sections of Particles, under Vertical Illumination. Photographs (a) and (b) show an active particle from the JANGLE Underground shot with essentially white, metallic particles imbedded in the larger particle. The particle in (c) was etched with nitric acid and had a surface structure similar to the Widmanstatten figure. Photograph shows an etched section of a particle from the fume of an open hearth furnace which exhibited typical Widmanstatten figures.

[redacted]

microcrystalline structure. Occasionally the particles were colored grey or brown. The composition of active fall-out particles was investigated using petrographic methods, chemical tests, X-ray diffraction measurements, and emission spectroscopy. Particles examined at Stanford Research Institute were composed almost entirely of calcium carbonate in the form of calcite. The original coral sand was also calcium carbonate, but almost entirely in the form of aragonite.

A large percentage of the active particles studied by NRDL were reported to consist of calcium hydroxide coated with calcium carbonate. Calcium nitrate was tentatively identified in a number of the particles.

Autoradiographs were prepared of sections of Ivy Mike particles (Figure 6). Activity was usually concentrated near the surface of the particles, although they were often, and possibly always, somewhat active throughout.

[redacted]

[redacted] ENERGY ACT

120

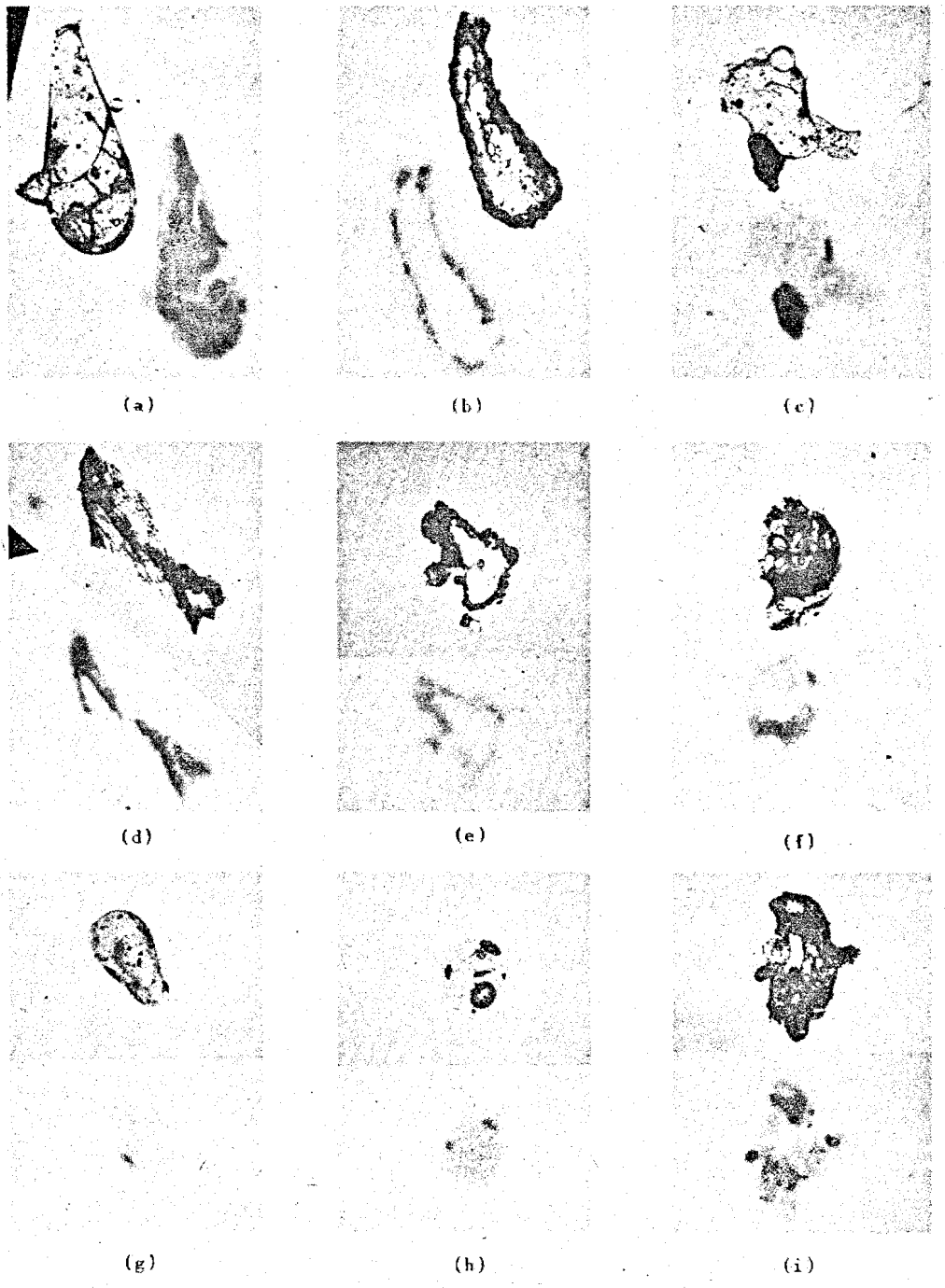

Figure 4 (a - i)

Photomicrographs of Active JANGLE Fall-out Particles with Corresponding Autoradiographs. Figures a, m, p, q, r, s, and t were from the surface shot. The remainder were from the underground shot.

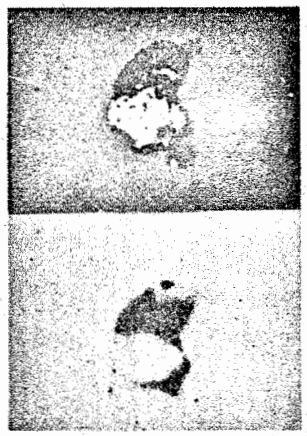

(j)

(k)

(l)

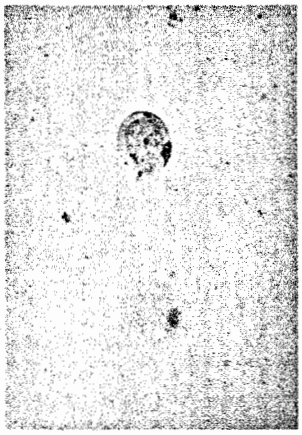

(m)

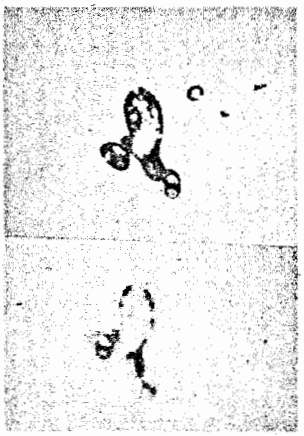

(n)

(o)

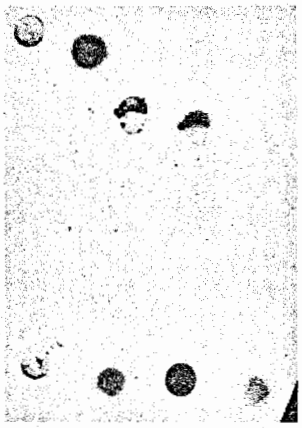

(p)

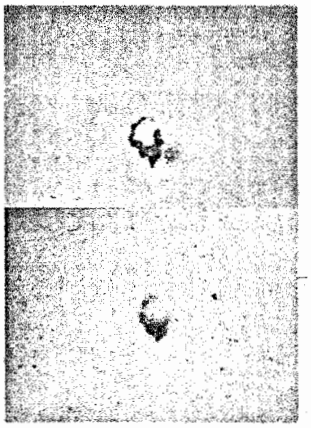

(q)

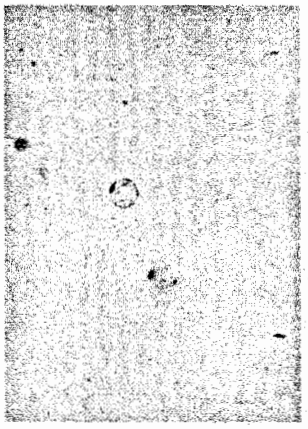

(r)

Figure 4 cont. (j - r)

(s)

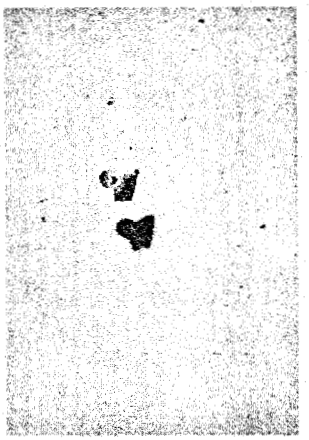

(t)

(u)

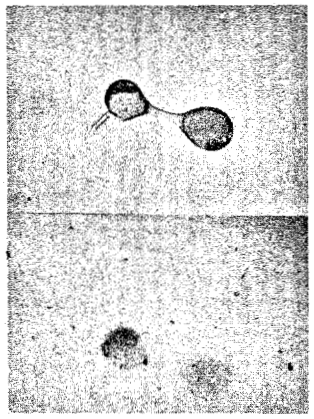

(v)

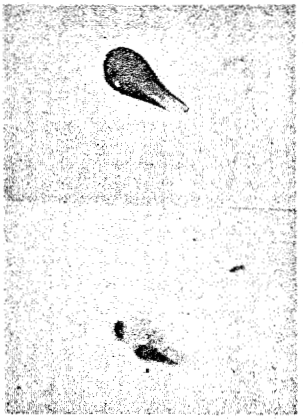

(w)

(x)

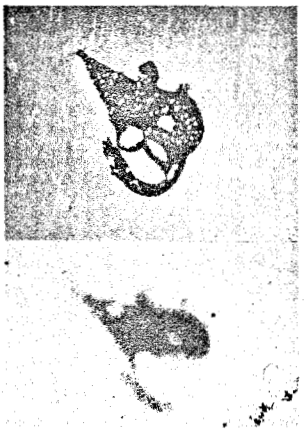

(y)

Figure 4 cont. (s - y)

[redacted]

123

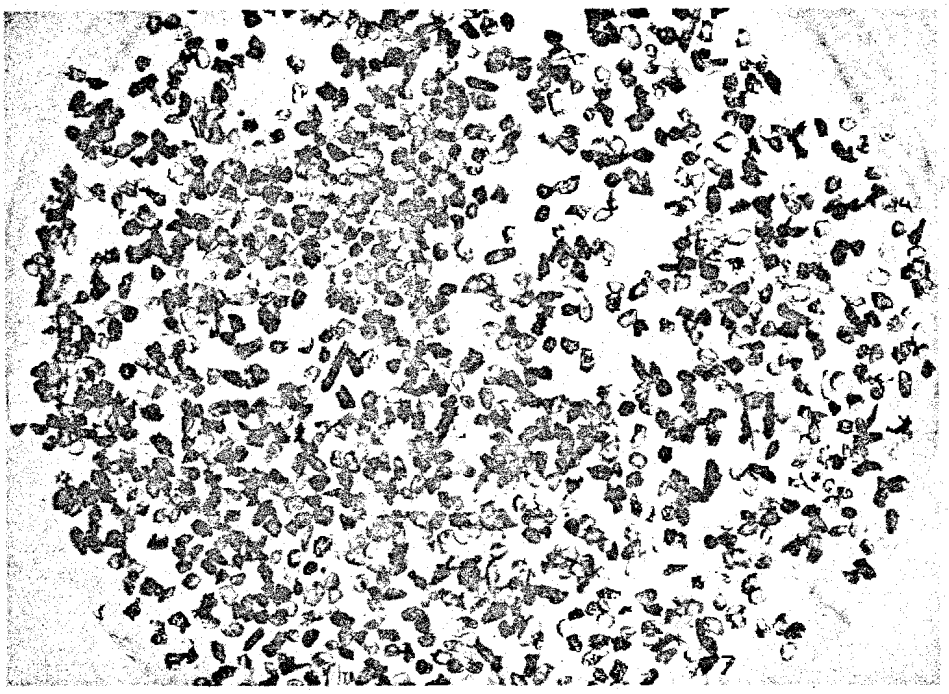

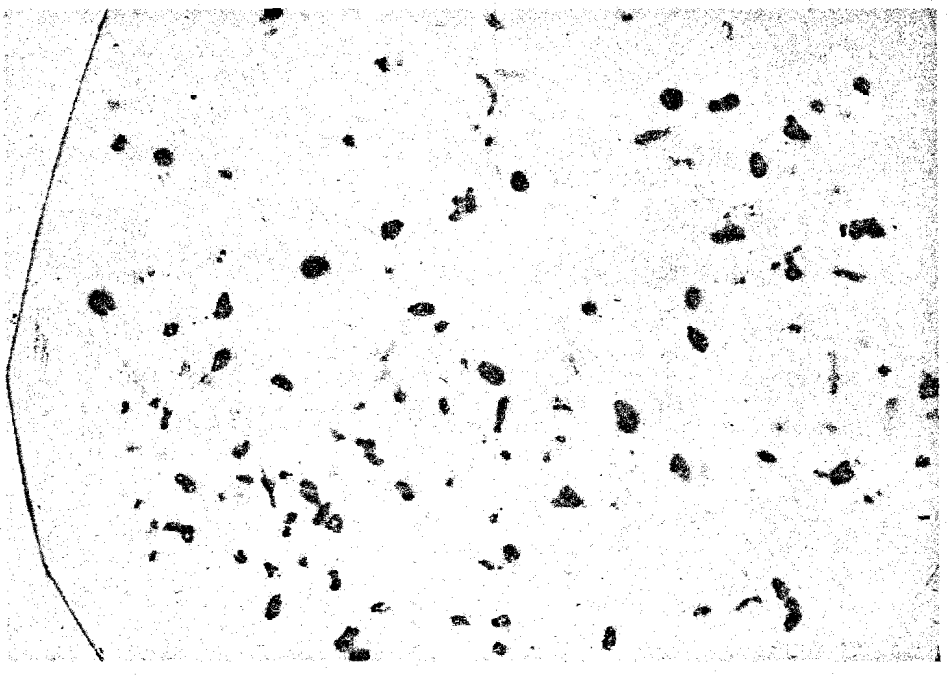

Figure 5
Photomicrographs (above) and Corresponding Autoradiographs (below) of JANGLE Underground Shot Fall-out Mounted and Sectioned in Plastic. The various types and relative abundance of active particles can be observed.

[redacted]

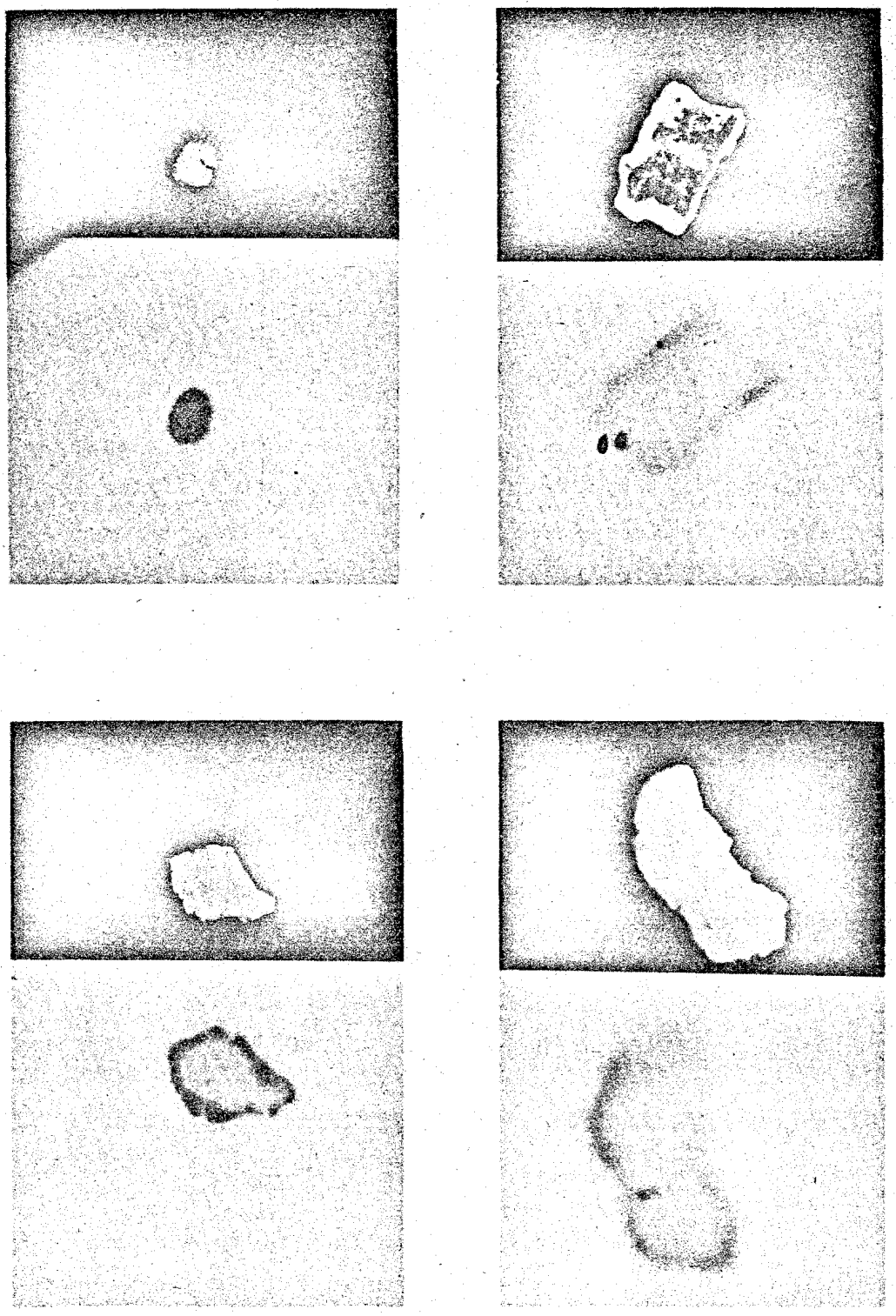

Figure 6
Photomicrographs of sections of IVY-Mike Particles with Corresponding Autoradiographs

[redacted]

[redacted]

THIS PAGE IS BLANK

[redacted]

126

[redacted]

PHYSICAL AND CHEMICAL NATURE OF THE CONTAMINANT INTERPRETATION OF CASTLE OBSERVATIONS

Dr. Carl F. Miller
U. S. Naval Radiological Defense Laboratory

The main objective of part of Project 2.6a was to determine the properties of the fall-out which were directly or indirectly related to countermeasures - that is, decontamination of the fall-out. In addition, many of the measured properties are those which determine the fall-out pattern.

A specific object of this paper is to show how the data can be used to specify, in a thermodynamic sense, a contaminated system. Such a system can be defined for a surface burst when four variants are given:

Site of detonation (environmental materials).

Yield of the device or weapon.

Amount of elemental structural components in the device.

Radiation contour in r/hr at 1 hour.

Once the above four items are given, data from the CASTLE Operations can be utilized to determine the kind and amount of materials which comprise the contaminated system produced by a surface burst.

The fall-out samples from which the data were derived are discussed in detail in the Project 2.6a final report. In general, the samples contained impurities of various kinds which had to be taken into account in interpreting the data. Fall-out from the first four shots was analyzed.

The contaminant properties of interest were of two general kinds: (1) contour properties and (2) chemical and physical properties. Both types, however, may be considered as giving a detailed picture of a given contour or the over-all fall-out pattern.

The contour properties are given by relationships between the radiation field and (1) the total mass of fall-out per unit area, (2) the specific activity or fraction of the device per unit area, and (3) the radiation characteristics of radioactive materials. Only the first two will be discussed at this time.

The physical and chemical properties which were determined included (1) distribution of the radioactivity into solid, liquid,

[redacted]

127

[redacted]

and colloidal fractions (or solubility of active constituents), (2) particle size distribution, (3) composition and structure of particles, (4) oxidation state of a few important radionuclides, (5) gamma spectra of the bulk radioactive source material, and (6) chemical composition of the fall-out.

A summary of the physical state fractionation of gamma activity (essentially solubility) is given in Table 1. An analysis of lead absorption data into three component energies for the various fractions is given in Table 2. The data in Table 1 are to be viewed as solubility effects. The weight of solid, for example, depended upon how much rain water, etc., fell into the sample collectors. The colloidal fraction was probably ionic material absorbed onto the ultrafilter membrane as indicated by the constancy of the fraction of ionic in the liquid phase for all shots and times of analysis. Decay of a sample from an island shot is given in Figure 1 and from a barge shot in Figure 2.

The particle size distributions are given in both Projects 2.5a and 2.6a final reports. The particles themselves were of several types: (1) inactive, unchanged coral particles (greater fraction of these from Shot 3 than Shot 1), (2) unchanged coral particles with radioactivity on the outside, (3) particles unchanged in the center with CaO or $Ca(OH)_2$ towards the exterior of the particle containing activity diffused inwards, (4) particles completely pyrolyzed with CaO or $Ca(OH)_2$ interiors with a thin shell of $CaCO_3$ around the exterior and radioactivity diffused inwards, and (5) particles of a very fluffy fragile nature containing spots of activity in them (apparently a "condensed" or agglomerated particle - like snowflakes). The most numerous or typical of the particles containing radioactivity were those typified by those given as (4) above of which an example of a thin section of a particle is given by Figure 3 in which the picture with polarized light shows the $CaCO_3$ shell, and the radioautograph shows the radioactivity diffusing into the $Ca(OH)_2$ center. The so-called "condensed" particles were relatively few in number. Hence, it is concluded that by far the majority of the radioactive particles were formed by the condensation of gaseous radioactive atoms (or particles of molecular size) onto larger solid particles which had never been vaporized, but which swept up through the radioactive gas cloud collecting both radioactive material as well as some vaporized environmental material. Later, as the cloud cooled, H_2O and CO_2 could have again reacted with calcined particles to form $Ca(OH)_2$ and the $CaCO_3$ shells. No definite information was obtained on the particles resulting from the water shots excepting that, as the fall-out reached the earth's surface, they must have been extremely small; the fall-out contained very little, if any, water.

[redacted]

[redacted]MIC ENERGY A[redacted]

128

Table 1

Summary, Physical State Fractionation of Gamma Activity

Shot Type	Shot No.	Number of Samples	Time After Detonation (days)	Wt. of Solid (%)	pH	Solid (%)	Ionic (%)	Colloidal (%)	Amount Ionic in Liquid Phase (%)(a)
Island	1	3	6.5-8.3	0.85-9.2	9.0-12.3	92.1-98.1	1.9-7.7	0.06-0.2	97.0-97.5
	3	2	4.2-5.5	0.18-0.23	10.5-11.2	92.4-94.2	5.6-7.3	0.23-0.23	96.1-97.0
Barge	2	1	3.4	0.01	7.5	24.7	72.9	2.4	96.8
	4	1	1.8	0.01	7.7	40.2	57.9	1.9	96.8

(a) Gamma count in ionic, as fraction of gamma count in liquid phase

Table 2

Average Photon Energy and Distribution of Apparent Photon Energies in Physical State Fractions

Shot Position	Low Energy Component Energy(Mev)	Low Energy Component Amount(%)	Medium Energy Component Energy(Mev)	Medium Energy Component Amount(%)	High Energy Component Energy(Mev)	High Energy Component Amount(%)	Average Photon Energy(Mev)
			A. Solid Fraction				
Island	0.15	50.3	0.34	22.2	1.18	27.5	0.47
Barge	0.15	45.0	0.34	23.4	1.02	31.6	0.47
			B. Ionic Fraction				
Island	0.16	44.1	0.41	19.7	1.19	36.2	0.55
Barge	0.15	55.4	0.34	24.2	1.42	20.4	0.41
			C. Colloidal Fraction				
Island	0.17	22.0	0.40	20.0	1.37	58.0	0.92
Barge	0.15	41.5	0.34	23.4	1.08	35.1	0.52

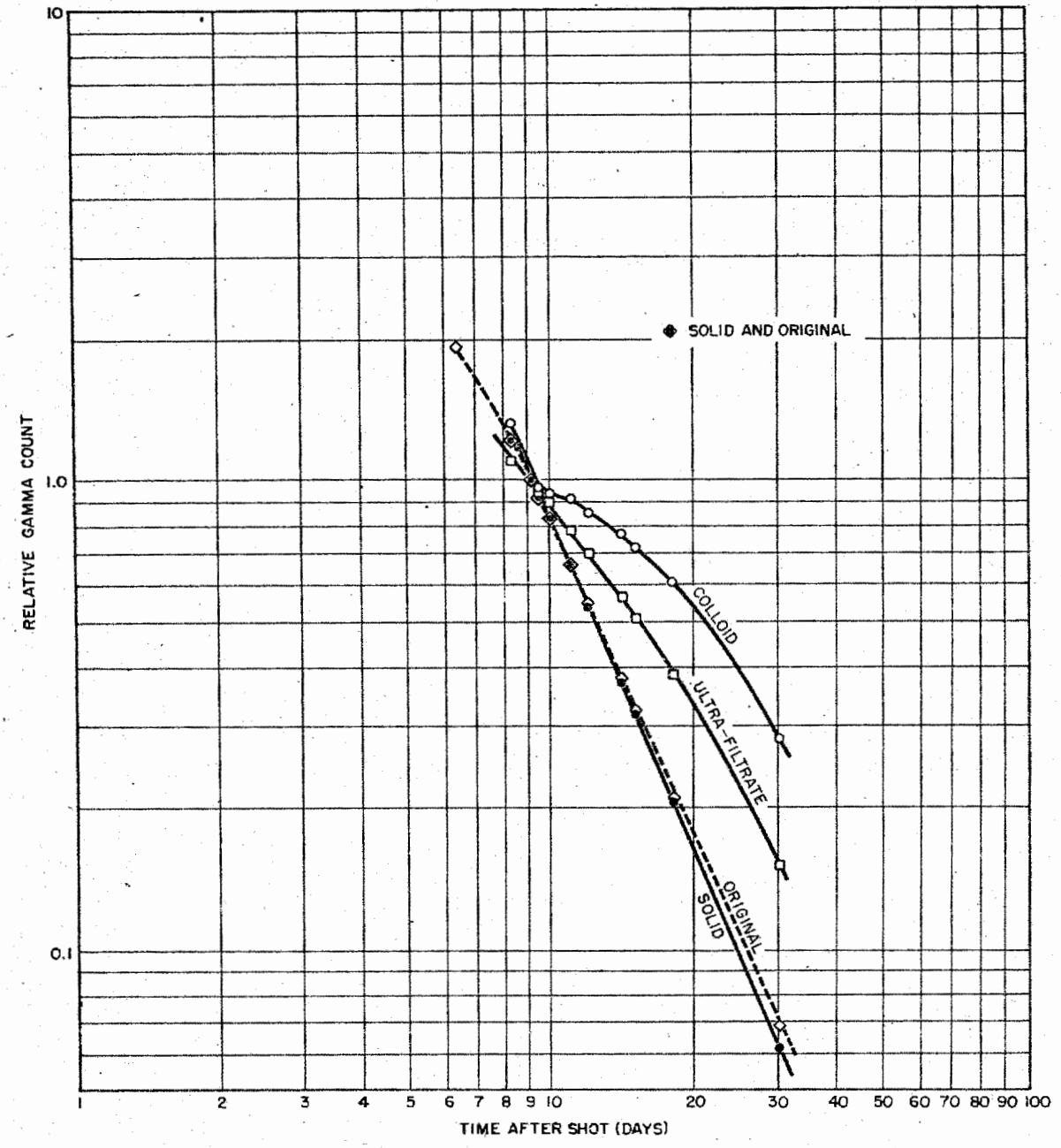

Figure 1
Gamma Decay of Physical State Fractions of Sample 1-251.03

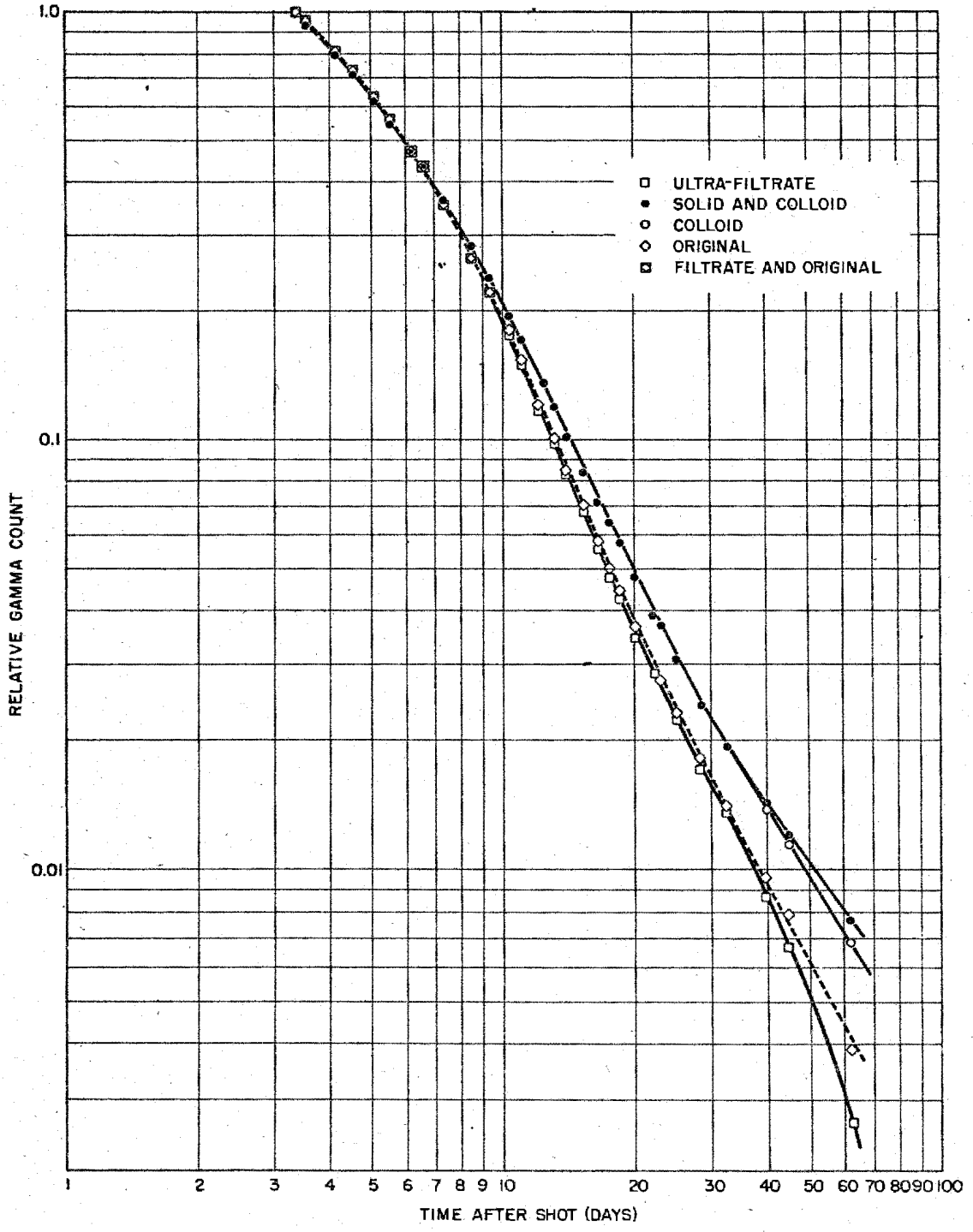

Figure 2
Gamma Decay of Physical State Fractions of Sample 2-A4

[redacted]

a. Photographed in ordinary light

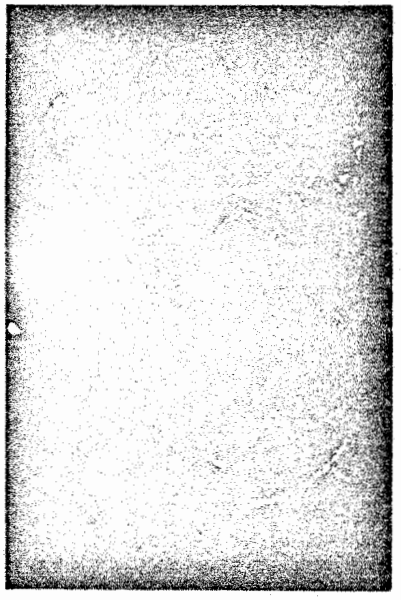

b. Photographed in polarized light

c. Radioautograph

1 mm

Figure 3
Typical Fall-out Particle from Operation CASTLE
Consisting Almost Entirely of Calcium Hydroxide

[redacted]

[redacted]

[redacted]

The oxidation states of Np and I were investigated. Np was found to be about 2/3 as NpIV and 1/3 as NpV and NpVI. For the barge shots, I was found in the liquid fraction, while for the island shots it was mainly in the solid fraction. With two phases present, I was apparently present in the -1 oxidation state (I as iodine is subject to air oxidation which is fairly rapid in the dry state).

Some 800 gamma spectral determinations were made in one month at the site. With a 1 in. NaI crystal, the data could not readily be reduced quantitatively but were used to demonstrate that, for samples obtained from various locations in the fall-out area up to about 200 miles distant from shot point, fractionation of the radioactive elements did not occur to any appreciable extent. The coincidence of the decay of such samples agree with the spectral data in this respect. The data do not prove that fractionation does (or did) not occur; they prove that if it did occur, the degree to which fractionation occurred was not sufficient to alter the over-all gamma spectral distribution and decay of the fall-out (each source sample was a dissolved aliquot representative of all the particles which fell out over a 7 in. diameter area). Spectral data for single particles have been taken and do, in fact, show a different gamma spectrum.

The chemical composition of the fall-out was determined by analyzing for Na, K, Mg, Ca, Sr, Al, Cl, Br, Cu, and Fe. Samples of the lagoon water, sea water, and coral were similarly analyzed as background constituents to obtain a ratio of the elements for coral and sea water. Using the ratios and the analysis of the fall-out samples, it was possible to reduce the composition of the fall-out into coral, sea water, and device-product components. The residual iron in the sea water and coral components was found to be about the same order of magnitude as that used in the device (barge, etc.). From the data, then, it was possible to determine the mass of coral per sq. ft., the mass (or apparent volume) of sea water per sq. ft., and the fraction of the device per sq. ft. which fell into each collector. Then knowing, or estimating, the radiation at each of the stations in r/hr (at 1 hr), a ratio can be calculated between the radiation field and each of the surface density quantities. For a given shot, the ratio should be constant providing the component in question has been thoroughly mixed with the total radioactive material available. The data are plotted as histograms in Figures 4 through 9. In the case of "double" distributions, it was noted that samples collected in the lagoon or at sea were high in sea water; samples collected on the islands were high in coral. In such cases, the lower distribution was considered a more reliable estimate of the quantity. The data are summarized in Table 3. The mass equivalents are in terms of weight of original material - coral or sea water - which was used to produce the stated ratio. For

[redacted]

133

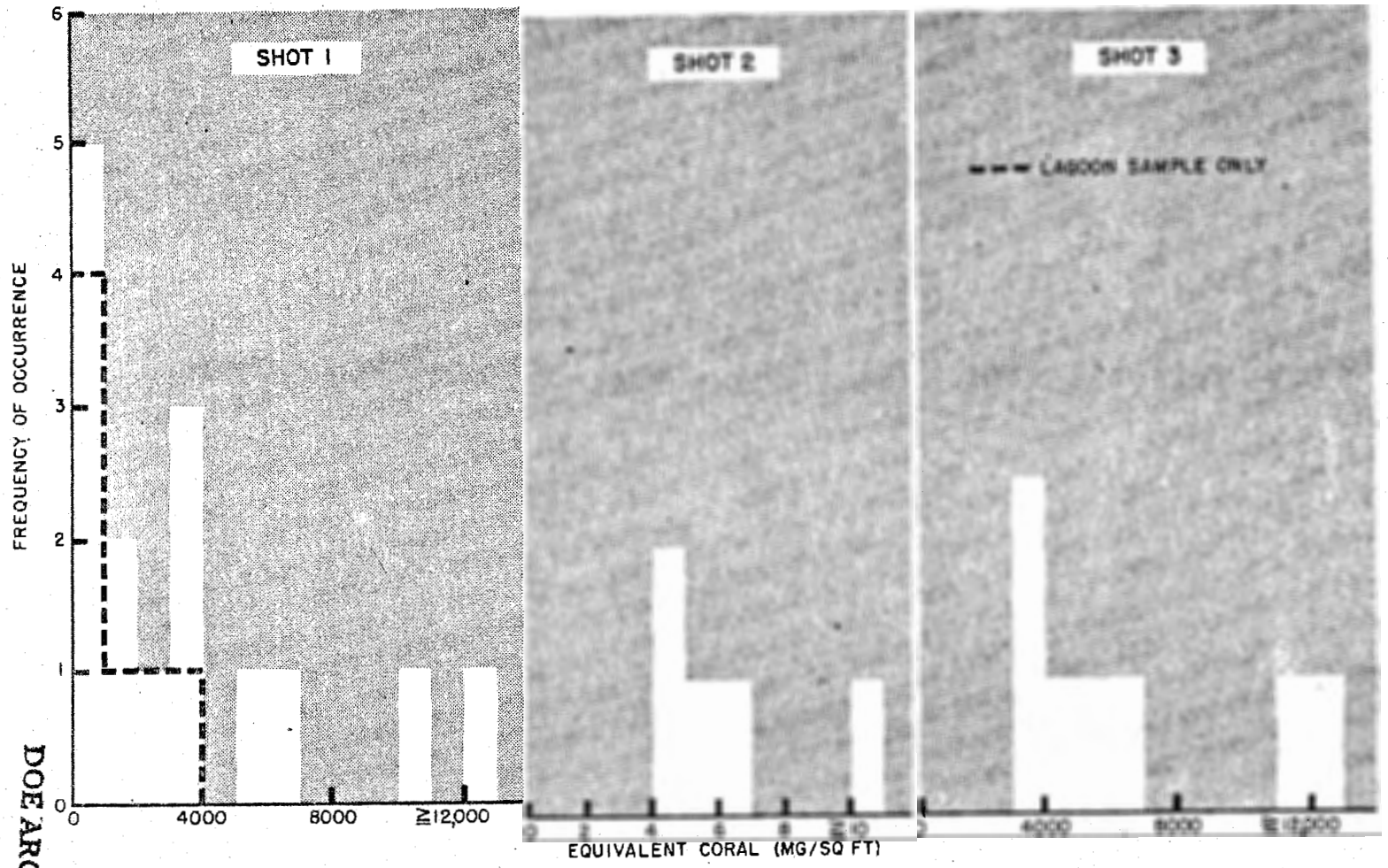

Figure 4
Density Distribution of Equivalent Coral for Shots 1, 2, and 3

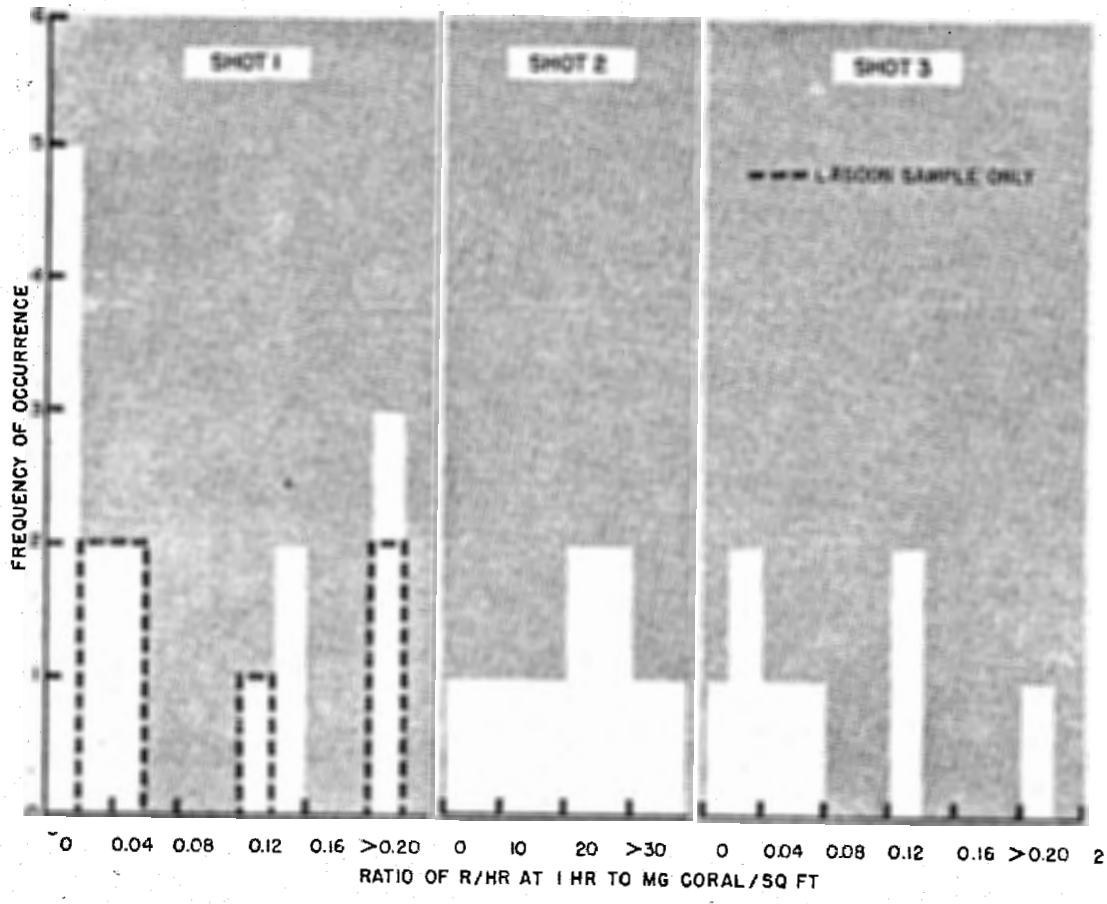

Figure 5
Distribution of the Ratio of the Radiation Field
to the Surface Density of the Coral Component

135

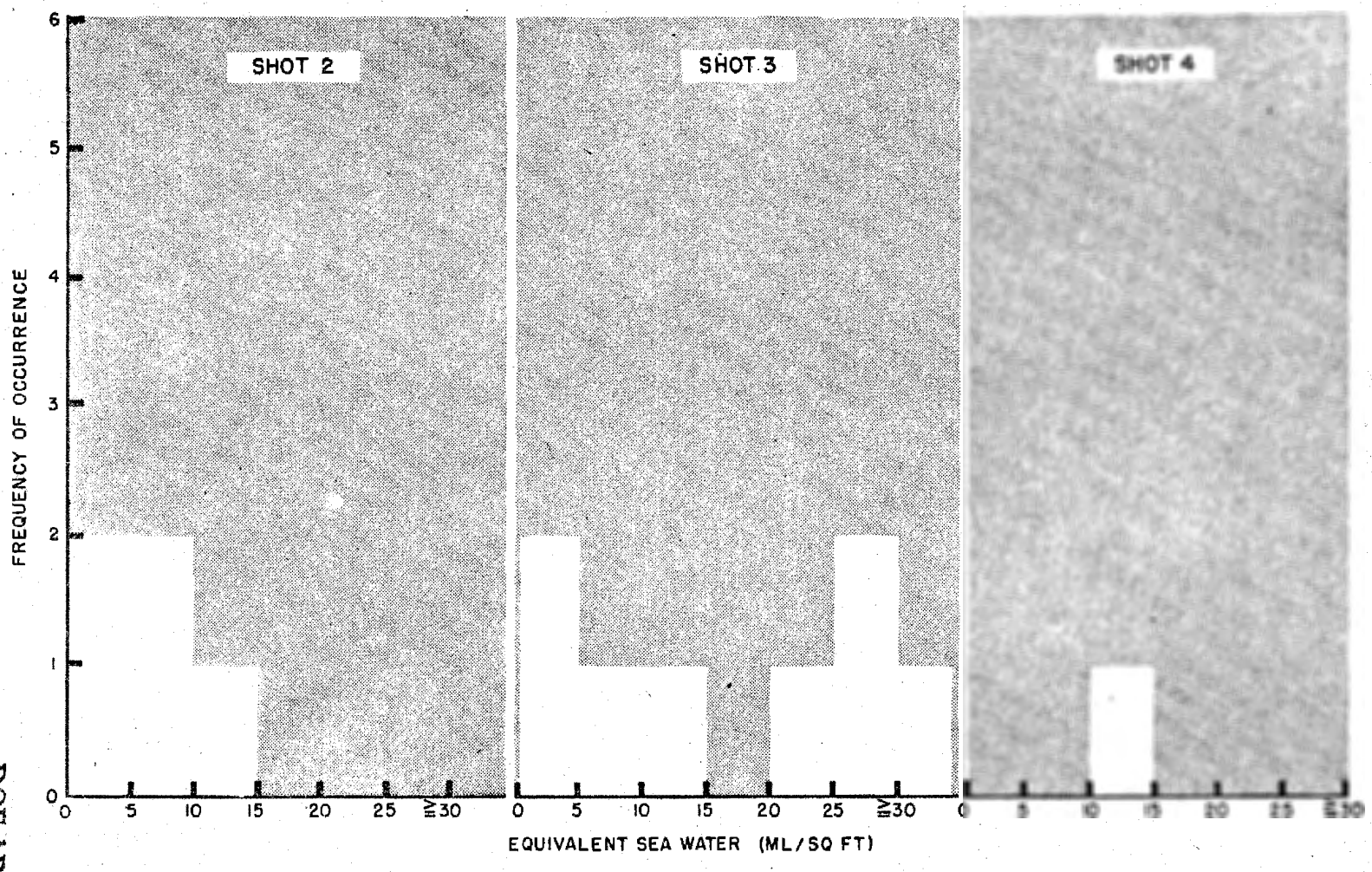

Figure 6
Density Distribution of Equivalent Sea Water for Shots 2, 3, and 4

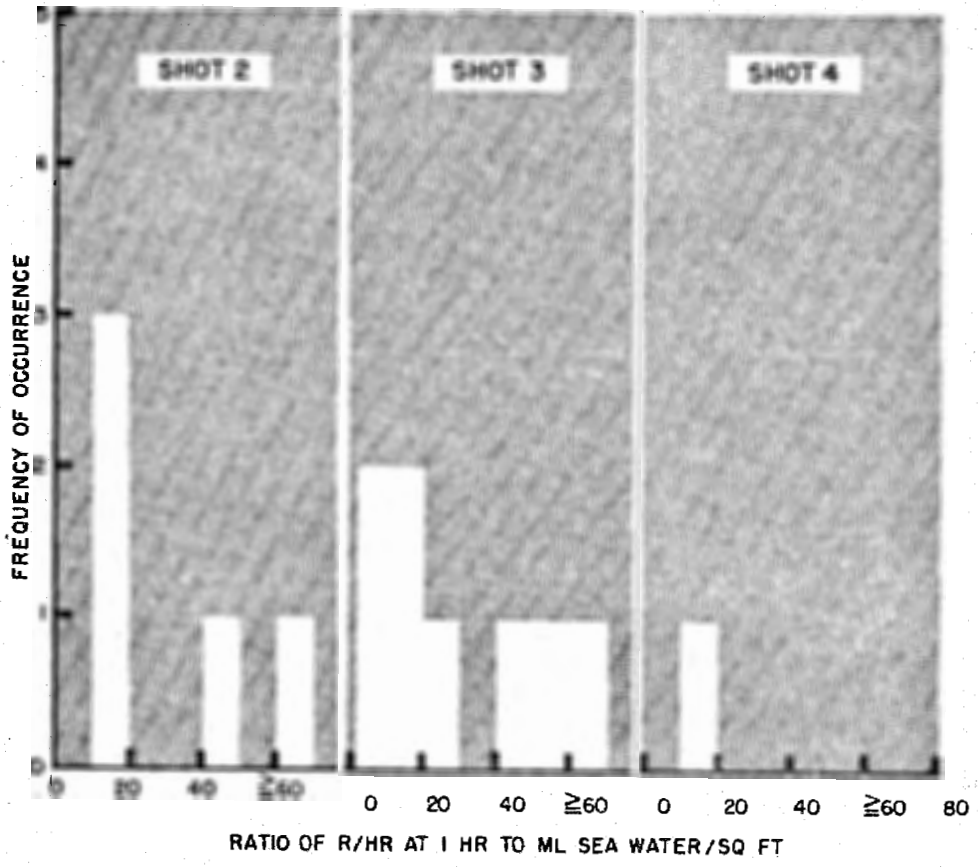

Figure 7
Distribution of the Ratio of the Radiation Field
to the Surface Density of the Sea Water Component

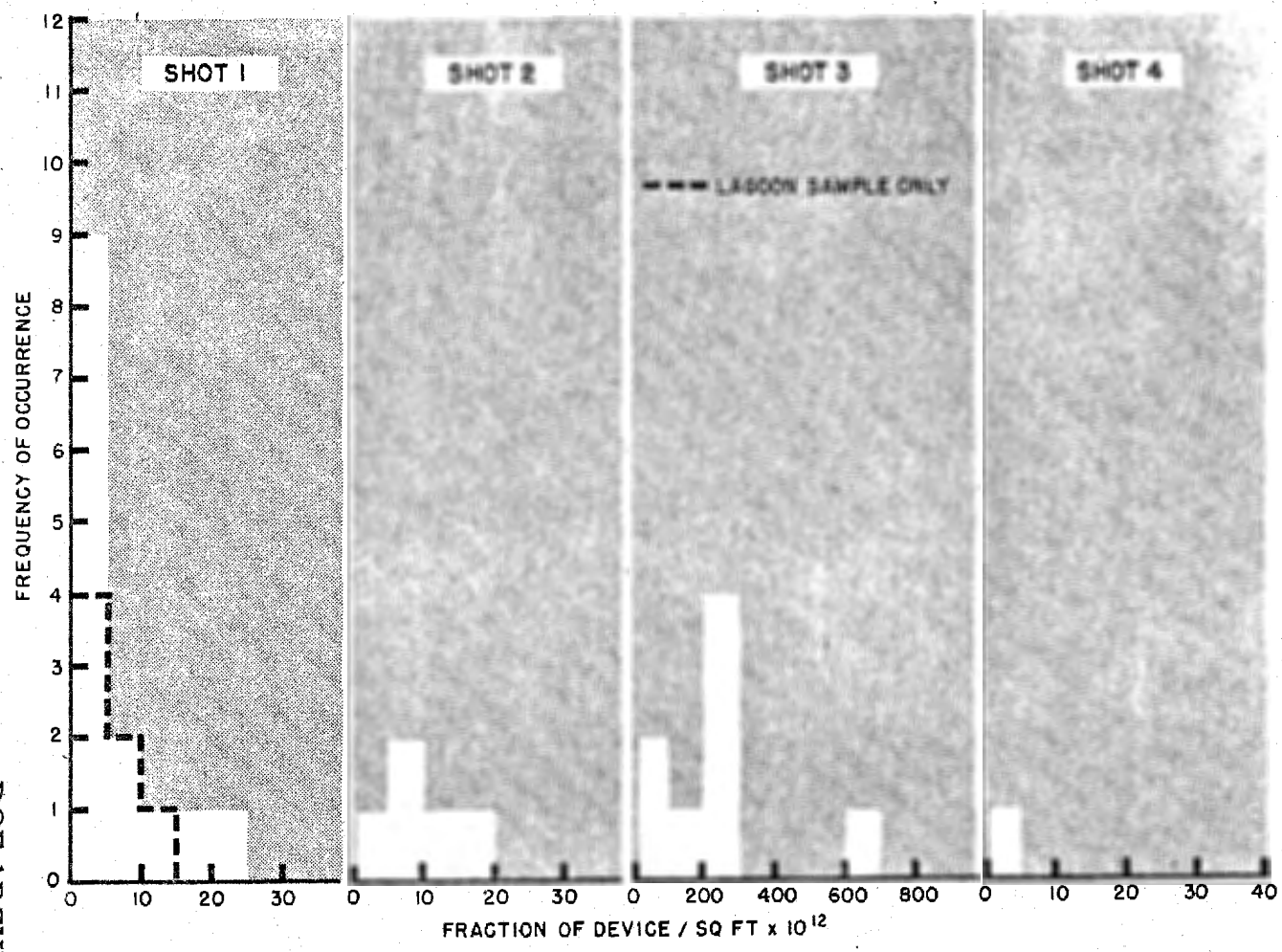

Figure 8
Density Distribution of Device Fraction for Shots 1, 2, 3, and 4

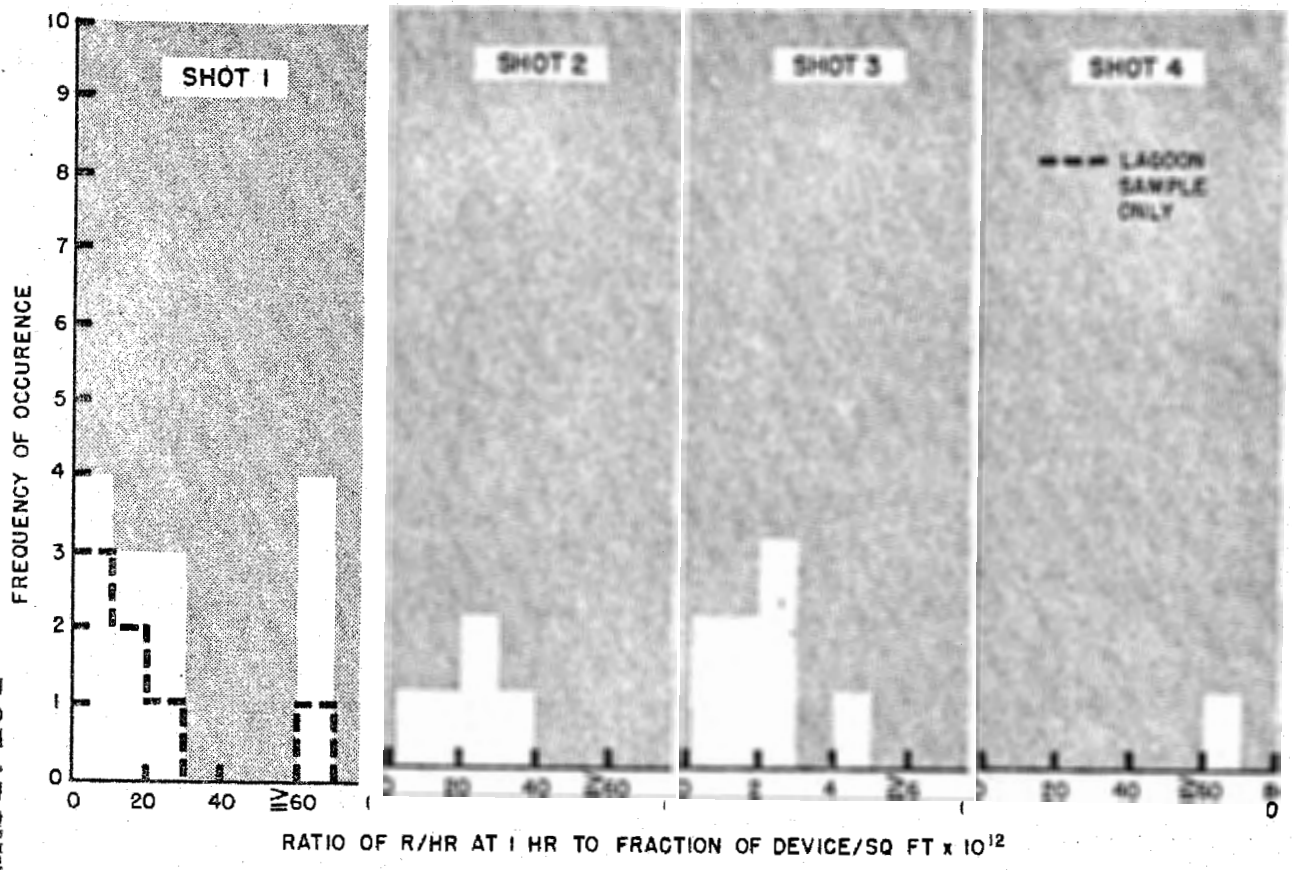

Figure 9
Distribution of the Ratio of the Radiation Field
to the Surface Density of the Device Fraction Component

Table 3

Contour Property Ratios

Event	mg.eq.coral/ft^2 r/hr at 1 hr	mg.eq.seawater/ft^2 r/hr at 1 hr	Total mass in mg/ft^2 r/hr at 1 hr	(a)Fraction Device/ft^2 r/hr at 1 hr	Yield
Castle No. 1	25	0	25	4×10^{-14}	14.5MT
Castle No. 2	0.04	77	77	5×10^{-14}	10.5MT
Castle No. 3	20	5	25	30×10^{-14}	110KT
Castle No. 4	0	91	91	2×10^{-14}	7MT
Jangle "S"	-	-	26	-	1.2KT

(a) $R_{f.d} = 2.4 \times 10^{-12} \cdot Y^{-0.42}$ (Y in KT)

[redacted]

Shots 2 and 4, for example, a ratio of 80 mg. sea water per sq. ft. to 1 r/hr at 1 hr would produce only an actual ratio of 2.7 mg. of residual salts per sq. ft. to 1 r/hr at 1 hr. The coral values would not be changed much by using $Ca(OH)_2$ for $CaCO_3$. For the JANGLE surface shot, the mass change would be less yet. The data show that the total mass contour ratio is essentially invariant with yield with the surface water shots producing a ratio greater by about a factor of [density (soil)/density (sea water) + 1] . The contour ratio for the fraction of the device varies with yield (from the Effects of Atomic Weapons, the variation of the ratio with yield would be $3 \times 10^{-11}/Y$). A more precise method for obtaining this contour ratio would be from a FP radiochemical analysis. The iron analytical are consistent within themselves but give a set of contour ratios which are apparently too high. This may be due to inadequate sampling of the background materials.

For Shot 1, the fall-out consisted of coral (mostly pyrolyzed) and device products (surface-land shot).

For Shot 2, the fall-out consisted of sea water (salts), device products, and small amounts of coral (surface-deep harbor shot).

For Shot 3, the fall-out consisted of coral smaller amounts of sea water (salts), and device products (surface-land shot on beach or harbor dock area).

For Shot 4, the fall-out consisted of sea water (salts), and device products (surface-water shot).

The above summary of the composition of the gross fall-out neglects rain water which fell during the collecting period by some of the sample collectors.

The following conclusions may be made from the data:

The site, or point of detonation, is the determining factor in the production of fall-out debris and its chemical and physical composition.

The contour properties which define a contaminated system (fall-out on a surface) can be utilized to specify experimental systems to evaluate countermeasures of various types for estimating the time, cost, and efficiency of a given recovery procedure. Such information is necessary for a practical countermeasure doctrine.

The chemical and physical properties not directly related to the contour properties are essential to the testing of experimental

[redacted]

systems; they serve as criteria by which a synthetic - or laboratory prepared - fall-out can be compared to the real fall-out. In addition, such determinations lead to a better understanding of the production and distribution of the fall-out and furnish such required data as are used in the calculation (or prediction) of the fall-out patterns themselves.

[redacted]

RADIOLOGICAL NATURE OF THE CONTAMINANT; SOURCE GAMMA ENERGY SPECTRA

Dr. C.S. Cook
U.S. Naval Radiological Defense Laboratory

Using a NaI(Tl) scintillation spectrometer, gamma-ray spectra have been determined for selected samples returned from the Pacific Proving Grounds to USNRDL.

The spectrometer is a single-channel analyzer developed in our laboratory. The block diagram of its electronics is shown in Fig. 1, and a photograph of the apparatus is shown in Fig. 2.

A 4-in. diameter by 4-in. high cylindrically-shaped crystal was used for the analysis in order to enhance the total absorption peak. The effect of a large crystal on this enhancement is seen by comparing the spectra of Cs^{137} as obtained by a 1-in. diameter by 1-in. high crystal, uncollimated (Fig. 3), and a 4-in. diameter by 4-in. high crystal (Fig. 4). The number of quanta at a given energy is determined through measurement of the area of the total absorption peak, followed by a peak-to-total area correction and a correction for the number of quanta which pass through the crystal without undergoing either a photoelectric or Compton interaction.

Further reduction to a dosage spectrum is made by correcting as a function of energy for the relative ionization produced in a unit mass of air per photon per unit time in accordance with the work of Marinelli et al.

The dosage spectrum as a function of time after shot is shown in Table I for a sample from CASTLE, Shot 4, (Union). This was one of the best sources from the point of view of having sufficient strength to produce relatively good statistical accuracy (approximately ±10 per cent).

The time-dependent characteristics of the spectra should be noted. Prior to ten days following the detonation, a large fraction of the radiations are concentrated in the vicinity of 100 kev. This is primarily the result of induced activities in the nuclear device. After ten days a growth in the relative amounts of activity in the regions of 500 kev and 1.6 Mev are noted. This can be attributed to the presence of the Ba^{140}-La^{140} radiations. As this dies away, a concentration of the spectra in the 700 kev region is noted. The primary contributant to this is the Nb^{95}-Zr^{95} fission product chain.

It should be remembered that the figures quoted are percentages. The absolute activity is constantly decaying.

[redacted]

[redacted] ENERGY ACT

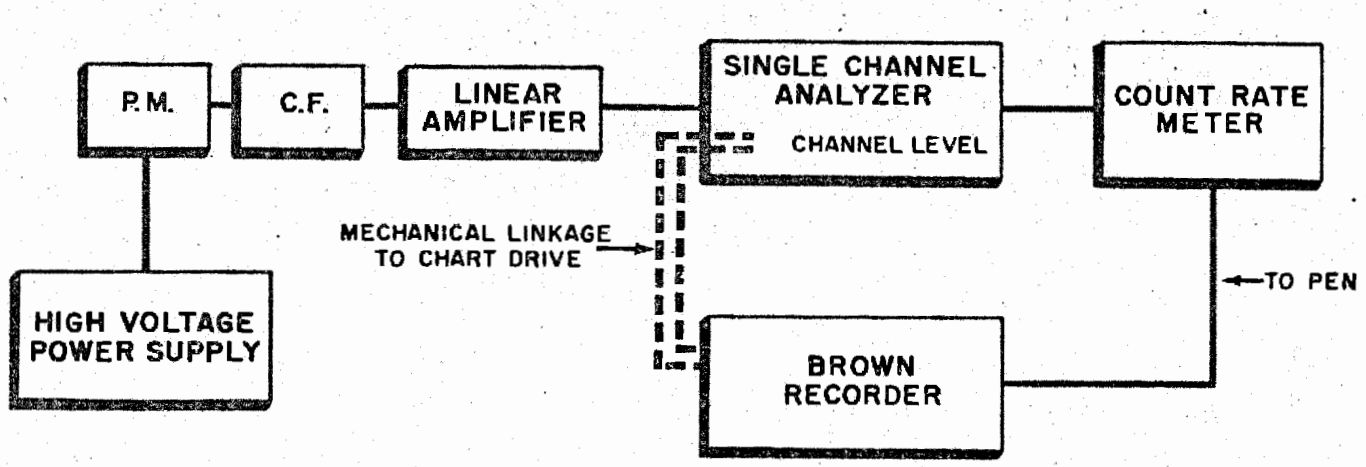

Figure 1
Block diagram of the Electronics for the Single Channel Scintillation Spectrometer. P.M. = Photomultiplier Tube, C.F. = Cathode Follower.

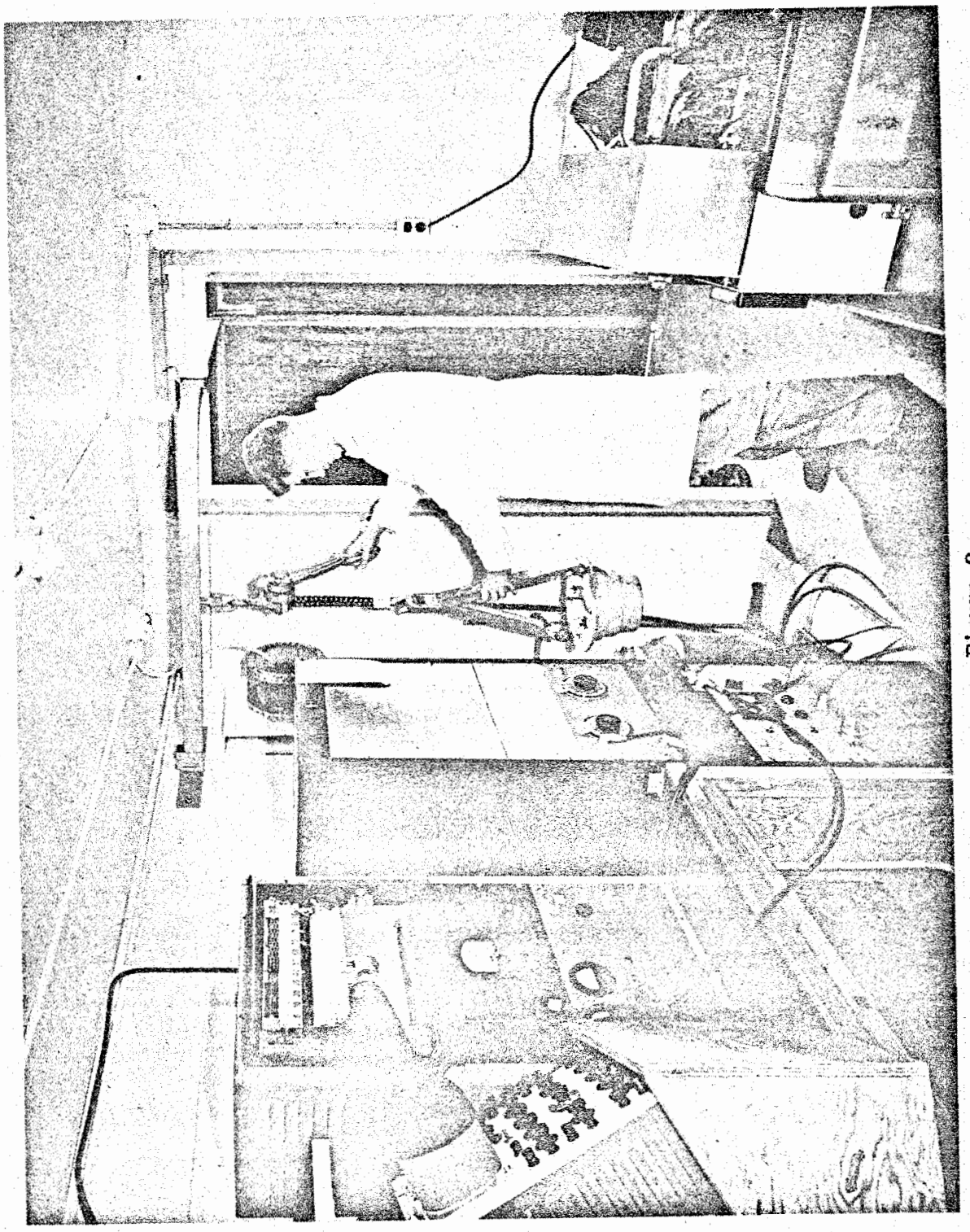

Figure 2
Single Channel Scintillation Spectrometer

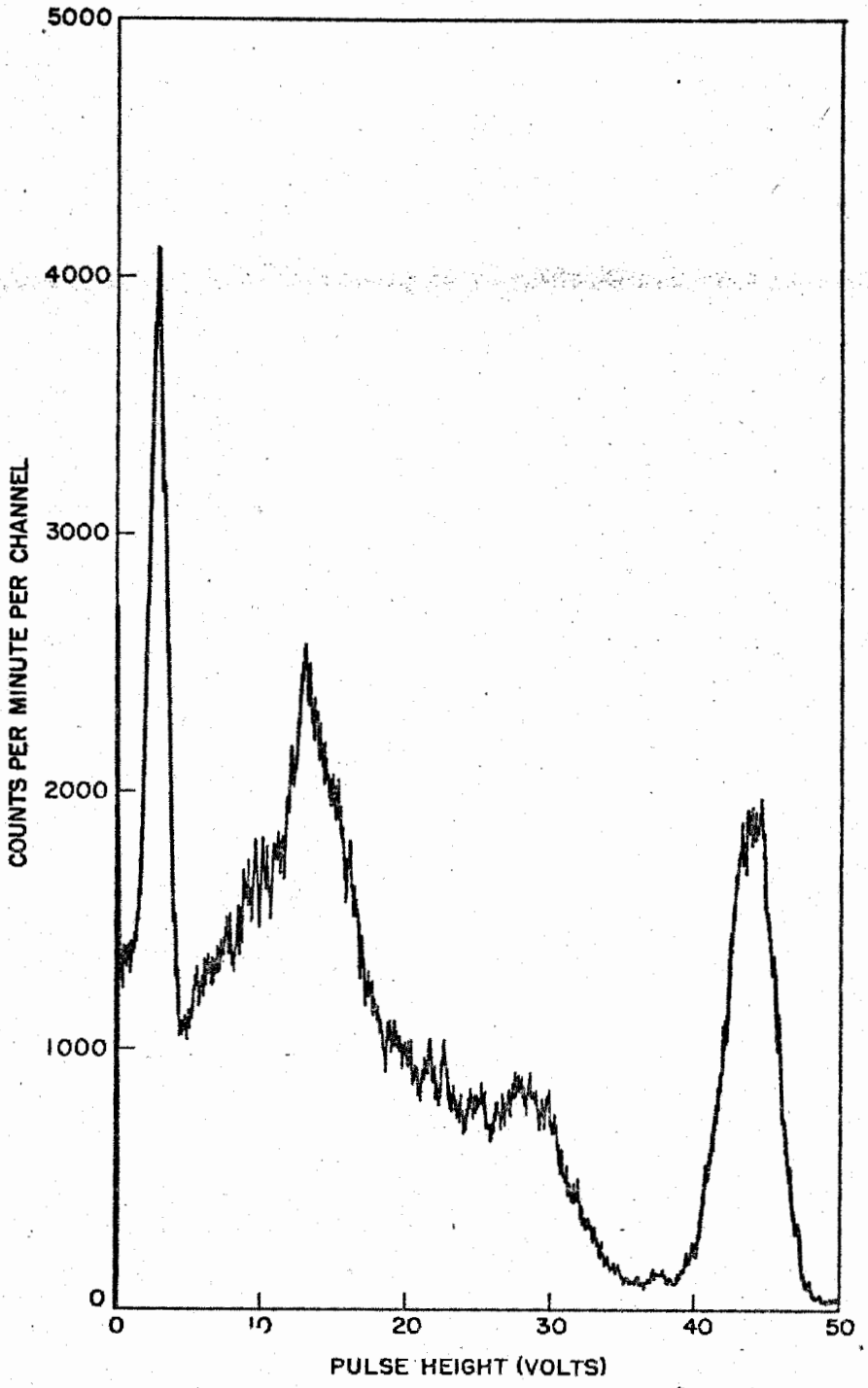

Figure 3
Spectrum of Cs^{137} as obtained by a 1-in. diameter by 1-in. high Crystal

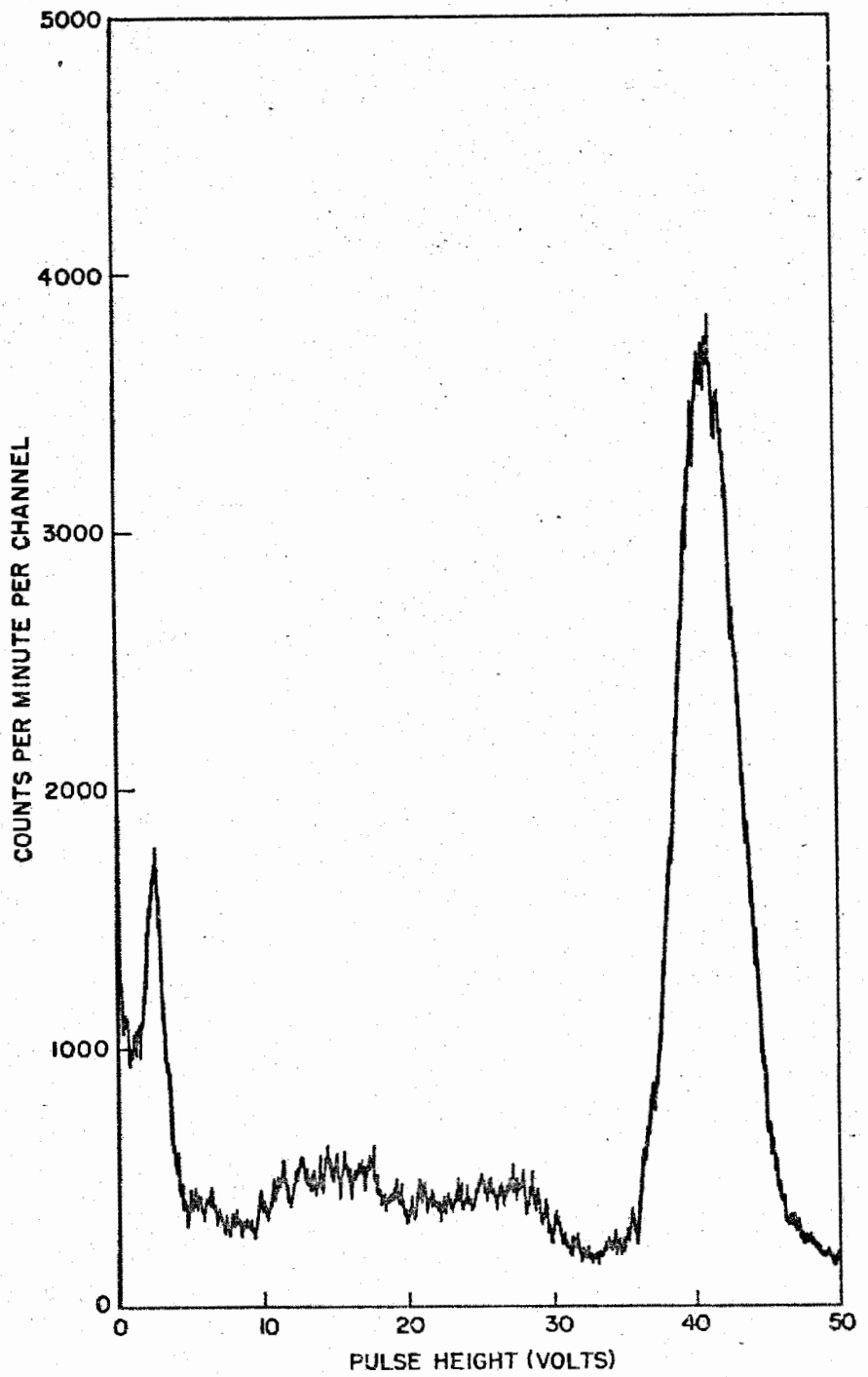

Figure 4
Spectrum of Cs^{137} as obtained by a 4-in. diameter by 4-in. high Crystal

147

TABLE I

Dosage Spectra for Sample 4-L in Per Cent of Dosage per 0.1 Mev Energy Interval

Days After Shot	0 .1	.1 .2	.2 .3	.3 .4	.4 .5	.5 .6	.6 .7	.7 .8	.8 .9	1.5 1.6
5.1	44.3	5.1	6.8		6.4		9.4	11.5	3.3	13.2
5.3	31.1	10.0	8.3		8.9		12.0	12.7	3.6	13.4
7.9	22.1	8.3	7.0	1.6	8.9		12.5	13.2	3.9	22.5
9.9	22.3	8.0	5.6	1.8	11.2		11.0	12.6	5.3	22.2
11.9	17.1	8.3	10.0	2.8	11.3		7.0	13.7	4.7	25.1
14.9	12.5	4.4	6.4	4.2	16.4		6.2	13.9	4.7	31.3
16.9	8.6	4.6	8.1	3.5	15.6		5.4	13.5	5.8	34.9
18.9	8.9	5.3	4.9	2.6	14.2		6.7	13.5	6.0	37.9
22.0	8.7	4.7	4.7	3.1	18.0		5.5	13.3	6.7	35.3
24.1	8.0	4.0	3.1	2.6	18.3		5.9	14.4	6.3	37.4
26.1	7.1	3.8	3.2	2.5	18.7		7.6	17.7	7.0	32.4
29.0*	5.3	3.7	2.1	2.6	17.5		7.9	16.9	9.0	35.0
29.1*	5.6	4.0	3.4	3.4	21.2			23.2	5.9	33.3
31.0	5.2	3.2	2.8	3.0	21.0			23.1	6.3	35.4
33.0	7.6	2.9	2.3	3.2	21.5			26.2	5.0	31.2
38.1	7.8	3.2	2.6	3.4	21.5			27.1	6.0	28.4
44.0	6.6	2.1	2.4	2.8	21.2			33.0	6.2	25.7
49.9	7.7	2.1	2.6	3.5	20.8			37.0	3.9	22.4
79.0	5.1	1.9	2.0	2.9	21.8			54.0		12.3
137.0		1.5		2.6	17.7			78.2		

* Sample 4-L consisted of two parts. Each contained approximately one cubic centimeter of liquid but one was prepared to have ten times the specific activity of the other. Measurements at 29.0 days and earlier were made on the lower specific activity source, and at 29.1 days and later on the higher specific activity source.

TABLE II

Dosage Spectra in Per Cent of Dosage Per 0.1 Mev Energy Interval for Several Samples, Each Recorded at Approximately 8 Days after Detonation

Sample	Days After Shot	0 .1	.1 .2	.2 .3	.3 .4	.4 .5	.5 .6	.6 .7	.7 .8	.8 .9	1.2 1.3	1.5 1.6	2.1 2.2
1-L	8	8.8	8.0	10.5	2.9	9.0	4.6	17.1	15.2	7.8		16.1	
1-L	5	14.5	8.3	17.0	2.7	9.9		16.8	14.9	5.9		10.0	
2-L	5	18.1	7.0	18.5	3.1		10.8	15.1	9.4	9.4		8.6	
2-L	7	14.0	8.1	15.5	2.8	10.6		11.7	14.5	2.8		20.0	
3-2	8	21.5	3.5	13.8	6.6	8.3		14.3	11.0	2.4	2.2	10.7	5.7
4-L	5	31.1	10.0	8.3		8.9		12.0	12.7	3.6		13.4	
4-L	8	22.1	8.3	7.0	1.6	8.9		12.5	13.2	3.9		22.5	
4-2	8	14.4	8.1	9.3	1.6	13.0		11.0	14.1	6.6		21.9	
4-3	8	23.9	10.2	16.6	3.7	9.7		8.6	11.6	5.0		10.7	
5-L	7	15.9	9.3	13.9	2.3	14.6		11.2	13.4	4.0		15.4	
5-L	8	12.7	6.6	9.5	1.6	13.7		15.7	20.5	3.3		16.4	
6-1	5	11.9	5.2	13.1	2.9	10.7		17.6	22.0	6.1		10.5	
6-1	7	13.0	6.4	11.0	2.4	10.0		17.5	19.9	7.1		12.7	
6-1	11	11.1	4.6	8.1	2.3	13.5		17.8	18.2	5.0		19.4	

TABLE III

Dosage Spectra in Per Cent of Dosage per 0.1 Mev Energy Interval for Several Samples, Each Recorded at Approximately 17 Days after Detonation

Sample	Days After Shot	0 .1	.1 .2	.2 .3	.3 .4	.4 .5	.5 .6	.6 .7	.7 .8	.8 .9	1.5 1.6	2.1 2.2	2.4 2.5
1-L	17	2.6	2.6	2.9	2.4	9.7	7.0	7.3	17.2	10.2	38.1		
2-1	17	7.3	2.8	4.6	4.2	19.2		3.0	20.5	3.4	35.0		
2-2	18	6.4	2.7	5.0	3.1	18.9		14.7	19.8	5.2	24.2		
3-1	17	12.4	10.8	3.2	10.3	17.3			11.4	6.4	21.9		6.3
3-4	17	17.1	8.0	7.2	12.2	16.3		11.0	11.8		14.0	2.4	
4-L	17	8.6	4.6	8.1	3.5	15.6		5.4	13.5	5.8	34.9		
4-2	17	11.1	4.4	7.7	3.6	17.0		8.1	14.6	6.6	26.9		
4-3	17	13.4	4.1	7.4	3.4	15.5		5.0	17.0	6.9	27.3		
5-L	17	7.0	2.9	5.8	2.9	19.2		10.0	16.5	7.5	28.8		
6-1	20	9.4	4.4	6.4	3.7	16.6		11.6	17.4	6.6	23.9		

[redacted]

To answer questions regarding variations in spectra from different detonations of the CASTLE series, intercomparisons have been made in the vicinity of 8 days following the detonation and 17 days following the detonation. These are respectively recorded in Tables II and III. Where a measurement at 8 days or 17 days was not available, measurements are shown at the nearest data recording time.

It will be noted that the spectra of all samples except those from Shot 3 show considerable agreement. Only from Shot 3 were radiations noted of energy higher than the 1.59 Mev La^{140} gamma-ray. No information is available to indicate the source of these radiations.

Energy and rate of decay measurements of the total absorption peaks allow most of the peaks of the spectrum of sample 4-L to be associated with particular radioisotopes. ~~In the low energy region, peaks were found whose energies and decay characteristics identified them with either Np^{239} or U^{237}.~~ Otherwise the identified peaks are associated with known fission products. Figure 5 indicates the relative contribution to the dosage spectrum. All peaks can be identified, with two exceptions. The contributions of the unidentified peaks are indicated by curves X and Y.

The results plotted in Fig. 5 are in reasonably good agreement with Heiman's predictions. The chief exceptions are the presence of two unknown radiations, X and Y, and the absence of iodine, also noted in the UPSHOT-KNOTHOLE report.

The unknown line, X, at approximately 75 to 85 kev, possesses decay characteristics similar to those of the Ba^{140}-La^{140} gamma-ray lines. In line with prior discussion it appears that at least part of this line may be spurious, attributable to the effect of a lower absorption coefficient immediately below the energy of the lead K-shell absorption edge. Although it makes an appreciable contribution to the quantum spectrum, its contribution to the dosage spectrum is quite small.

The higher energy unknown line has a half-life of approximately seven days. Its energy is not known uniquely since it appears in a group of at least three lines which overlap in the pulse height spectrum. However, if the total area under these lines is plotted as a function of time, normalized to the standard Cs^{137} peak, two half-lives expected in this energy region from the fission products and the unknown seven day half-life are observed. A search for possible sources of this gamma-ray was not too successful. One of the few which appeared feasible was the decay of Bi^{206} to Pb^{206}. It appears possible to fit the radiations of Bi^{206} into the pulse height gamma-ray analysis for sample 4-L.

Gummed paper samples were placed for observation in a Lustroid test tube having walls 0.028 gm/cm^2 thick. The aluminum cover for the

[redacted]

[redacted]

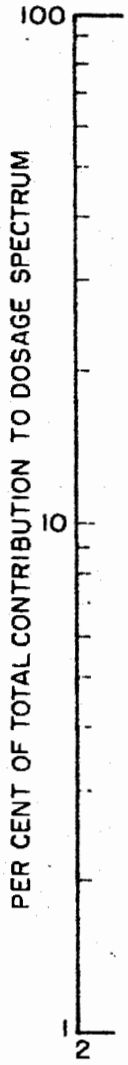

DELETED

DOE ARCHIVES

Figure 5
Relative Contributions to the Dosage Spectrum

152

[redacted]

crystal was 0.068 gm/cm^2 thick and the MgO powder reflector approximately the same as the aluminum. No betas having energies less than 500 kev should penetrate this material. However, there are several fission products, whose gamma-rays were observed in the spectrum, which emit beta radiation whose maximum energy end point is above 500 kev. To see whether a sufficient number of beta particles are able to get into the crystal to produce an error in the gamma-ray dosage spectrum, a number of tests were made in which the gamma-ray pulse height spectrum was recorded, both in the normal manner and with an aluminum cap whose minimum wall thickness was 0.880 gm/cm^2 covering the end of the Lustroid test tube. Typical plots are shown in Fig. 6 of the results in the low energy region at times when beta energies up to at least 1.5 Mev are expected. The black line is the spectrum as recorded without the aluminum cap and the white line as recorded with the aluminum cap. The only difference is observed below 75 kev and this can be explained by the absorption of the low energy gamma radiation in the aluminum cap. Therefore, it is concluded that no correction is required for the underlying continuous beta spectrum in the pulse height spectrum, and no such correction was made in this study.

The Shot 1 samples of radioactive coral from the four locations of Table 1 were initially treated as four radioactive sources. From three to six pieces of coral had been removed from each gummed paper and collected together as individual samples for analysis in the pulse height spectrometer. Although similar spectra were obtained, there were sufficient differences to introduce questions regarding possible fractionation of the samples as a function of position of the sample collector. Because of these differences, the pulse height spectra from individual coral particles were observed. The particles were found to fall into two classifications with regard to spectra, and both classifications appeared both downwind and crosswind. The two general types of pulse height spectra, henceforth called type 1 and type 2, are shown in Figs. 7 and 8, respectively. The spectrum of type 1 appears to consist primarily of radiations from $Ba^{140}La^{140}$, with perhaps a small amount of $Zr^{95}Nb^{95}$ radiation. On the other hand the spectrum of type 2 shows very little $Ba^{140}La^{140}$ radiation, but sizable quantities of Ru^{103}, Zr^{95}, and Nb^{95} radiations.

These measurements begin at approximately five days after detonation. Source spectral measurements should be made at earlier times. Such measurements are contemplated for Operation TEAPOT. Overlapping times with the currently reported measurements will allow comparisons between low and high yield weapons. Although there is no reason to believe that there should be any drastic difference except for differing amounts of induced activities, spectral measurements at times corresponding to the currently reported measurements will be made.

[redacted]

[redacted]
ATOMIC ENERGY ACT

153

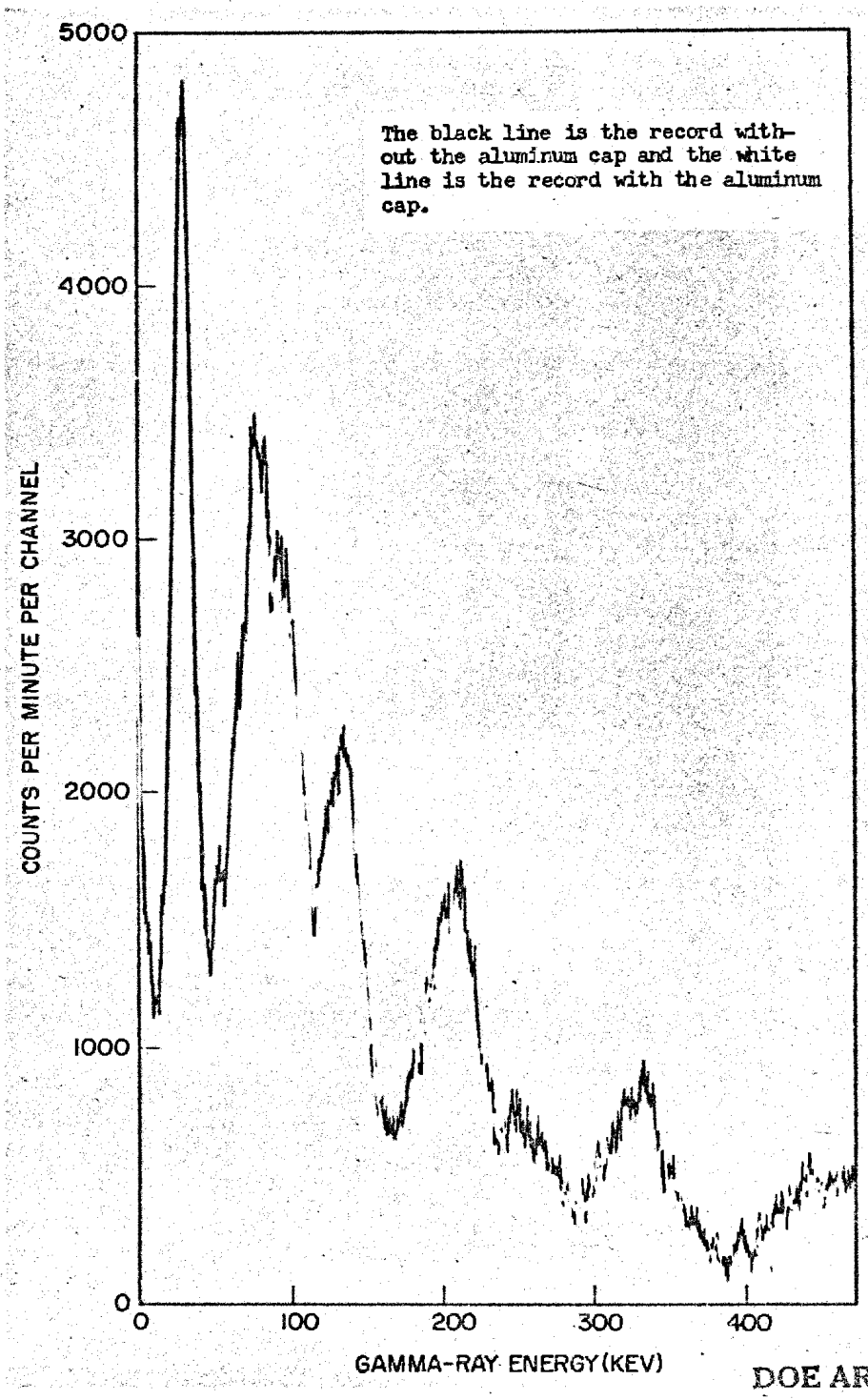

Figure 6
Low Energy Region Spectra

[redacted]

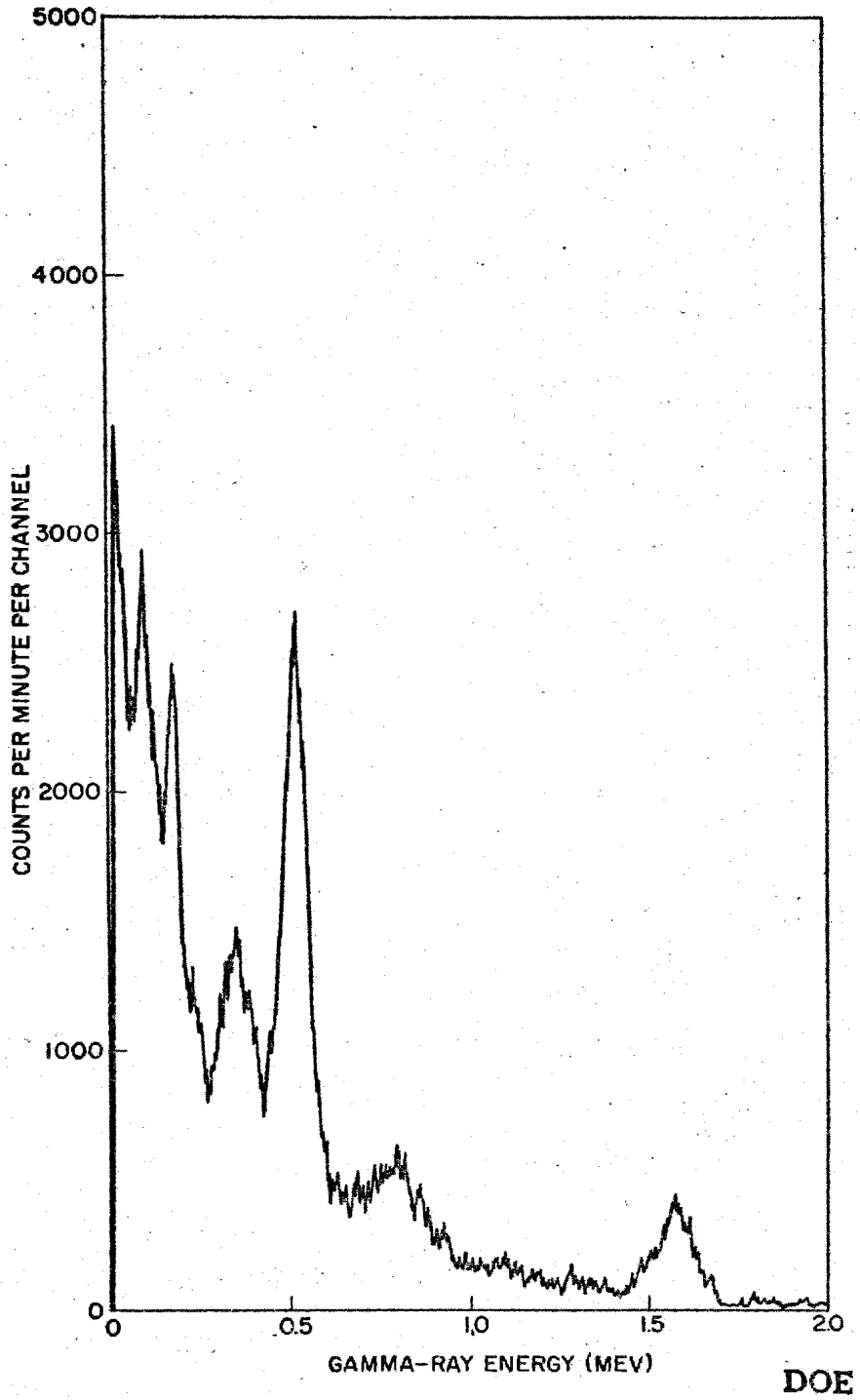

Figure 7
Type 1 Pulse Height Spectrum

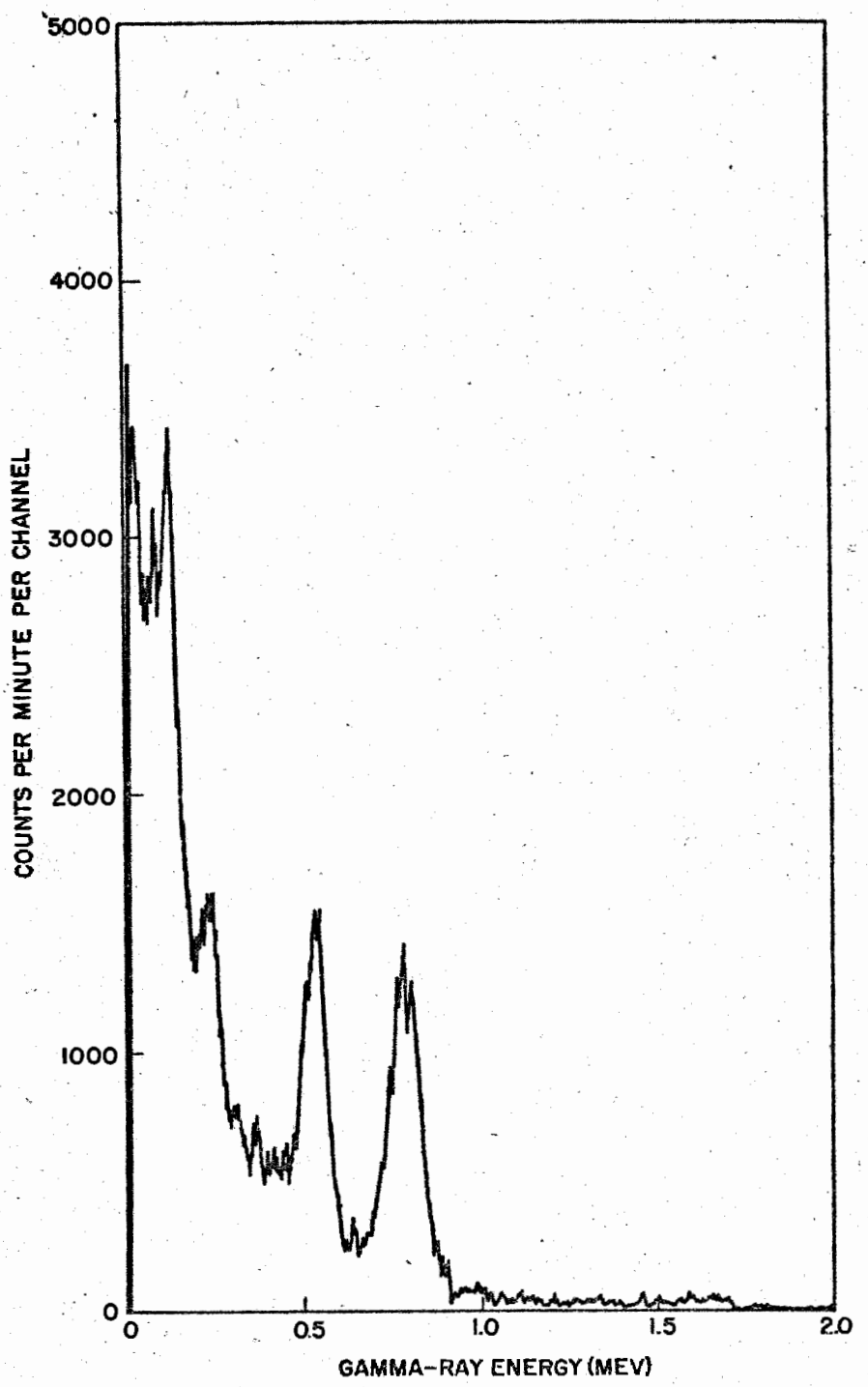

Figure 8
Type 2 Pulse Height Spectrum

[redacted]

Controlled experimental determinations of the spectra from distributed sources are also needed. These are relatively straight forward, although time consuming once experimentally determined source spectral characteristics are known. A limited amount of this type of information can be obtained at weapons effects tests, and some measurements of this type will be made at TEAPOT.

[redacted]

[redacted]

THIS PAGE IS BLANK

[redacted]

[redacted]

[redacted]

RADIOLOGICAL NATURE OF THE CONTAMINANT; DECAY OF THE GAMMA RADIATION FIELD

N. E. Ballou
U. S. Naval Radiological Defense Laboratory

It is the purpose of this paper to present a general discussion of decay and radiation characteristics of nuclear weapons debris and to report on the results of measurements of these characteristics of fallout material produced in Operation CASTLE. It is clear that the decay and radiation properties of nuclear bomb debris are necessarily among the predominant determinants of radiation hazards resulting from such detonations, and thus good information on them is required for many purposes.

The contributing species to the radiation field consist of fission product radionuclides in addition to other radionuclides formed by neutron induced reactions. The relative amounts of the various fission products are determined by their fission yields; the fission yields are functions of the identity of the nuclide undergoing fission and the energies of the neutrons causing fission. The non-fission product radionuclides result from neutron reactions with the components of the nuclear devices and with the environmental materials in the detonation area. The relative amounts of these products depend on the quantities of material exposed to neutrons, the cross-sections for the reactions producing them, and the total number of neutrons to which the material is exposed.

Determination of gross decay curves from nuclear detonations can be made either by direct observations on the debris or by calculations. In order to calculate a gross decay curve, knowledge of the yields and half-lives of all contributing radionuclides must be known. At the present time, there is much good information available on yields and half-lives of fission products whose half-lives are approximately one hour or longer. The yields of neutron induced radionuclides vary from one weapon type to another and with the nature of the surrounding detonation medium. The contributions of induced radionuclides have been determined radiochemically in a large number of nuclear detonations. Under most circumstances, the major contributors are those derived from the components of the nuclear weapon and only to a small extent from the materials present in the detonation area.

It is of importance to measure the gross decay curves from various nuclear detonations and to compare them to the calculated curves. The main cause of lack of agreement between such curves would be the use of inaccurate fission yield and half-life values in the calculations and

[redacted]

[redacted]

the existence of fractionation among the products of a nuclear detonation. Since half-life and yield values are believed to be fairly well known, fractionation is the most likely source of discrepancy. Fractionation has been observed radiochemically in some detonations, especially in the surface type shots. This was markedly demonstrated in measurements on Operation JANGLE debris.

Because of these and other considerations, it seemed worthwhile to measure the gross decay curves of material resulting from Operation CASTLE. Both beta and gamma ray decay curves were measured. In order to obtain information on beta and gamma ray energies as a function of time, decay rates were measured with various lead and aluminum absorbers placed between the sample and detector. The measurements were started at the site as soon after detonation as possible and were eventually continued at USNRDL. The beta and gamma ray decay curves (Figure 1 and Figure 2, respectively) have the same shape except at longer times, approximately two weeks, at which times the gamma curves have a somewhat steeper slope. Although the gamma ray counting rates were rather low by this time, the differences may be real. Computations of the gamma ray decay curves have not been completed, consequently, the extent of similarity to be expected between the beta ray and gamma ray decay curves is as yet not known. In order to compare beta ray disintegration rate and gamma ray ionization decay curves, measurements of these two were made at the site for approximately two weeks following detonation. The shapes of the two were the same. Comparisons between observed and calculated beta ray decay curves (Figure 3) show that there is moderately good agreement among these curves. Absorption curves on samples of fallout material gave information on beta ray and gamma ray energies. Although details cannot be derived from the curves, the expected occurrence of soft and hard beta and gamma ray components was found. The results are in general agreement with the more detailed information on energies obtained from spectral measurements, as reported by Dr. Cook in the preceding paper.

DELETED

The slopes of the logarithmic beta ray decay curves can be approximated by certain values over given periods of time. For most of the CASTLE shots, the slope was approximately -1.0 from about three hours to six days. From

[redacted]

160

[redacted]

this page stamped in. was marked in red by mistake

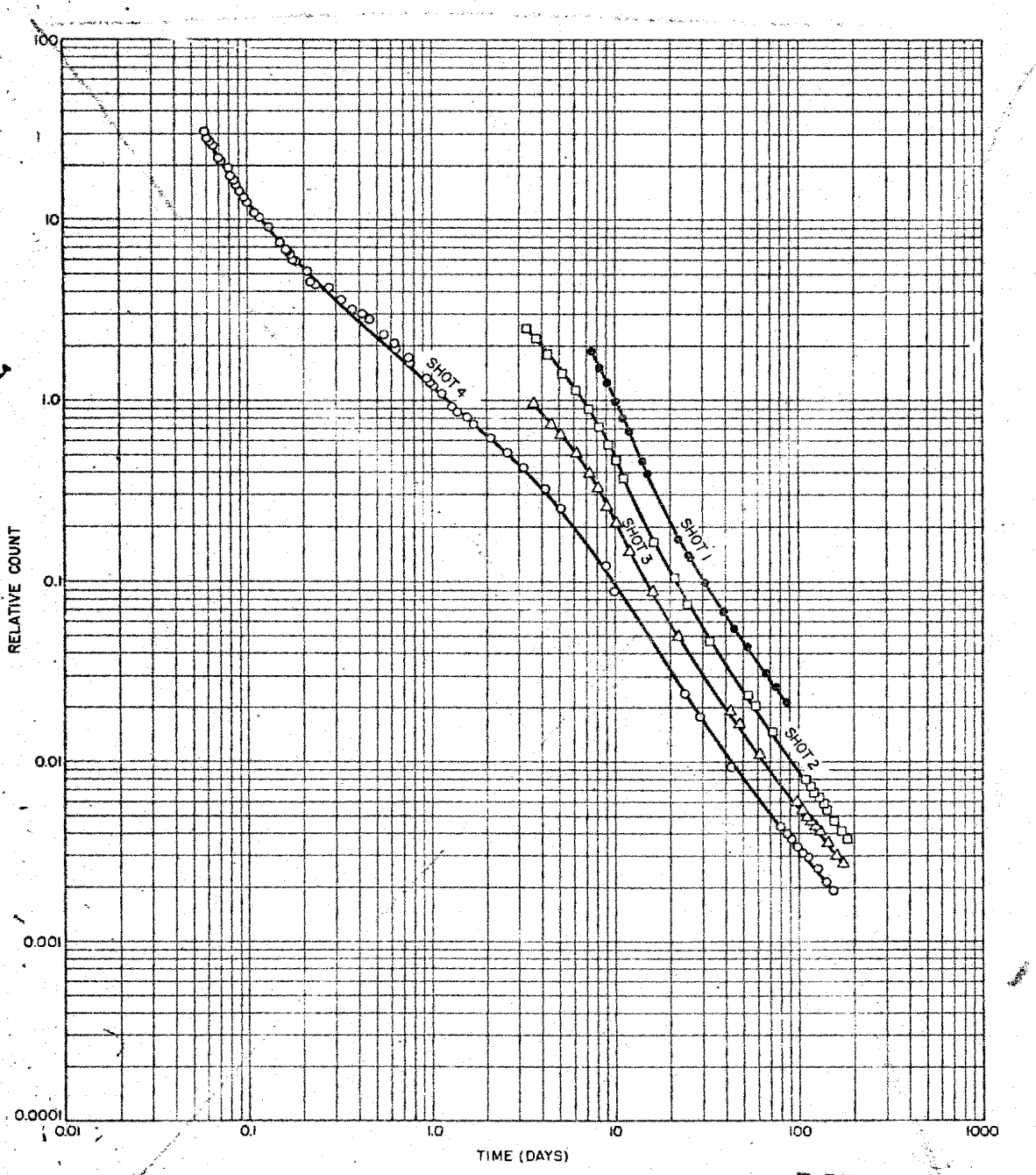

Figure 1
Gross Beta-Ray Decay of Fall-out Samples from Shots 1, 2, 3, and 4

[redacted]

[redacted]
MIC ENERGY ACT

161

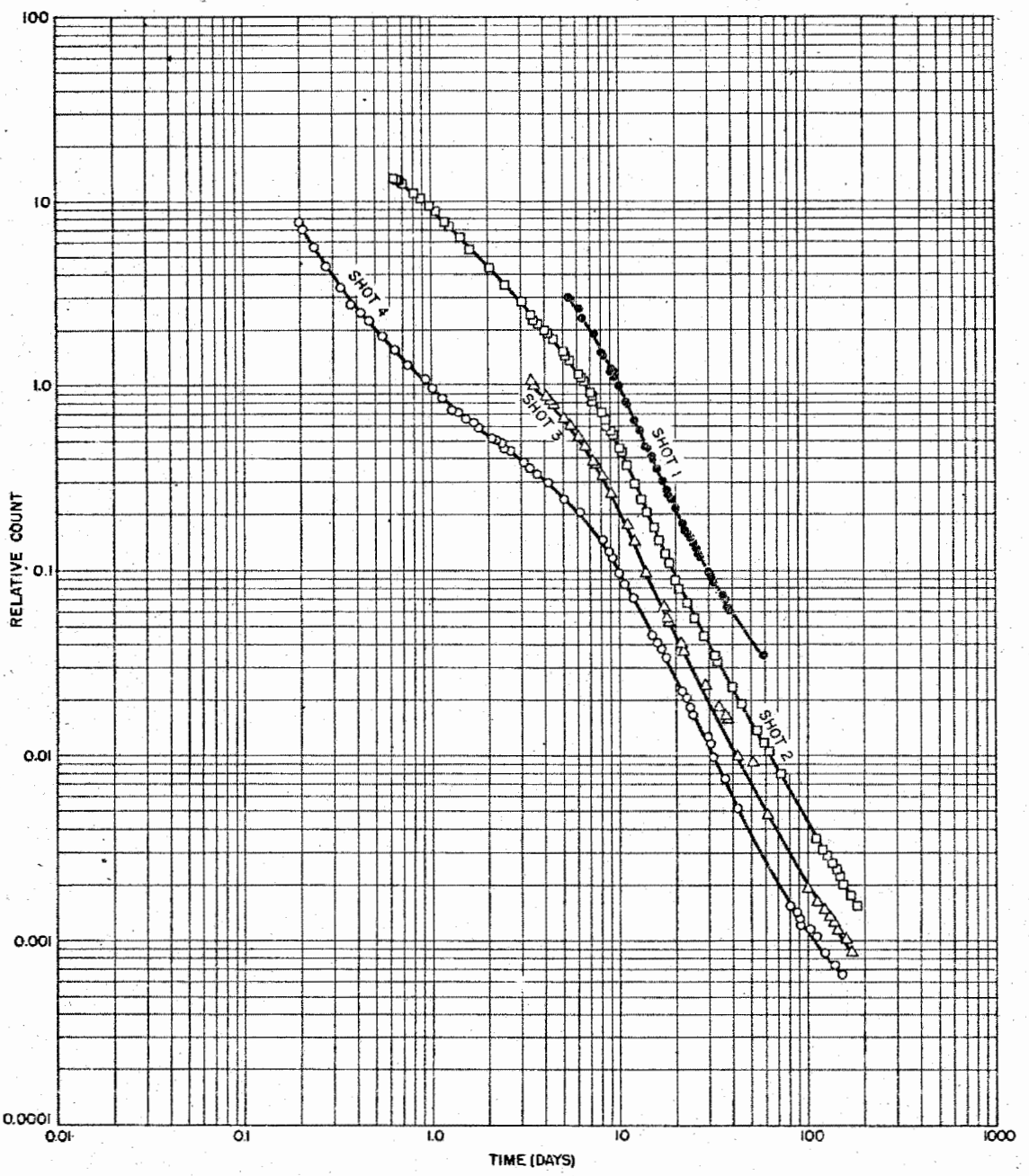

Figure 2
Gross Gamma-Ray Decay of Fall-out Samples from Shots 1, 2, 3, and 4

[redacted]

DELETED

DOE ARCHIVES

Calculated and Observed Gross Beta-Ray Decay Curves of Fall-out Sample

159

[redacted]

[redacted] OMIC ENERGY ACT 19

six days to fifty days, the slope was about -1.7. The observed slope at the earlier times agrees with the calculated value. The slope at later times is somewhat greater than the calculated value of -1.5.

It is now possible, as a result of radiochemical measurements, to make certain statements about gross decay rates of debris from various types of weapon detonations. Relative production of non-fission product radionuclides is in general greatest with thermonuclear weapons of the type tested so far; is appreciably less with normal fission type weapons; and is very small with the type of gun weapon tested in the UPSHOT-KNOTHOLE test series. Gross beta ray decay curves of debris from representative weapons of these three types are given in Figure 4.

DELETED

On the basis of studies made so far, several conclusions can be reached. First, the radiochemical composition of unfractionated nuclear weapons debris is moderately well established for weapons of various types. Second, fractionation of products of nuclear weapons detonation does occur, especially in surface type shots. Third, calculated gross beta ray decay curves agree with the experimentally observed curves for unfractionated material. Fourth, in the absence of well established gamma ray decay curves, calculated beta ray decay curves can be used to approximate the gamma ray decay curves.

In view of the present state of knowledge, it is recommended the following be done in order to obtain necessary information on radiation characteristics of nuclear weapons debris:

Calculate beta and gamma ray energies as a function of time for various weapon types.

Measure radiochemical composition of debris from nuclear weapons test and determine nature and extent of fractionation.

[redacted]

DELETED

Figure 4
Calculated Gross Beta-Ray Decay Curves from Thermonuclear, Fission and Gun Type Nuclear Weapons

[redacted]

[redacted] DATA
[redacted] ENERGY ACT [redacted]

[redacted]

Measure gamma ray decay curves and energy spectral distributions of nuclear weapons debris and determine extent of agreement between measured and calculated curves.

[redacted]

[redacted]

RADIOLOGICAL NATURE OF THE CONTAMINANT; RADIATION FIELD GAMMA ENERGY SPECTRA

Mr. Stanley Ungar
Evans Signal Laboratory

Radiation survey instruments are used in monitoring dose rate levels in contaminated areas. Design requirements for these detectors call for an energy response of ± 20% down to 80 Kev. In order to determine the adequacy of present specifications, a determination of the fraction of the radiation dose due to photons in the energy range below 80 Kev is essential. In addition, knowledge of the spectral distribution of the gamma ray fields is desirable in order to predict the relative biological effectiveness of the radiation. This paper will concern itself with a brief survey of previous field determinations of parameters of the gamma spectra of residual contamination and a summary of the techniques and results of scintillation spectrometer measurements made during Operation UPSHOT-KNOTHOLE.

Several experimental approaches to these determinations have been made. The gamma spectral quality was investigated at Operation GREENHOUSE and at subsequent test operations. Data available have been obtained by essentially three techniques: absorption measurements, energy dependent chambers, and scintillation crystal spectrometers.

Absorption Type Measurements

Depth dose studies have been made by several groups during past operations. In these measurements, dosages are obtained as a function of depth from surface. Pressed wood phantom men and spherical absorbers made of tissue-equivalent or unit density materials are unusable in the field as effective energy measuring devices. Numerous experiments have demonstrated that the shape of the depth dose curve is not very sensitive to the effective energy of the gamma radiation over a wide range of energies. This is due in part to the fact that the radiation is incident on all sides and to the high ratio of scatter to actual absorption taking place. Comparison of various absorption curves indicates that the high surface readings obtained are due to high energy β particles which are rapidly attenuated by the first two gm/cm^2 of absorber, rather than low energy gamma radiation.

Aluminum lined and air wall chambers used in depth-dose studies have shown that the effective energy inside the phantom decreased relative to the effective energy of the gamma radiation near the surface of the phantom. This was attributed to the increased effect of scatter within the phantom.

[redacted]

[redacted]

167

[redacted]

Measurements have also been made with film badges as detectors using copper spheres of various thicknesses around the film as absorbers. The results of measurements of residual radiation quality were expressed in the form of copper absorption curves. No evaluation was attempted, however, of the effective energies of the composite spectra.

Although these absorption measurements did not provide the gamma spectral distribution or the effective energy of the residual contamination, the depth-dose curves may be of use in themselves for predicting total-body dose from readings of surface detectors. In addition information was obtained regarding the presence of β particles in the soft component of the radiation.

Energy Dependent Chambers

Lining the walls of an ionization chamber with a material which is not air equivalent changes the relative response such as to make the instrument energy dependent. This response will depend on the true absorption coefficient of the wall material and its stopping power for electrons. Numerous measurements have been made using ionization chambers lined with materials such as aluminum, copper, tin and lead of various liner thicknesses. Prior to field use, theoretical and experimental curves were obtained for the chamber response as a function of energy, heavily filtered X-ray beams being used in these calibrations as well as any monoenergetic gamma sources available. Field measurements were made using both lined and unlined chambers. The ratio of lined and unlined chambers gave an indication of an "effective" energy of the radiation. The effective energy value at any one time or place was in general somewhat dependent upon the liner material used. This is due in part at least to the fact that instruments calibrated by beams of relatively narrow photon energy distribution were used to evaluate a photon beam containing a broad band of energies. The significance of such effective energy determinations is reduced as the broadness of the photon energy distribution increases. Extensive sets of data on effective energies at various positions and times have been obtained. Effective energies for a number of distances for two shots at Operation GREENHOUSE ranged from 83 to 127 Kev. At Operation JANGLE over a large area of contamination the effective energy measured near a surface burst and an underground burst ranged from 84 to 140 Kev and 113 to 144 Kev respectively. Measurements during UPSHOT-KNOTHOLE gave effective energies ranging from 96 to 230 Kev. The effective energies were highest in the crater and fall-out areas and were observed to decrease for several days subsequent to detonation after which time they increased.

Data obtained during UPSHOT-KNOTHOLE with lined chambers were used to determine mixtures of X-ray beams which would yield results

[redacted]

[redacted] ENERGY ACT

[redacted]

equivalent to those obtained in the field measurements. These field equivalent X-ray beam mixtures were then considered to be representations of the quality of the gamma radiation. Considering these mixtures, the UPSHOT-KNOTHOLE field results indicated the percentage of energy flux of photons of energy below 200 Kev varied from approximately 5 to 25 percent of the total energy flux.

An attempt was made to obtain more spectral information by extending the lined ionization chamber technique. Here use was made of the fact that the energy response curves of aluminum, copper, tin and lead peak at different energies. An estimate was made of the percent of gamma dose rate contributed by gamma rays of energy less than 200 Kev as well as the approximate spectral extent. The Operation JANGLE results indicated, for a number of locations within several days after detonation in the fall-out area, that the soft component contributed 60 to 70 percent of the total dose for the surface shot and 40 to 50 percent of the total dose for the underground shot and that the hard band extended to beyond 1 Mev in energy. The Operation SNAPPER data indicated that for the times after detonation and distances from ground zero over which measurements were made 15 to 35 percent of the gamma dose was contributed by gamma rays less than 200 Kev in energy. Operation UPSHOT-KNOTHOLE results indicated for the first two days after detonation 9 to 30 percent of the total being contributed by gamma rays with less than 200 Kev energy.

Scintillation Spectrometers

Gamma spectral distribution curves were obtained during Operation UPSHOT-KNOTHOLE using a scintillation crystal-type spectrometer. Measurements were made for several shots at various times after detonation and at various distances from ground zero. This instrument is well suited as a field device as it can be made relatively compact with a minimum of shielding and can readily be moved to various locations in the fall-out area. The gamma ray energy distribution was determined over the approximate photon energy range from 40 Kev to 2 Mev. The spectrometer incorporated a low energy NaI-Tl crystal detector head to cover an energy range from 40 Kev to 200 Kev and a high energy anthracene crystal detector head which covered an energy range from 200 Kev to 2 Mev.

The gamma ray photons incident on the NaI and anthracene crystals undergo photoelectric and Compton absorption, producing secondary electrons. These electrons for the most part are completely stopped within the crystal, giving rise to the emission of a quantity of light of a quality characteristic of the crystal. The integrated light flux of each incident photon is proportional to the energy of the secondary

[redacted]

[redacted]

[redacted]

electron produced. The pulses from the photomultiplier which are amplified are therefore proportional in height to the energies of these secondary electrons produced. Knowing the absorption processes taking place, an analysis of the pulse height distribution of the secondary electrons leads to a determination of the incident photon spectrum. Measurements made were of the detected count rate per channel width versus pulse height using a single channel analyzer.

The response of the NaI-Tl crystal is due predominantly to the photoelectric absorption process, Compton interactions being minimized by low Compton absorption cross section and small crystal thichness (0.2 cm). A thick tin absorber around the crystal decreased the total number of events. In order to correct for Compton electrons due to higher energy photons contributing to the observed pulse height distribution measurements were made with and without a removable tin disc of 1.75 gm/cm^2 thickness over the top face of the crystal and the difference in these two curves was considered to represent the pulse height distribution of the photoelectrons. An In^{114} source of known strength was used to absolutely calibrate the NaI crystal used, and to determine energy scale (Figure 1). The effects present and the assumptions employed in the analysis were such as to somewhat over estimate the photon intensity at the low energy end of the spectrum so that if the low energy region of the gamma dose spectral distribution is not of great importance, then it may be concluded that present radiation survey instrument design parameters are adequate.

The portion of the spectrum extending from 200 Kev to 2 Mev was determined using the anthracene crystal. In this energy region Compton absorption predominates and with the anthracene crystal used is the only process of importance. Analysis of the data obtained is based on the assumption that the pulse height distribution due to absorption of monoenergetic photons may be approximated by a rectangle, the area of this rectangle being proportional to the incident photon flux. The gamma ray spectrum is then given by the derivative of the measured pulse height distribution curve, correcting for crystal efficiency and energy scale distortion. Absolute calibrations of the anthracene crystal used were performed using both Co^{60} and Cs^{137} sources of known intensities (Figure 2). Co^{60} was used to determine the energy scale. The calibration procedure was performed both prior and subsequent to each field run in a radiation free area. The assumption of the rectangular distribution limits the resolution of the results in this region although the general shape of the spectrum may be obtained. The intensities measured with the two crystals were normalized using the absolute calibration of each crystal.

[redacted]

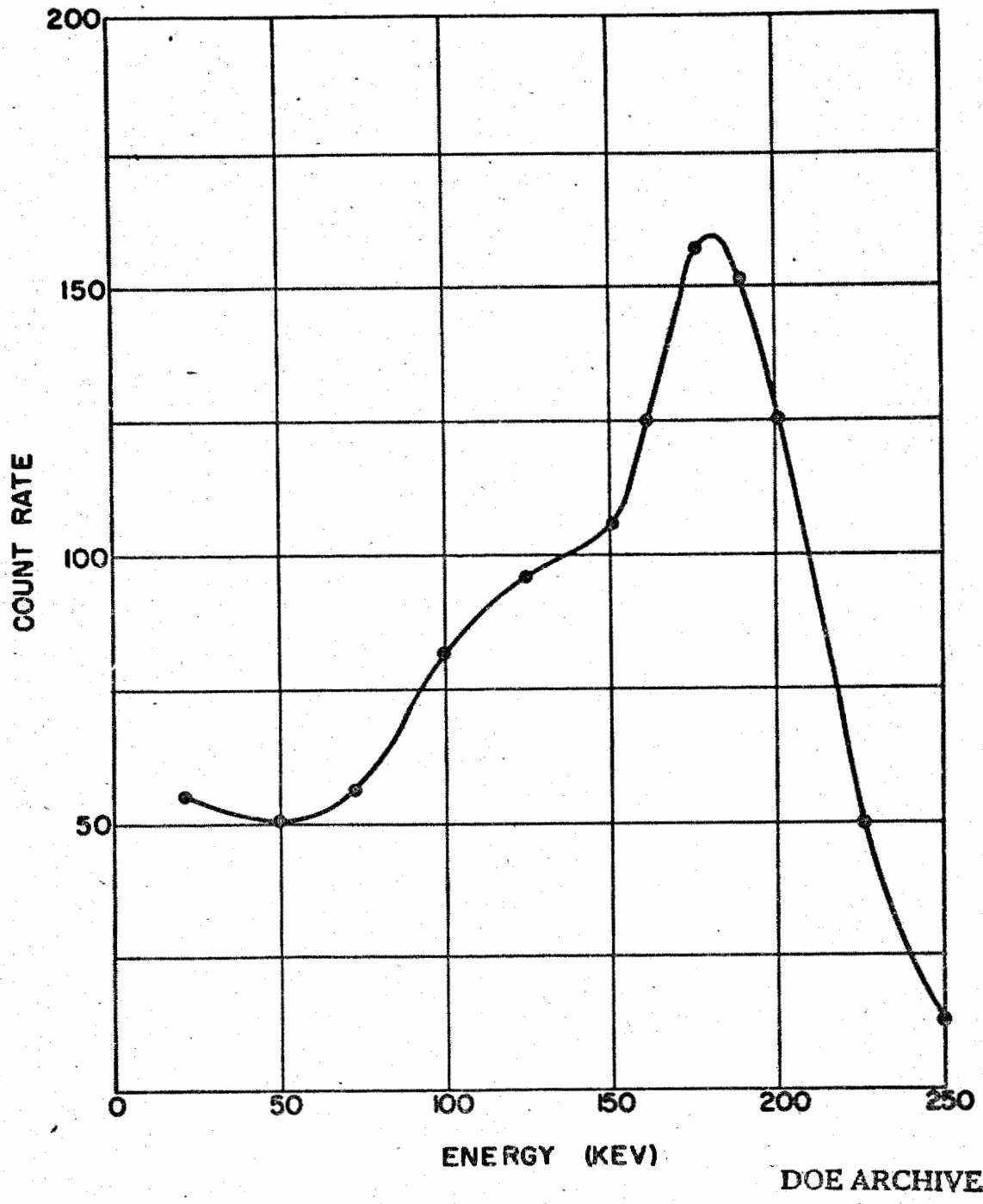

Figure 1
NaI-Ti Response for In^{114}

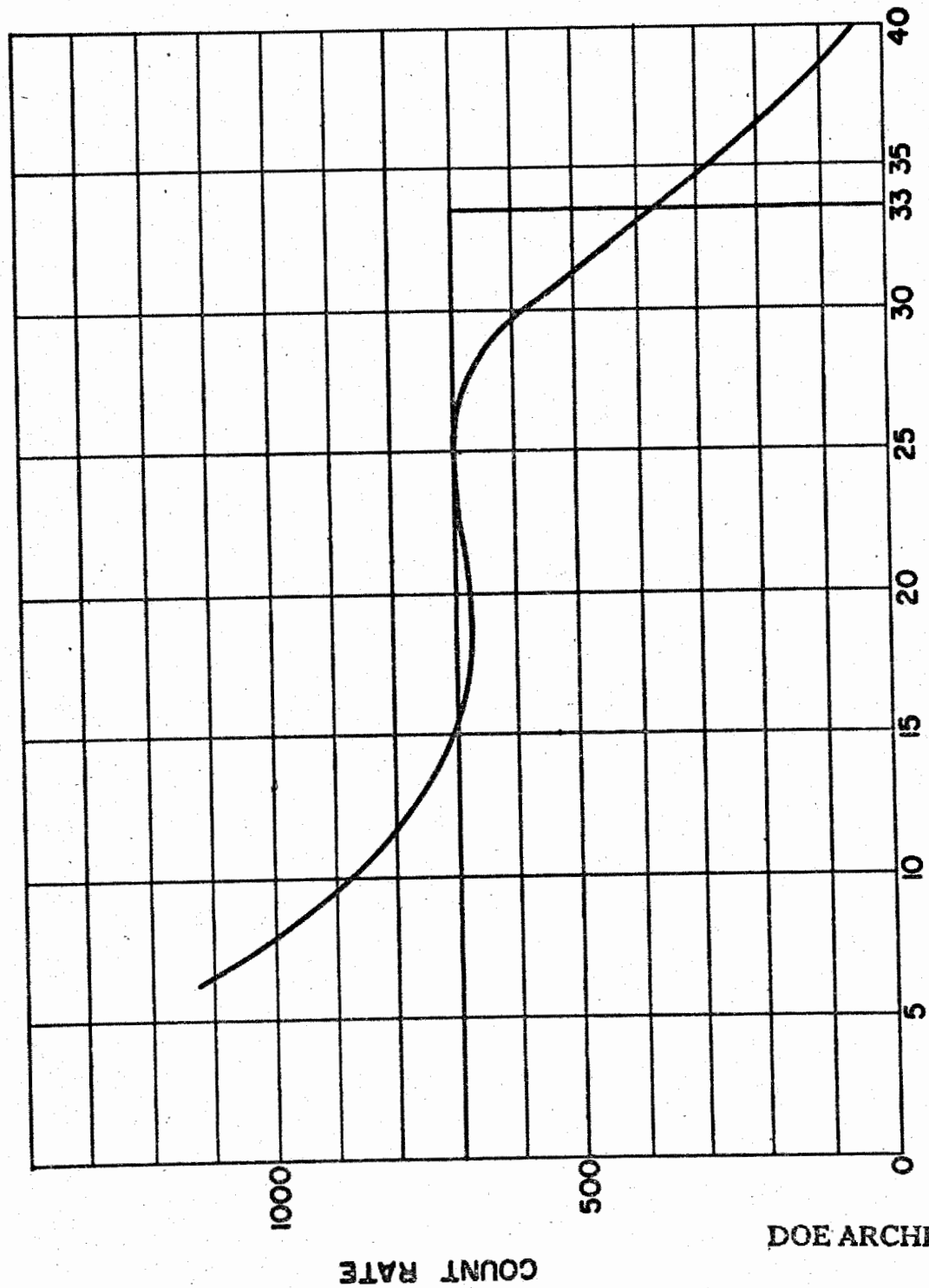

Figure 2
Anthracene Crystal Response for Cs^{137}

[redacted]

[redacted]

Comparison of the results of scintillation spectrometer and lined ionization chamber measurements taken at the same location at the same time showed excellent agreement. Insufficient data was obtained to make any generalizations regarding the variations of spectral quality with distance. Indications were that the spectrum softens for several days subsequent to the shot after which time a progressive hardening occurs. Results (Figures 3, 4, 5, 6) also disclose a large contribution to the gamma dose rate by photons with energies up to approximately 2 Mev. In addition to the low energy peak below 200 Kev, most of the data indicated peaks in the 600 to 800 Kev and 1.5 to 1.8 Mev energy regions. Results indicate that for measurements made on subsequent days and closer distances from the point of detonation, the peak in the highest energy region becomes increasingly important. In general, as was to be expected because of multiple scattering, the contribution to the low energy peak was greatest from the upward direction. It was concluded that for the tower and air detonations following which there was an extensive contaminated area, the contribution to the gamma dose rate by photons with energies less than 100 Kev is but a small percentage of the total. When making gamma measurements in these residual fields, currently used radiac instruments with their associates energy response are adequate. For surface and subsurface detonations the spectral distribution in the fall-out area is significantly altered so that additional information is required before adequacy of radiation detectors under these conditions may be determined.

The use of a total absorption spectrometer for future measurements will enable better resolution of the spectral distribution and eliminate the need for normalization of two crystals, thereby increasing the overall accuracy. It is recommended that these measurements include the energy region down to 20 Kev, that the angular dependence be investigated in greater detail, that more data be obtained regarding the variation of spectral quality with distance from ground zero, and that lined chamber measurements be made simultaneously for the subsurface detonation to enable further conclusions regarding the adequacy of this technique for rapid evaluation of spectral quality. It is further recommended that the spectral measurement be absolute so that a comparison of the integrated dose rate with radiac readings can be made.

[redacted]

[redacted]

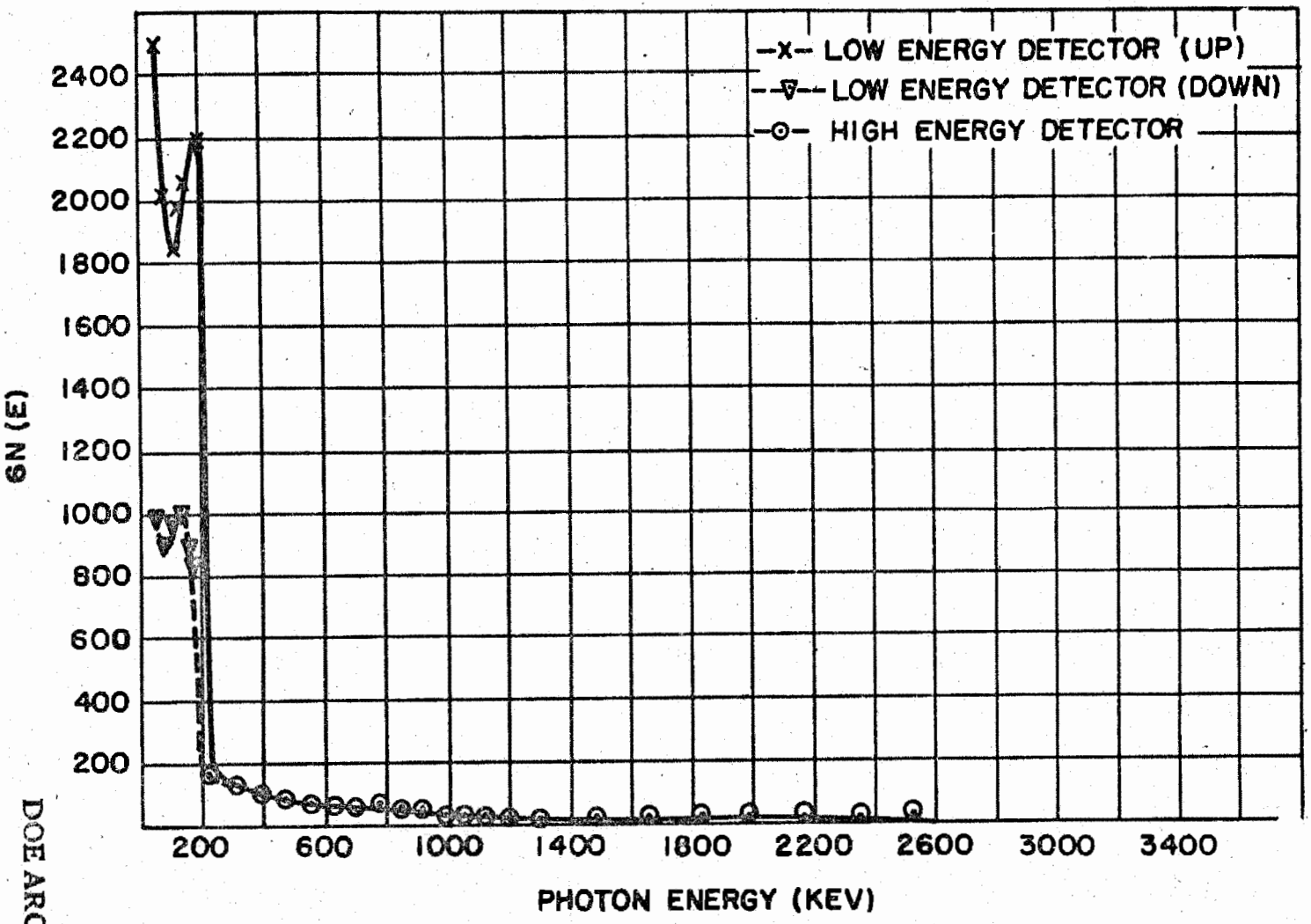

Figure 3
Photon Spectral Distribution - Shot 8 (D+2)

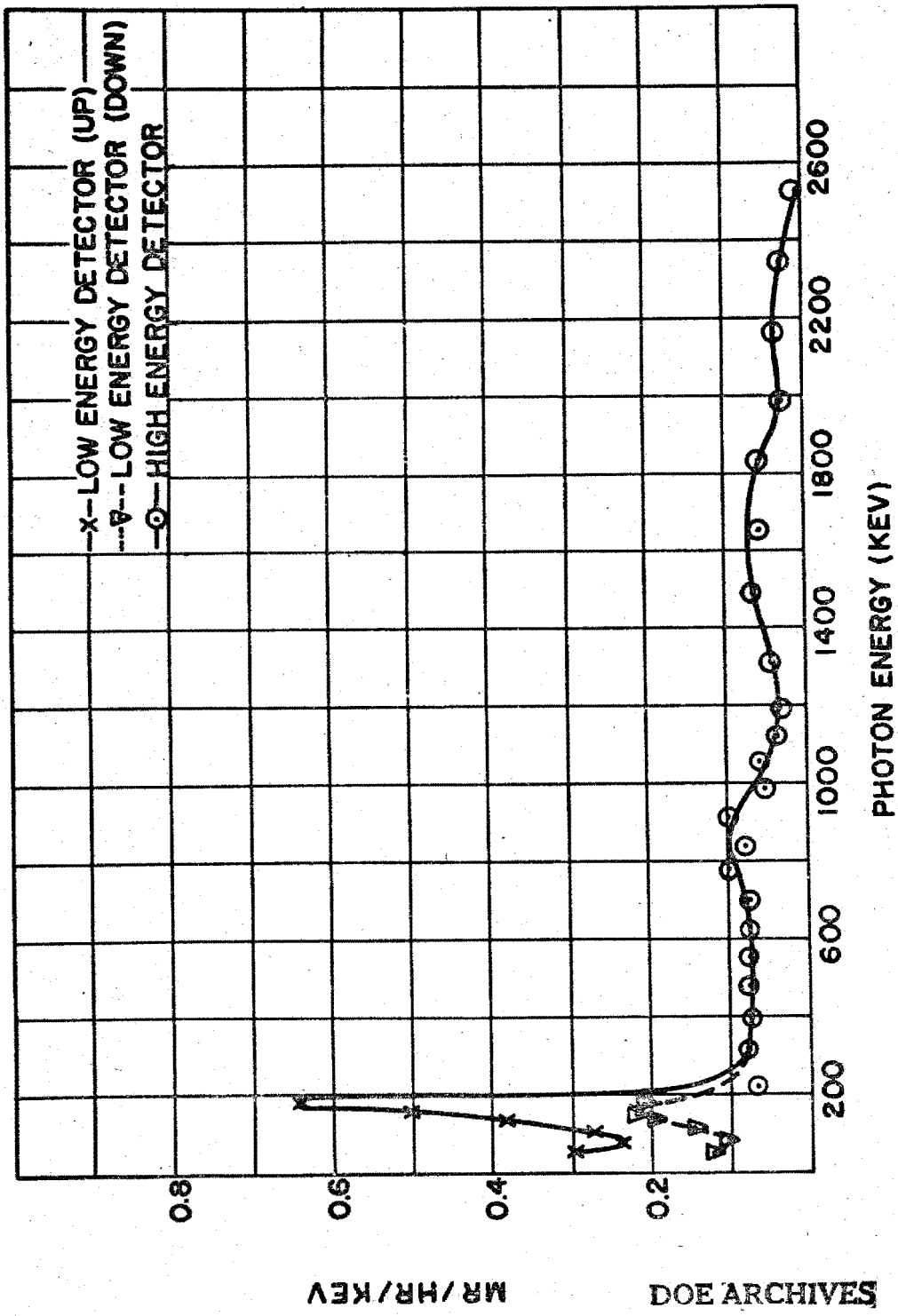

Figure 4
Dose Rate Spectral Distribution - Shot 8 (D+2)

[redacted]

[redacted] ENERGY A[redacted]

175

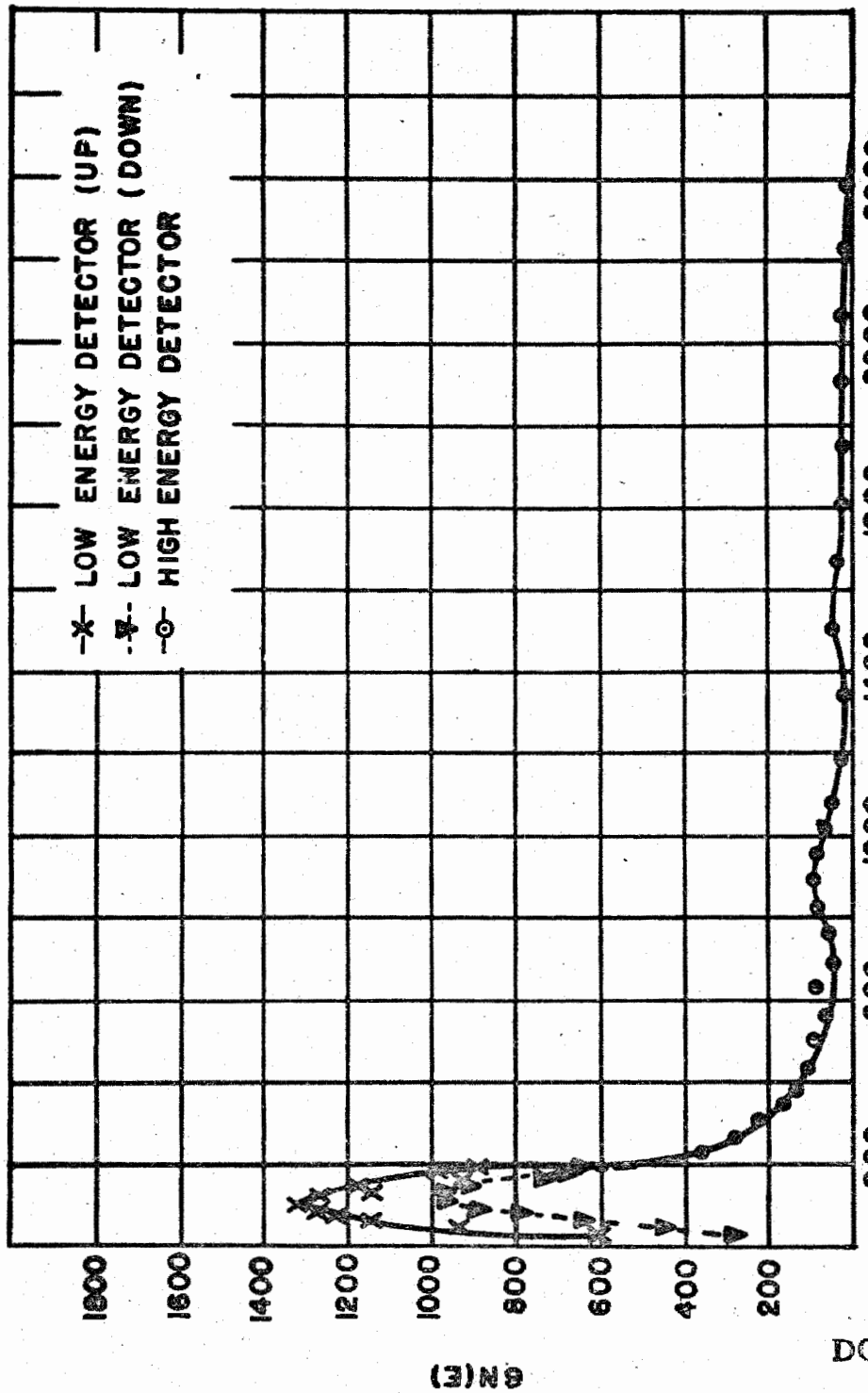

Figure 5
Photon Spectral Distribution - Shot 11 (D)

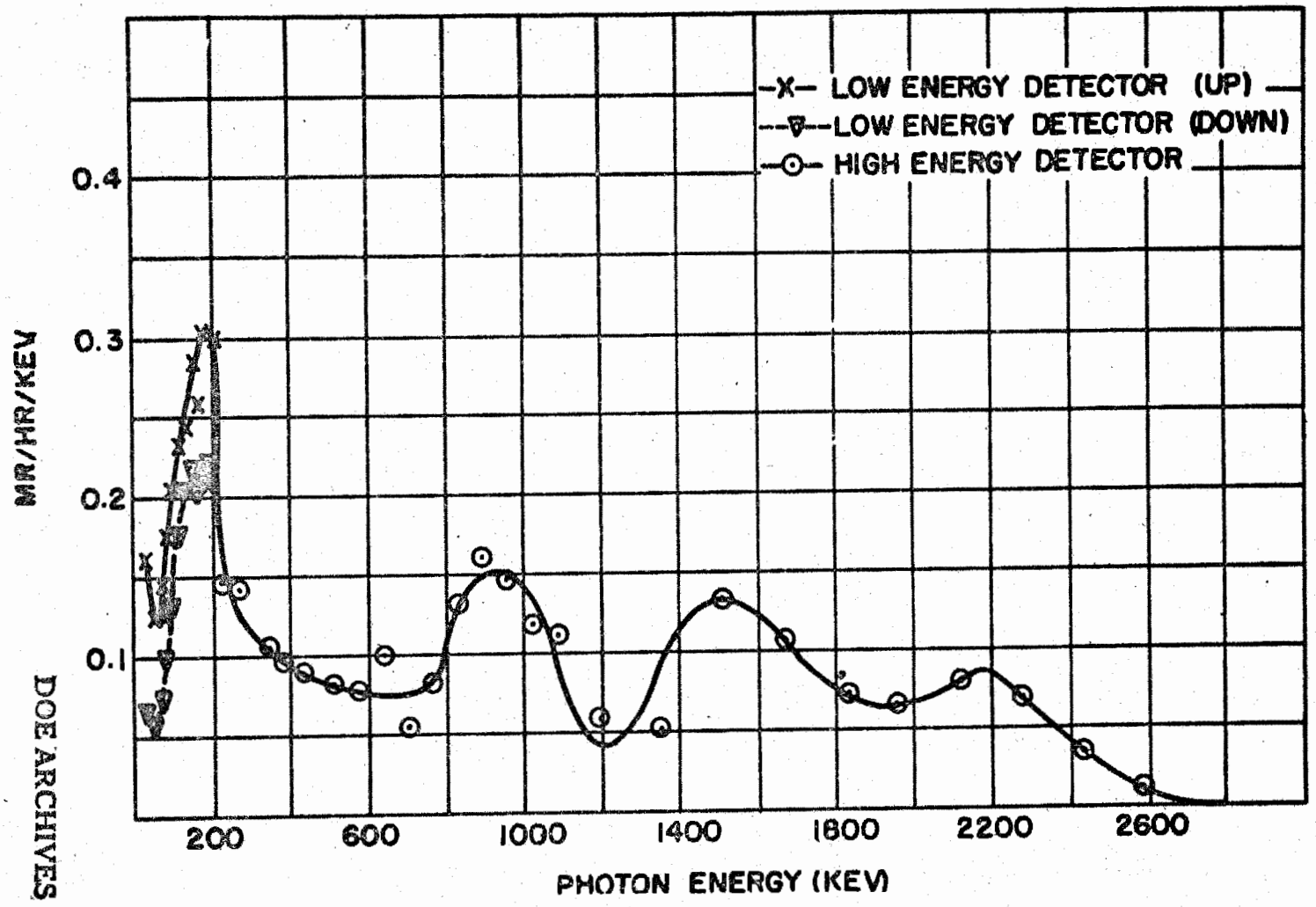

Figure 6
Dose Rate Spectral Distribution - Shot 11 (D)

[redacted]

THIS PAGE IS BLANK

[redacted]

[redacted]

RADIOLOGICAL NATURE OF THE CONTAMINANT; FRACTIONATION OF ACTIVE NUCLIDES WITH DISTANCE

Philip Krey
Chemical and Radiological Laboratories

Introduction

Before going into the main topic which is, Fractionation as a Function of Distance From Ground Zero, it may be useful to explain what we mean by fractionation. Fractionation is any change in the relative concentrations of the radioactive nuclides present in one sample as compared to another sample of the same event. It is a relative concept such that one nuclide cannot fractionate alone but must fractionate with respect to another constituent in the same sample. For example, consider the hypothetical situation shown in Table I. The Ba^{140} activity in sample 1 is four times the Sr^{89} activity and twenty times the Ce^{144} activity. In sample 2 the magnitude of these activities have changed but their relative concentrations are the same. Consequently, there is no fractionation. In sample 3, Ba^{140} activity is still four times the Sr^{89} activity but the Ce^{144} activity has increased from one-twentieth to one-fourth of the Ba^{140} activity. Here there is fractionation. Ce^{144} fractionates with respect to Sr^{89} and Ba^{140} in sample 3 as compared to the other two, but the Sr^{89} and Ba^{140} still do not fractionate with respect to each other.

Table 1 - Activities in Microcuries

Nuclide	Sample 1	Sample 2	Sample 3
Sr^{89}	10	1.0	0.10
Ba^{140}	40	4.0	0.40
Ce^{144}	2	0.2	0.10

Fractionation between samples can be identified in three ways. First, a radiochemical analyses of the samples, as would be expected, reveals this effect. Secondly, different decay rates between samples indicate corresponding changes in the relative concentrations of the radioactive nuclides present. Small variations in decay rates signify large changes in the radiochemical composition. The dosage accumulated over a period of time is also very sensitive to decay rates. For example, if we are given the dose rate in an area at ten days after detonation and if we assume that the dose rate decayed as the equation,

[redacted]

[redacted]

$D = kt^{-n}$, what would be the dosage accumulated by a person in this area during one to ten days? A change in the exponent from 1.2 to 1.4 increases the accumulated dose by 28 per cent. An increase in the exponent from 1.2 to 1.7 doubles the cumulative dose over this same period of time. Finally, different energy spectra (either beta or gamma) between samples indicate that fractionation has taken place.

This phenomenon of fractionation has received considerable attention in the last few years of atomic weapons testing. Oddly enough there is only a limited amount of data describing this behavior as a function of distance from ground zero. However, if fractionation can be shown to be dependent upon such variables as particle size of fall-out, altitude in the cloud, and time of collection after shot, then its dependence upon distance from ground zero is a necessary conclusion. This follows because each of the previously mentioned conditions will of itself produce fractionation with distance from the point of detonation. Therefore, a review of the existing data from previous operations is in order to point out the frequency and magnitude of these effects.

Experimental Data and Discussion

Operation GREENHOUSE

Fractionation at Operation GREENHOUSE was clearly established. The dependence of radiochemical composition on particle size is shown by the cascade impactor data presented in Figure 1. The cascade impactor separates particles below 10 microns into size ranges by the impaction of each size range on separate glass or plastic slides. The gross beta decay of each slide was measured from about 250 to 1300 hours after shot time and it followed the equation, $A = A't^{-n}$. A definite relationship existed between the exponent (n) of the decay equation and the particle size on the slide. In this figure, the logarithm of the number median diameter is plotted against the exponent (n). The number median diameter is that diameter for which 50 per cent by number of the particles measured are less than this size. The actual relationship is $NMD = ke^{fn}$. This particular cascade impactor sampled the Dog shot cloud at 30,000 feet. Similar relationships were found in the Easy and George shots at this operation.

[redacted]

[redacted]

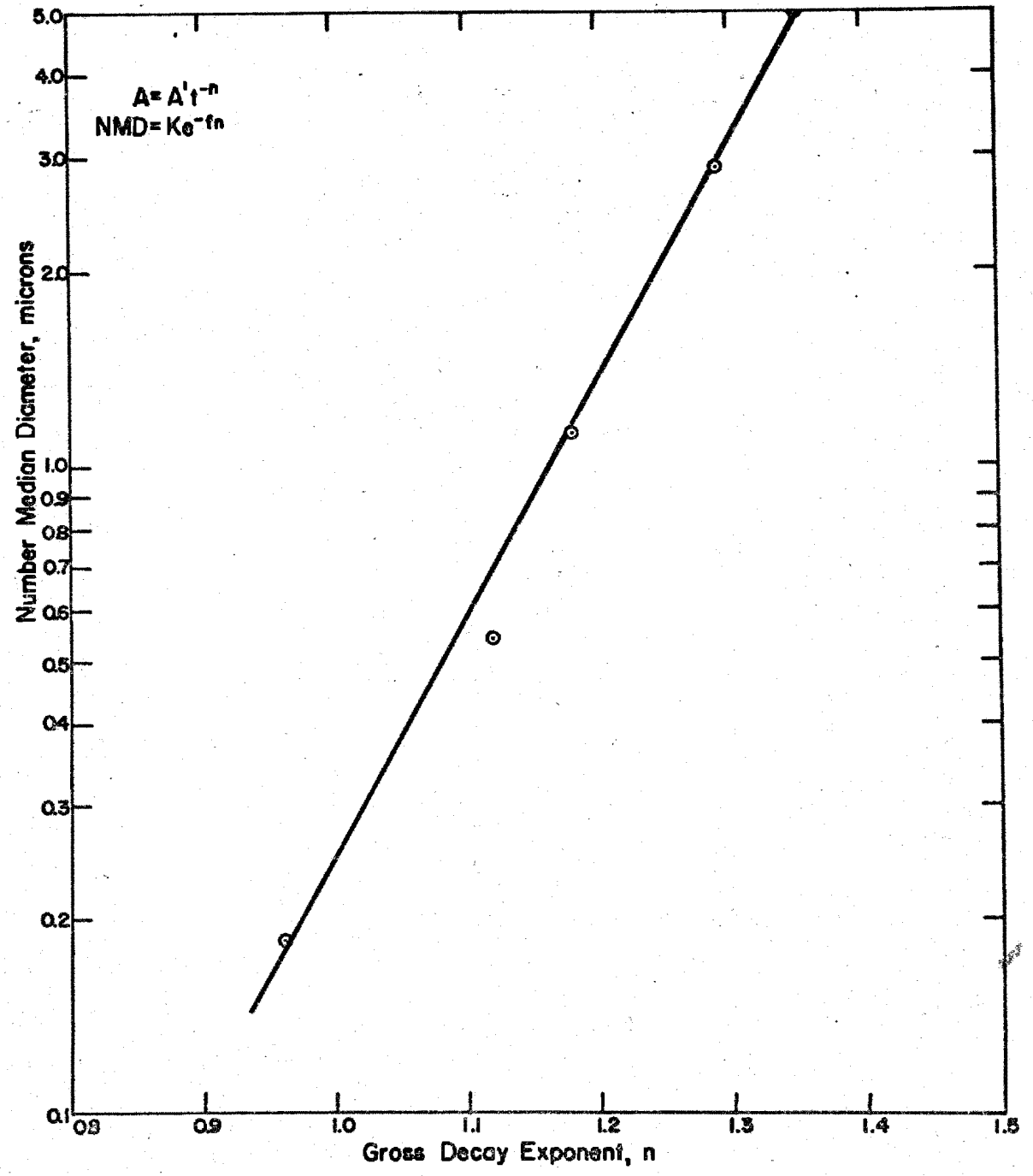

Figure 1

[redacted]

DELETED

DOE ARCHIVES

[redacted]

[redacted]

182

[redacted]

DELETED

Table 3 - Relative Fractionation

	Ce^{144}/Mo^{99}	Zr^{95}/Mo^{99}	Ba^{140}/Mo^{99}	Ag^{111}/Mo^{99}	Cd^{115}/Mo^{99}	Sr^{89}/Mo^{99}
Surface Shot						
Crater Area	1	1	0.6	0.7	0.4	0.1
Low Altitude	3.4	1.3	0.5	1.5	2	0.3
High Altitude	1.8	0.9	4	4.6	6	7
Long Range (1200 mi)	1	1	6	8	8	10
Underground Shot						
Crater Area	0.8	0.7	0.5	0.3	-	0.1
Low Altitude	1.3	1.0	9.3	12	9	8
High Altitude	1.5	1.8	46	28	29	96
Long Range (1200 mi)	17	11	97	55	-	200

[redacted]

183

[redacted]

Operation JANGLE

The most severe fractionation to date was observed at Operation JANGLE. (Table 3) This table of relative fractionation was calculated by taking the average R values for the different sampling areas and dividing by the corresponding R values obtained at Operation RANGER, Able shot. An R value is the counting rate ratio of two fission products obtained from a shot sample divided by the counting rate ratio of these same fission products obtained from the thermal fission of U^{235}. [redacted] For the surface shot the Ce^{144} and Zr^{95} to Mo^{99} values do not change drastically while the Ba^{140}, Ag^{111}, Cd^{115} and Sr^{89} to Mo^{99} ratios all show a definite increase with overall distance from ground zero. In the Underground shot all six fission products fractionate with respect to Mo^{99} in the same way. The Sr^{89} and Ba^{140} are the most severe followed by Cd^{115}, Ag^{111} and then by Ce^{144} and Zr^{95}. The Ce^{144} and Zr^{95} to Mo^{99} ratios increase at the same rate which indicate that perhaps the Mo^{99} activity might be falling off very rapidly with distance from ground zero and causing the ratios to Mo^{99} to soar. A similar possibility of an odd behavior of Mo^{99} was pointed out in discussing the GREENHOUSE results. Rather than attempt a lengthy explanation here, I would prefer to just mention that the Sr^{89} and Ba^{140} behavior can be explained on the basis of their relatively long-lived rare gas precursors, Kr^{89} and Xe^{140}. The fractionation of Ag^{111} and Cd^{115} to Mo^{99} is more difficult to explain since the proper physical properties are lacking.

The dependence of radiochemical composition upon particle size was also verified at JANGLE as shown in Figure 2. This is a log-log plot of fission product counting rate ratios against particle size of the fall-out. The Zr^{95} and Ce^{144} to Sr^{89} ratios behave similarly, both decreasing with decreasing particle size. Ba^{140} also follows this trend but not so steeply. It is obvious that if two JANGLE samples did not have the same particle size distribution, there was a corresponding difference in the radiochemical composition. As further support the gross decay of these samples measured from 1000 to 2000 hours after shot did change with particle size. There was a good deal of scatter of the original points but the general trend was as indicated, a gradual increase of the decay exponent with decreasing particle size.

Operation TUMBLER-SNAPPER

At Operation TUMBLER-SNAPPER, fractionation as a function of distance from ground zero can be clearly seen even though the data are

[redacted]

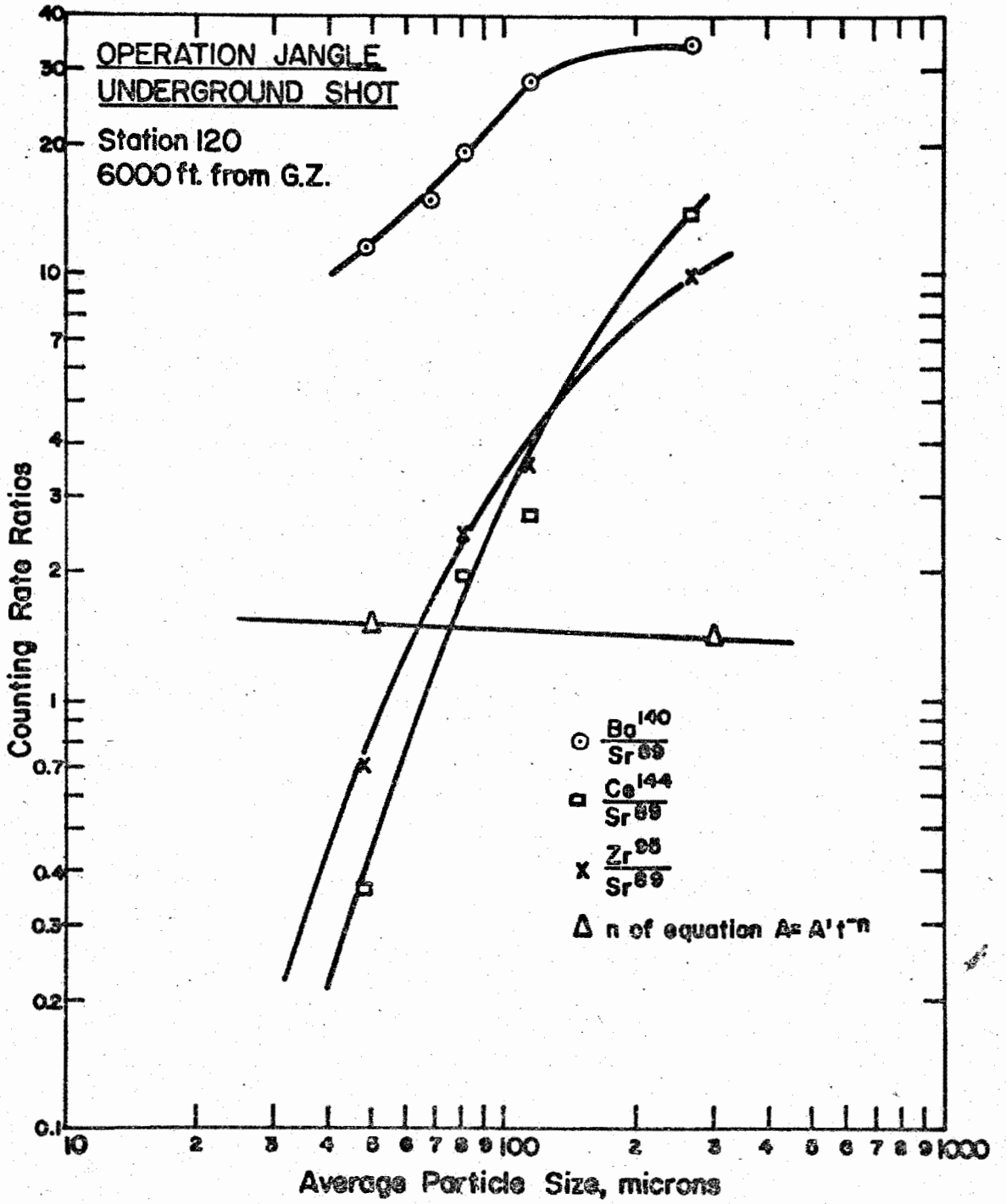

Figure 2

185

very limited. (Figure 3) The University of California collected the small amount of fall-out resulting from the tower shot, SNAPPER 6, at downwind distances of almost 60 miles. The logarithm of the average gross decay exponent for each station is plotted against the logarithm of the station distance from ground zero. The general trend indicates that a relatively greater concentration of a faster decaying nuclide or nuclides is present in areas closer to ground zero.

Operation IVY

The first large scale thermonuclear device detonated at Operation IVY produced fractionation but it was not well documented. A total fall-out sample was separated into various particle size fractions and the decay rates of each fraction was measured from 600 to 1100 hours after shot. The variation of rate of decay with particle size is shown in Figure 4. Radiochemical analyses for Sr^{89}, Zr^{95}, Mo^{99}, Ru^{103}, Ru^{106}, Ba^{140} and Ce^{144} performed on these IVY size-separated samples indicated only a slight amount of fractionation among these nuclides. The radiochemical results cannot explain the decay variations.

DELETE

Operation CASTLE

Operation CASTLE was much more successful with regard to the study of fractionation. The dependence of radiochemical composition upon particle size of fall-out at Bravo shot is clearly shown in Figure 5. Here the logarithm of the R value is plotted against the logarithm of the particle size. The $\frac{Ba^{140}}{Ce^{144}}$ pattern is the same as the $\frac{Sr^{89}}{Ce^{144}}$ pattern which indicates that Ba^{140} and Sr^{89} both fractionate with respect to Ce^{144} but they do not fractionate with respect to each other. The Mo^{99}/Ce^{144} data shows how the relative concentrations of these nuclides vary with particle size. The discontinuity at 50 microns, as was explained this morning by Dr. Barnett, is caused by the methods used to separate the particles of the fall-out into their respective sizes. Here as at JANGLE, samples having different particle size distributions, had corresponding changes in radiochemical composition. The gross beta decay of these samples was measured from 110 days to 170 days after detonation and the exponent of the decay equation ($A = A't^{-n}$) is plotted against particle size. There is good correlation with the radiochemical data and the decay data because any increase in the relative Sr^{89} concentration at this time will increase the decay rate of the sample. The contributions of the Mo^{99} and Ba^{140} have decayed below significant levels, at the time these decay measurements were made.

[redacted]

Figure 3

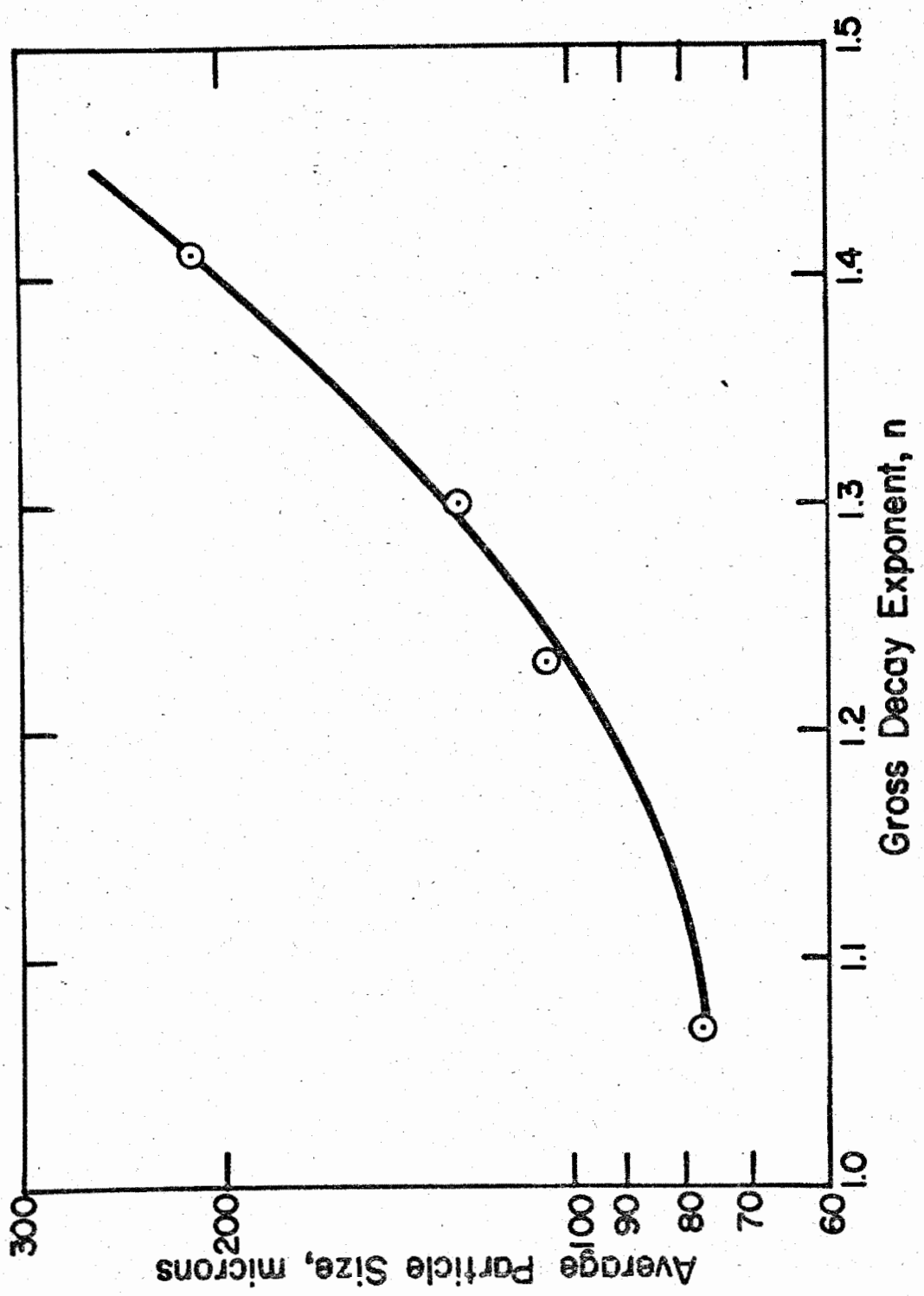

Figure 4

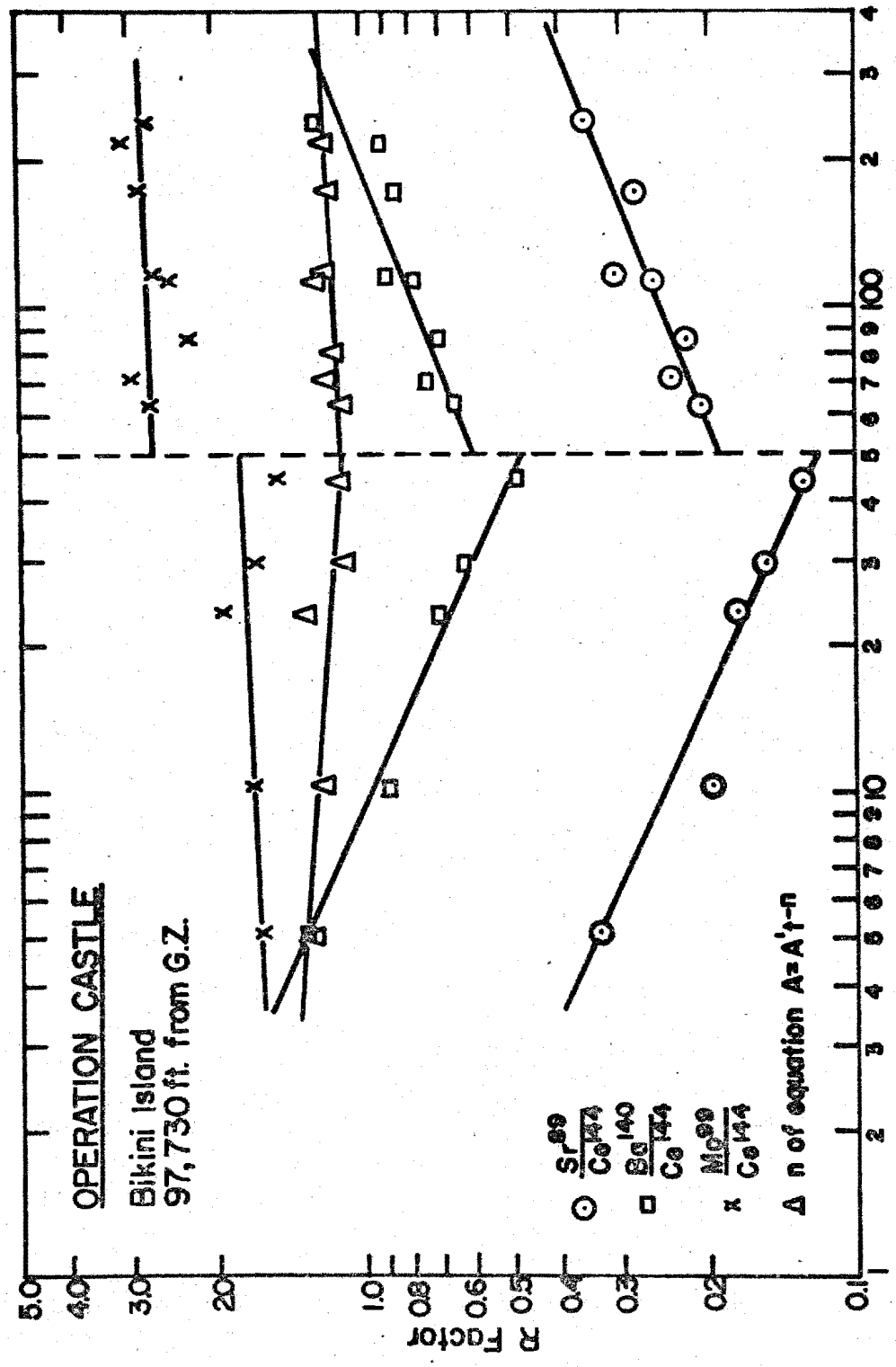

Figure 5

[redacted]

Analyses of a few time differentiated samples at Union shot (a surface water detonation) revealed a change in the radiochemical composition with time of collection after shot. Figure 6 is a logarithmic plot of the R values against the time the sample was collected. It can be seen that Sr^{89} and Ba^{140} fractionate with respect to Mo^{99} at different times but are fairly consistent with each other. The Ce^{144} data are included but are not too reliable. The gross beta decay of these samples was measured from 7 to 20 days after shot. The exponents of the gross decay equations are also included in this figure to substantiate the presence of severe fractionation.

Summary

To summarize briefly, the limited amount of fall-out sampling at significant downwind distances from ground zero indicates that there is fractionation as a function of distance. The existence of fractionation as a function of particle size of fall-out, altitude in the atomic cloud and time of collection lends additional weight to this observation.

Further investigation of this phenomenon is essential for a better understanding of the vital processes that take place following an atomic detonation. Such information has very important applications. How can one confidently predict the residual contamination patterns caused by an atomic detonation under a variety of conditions if he is not certain of how the fission products are associated with the fall-out material? The value of any scaling law suffers when different decay rates of the same isodose line may cause wide variations in the cumulative dose acquired over a period of time. The agencies determining the fission yields of the weapons by radiochemical methods are well aware of the existence of fractionation. For nominal weapons these effects may be significant for only small localized areas. However with the advent of thermonuclear weapons by which casualty producing radiation effects can be realized over a 100 mile downwind direction, the possible effects of fractionation assume alarming proportions. The studies of fireball mechanics and fractionation will proceed simultaneously until a complete understanding of the effects and capabilities of these weapons are realized.

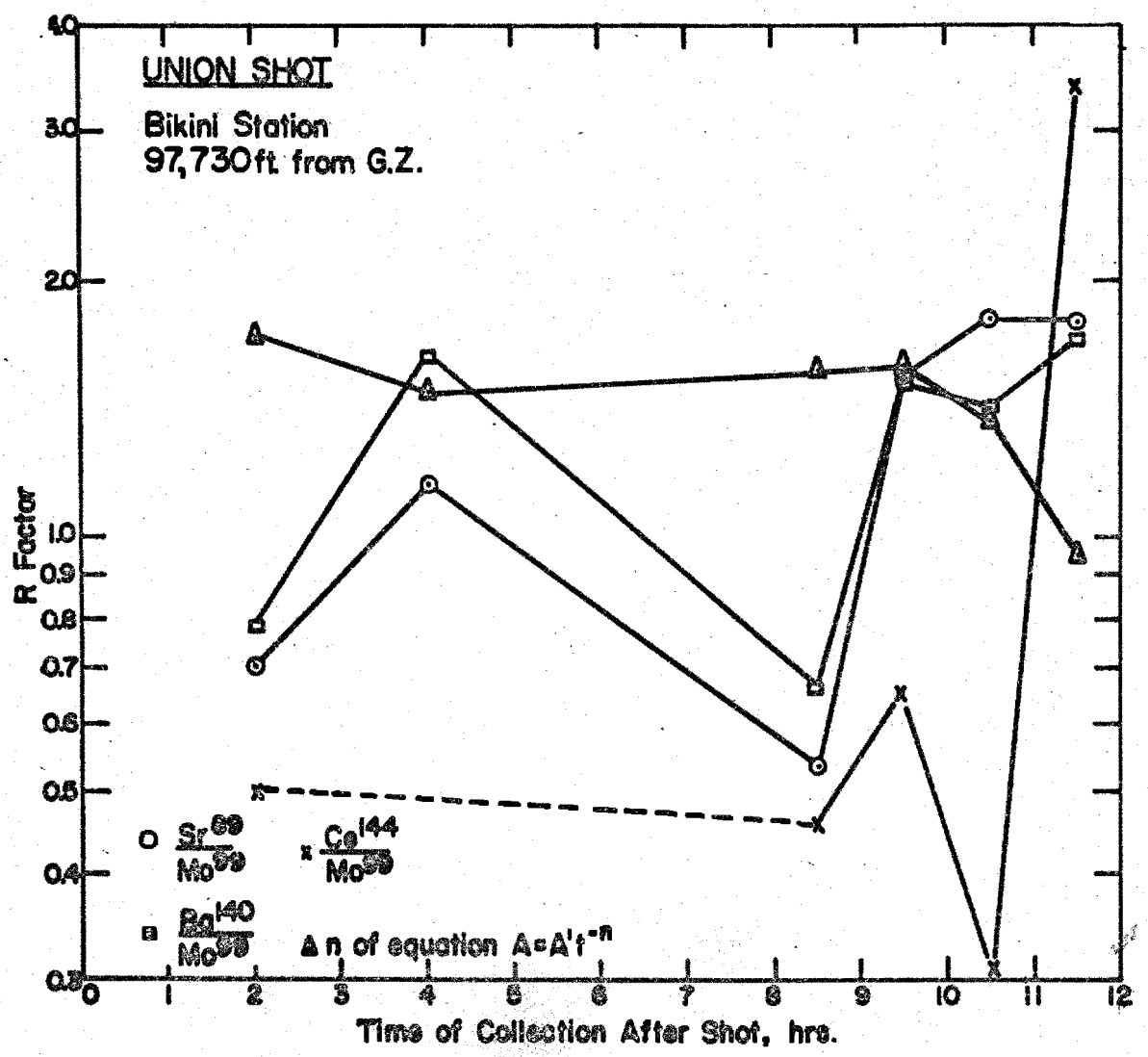

Figure 6

[redacted]

THIS PAGE IS BLANK

DOE ARCHIVES

[redacted]

[redacted] ENERGY [redacted]

RADIOLOGICAL NATURE OF THE CONTAMINANT; PERCENTAGE OF TOTAL ACTIVITY IN FALLOUT AS A FUNCTION OF HEIGHT OF BURST

Lt. Col. N. M. Lulejian
Air Research and Development Command

By studying the fallout from the TUMBLER-SNAPPER and UPSHOT-KNOTHOLE atomic test operations, we were able to determine that there was some simple function of the percentage fallout as a function of scaled height. Figure LA shows this simple curve. We have also plotted in this figure the JANGLE-Surface and JANGLE-Underground as well as the IVY-Mike and the CASTLE-Bravo shots. The data for this curve was obtained from Headquarters, ARDC Report C3-36417 and its supplement, and ARDC Report No. C4-23676. In this work, we define scaled height as λ, where

$$\lambda = \frac{h}{W^{1/3}}$$

h = height of burst in feet above target

W = kiloton yield of bomb

Percentage fallout is defined by P, where $P = \frac{\Sigma AR}{k\, Wt^{-1.2}}$

where A = area covered by fallout in nautical square miles

R = dose rate in r/hr at time of fallout

t = time of start of fallout

W = bomb yield in kilotons (fission yield)

k = constant (we have taken this as 10 in our reports)

As we study the curve shown in Figure 1A, we see that between 70 and 90% of the total residual activity is assumed to fall out downwind within 24 hours or less. This fallout is that due to those particles that are sufficiently large to have significant rate of fall (1000 to 30 microns). Many organizations analyzed in detail fallout from the JANGLE-Surface and JANGLE-Underground shots. They concluded that only 10 to 15% of the JANGLE-Surface residual activity was found within 3 to 5 miles downwind of ground zero. This data closed the 100 roentgen/hr contour line. Now the 10 - 15% fallout from JANGLE-Surface shot perturbed us greatly because we had developed a curve (Figure 1A) which showed that surface fallout ($\lambda = 0$) should be above 50% and probably less than 90%. This gave us the strong suspicion that either our beloved curve was wrong, or the

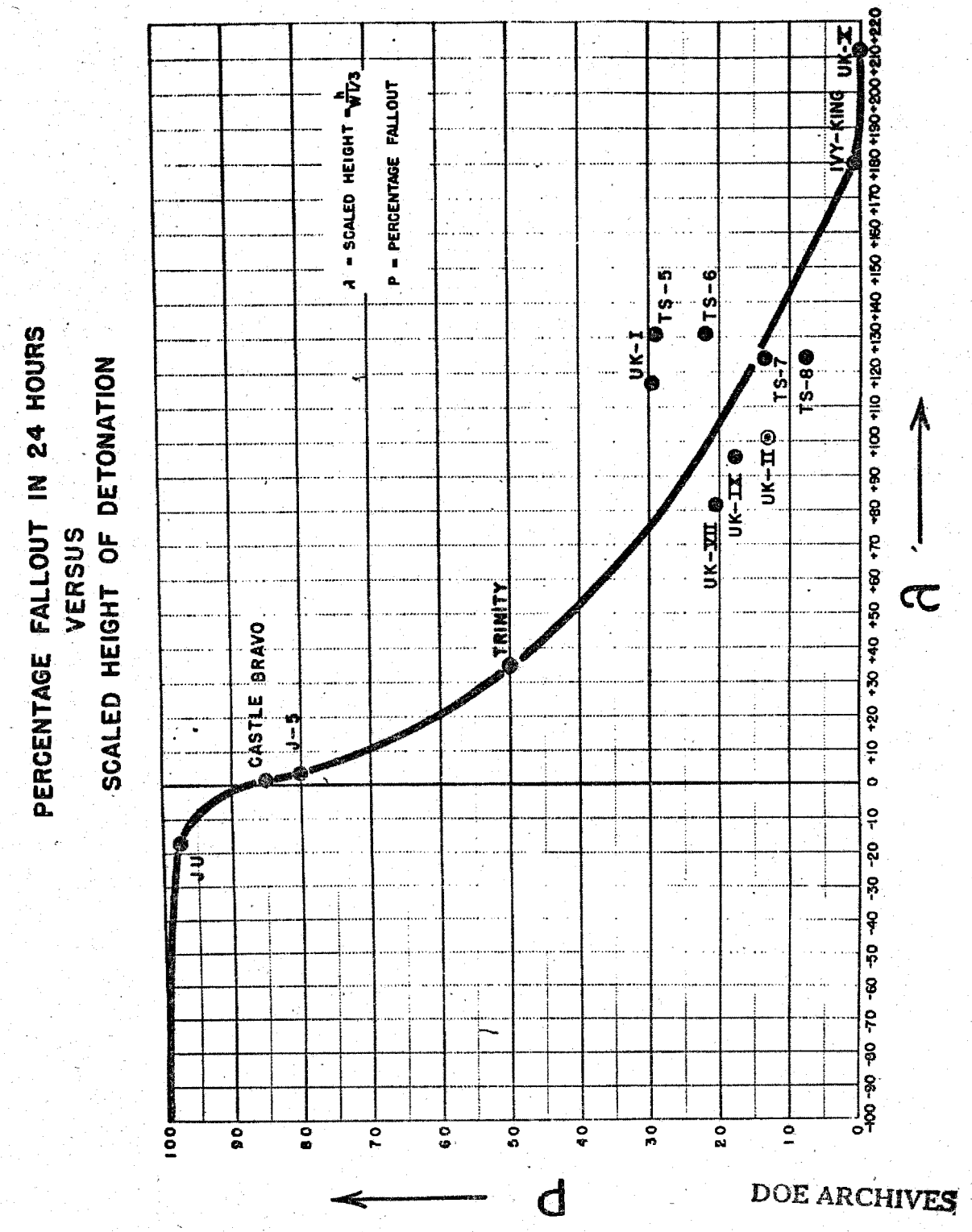

Figure 1A

[redacted]

[redacted]

194

[redacted]

workers in the field of fallout had only measured a very small portion of the total. To this end, we started hunting the classified literature. We found that in AFSWP Report WT-370, hidden under Project 2.1c-1, there were figures showing that fallout occurred 50 to 100 miles downwind of ground zero. Unfortunately, this fallout data was in relative units and contact with the project officer indicated that he had no idea of the actual amount of contamination on the ground. He agreed it could have been in roentgens or tenths of roentgens. Further search brought out the fact that the Air Force Special Weapons Center of ARDC had made repeated aerial survey of the downwind area for both JANGLE-Surface and JANGLE-Underground shots at D-day and also at D+1 day. This excellent work done by SWC under the direction of Colonel Fackler resulted in the fallout plot shown in Figure 1C. We were able to prepare this fallout plot by utilizing the following attenuation factors with height:

Height Above Ground in Ft	Attenuation Factor
3	1.
10	1.2
20	1.4
30	1.5
40	1.7
50	1.8
100	2.6
200	4.0
300	5.1
400	6.8
500	8.5
1000	30.

A study of Figure 1C shows that the total fallout downwind is not 10 or 15%, but more in the order of 70 ± 20%. This quite satisfactorily fits our curve shown in Figure 1A.

I would now like to touch on one more point in our analysis which I consider to be very significant. During TUMBLER-SNAPPER test operations, the percentage fallout from the stem of the cloud was approximately equal to that coming from the mushroom. Now the TUMBLER-SNAPPER tower shots were from 12 to 14 KT bombs detonated from 300 ft. towers. During the UPSHOT-KNOTHOLE test operation, however, the yields varied from 17 KT to 50 KT (I am now referring to the large yield tower shots) and the tower heights were 300 feet. During UPSHOT-KNOTHOLE, where the scaled heights were significantly lower than during TUMBLER-SNAPPER, the percentage activity in the stem was two to three times the percentage fallout coming from the mushroom. This was amazing to us at the time. We had anticipated that as the tower height remained constant while the

[redacted]

[redacted]

195

yield was increased (by a factor of 2 or 3), then the percentage fallout coming from the taller and wider mushroom would be greater. We found the contrary to be true. Also, as we studied Figure 1C, we noted that approximately 50% of the fallout came from the stem and only 15 to 25% came from the mushroom. It was this increased percentage fallout from the stem that made us take the gamble of predicting in November 1953 (see ARDC Report No. C3-36417) that if a 5 to 10 MT weapon were detonated on the surface in Washington, D. C., then Baltimore, which is 40 miles downwind, may have to be evacuated. We further stated in this report that 50 to 75% of the total activity of a surface detonated multi-megaton weapon would fall out downwind and cover an area of approximately 5000 square miles. We also stated that this prediction was based only on small yield weapons and that it had to be proof-tested in a high yield test before we developed any confidence in it.

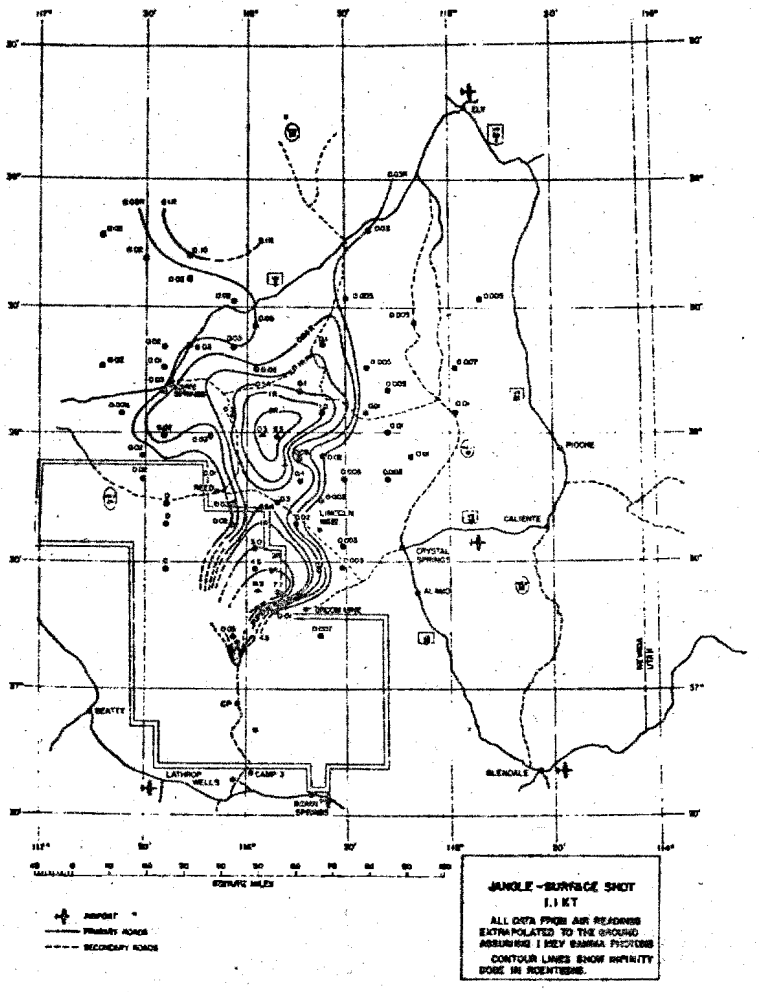

Figure 1C

[redacted]

ATOMIC CLOUD HEIGHT AND SIZE AS A FUNCTION OF YIELD AND METEOROLOGY

Dr. W. W. Kellogg
Rand Corporation

Introduction

Yesterday we were in the microscopic realm of micron-sized particles. Today we abandon the particles--for a while at least--and talk about the very biggest part of an atomic explosion, the cloud which forms after the blast has gone off.

Why, you may ask, are we particularly concerned with the cloud in a symposium devoted to fall-out? The answer is simple--only by a careful study of all the available evidence on the behavior of the atomic cloud can we hope to determine where the radioactive debris goes initially. In a very real sense the atomic cloud defines the initial spacial boundary condition for the fall-out process.

With this in mind, the purpose of the present paper should be twofold:

To get an idea of the circulation which an atomic explosion sets up, in order to tell where, within the cloud, the radioactive debris of the fireball will go.

To describe the dimensions and heights of atomic clouds as precisely as possible. These will vary primarily with yield, of course, but the meteorological situation also has an effect.

Early Development and Circulation

In order to fix our ideas a bit, consider the first few minutes in the life of an atomic cloud (Figure 1). It will not be necessary to dwell on this schematic diagram at any length, but a few points are very pertinent to the question of fall-out.

Notice that, in the high air burst, the surface material never reaches the mushroom. In the low air burst it often does reach the mushroom, and we have looked at many pictures (for example, BUSTER Easy) where the material from the ground passes completely through the doughnut-shaped mushroom, and then flows out and around the outside. Yet, in such cases there is no fall-out, as LTCOL Lulejian pointed out. The toroidal circulation is so strong, apparently, that the dirt can only circulate around the doughnut which contains the fission products, and never comes in contact with them.

[redacted]

[redacted] ENERGY ACT

197

[redacted]

SCHEMATIC CROSS-SECTION, SHOWING THE WAY IN WHICH SURFACE MATERIAL RESPONDS TO THE INDRAFT CAUSED BY THE RISING ATOMIC CLOUD.

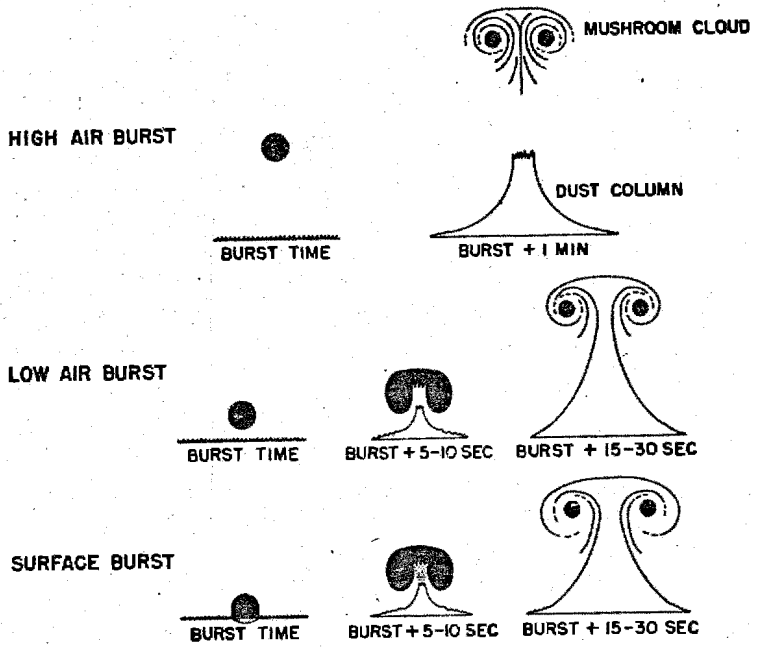

Figure 1

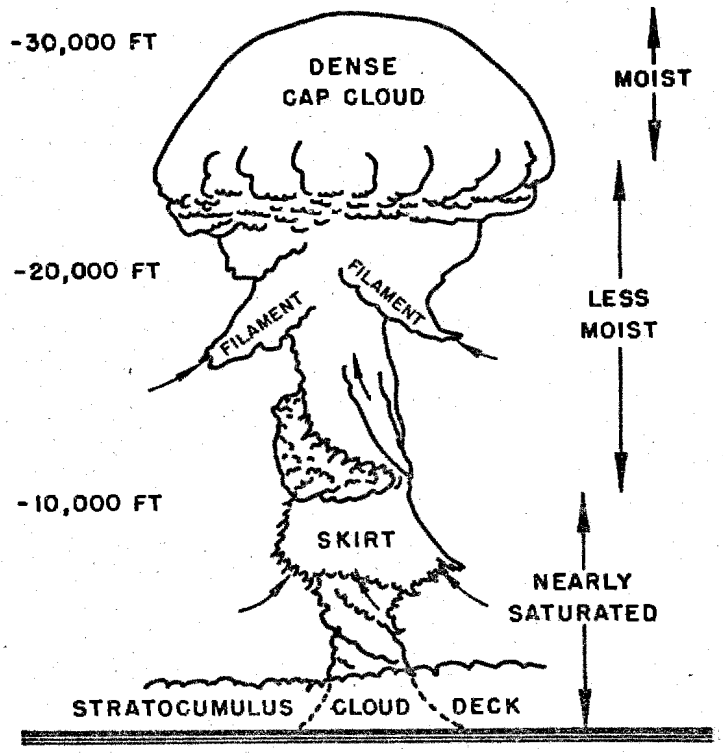

Figure 2

[redacted]

[redacted] ENERGY ACT

198

[redacted]

In the surface burst, contact between the dirt and the fission products is achieved initially, and the dirt is drawn up with the fireball in a mixture of vapor, liquid, and solid particles. The evidence from the particle sampling makes this fact quite certain. After a few seconds, however, one would expect exactly the same influences that dominated the low air burst to exert themselves, and there will be little or no further mingling of soil and fission products.

Now follow the cloud upwards. From the outside it may look like the sketch of the DELETED cloud (Figure 2). We cannot actually see the inside, but we can deduce a good many things about the circulation just the same. First, we are certain of the strong convergence and updrafts along the stem. The existence of the skirts and filaments, which are an invariable feature of these clouds, is proof that there is an upward motion, since only by a forced lifting will the air be made to form a cloud. Moreover, we can get an idea of the rate of the toroidal circulation of the mushroom by a simple experiment. In a movie, taken with a fixed camera, mark with a pointer on the screen some bump or spur on the side of the upward rushing mushroom. You may be surprised to find that, relative to the ground, the outside of the mushroom is standing still or even descending slightly (Figure 3).

SKETCH OF TORUS OF A 30 Kt WEAPON ABOUT 1 MIN AFTER BURST

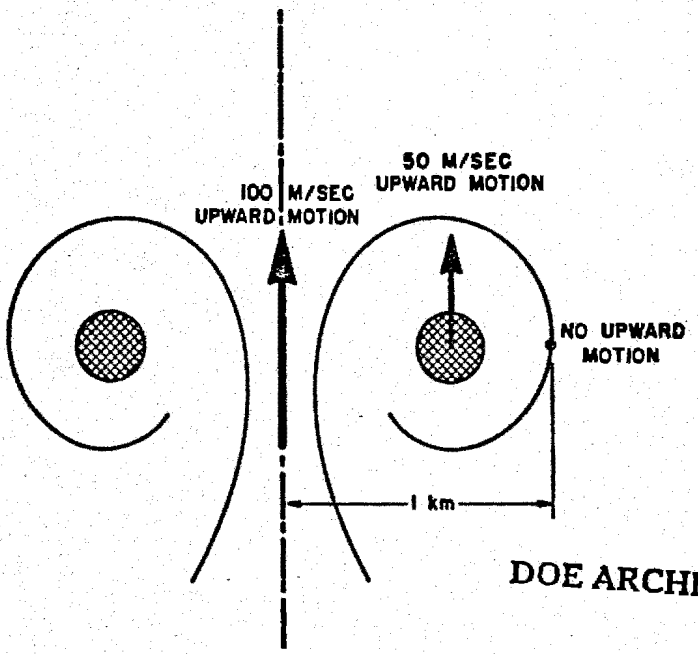

Figure 3

[redacted]

199

[redacted]

This means that the material in the middle of the mushroom must be moving upward even faster than the cloud as a whole. The figure shows a 30 KT case (a schematic drawing of the situation in TUMBLER-SNAPPER 3). Imagine the upward motion in the larger clouds, such as CASTLE Bravo, which, as LTCOL James showed, were moving at the rate of about 150 meters per second during the first minute or two!

It is clear, from these considerations, that very little debris from the mushroom could ever remain behind in the stem. It would be swept upward far too rapidly. If there are any particles left behind, they must be large particles which have been thrown outward by the two or three "g" force of the toroidal motion, and fall in a thin veil outside of the stem. Actually, when the light is right one can sometimes see this thin fall-out veil around the stem--though it must constitute but a small fraction of the total radioactive material.

There always comes a time in the life of an atomic cloud when it reaches its ceiling. The cloud, as it rises, draws in or "entrains" a great deal of the surrounding air, and its mass increases by a factor of over 100 in going from, say, 5 or 10 seconds, to its stabilization height. This large entrainment, coupled with the natural stability of the atmosphere, means that it will eventually use up all its thermal energy and acquire the same temperature and density as the surrounding air at its level. However, it may still have the kinetic energy of its toroidal circulation, and if it is a cloud from a large yield weapon it will have a great deal of this kind of energy.

There are two good pieces of evidence for this in the larger yield clouds. First, a study of pictures of these clouds shows that they keep on turning and boiling after they stabilize. In addition, to clinch the matter, the cloud often behaves just the way a smoke ring behaves when it stops moving—it suddenly starts to grow radially. The GREENHOUSE George cloud showed this, and the Easy cloud did to a lesser degree (Figure 4). Several of the larger Nevada clouds have shown this behavior also. In the case of the very large clouds, in the megaton range, this rapid expansion is so pronounced that, as we heard yesterday, the mushroom quickly grows right out of the picture, and we hardly know how large it did get before it settled down. All we know is that, according to EG&G's analysis, at 10 minutes after shot time the rate of horizontal growth for several of the CASTLE clouds was two or three hundred miles per hour—far too fast to be accounted for by the prevailing winds and wind shears.

This feature will be noted again in the next section.

[redacted]

200

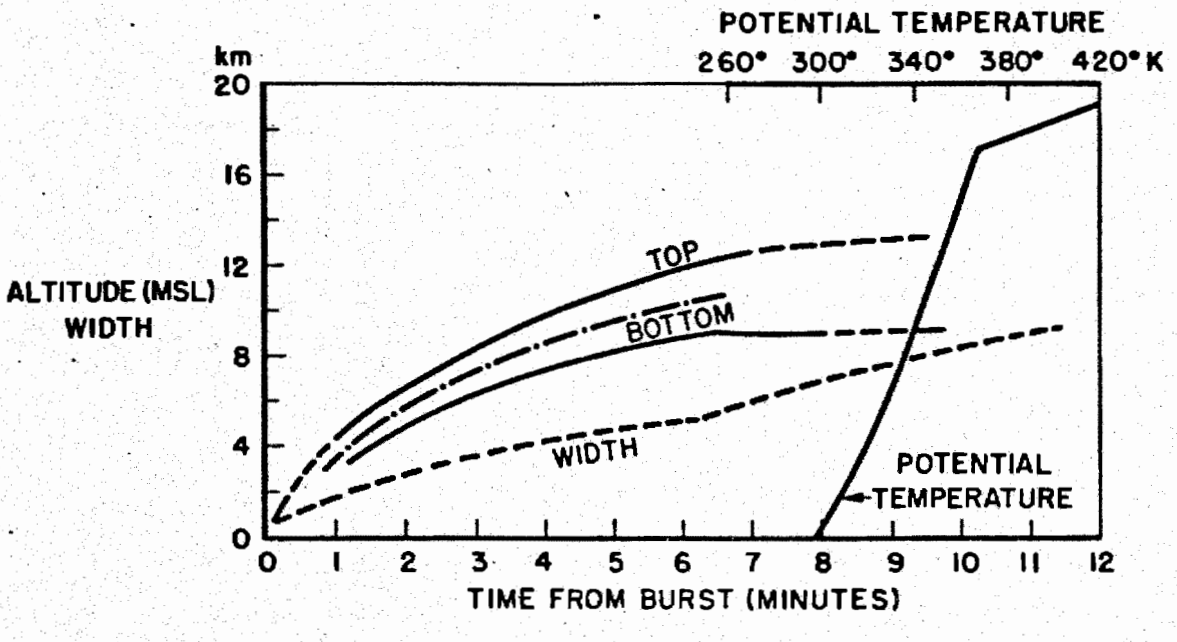

RISE AND GROWTH OF GREENHOUSE EASY CLOUD

DELETED

RISE AND GROWTH OF GREENHOUSE GEORGE CLOUD

Figure 4

201

[redacted]

Measurements of Size and Altitude

In the earlier atomic tests, TRINITY, CROSSROADS, SANDSTONE, and RANGER, the emphasis of the observations was on the devices themselves, and on the events of the first few seconds or milliseconds. After the fireball glow died and the boiling mushroom cloud started rising the test was "over", and what went on after that was the province of the documentary photographers--and a handful of weather men with theodolites who tried excitedly to get angles on the rushing cloud. If it has not been for these weather men, I believe that we would have virtually no information on the heights to which these clouds went.

Starting with the GREENHOUSE tests, however, carefully planned programs to observe the cloud were instituted, and photographic measurements were made. You have heard from LTCOL James about the most recent--and most elaborate--efforts to photograph the CASTLE clouds. So now we do have a fairly good set of data on a number of atomic clouds, covering a wide range of yields.

Before showing you the collected data on all the shots to date, a few caveats are in order about the quality and accuracy of these measurements. (I believe Dr. Machta will have more to say about this matter.) Whether the measurement is by theodolite or by camera, the basic observation is a set of angles. Before these angles can be reduced to dimensions two important factors must be taken into account:

Wind drift

Cloud shape

It will not be necessary to go into the details of just how these are handled in the analysis, but you should understand how an erroneous treatment can introduce large errors.

First, concerning the wind drift, the motion of the cloud relative to the observer will change the distance, and this will give the impression of a vertical motion or a change of size. For example, movement towards the observer of the cloud top will give the impression that the cloud is still rising. Fortunately, wind observations are nearly always available at the test site, so, though the correction may be laborious, it can be made with some degree of confidence.

The cloud shape is more illusive and has resulted, I believe, in some rather serious errors in height estimates. The natural assumption to make about a mushroom cloud is that it is round on top (Figure 5). This is not a bad assumption for the smaller yield clouds, but even here it must be noted that there may be an appreciable difference

[redacted]

[redacted] ENERGY

DIAGRAM OF THE OPTICAL SYSTEM OF A CAMERA, SHOWING THE RELATIONSHIP BETWEEN THE VARIOUS ANGLES AND DISTANCES.

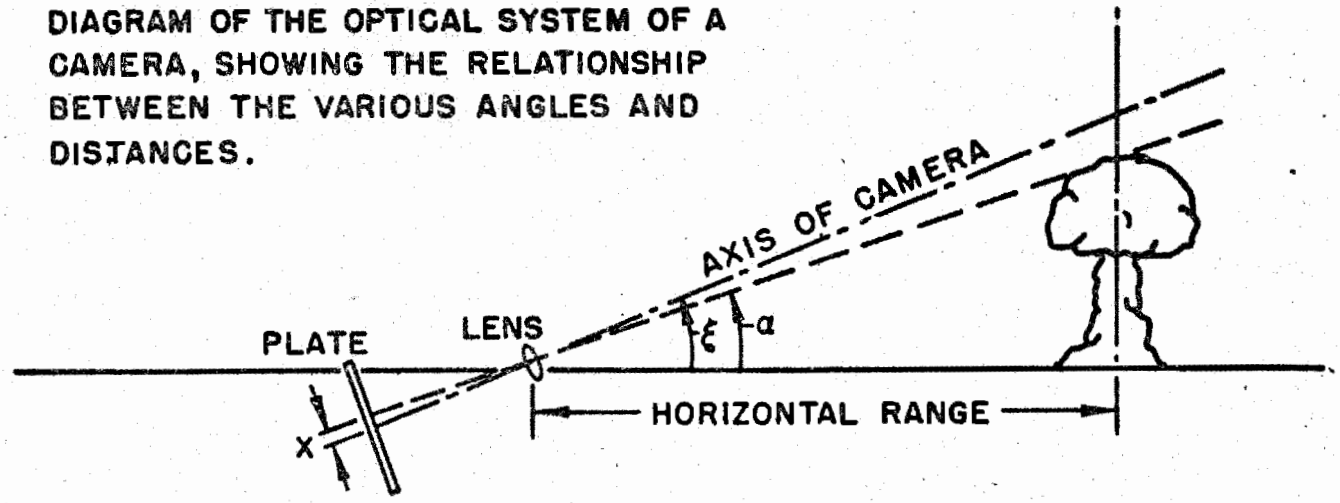

IDEALIZED SKETCH OF THE ATOMIC CLOUD SHOWING THE METHOD OF CORRECTING FOR THE ANGLE OF VIEW.

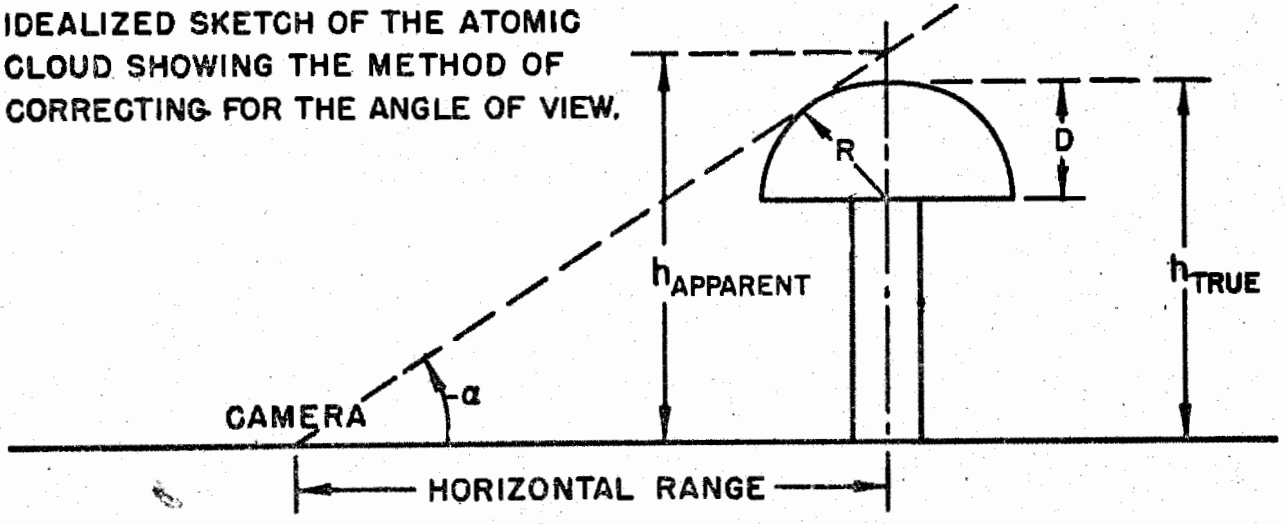

Figure 5

[redacted]

between the true height and the apparent height, as indicated in the figure.

Imagine, now, that the rapid expansion of diameter, shown in Figure 4, takes place while the observer is measuring the elevation angle, α, between the horizon and the cloud edge nearest him. Clearly, the expansion will push the edge towards him, and he may interpret this as a continued increase in height instead of an increase in size. Of all the clouds which I have studied carefully, none have, as far as I could judge, continued to rise for more than six to seven minutes, and many stabilize at four to five minutes. However, at around six minutes many have shown the pronounced diameter increase, with its accompanying flattening. Therefore, where height versus time curves are presented which show the cloud continuing upward for eight, ten, or even fifteen minutes, it is probably justified to chop it off at around six minutes, and to ascribe the remainder to an illusion in space.

The results of all the observations which are available to date are shown in the next two figures. In the height data (Figure 6) I have taken the best estimates, and in two cases (SANDSTONE Yoke and X-Ray) have cut them down, in line with the previous statement about stabilization time. You should note that these are heights of centers. Should you want height of top or bottom, the vertical extent is shown as a solid line.

The various curves through the data points are theoretical curves, whose derivations are described in the Rand "Aureole Report" and so will not be repeated here. They show the effects of atmospheric stability and the height of the tropopause, and appear to agree fairly well with the data. The extension of the Marshall Islands curve to yields above 1 MT is done so as to roughly fit the data, and the same applies to the extension of the two winter cases below 5 KT.

You have all noticed, by now, that there is quite a discouragingly large spread in the data points. Part of this is certainly due to poor measurements, and part is a real effect due to the change in atmospheric conditions of stability and wind or wind shear between shots of the same yield. It is also possible that certain characteristics of the device, in addition to the yield, have an effect on the cloud behavior.

The yields, incidentally, have all been corrected to sea level by the ratio of the sea level pressure (standard) to the pressure at burst altitude. This is to take into account in a rough way the fact

[redacted]

[redacted]

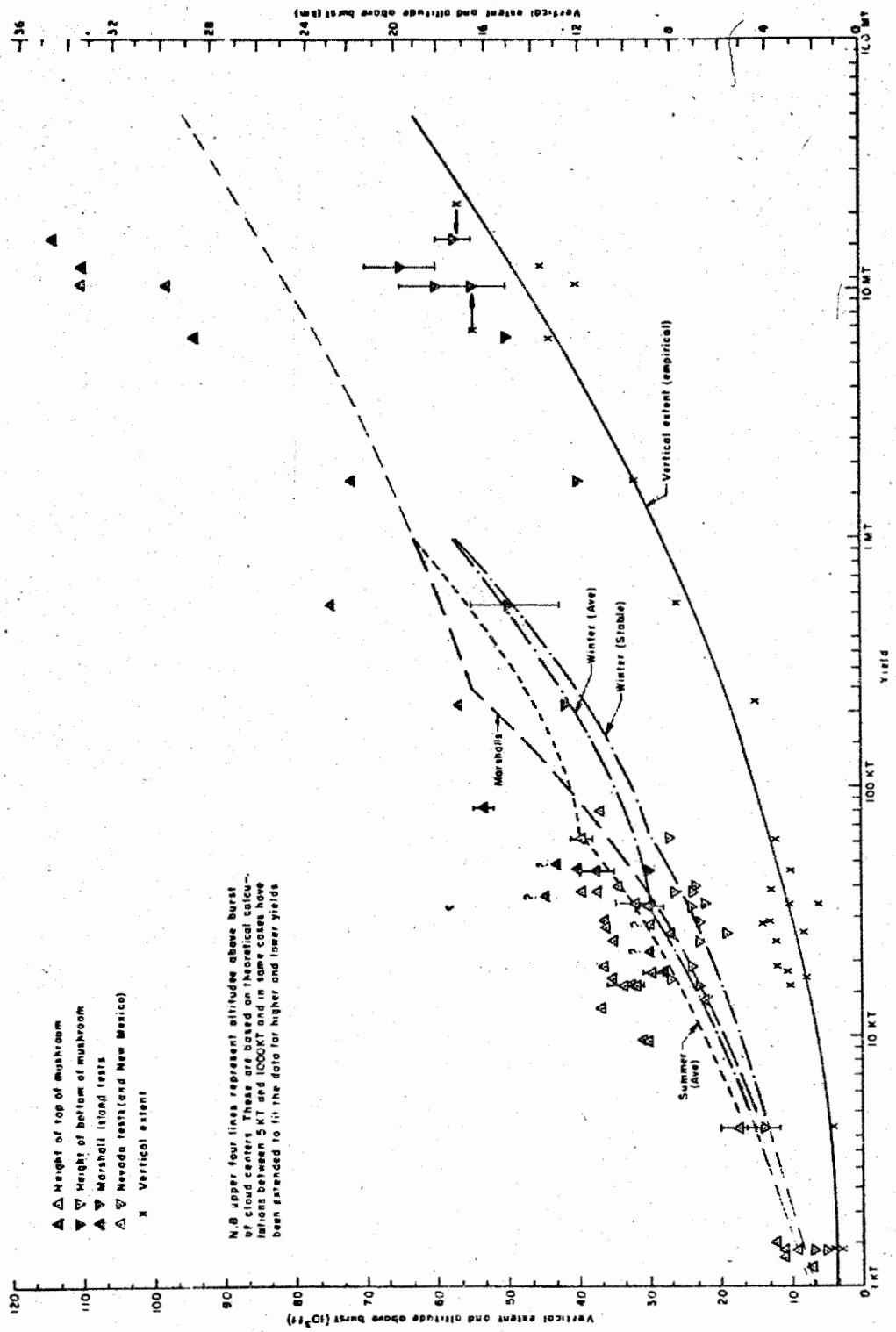

Figure 6

[redacted]

[redacted] OMIC ENERGY ACT

205

[redacted]

that a burst at, say, 750 mb pressure has to do less work in pushing outward against the atmosphere than a burst at sea level, and so will grow bigger. This correction factor amounts in some cases to 20 to 25 percent of the yield.

Figure 7 shows the diameters versus yield. Note the change in scale at 1 MT to accomodate the tremendous growth in the megaton range. The curves here are drawn as best fits to the data. You will note the arrows attached to the points showing the 10 minute diameters above 1 MT. As previously mentioned, these clouds, even at 10 minutes from shot time, were still growing at a rate which was too great to be accounted for by wind shear, so their "final" diameters, a difficult thing to define even if we could observe it, may be considerably larger than shown.

In conclusion it should be admitted that our information on atomic cloud dimensions and heights leaves much to be desired from the point of view of precision, but I have the feeling that these clouds share to some degree the sloppy behavior of natural clouds. Turbulence, winds, layers of stable and unstable air encountered during the atomic cloud's rise are bound to have some effect, and make each case a unique one. Therefore, I doubt if we will ever be able to be much more precise than we are now.

Fortunately, as you will see later in the day, a few thousand feet in positioning of the cloud will not have any great effect on the fall-out computation.

[redacted]

[redacted]

206

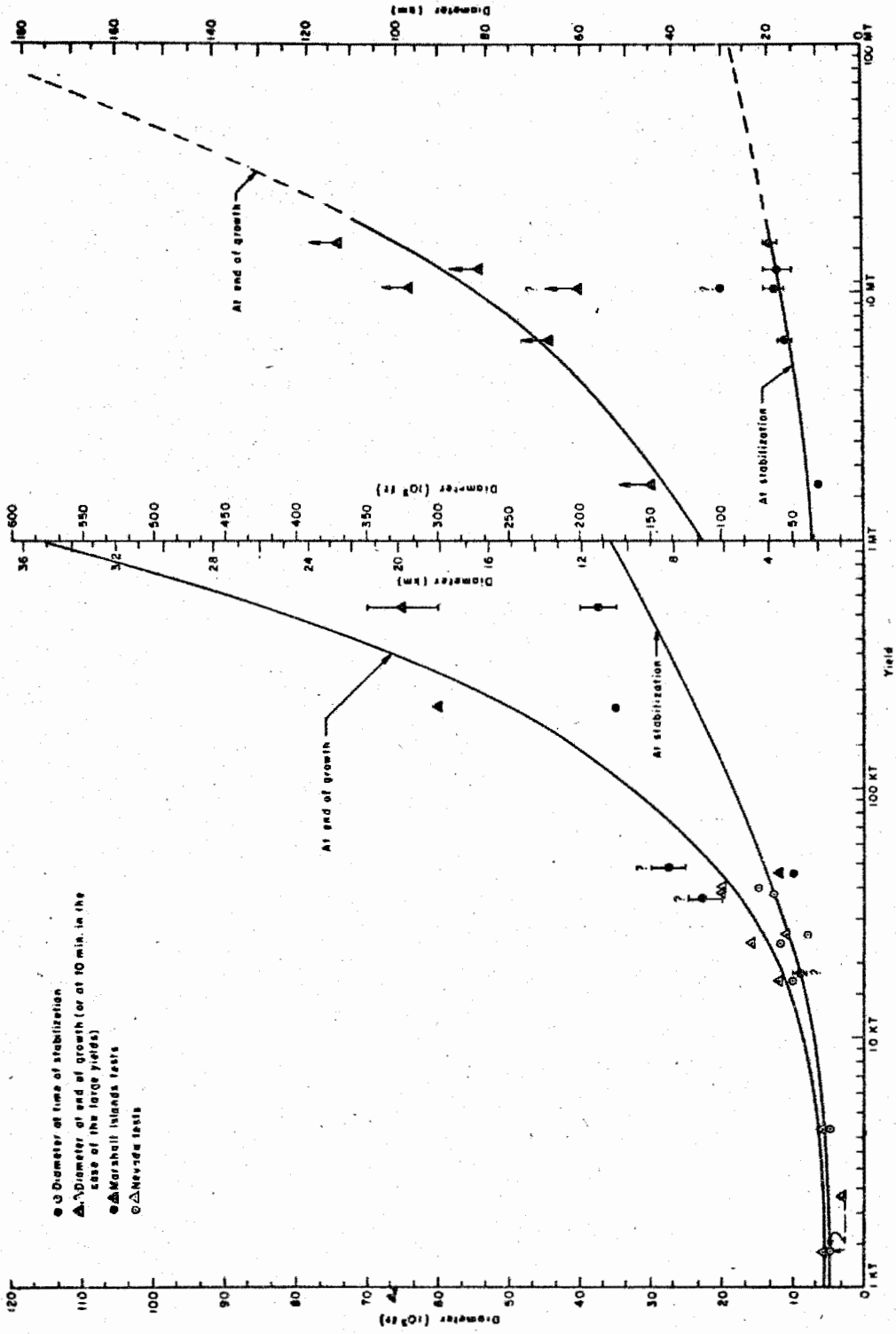

Figure 7

[redacted]

THIS PAGE IS BLANK

[redacted]

ATOMIC CLOUD HEIGHT AND SIZE AS A FUNCTION OF YIELD AND METEOROLOGY

Dr. Lester Machta
U. S. Weather Bureau

The Weather Bureau under contract to the AFCRC in connection with TEAPOT Project 9.4 is attempting to determine whether there is any relationship between the physical characteristics of the various atomic clouds and available meteorological parameters.

The study has just begun so that only a limited field of interest can be reported upon today; namely, the tops of the clouds detonated in the Nevada Test Site. These data were examined first because they are most numerous and probably most reliable. Any conclusions derived from such a study of Nevada shots would then be applied to both kiloton and megaton weapons in the Pacific as well as being useful in the forthcoming TEAPOT series.

It is evident that the quality of the cloud top and meteorological information will bear strongly on the success of the study. The conventional upper air weather data collected by the Air Weather Service for the test operations is among the best that weathermen may work with, although it is true that we may not be measuring all of the pertinent meteorological elements because of lack of proper instruments as, for example, the failure to measure vertical currents or atmospheric turbulence.

The matter of the cloud tops is another question, however, and some background information is necessary.

It is perhaps, convenient to review the three methods by which we may ascertain the tops of the atomic clouds in Nevada. First and simplest is to fly an airplane at the same level as the cloud and read the altimeter. This is routinely done and except for small altimeter corrections and cases where the cloud is well above the aircraft one should assign relatively small errors to this method. However, I understand that this determination of the cloud top data is not a primary function of the pilots and probably no attempt is made to obtain precise measurements.

A second method of height determination is the measurement of the elevation angle of the cloud top and together with a knowledge of the point of burst and the drift of the cloud compute the cloud rise. This may be done either by theodolite or by photography. Uncertainties in the drift and inability to sight the top of the cloud are the main limitations in this method. In general, when the elevation angle is

[redacted]

[redacted]

209

small and the cloud outline still sharp, during and immediately following the ascent, the errors ought to be small.

The third method uses two or more cameras or theodolites focused on the same point at the cloud top and applies trigonometric computations to find the cloud rise. Drift corrections are unnecessary, but for this benefit we substitute the uncertainty in the location of the same point on the cloud. Only during BUSTER-JANGLE has there been any attempt to use this method--by EG&G with photographic film.

There are some minor ambiguities in the definition of the irregular cloud top which may account for some of the discrepancies to be seen later. EG&G, for example, uses the average top rather than the highest point of the cloud while I suspect that the theodolite measurements are based on the highest point of the cloud. Further, since the cloud frequently overshoots the final levelling off height, it is not always clear which height; (the absolute maximum or the final maximum) is being referred to. In time, some sort of agreement should be reached as to the definition of a cloud top.

I have surveyed, to the best of my ability, the documented heights of all the atomic clouds detonated in Nevada, discarding insofar as possible, values which were subsequently changed by later computations. I should like to illustrate a few of the cases of discrepancies which were found by the different methods. Table 1 shows two BUSTER-JANGLE

Table 1

Examples of Cloud Top Observations

Heights in feet MSL

BUSTER/BAKER			
AWS Theodolite	27,000	at	15 minutes
EG&G Photographs	22,000	at	8 minutes and still rising
Rand Photographs	29,000	at	7 minutes and still rising
Aircraft (at 26,500)	25,000	at	50 minutes
	Value used 27,000		
BUSTER/DOG	(48,000	at	20 minutes
AWS Theodolite	-(46,000	at	8 minutes (data confusing)
	(21,000	at	21 minutes
EG&G Photographs	40,000	at	8 minutes & rising fast
Rand Photographs	37,000	at	7 minutes and still rising
Aircraft (at 41,000)	41,000	at	1 hr., 50 minutes
	Value used 40,000		

[redacted]

cases—illustrations of poor agreement. Let me make it clear that the individuals making the observations during these early series make no pretense of great accuracy. Nevertheless, this is what we must work with.

These BUSTER shots were selected for illustration because there were four sets of measurements available. EG&G used double triangulation—Rand, single camera and drift, but checked their results from a second observing point. The differences between the cloud tops speak for themselves. In the case of BUSTER Dog the cloud moved toward both the theodolite and cameras so greater credence was associated with the aircraft, tempered by the photographic analysis which incorporates the spherical shape of the cloud.

Table 2 shows two of the UPSHOT-KNOTHOLE clouds. In the case of Shot 4, the discrepancy between EG&G and the others is more than might

Table 2

Examples of Cloud Top Observations

Heights in feet MSL

UPSHOT-KNOTHOLE-DIXIE (4)			
AWS Theodolite	43,000	at	12 minutes
EG&G Photographs	38,500	at	10 minutes
Aircraft	43,000		
	Value used 41,000		
UPSHOT-KNOTHOLE-ENCORE (8)			
AWS Theodolite	43,000 & 41,500		
	42,500	at	13 minutes
EG&G Photographs	42,000	at	9 minutes
Aircraft	40,500		
	Value used 42,000		

be expected. In the case of Shot 8, only the aircraft is out of line and the 42,000 feet value looks fairly reliable. The two AWS numbers: 43,000 and 41,500 are the tops reported by two different theodolite observations - the 42,500 number is a compromise. The comparison between various methods of measurements for the UPSHOT-KNOTHOLE cloud tops reveals better agreement than the earlier series suggesting a trend toward better observations.

In summary, I feel that the cloud top data are acceptable for this study in no more than half of the 29 cases.

[redacted]

211

It is evident that a more powerful explosion will, in general, yield a cloud which rises higher than a weaker blast. Figure 1, typical of the kind which everyone working in this field prepares, shows a plot of the adjusted yield of the device as the abscissa against the amount of rise of the cloud as the ordinate. This adjusted yield is the fireball yield multiplied by the standard sea level pressure (1013 millibars) and divided by the pressure at the point of burst. The correction factor for pressure, about 1.2, is roughly the same for all shots except the two high air bursts--shown by the double circles--so that the results of this and later figures would be just about the same if we used the actual rather than the adjusted yields. The amount of rise is the difference between my interpretation of the top of the atomic cloud and the height of the burst. The circles represent air bursts and the crosses tower bursts (all 300-foot towers); the gun shot by a circle and cross since it was a true air burst, but detonated much lower than the other air bursts. The letters and numbers denote the names and numbers of the Nevada test series - R for Ranger, B/J for BUSTER-JANGLE, S/T for SNAPPER-TUMBLER, and U/K for UPSHOT-KNOTHOLE. The curve denotes my subjective interpretation of a best fit of the data.

It is clear that up to about 15 KT, the rise is generally greater the larger the yield, but between about 20 and 75 KT, I suspect that a least squares analysis would indicate almost a horizontal line showing little or no dependence of the amount of rise on the yield.

Since, in Nevada, the tropopause lies in the range of about 30-45,000 ft. above mean sea level, the same height range at which the bombs over 10 to 15 KT appear to stop, it seems logical to see what the relationship between the top and the tropopause may be. Figure 2 shows the adjusted yield as the abscissa once again with height above sea level as the ordinate this time rather than the amount of rise. For those shots which rose above 20,000 feet, the corresponding tropopause is given as either a line or a thin or a broad shaded area. The line indicates a weak tropopause with little tendency to stop the rising cloud, while the broad area indicates an intense tropopause with a strong tendency to stop the cloud. The narrow shaded area lies between the two extremes and the question marks on two cases mean that the tropopause has not yet been reached at the indicated heights. Up to about 15 or 20 KT none of the tops really rise above the tropopause but between 20 and 40 KT adjusted yields there are cases in which the clouds tops overshoot and undershoot the tropopause. All three cases above 40 KT exceeded the height of the tropopause slightly. Aside from these remarks there appears to be very little relationship between the height of the tropopause and the height at which the atomic clouds stop.

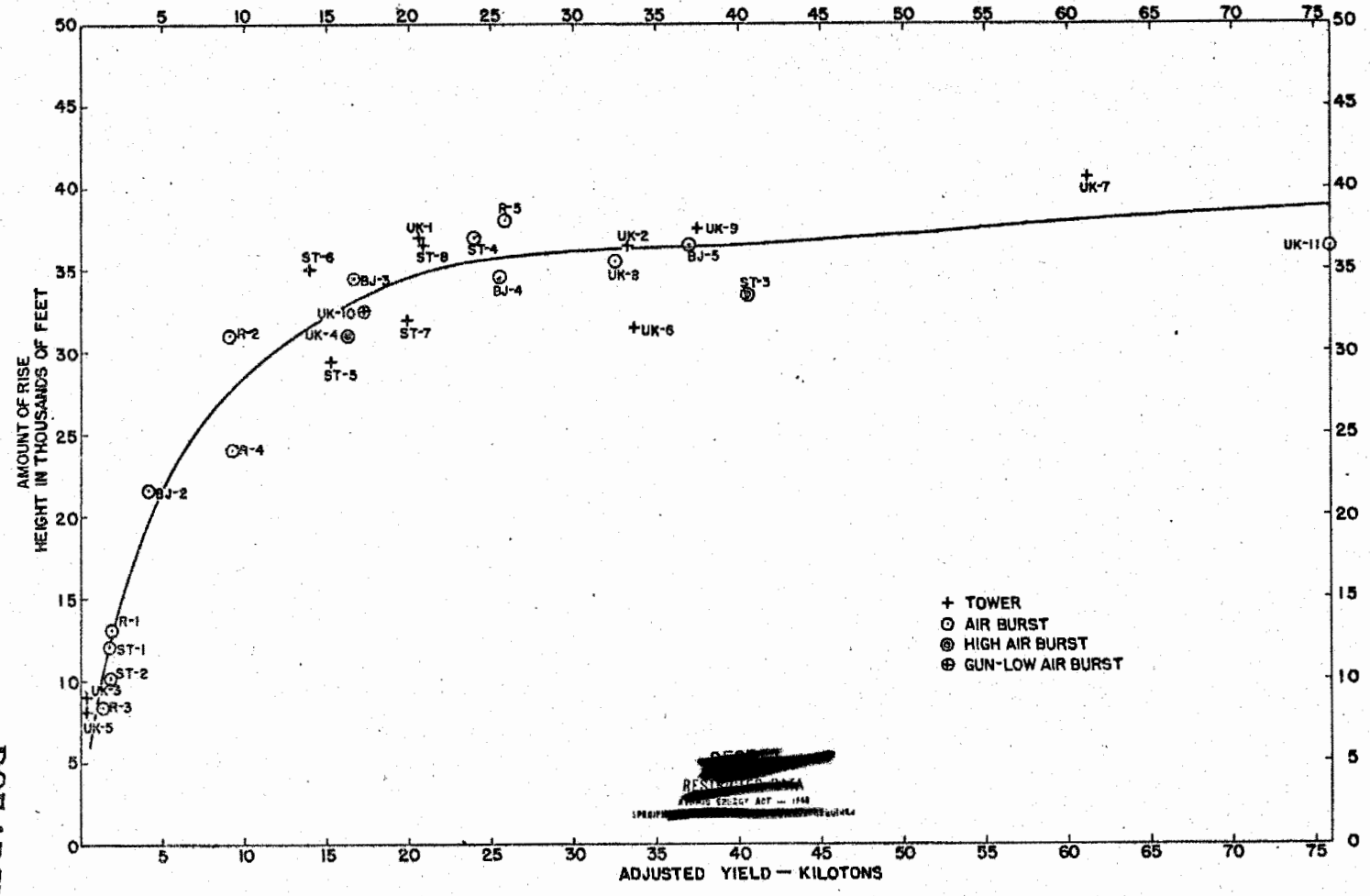

Figure 1
Amount of Rise of Atomic Cloud as a Function of the Adjusted Yield

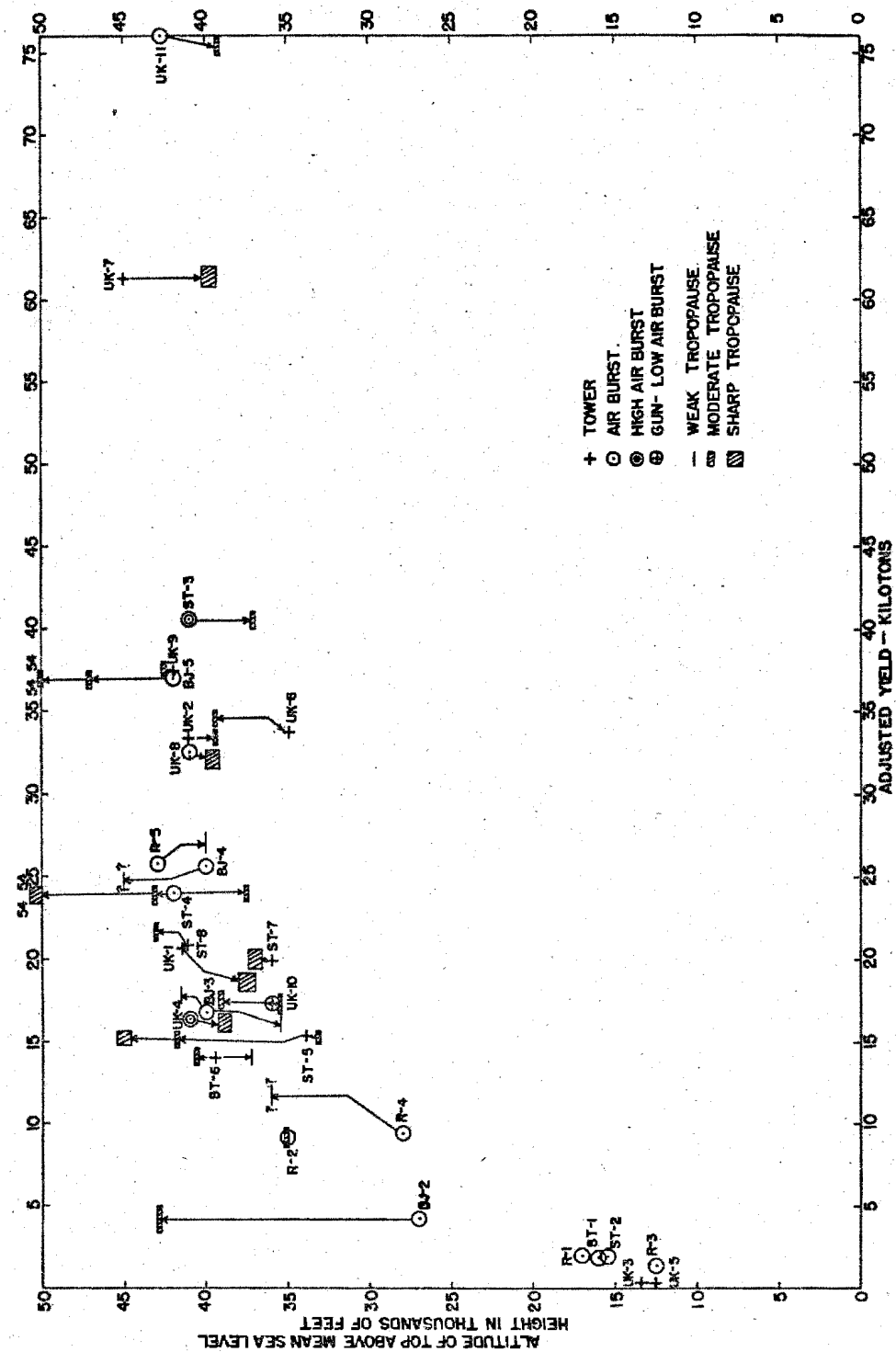

Figure 2
Altitude (MSL) of Atomic Cloud Top as a Function of the Adjusted Yield

[redacted]

In theory, an isolated parcel of air heated above its environment will rise and expand until its density is again similar to that of its new surroundings. Thus, the greater the heating the greater the rise. After the initial effects of radiation loss of the fireball have passed, it is believed that cooling will be accomplished in part by expansion as the parcel moves into regions of progressively lower pressure aloft. During this rapid rise a meteorological property called the potential temperature remains approximately constant even though the actual temperature of the cloud decreases rapidly. If the amount of initial heating available for bouyancy is proportional to the yield of the weapon, then the potential temperature difference of the atmosphere between the elevation of burst and the stopping point of the cloud should, according to one simple concept, be proportional to the yield.

Figure 3 shows the adjusted yield as the abscissa again and the potential temperature difference between point of burst and stopping as the ordinate. θ is the symbol for potential temperature. The simple theory states that the cases should arrange themselves so that greater differences in potential temperature go with greater yields. I do not believe that one can argue for more than the vaguest suggestion that the simple theory is verified in the range above 15 or 20 KT.

In a RANGER report, Holzman and Kent recommended using the difference in potential temperature between cloud top and 750 millibars (about 8,000 feet above mean sea level) rather than the top and burst height. Figure 4 shows this potential temperature difference as the ordinate. It is seen that the picture in this figure is very similar to that of the previous one and that the predicted theory is not verified. In passing, you might note that if you look only at the five RANGER shots you can see why with the limited data, the simple theory appeared to be verified in 1951.

I shall not bore you with the details of all the other studies associating the cloud tops with weather elements. The wind shear, the mean wind during ascent and the conditions at the point of burst have so far been looked at with, in my opinion, negative results. I have not by any means exhausted the possibilities nor yet looked into combinations of parameters as controlling the rise of the cloud.

Table 3 emphasizes the present state of ignorance on the part of meteorologists to utilize meteorological factors in predicting the tops of Nevada clouds. Based on regression equations prepared from all the pre-U/K shots in the range between about 10 and 50 KT, LTCOL Spohn made predictions for each of the U/K shots. The equations incorporated the yield, the stability of the air - or essentially something similar to the potential differences shown in the previous figures - and the wind

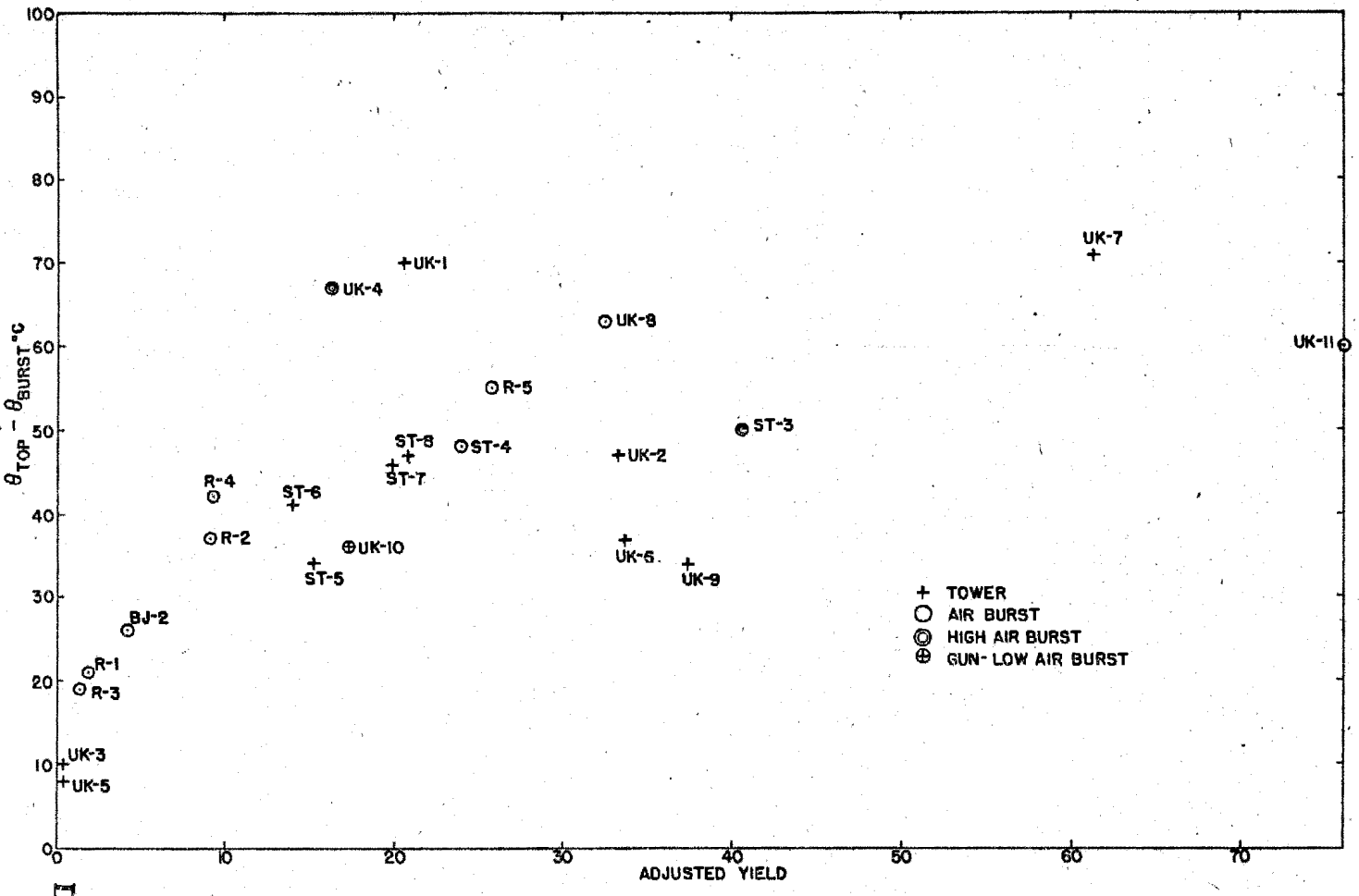

Figure 3
Potential temperature (θ) difference between the Cloud Top and the Point of Detonation as a Function of the Adjusted Yield.

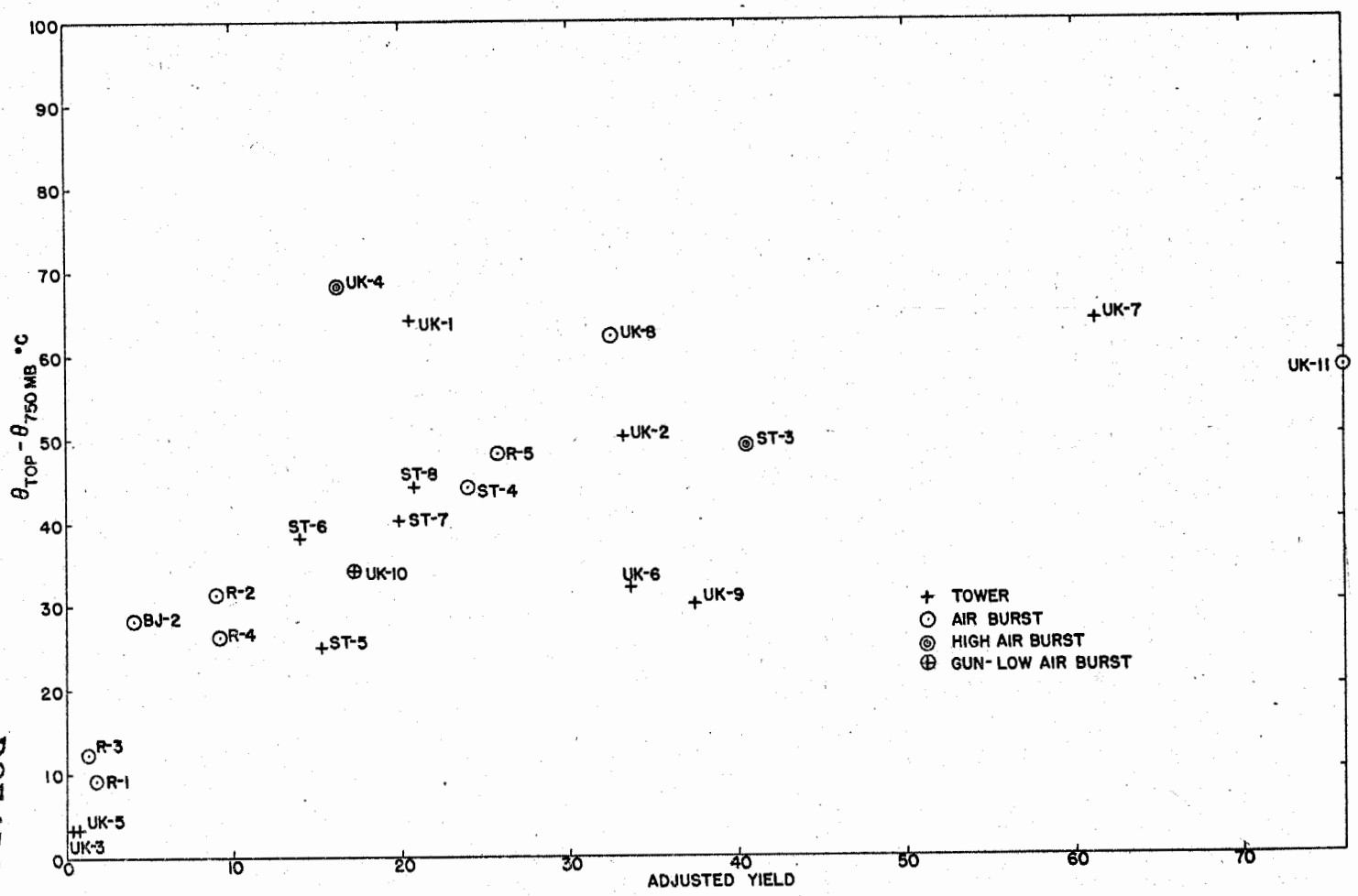

Figure 4
Potential temperature (θ) difference between the Cloud Top and the 750-mb. Level as a Function of the Adjusted Yield.

[redacted]

Table 3

Verification of U/K Cloud Tops

Absolute Mean Errors in Feet

LASL pre-U/K Regression Equation	Cloud Top at Tropopause	Cloud Top at 40,700 Feet (Mean of pre-U/K Tops)
3,500	3,300	2,800

1. 9 of 11 U/K shots.
2. U/K tops taken from WT-703.
3. Tropopause data also taken from WT-703.

speed. I show here the verification of his predictions for all but the two smaller U/K shots (numbers 3 and 5). The average absolute error is about 3,500 feet and, this error, incidentally, is unchanged for his predictions even if the two smaller shots are included. Two other simple predictive schemes suggest themselves for comparison. First, that the clouds stop exactly at the tropopause. The verification for this case, 3,300 feet, is better than the regression equations, but probably not significantly so. I understand that the present revised version of the Los Alamos regression equations now includes the tropopause height as an additional parameter. Finally, one might argue that all clouds in the 10 to 75 KT yield range stop at the same height above sea level as suggested from one of the earlier figures. The heights of all shots above about 10 KT prior to UPSHOT-KNOTHOLE stopped at about 40,700 feet above mean sea level and using this height for the nine larger U/K shots, the verification, 2,800 feet, turns out to be better than either of the previous cases. Taken literally, it means that, as yet, we have found no reason why the cloud tops should be a function of either the yield or weather conditions for the Nevada shots provided the yield is in the range of about 10 to 75 KT.

I should like to indicate what, in my opinion, represents the most likely explanations for the failure to satisfactorily use meteorology in cloud top analyses.

I feel that there is ample reason for doubting the accuracy of most of the cloud top measurements.

Perhaps the changes in atmospheric conditions play little or no role in controlling the cloud rise or if meteorology is important,

[redacted]

[redacted]

we may not be measuring the right meteorological parameters or interpreting the weather observations in the proper fashion.

Perhaps, it is the center of the mushroom or some other feature not yet studied which is related to changes in atmospheric parameters.

If the construction or detonation of atomic weapons possess differences other than their yields of which we are not aware, but which determine, say, the bouyancy of the cloud, this may well account for some of the height differences.

In conclusion, where does this state of affairs leave us? First, I would say that if there is no systematic arrangement of cloud tops in the Pacific for weapons in a broad megaton range, this should not surprise us. Second - for TEAPOT - unless someone produces a rather convincing demonstration of yield and meteorology as controlling features in the cloud tops, I would say that in the 10 to 40 KT range and for normal tropopause elevations, a constant height of about 40,000 feet is as good a predictive rule as any.

[redacted]

[redacted]

THIS PAGE IS BLANK

[redacted]

TYPICAL U. S. AND EUROPEAN WEATHER AS IT AFFECTS FALLOUT, WITH EMPHASIS ON WIND STRUCTURE

Dr. Lester Machta
U. S. Weather Bureau, Washington 25, D.C.

I believe there are two types of fallout information which Civil Defense officials and military commanders would want from the meteorologist; first, material based on past weather records which can be used for planning purposes - it is this which we will discuss primarily - and second, day-to-day forecasts of where and how much fallout would occur from a potential or actual bomb dropped at a specific time and place.

It is clear that what is desired is information both on where fallout will occur and what the distribution of dosages within the fallout area will be. For a variety of reasons, I do not know how to predict dosages from a given wind field. My discussion will describe only the areas of fallout with some clues as to where particles of a given size will fall or when the fallout will occur downwind of the blast. Further, even in providing the areas without giving dosages, I am handicapped because I don't know the width of the radioactive cloud or how high the radioactive part of the clouds from megaton weapons will rise. So, if you will forgive some arbitrary decisions which, strictly, should represent conclusions of this symposium, I can proceed.

The central and northern United States and Europe lie in the temperate latitudes and, by and large, have marked similarities in weather and winds. Thus, though most of what I will show represents data from the United States, the conclusions to be drawn are generally applicable to Europe as well.

Figure 1 shows the mean fallout sectors in winter. The radial lines show the extremities of the fallout sector for a very narrow cloud. The inner envelope shows the outline of the fallout area if the mushroom (here defined as the portion of the cloud above the tropopause) were 50 miles wide and the outer lines, if the mushroom were 100 miles wide. The shaded area represents the sector in which fallout comes from the center of the mushroom. Fallout is assumed to originate from heights up to 90,000 feet. The heavy line running across the radial lines indicates the approximate position of fallout 6 hours after burst. The arcs are drawn at a distance of 100 miles from the burst to provide a distance scale.

The main feature of the winter chart is that fallout occurs primarily to the east of the burst. The New England area contains many of the stronger wind speeds experienced in the country.

[redacted]

[redacted]